

**A Tale of Two Alpha's: Design of Selective
Agonists and Modulators Targeting the $\alpha 4$ - $\alpha 4$
Binding Site of $(\alpha 4)_3(\beta 2)_2$ Nicotinic
Acetylcholine Receptors**

**A thesis submitted for the degree of Doctor of Philosophy at the
Australian National University**



**Australian
National
University**

By

**KESHAV KUMAR GUPTA
RESEARCH SCHOOL OF CHEMISTRY
COLLEGE OF SCIENCES
THE AUSTRALIAN NATIONAL UNIVERSITY
2020**

DECLARATION

I certify that the work in this thesis has not previously been submitted for a degree nor has it been submitted as part of requirements for a degree except as fully acknowledged within the text. I declare that, to the best of my knowledge, the material presented in this thesis represents the result of original work I carried out, under the supervision of Associate Professor Malcolm D. McLeod.

I also certify that the thesis has been written by me. Any help that I have received in my research work and the preparation of the thesis itself has been acknowledged. In addition, I certify that all information sources and literature used are indicated in the thesis.

KESHAV KUMAR GUPTA

Keshav Gupta

ACKNOWLEDGEMENTS

It has been an extremely long and tough journey towards my doctoral degree, and the first person to whom my deepest appreciation comes for is my committee chair and supervisor, Associate Professor Malcolm D. McLeod. It was due to your tremendous support, guidance and encouragement that I am able to accomplish, what seemed impossible at so many instances. You have been exceptionally understanding and patient, especially during the final year of my PhD when I was facing critical health issues, that I cannot thank you enough for what your support meant to me and the way it kept me motivated. Your continued supervision and inspiration are much appreciated, as is the considerable time spent reading through the many drafts of this thesis. I also wish to thank the remaining members of my supervisory panel, Professor Chris Easton, Professor Mary Collins and Associate Professor Thomas Balle, our collaborator, for their constant support and directions.

I would like to thank my dear friend and colleague Dr. Nick Kanizaj, for teaching and demonstrating me several chemistry techniques and instruments that were of great help in the lab and in completing my research. His own personal experiences provided a thorough insight on how to excel in organic chemistry research without compromising on personal health and safety. I also wish to express gratitude to Dr. Bradley Stevenson, who's calm nature aided me in achieving the necessary endurance to carry out research as well as for his help with running and troubleshooting the LCMS. Special thanks to Dr. Komba Thomas and Dr. Christoph Nitsche for their support in and out of the lab, whether discussing chemistry or my future after PhD. I extend my appreciation to the various technical staffs at the Research School of Chemistry, especially Anitha for running my mass spectrometry samples, Hideki for analysing my chiral samples on UPLC and Chris Blake for his training and help with the NMR.

I wish to thank the past and present members of the McLeod group; Ryan, Andy, Paul, Chris Waller, Eric, Natasha, Jacob, Sumudu, Dimanthi, Patrick, Chris Fitzgerald, Maryam, Connor, Katelyn, Karen and Jack. It was great to bounce ideas off each other and you all made life in the lab a lot more entertaining. I would also like to thank my friends and peers from other lab groups; Junna, Michael, Manjeet, Ayana and Josemon for great laughs and discussing completely unrelated issues to keep my mind sane.

Finally, I wish to thank all the members of my family for supporting me over the years. To my beloved Maa and Papa, thank you for always believing in me and building my confidence to find the right career path. To my elder brothers and sisters-in-law, thank you for supporting me and helping me relocate to Australia, also for giving me two sweet little munchkins that kept me going through the hard times with their cute smiles and naughtiness. To my late father-in-law, for all the unparalleled love and support you gave me, I wish you were still here to see me fulfil your dream.

Lastly, nothing is complete without mentioning my wife Shweta, as I am lucky to have found such a wonderful person, who left her everything in India to accompany me on one of the toughest journeys of my life and help me fulfil our parents shared dream to accomplish a PhD degree from one of the prestigious university in the world. Whether it was taking care of the finances, when I ran out of my scholarship or if it was about cooking your awesome food during those tiring days or keeping me warm with your candid love when I was down and out, I just want to say thank you for never leaving my side.

Happiness, health and success to all of you!

TABLE OF CONTENTS

Declaration	i
Acknowledgements	ii
List of Abbreviations	vi
Abstract	x
1. Introduction	2
1.1. Nicotinic Acetylcholine Receptors	2
1.1.1. General Structure	3
1.1.2. Types of Nicotinic Acetylcholine Receptors	10
1.1.3. Functional and Kinetic Characteristics	12
1.2. Nicotinic Acetylcholine Receptor Ligands	16
1.2.1. Agonists	17
1.2.2. Antagonists	20
1.2.3. Allosteric Modulators	22
2. Design of Selective Agonists For $\alpha 4$-$\alpha 4$ Binding Site	27
2.1. The $\alpha 4\beta 2$ Nicotinic Acetylcholine Receptors	27
2.1.1. X-Ray Crystal Structure of Human $\alpha 4\beta 2$ Receptors	28
2.1.2. The Two $\alpha 4\beta 2$ Nicotinic Receptor Stoichiometries	31
2.1.3. Ligands Targeting $(\alpha 4)_3(\beta 2)_2$ Nicotinic Receptors	41
2.2. Design and Syntheses of NS9283-NS3920 Hybrids	53
2.2.1. Project Aims	53
2.2.2. Retrosynthetic Analysis	55
2.2.3. Synthesis of Hybrids	56
2.2.4. Biological Evaluation of Hybrids	71
2.3. Design of Substituted Pyridines	75

2.3.1. Project Aims	75
2.4. Chapter Conclusion and Future Work	79
3. Design of Novel Positive Allosteric Modulators	83
3.1. The (α 4) ₃ (β 2) ₂ Nicotinic Acetylcholine Receptor	83
3.1.1. Identification of New Pocket in the α 4- α 4 Subunit Interface	84
3.1.2. Targeting the Newly Recognised Site in the α 4- α 4 Interface	87
3.2. Design of Anabasine and Nicotine Analogues	92
3.2.1. Project Aims	92
3.2.2. Retrosynthetic Analysis	95
3.2.3. Synthesis of Unsubstituted Anabasine and Nicotine Analogues	96
3.2.4. Synthesis of Substituted Anabasine and Nicotine Analogues	117
3.2.5. Biological Evaluation of Anabasine and Nicotine Analogues	129
3.2.6. Determination of Enantiomers from Chiral HPLC	131
3.3. Chapter Conclusion and Future Work	134
4. General Information	138
4.1. Experimental for Chapter 2	139
4.2. Experimental for Chapter 3	150
References	181

LIST OF ABBREVIATIONS

5-HT₃	5-Hydroxytryptamine receptor
ACh	Acetylcholine
AChBP	Acetylcholine-binding protein
AChE	Acetylcholinesterase
ACN	Acetonitrile
AcOH	Acetic acid
ADHD	Attention deficit hyperactivity disorder
BnBr	Benzyl bromide
Boc	Di- <i>tert</i> -butyl dicarbonate
CAN	Ceric ammonium nitrate
CDCl₃	Deuterated chloroform
CDI	Carbonyldiimidazole
cDNA	Complementary deoxyribonucleic acid
CMPI	3-(2-Chlorophenyl)-5-(5-methyl-1-(piperidin-4-yl)-1 <i>H</i> -pyrrazol-4-yl)isoxazole
cRNA	Complementary RNA
DBU	1,8-Diazabicyclo[5.4.0]undec-7-ene
DCC	Dicyclohexylcarbodiimide
DCM	Dichloromethane
DEE	Diethyl ether
dFBr	Desformylflustrabromine
DIBAL	Diisobutylaluminium hydride
DIPA/(<i>i</i>-Pr)₂NH	Diisopropylamine
DMAP	4-Dimethylamino pyridine
DMF	Dimethylformamide

DMPP	1,1-Dimethyl-4-phenylpiperazinium
DMSO	Dimethyl sulfoxide
DMXBA/GTS-21	3-(2,4-Dimethoxybenzylidene)-anabaseine
DRC	Dose-response curve
EC₅₀	Agonist concentration required for 50% of the maximal response
ECD	Extracellular Domain
ELIC	(<i>Erwinia chrysanthemi</i>) Ligand-gated ion channel
EM	Electron microscopy
Fab	Antigen-binding fragments
GABA_A	γ-Aminobutyric acid receptor
GLIC	(<i>Gloeobacter violaceus</i>) Ligand-gated ion channel
HEK	Human embryonic kidney
HMBC	Heteronuclear multiple bond correlation
HRMS	High resolution mass spectrometry
IC₅₀	Antagonist concentration required for 50% inhibition
I_{max}	Maximal current generated on receptor activation by agonist
<i>i</i>-PrMgBr	Isopropyl magnesium bromide
IprOH	Isopropanol
IR	Infrared
K_i	Inhibition constant or binding affinity
LGIC	Ligand-gated ion channel
LRMS	Low resolution mass spectrometry
<i>Ls</i>	<i>Lymnaea stagnalis</i>
mAChRs	Muscarinic acetylcholine receptors
MeOH	Methanol
MLA	Methyllycaconitine

MsCl	Methanesulfonyl chloride
MWC	Monod-Wyman-Changeux
MYA	Million years ago
nAChRs	Nicotinic acetylcholine receptors
NAM	Negative allosteric modulators
NaOtBu	Sodium <i>tert</i> -butoxide
NBS	<i>N</i> -Bromosuccinimide
<i>n</i>-BuLi	<i>n</i> -Butyllithium
NIS	<i>N</i> -Iodosuccinimide
NMR	Nuclear magnetic resonance
nOe	Nuclear Overhauser effect
NS3920	1-(6-Bromopyridin-3-yl)-1,4-diazepane
NS9283	3-[3-(3-Pyridinyl)-1,2,4-oxadiazol-5-yl]benzotrile
PAM	Positive allosteric modulator
PCP	Phenylcyclohexylpiperidine
PDA	Photodiode array
PDB	Protein data bank
PMP	<i>p</i> -Methoxy phenyl
R_f	Retention factor
R_t	Retention time
rt	Room temperature (25 °C)
SFC	Supercritical fluid chromatography
TEA	Triethylamine
TEVC	Two-electrode voltage clamp
TFA	Trifluoroacetic acid
THF	Tetrahydrofuran

TLC	Thin layer chromatography
TM1-4	Transmembrane helix 1-4
TMD	Transmembrane Domains
TMS	Trimethylsilyl
UPC²	UltraPerformance Convergence chromatography
UV	Ultraviolet
WT	Wild type
XPhos	2-Dicyclohexylphosphino-2',4',6'-triisopropylbiphenyl

ABSTRACT

The $\alpha 4\beta 2$ nicotinic acetylcholine receptor (nAChR), belonging to the family of ‘Cys-loop’ pentameric ligand-gated ion channels, is one of the most abundant subtypes found in the brain. Several researches have concluded its important role in modulating memory, sleep and attention. Thereby, making it an attractive druggable target due to its implication in several neurological, and psychiatric disorders such as Alzheimer’s disease, Attention Deficit Hyperactivity Disorder (ADHD) and nicotine addiction. The heteropentameric $\alpha 4\beta 2$ nAChRs are known to arrange in two different stoichiometries; $(\alpha 4)_2(\beta 2)_3$ and $(\alpha 4)_3(\beta 2)_2$. Apart from the known and extensively targeted $\alpha 4$ - $\beta 2$ binding sites that are present in both stoichiometries, the distinctive $\alpha 4$ - $\alpha 4$ binding site located only in the $(\alpha 4)_3(\beta 2)_2$ stoichiometry, has become a desirable target to exploit its site-specific functions in formulating treatments for the neurological disorders. The key challenge lies in developing $\alpha 4$ - $\alpha 4$ site-selective ligands, as structurally both are closely matched binding sites with only minor differences. Understanding these key differences could pave the way for more potent and selective ligands for the $\alpha 4$ - $\alpha 4$ binding site.

NS3920, a pyridine-diazepane compound and NS9283, an oxadiazole analogue has been found to be active at the $\alpha 4$ - $\alpha 4$ binding site. Based on the potency of NS3920 and selectivity of NS9283, diazepane substituted pyridyl/phenyl hybrids harbouring common structural features of both ligands were designed, with an aim to improve the biological profile of ligands at the $\alpha 4$ - $\alpha 4$ binding site. The synthesis of 5- and 6-monosubstituted as well as 5,6-disubstituted pyridyl/phenyl hybrids was achieved through the Buchwald-Hartwig reaction conditions. The biological evaluation of these hybrids was carried out by employing the TEVC electrophysiology and receptor binding assays on $(\alpha 4)_2(\beta 2)_3$, $(\alpha 4)_3(\beta 2)_2$ and mutated $(\alpha 4)_2(\beta 2^{\text{HQT}})_3$ receptor harbouring three interfaces resembling $\alpha 4$ - $\alpha 4$ binding site. The results obtained remained largely inconclusive, thus, leading us to the design of modulators.

Positive allosteric modulators or PAMs are a newfound interest of the scientific community due to their ability to increase the frequency of channel opening without directly activating the receptor itself, thus, reducing the chances of receptor desensitisation, as PAMs bind at a site away from the orthogonal binding site of classical agonists, like ACh. A small pocket in close proximity to the $\alpha 4$ - $\alpha 4$ binding site was identified recently by the collaborators at the University of Sydney, which could prove beneficial in unlocking the full potential of

receptor. Several co-crystal structures of known agonists and antagonists were analysed that may have a bond vector directed towards the new pocket. Anabasine and nicotine were chosen as the two lead templates to design and synthesise analogues, because of the presence of a bond vector directed straight towards the newly identified pocket. L-proline catalysed Mannich reductive cyclisation principle was employed for the synthesis of several anabasine and nicotine analogues. Side chain substitution was carried out either via CDI-mediated esterification or base-promoted etherification, to install substituents that can directly interact with the site residues of the identified pocket. Preliminary biological studies have shown that four anabasine ester analogues possess positive modulatory activity at $\alpha 4$ - $\alpha 4$ binding site which could be due to direct interaction of sidechain substituents with the site residues.

CHAPTER 1

1. INTRODUCTION

The generations of research involving diverse disciplines, like biochemistry, genetics, structural biology, and pharmacology have uncovered the many intricacies of neuronal networks, neurotransmitter release, and nerve transmission. Progress has been made at all frontiers since the high-resolution structures of various neuronal receptors were made available and electrophysiology studies were conducted on isolated or whole-cell receptors. However, the complexities associated with neuronal receptors like the nicotinic acetylcholine receptors (nAChRs) still outshine our current knowledge and thus, necessitates a multidisciplinary approach to achieve greater insight.¹ The forthcoming sections will provide detailed discussions on various aspects of nAChRs, ranging from structure and function to its role in various disorders as well as the development of ligands, and what the future holds, especially in regard to $\alpha 4\beta 2$ subtype.

1.1. NICOTINIC ACETYLCHOLINE RECEPTORS

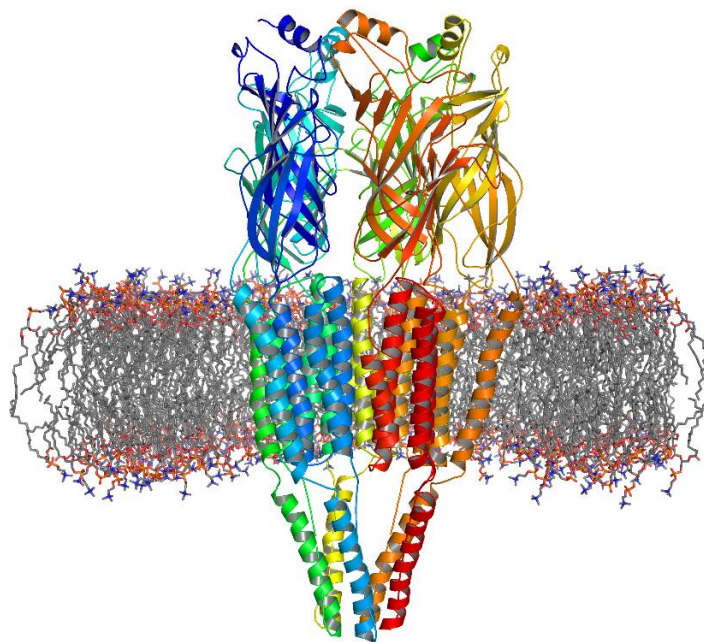


Fig. 1.1: *Lateral view Torpedo marmorata nAChR structure, using ribbon representation generated from PDB 2BG9.*²

The first nicotinic acetylcholine receptor was discovered and studied almost five decades ago. (**Fig. 1.1**). Since then, a multitude of receptors homologous to the nAChRs have been unearthed, not only in eukaryotes (GABA_A, glycine and 5-HT₃) but also in prokaryotes (GLIC and ELIC). This makes nAChRs the prototypical members of pentameric ligand-

gated ion channels superfamily.³ The ubiquitous pair of disulphide bonded cysteine residues, separated by 13 amino acids, forms the Cys-loop. It is the most defining feature of LGIC superfamily, classifying them as Cys-loop receptors.^{1, 4} In vertebrates, the genome encodes a total of 17 genes translating into different nAChR subunits, forming a distinctive set of integral allosteric membrane proteins responsible for fast synaptic transmission.^{5, 6}

The nAChRs are found on the presynaptic, postsynaptic, and some non-neuronal cells, where they expedite neurotransmission via binding of the neurotransmitter acetylcholine. They play a significant role in memory formation, learning, cognition, muscle contraction, arousal, and pain alleviation.^{7, 8} The distinct physiological and pharmacological facets of nAChR makes it a potential therapeutic target for several neurodegenerative and psychiatric disorders, such as myasthenia gravis,⁹ Parkinsonism,¹⁰ attention deficit hyperactivity disorder (ADHD),¹¹ Alzheimer's,¹² schizophrenia,¹⁰ neuropathic pain,¹³ depression,¹⁴ and nicotine addiction.¹⁵ This underpins the need to use combined knowledge of medicinal chemistry and chemical biology in developing diverse therapeutics to treat nAChRs linked disorders as well as devise chemical probes to study and validate the targeted protein.⁸

1.1.1. GENERAL STRUCTURE

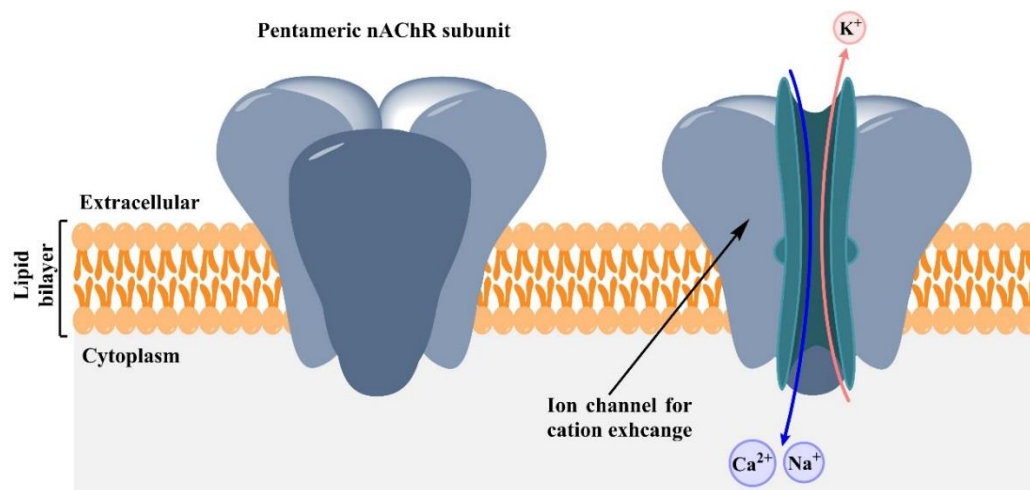


Fig. 1.2: Standard depiction of a pentameric nAChR subunit, both complete and cross-sectional view, traversing the lipid bilayer to establish an ion channel.⁸

The isolation of the nAChR prototype from an electric organ of a ray fish *Torpedo marmorata*² and that of soluble acetylcholine-binding protein (AChBP) secreted by fresh pond snail *Lymnaea stagnalis* (*Ls*) and sea snail *Aplysia californica* (*Ac*),¹⁶ are the two major scientific findings that paved way for a comprehensive investigation of nAChRs

structure and function. The detailed structure established through electron microscopic (EM) studies and crystallised assemblies, revealed the membrane topology of nAChRs. The pentameric structure consists of five subunits, which are symmetrically organised around a central pore for passive diffusion of cations across the membrane (**Fig. 1.2**).

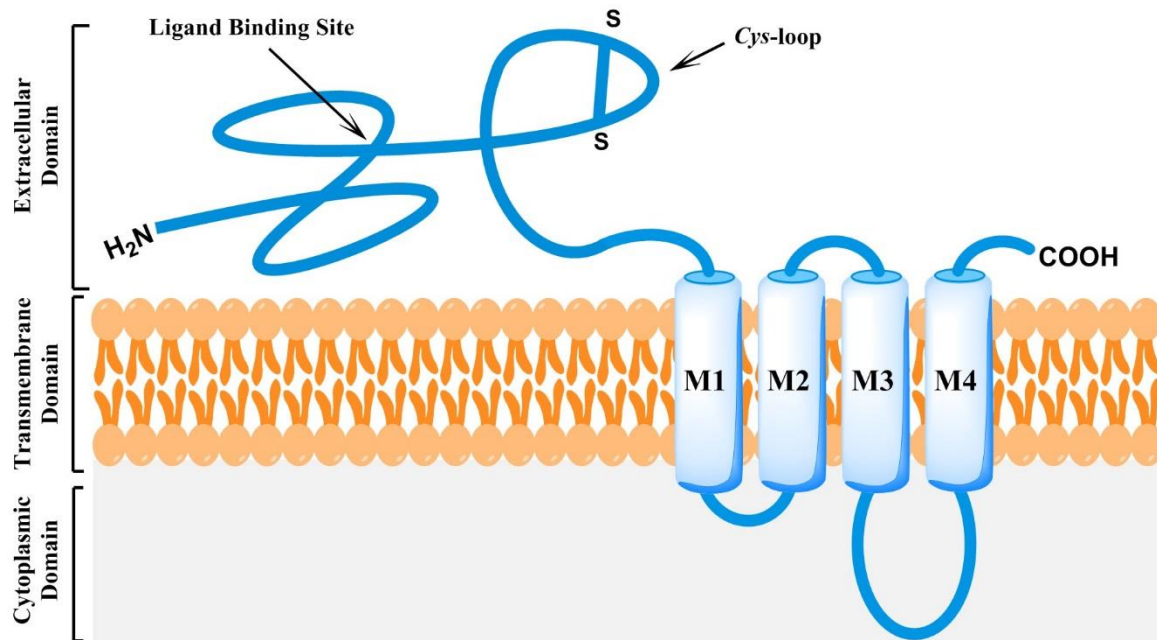


Fig. 1.3: Representation of a single nAChR subunit transmembrane topology, showing the ligand binding site and Cys-loop on the N-terminal region, variable cytoplasmic domain, and short C-terminal domain.⁸

The high similarity in the protein construct amongst nAChRs of different species led to utilisation of the EM-image of the isolated *Torpedo* nAChR as a model, to study the complete structure of nAChRs present in vertebrates. Every monomeric subunit of *Torpedo* receptor is divided into (**Fig. 1.3**): (i) a hydrophilic extracellular domain harbouring the ligand binding site, (ii) four α -helical transmembrane domains lining the channel pore, (iii) a short amino acid sequence of cytoplasmic domain, and; (iv) a short carboxy terminus extending to extracellular domain.^{2, 4, 16}

Extracellular Domain (ECD): Ligand Binding Site

In the *Torpedo* receptor,² the nAChR-ECD is made up of a large single polypeptide with N-terminal α -helix and a continuous sequence of 10 hydrophobic β -strands, linked through signature disulphide bonded cysteine residues. Some loop regions essential for receptor function, such as loops A-F, Cys-loop and the β 1- β 2 loop, are present in this domain. The

ligand binding site is formed at the interface of two adjacent subunits in the ECD. In all cases, one side will have α subunit that forms the positive (+) or principal side, while the other can be α , β , γ , δ or ϵ subunit, which is labelled as the negative (-) or complementary side. A pair of cysteine residues present on loop C in the agonist binding site defines the receptor subunit as α -subunit or principal side.^{2, 8} To gain a better understanding of the ligand binding site in nAChRs, the crystal structure of AChBP is considered in current discussion, as they are most closely related to nAChRs.

The structural features of the binding site preserved in proteins related to nAChRs, are highly valuable to deeply analyse the ligand interactions in receptors. Breakthrough analysis of AChBP crystal structures marked the paradigm shift in nAChR structural studies, serving as a blueprint for the nAChR-ECD.^{17, 18} Here, the co-crystal structure of *Ls*-AChBP with nAChR agonist nicotine (**Fig. 1.4**)¹⁷ is used as a model for the nAChR binding site. *Ls*-AChBP is preferred over other proteins, as it contains a conserved set of five aromatic residues (discussed later) relevant for ligand interaction in nAChR. The AChBP is a homopentamer resembling the ECD of receptor but lacks transmembrane and cytoplasmic domains. It shares 15-28% sequence identity with the receptor ECD across the Cys-loop superfamily and 20-24% with the nAChR-ECD, especially ~28% with $\alpha 7$ receptors.¹⁹



Fig. 1.4: Co-crystal structure of *Ls*-AChBP (PDB 1UW6) showing principal (purple) and complementary side (orange), with nicotine (pink spheres) located in the binding pocket.¹⁷

Each ligand binding site is positioned at the interface between the principal side of the α -subunit and complementary side of a neighbouring subunit.²⁰ Affinity labelling and mutagenesis studies of AChBP show that the binding site consists of the following residues: Tyr89, Trp143, Tyr185, Cys187-188, Tyr192 from the principal side, and Trp53, Gln55,

Leu112, Met114, Tyr164 from the complementary side (**Fig. 1.5**). The binding site core enclosing the ligand, is constructed by a set of five highly conserved aromatic amino acids-Tyr89, Trp143, Tyr185, Tyr192 and Trp53, with the cysteine pair encapsulating from the top, thus, transforming it into an ‘aromatic cage’ like structure.^{18, 19} Polar amino acids associated with the side chains of every subunit are responsible for maintaining charged contacts to keep the assemblies intact. Despite the conservative cysteine and aromatic residues forming the binding domain, the accompanying amino acids in the interface varies from receptor to receptor subtypes, providing scope for developing selective ligands.⁶

X-ray crystallographic analysis of nicotine bound *Lymnaea* AChBP¹⁷ and epibatidine bound *Aplysia* AChBP,²¹ shows that the ligand is completely encased in binding site with cysteine pair capping the entrance. Ligands like nicotine (protonated at physiological pH) containing a charged ammonium moiety, accommodates itself into the receptor site and form a strong π -cation interaction with the aromatic residues. Other contacts including hydrogen bonding and van der Waals forces, also contribute to ligand binding and stabilisation.^{20, 22}

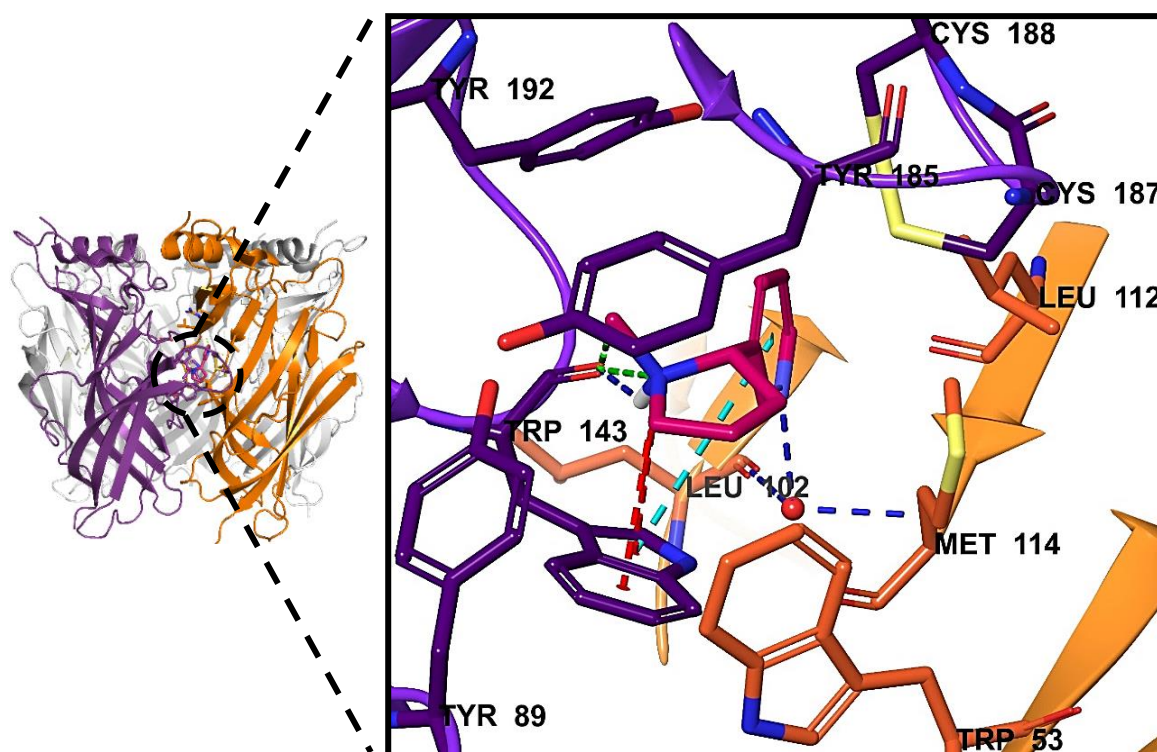


Fig. 1.5: Residues from principal (purple) and complementary side (orange) forming an ‘aromatic cage’ with pair of cysteine residues (purple) enclosing nicotine (hot pink) from the top. Image generated from *Ls*-AChBP X-Ray crystallographic data (PDB 1UW6).¹⁷

The Trp143 residue forms the central floor of the aromatic structure, where the cationic ligands position itself via hydrogen bonding and π -cation interactions.^{6, 20} Four other aromatic residues along with Leu112, Met114 and Arg104 build the confined walls of the cage and further provide stability to the ligand through hydrogen bonding with polar motifs of agonists as well as hydrophobic van der Waals forces. A water molecule present in the binding site also sometimes acts as a bridge, by hydrogen bonding between the ligand and side chain residues Leu102 and Met114.²³ In the end, loop-C with its pair of adjacent cysteine residues, covers the entrance to cap the agonist in the binding site (**Fig. 1.5**).²⁰ Once the agonist binds to the receptor, consequently, the energy generated is transferred to TMDs inducing twists and turns that lead to channel opening.¹⁸

Transmembrane Domains (TMD): Channel Lining and Gating

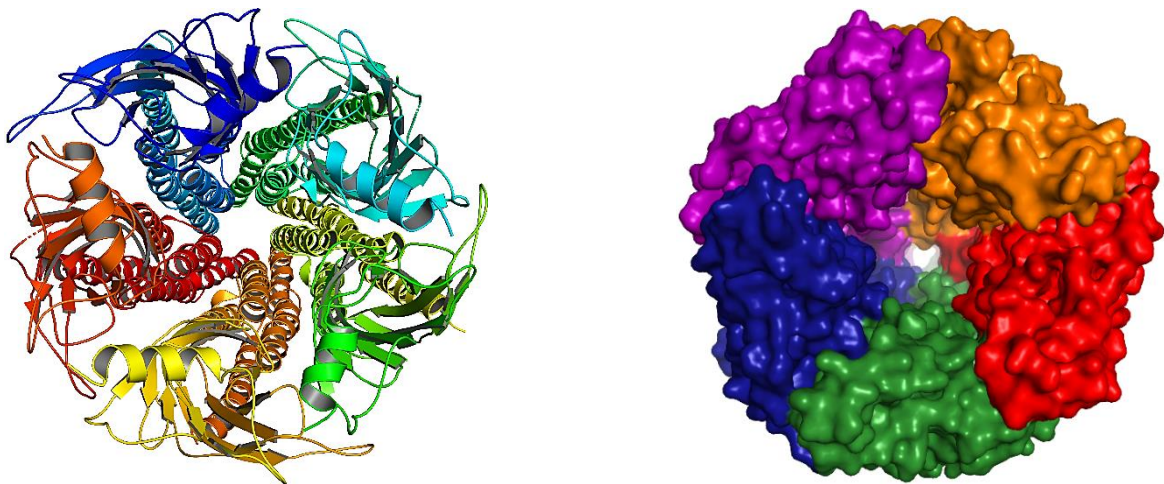


Fig. 1.6: Cartoon (left) and surface (right) representation of the EM-image of *Torpedo* nAChR (PDB 2BG9) from the top, clearly showing the conical shape of the ion channel.²

When viewed from the top, the EM-image² of the *Torpedo* nAChR illustrates the ECD of ligand-free receptor as blades of a turbine with a tapered pore of the channel surrounded by TMDs (**Fig. 1.6**). Each subunit's TMD is made up of four highly conserved α -helices which traverse the membrane bilayer and delineates the hydrophilic ion channel. The TM2 helix from each subunit lines the channel pore, while TM1, TM3 and TM4 protect it from the surrounding non-polar lipid bilayer.⁴ The hydrophobic groups present in sidechains of the TM α -helices (1, 3 and 4), interact via van der Waals forces providing stabilisation.⁶ In ligand free state, TM2 of every subunit maintains a contracted state with non-polar groups placed towards the central axis of the pore to create a layered hydrophobic barricade, thus, restraining ion conduction across the membrane. Both ends of the tapered pore employ

negatively charged amino acids, functioning as an ionic screen to only allow cations to flow through the channel and reflect anionic species out into the extracellular space.¹⁶

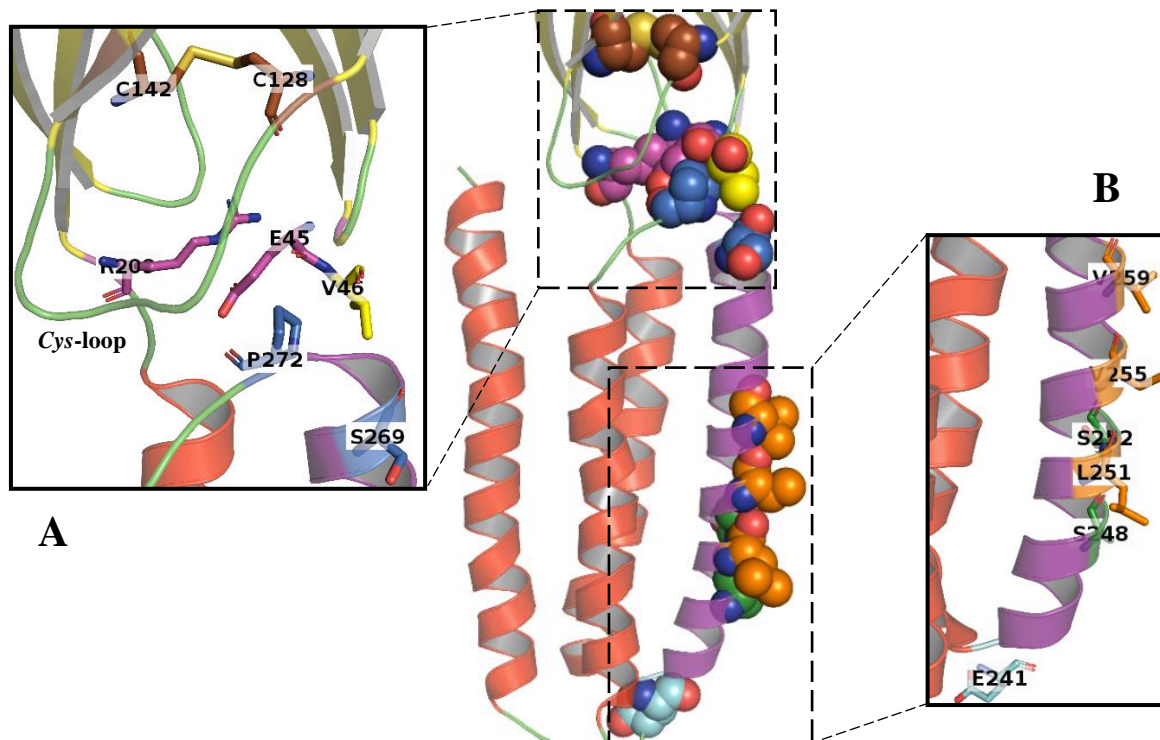


Fig. 1.7: Coupling and gating region (spheres) enlarged to show the residues responsible for channel gating, ion selectivity and conduction in the Torpedo nAChR. **A-** Interlocking residues (sticks) at ECD-TMD junction needed for TM2 rotation. **B-** Essential residues (sticks) responsible for hydrophobic barrier (orange) as well as channel gating (green) and ion selectivity (E241-blue). Image generated from PDB 2BG9.²

Single-channel steady state kinetic studies of nAChR^{24,25} demonstrated highly sophisticated organizational interchanges, which transpire within a span of few microseconds. Residues present at the Cys-loop and covalently linked β 10-TM1 loop play a major role in gating, ion selectivity, and conduction.²⁰ Once an agonist binds to the receptor, the cysteine pair present on loop-C encloses the agonist in the binding site. This converts the ‘distorted’ state of α -subunits to a relaxed conformation, generating enough torque for rotation of the β -sheets.² This energy is transduced to terminal loop residues, which result in the interlocking of the Cys-loop to the adjoining transmembrane residues present at the ECD-TMD junction. It forces overall conformational changes in the TMD, triggering rotation of TM2, and a repositioning of its residues. The relocation of non-polar residues lining the channel with polar residues disrupts the hydrophobic barrier and creates a hydrophilic environment. This allows the pore to be filled with water molecules and thus, facilitate ion conduction.^{16,26}

Charged residues present at both ends of the channel act as an ionic screen and maintains cation flow, especially Glu241 near the cytoplasmic entrance (Fig. 1.7 and 1.8).^{6, 25}

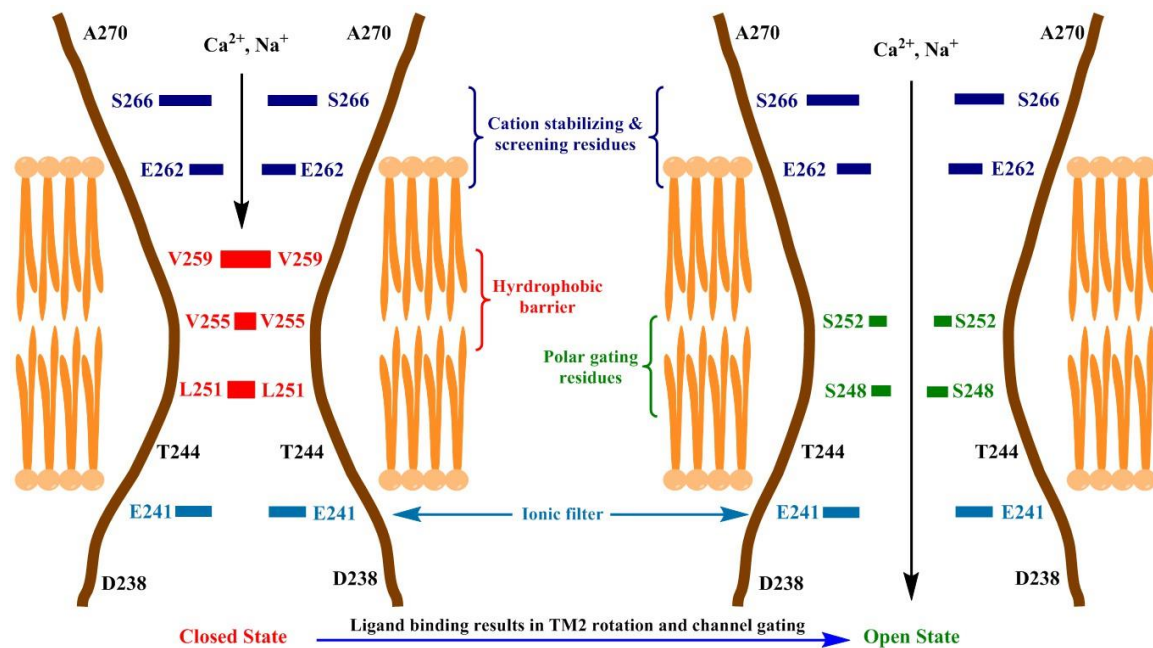


Fig. 1.8: Channel residues lining pore of *Torpedo* nAChR. Image on left shows hydrophobic barrier (closed state), while on the right displays gating residues (open state).⁶

Changeux termed this allosteric transition as a global quaternary twist mechanism.^{27, 28} It involved concerted, opposite rotation of ECD (counter-clockwise), and TMD (clockwise) quaternary constructs with rearrangement of tertiary structures within every subunit (Fig. 1.9).^{3, 6} The gating mechanism was further backed by comparison of X-ray crystal structures of prokaryotic nAChRs, *Erwinia chrysanthemi* (ELIC protein-closed channel)²⁹ and *Gleobacter violaceus* (GLIC protein-open channel),^{30, 31} with its structural homologue *Torpedo* nAChR. Both the prokaryotic structures account for a minimum of 29% of the total quaternary twist models responsible for channel gating.³

Cytoplasmic Domain (CD): Ionic Screen

The eukaryotic cytoplasmic domain is formed by an arched α -helix (Fig. 1.1), preceding TM4, linked to the extended loop connecting the TM3-TM4 domain. The only identifiable part of this domain is the α -helix, termed as a membrane-associated (MA) extension of the receptor subunit,³² as the extended loop is highly variable and disordered throughout the receptor family.⁶ The cytoplasmic conduit is shaped as an inverted cone, lined by the α -helices from each subunit, similar to the extracellular passageway. The inverted cone walls

are made up of negatively charged amino acids with intervening windows present between α -helices.³ The width of these openings is wide enough (~ 8 Å), to allow the speedy passage of hydrated sodium or potassium ions through electrostatic interactions while avoiding strong contact to decelerate ion movement. They also act as an ionic screen, repelling anions and large cations, as the windows are lined with negatively charged residues and are only ~ 8 Å wide.² The CD also plays a role in upregulation, trafficking, desensitisation via phosphorylation, and interactions with other cytoplasmic structures such as G-protein assemblies, to regulate intracellular signalling pathways.^{4,6}

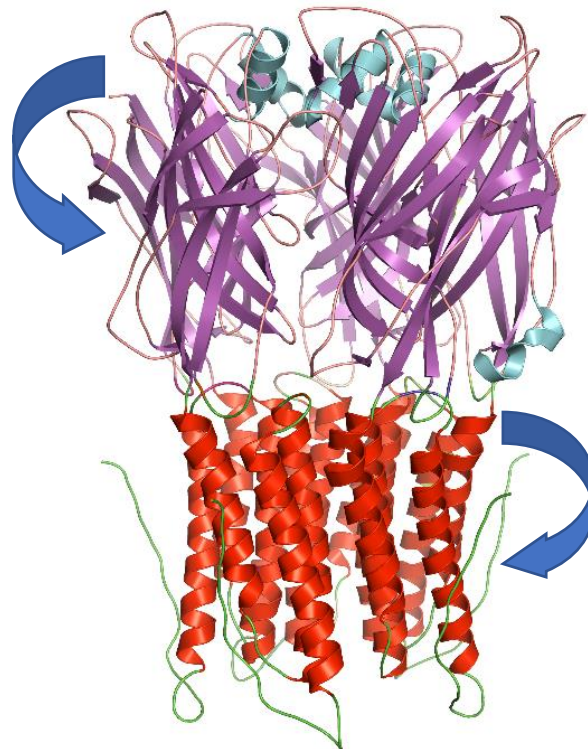


Fig. 1.9: *Quaternary Twist Mechanism showing anticlockwise rotation of ECD (purple) and clockwise rotation of TMD (red), in ELIC X-Ray crystal structure PDB 2VL0.²⁹*

1.1.2. TYPES OF NICOTINIC ACETYLCHOLINE RECEPTORS

Cloning studies of cDNAs from different vertebrate species identify a large multigene family that encodes a total of 17 homologous subunits: $\alpha 1$ - $\alpha 10$, $\beta 1$ - $\beta 4$, γ , δ and ϵ .^{33,34} The subunits organize in different combinations to form the pentameric structure of nAChRs with diverse physiological, pharmacological, and functional profiles.⁴ Based on the subunit composition, nAChRs are classified as homopentameric or heteropentameric receptors, while the subunits are divided into four subfamilies based on sequence analysis and genetic makeup (**Fig. 1.10**).⁷

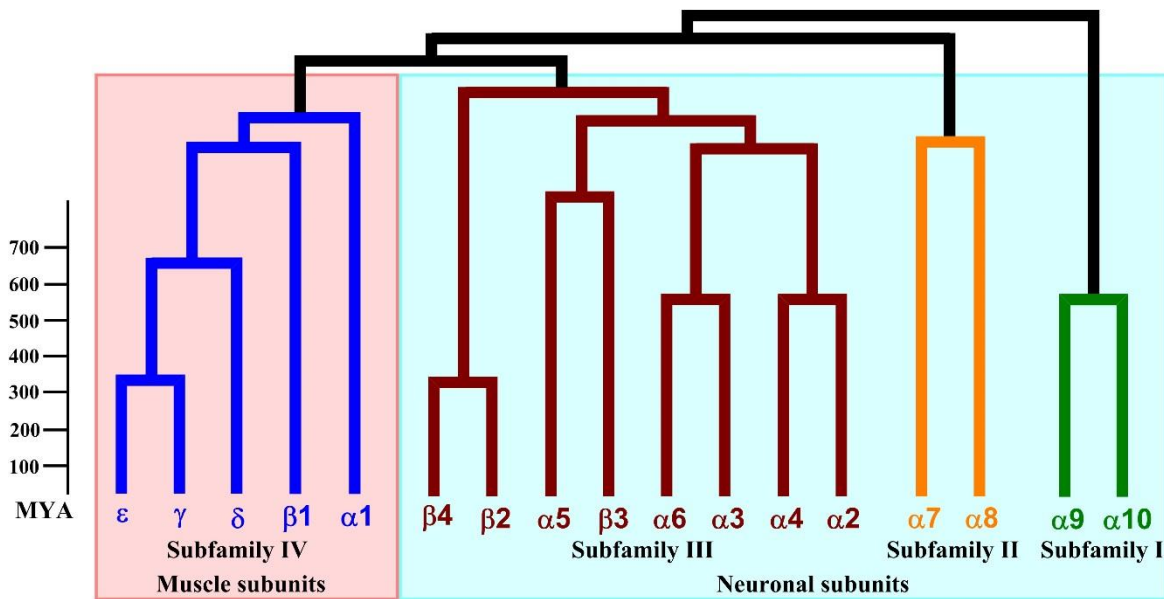


Fig. 1.10: Cladogram of all nAChR subunit gene family based on cloning studies.³⁴

The neuronal nAChRs are composed of complex organization of α and β subunits, constructing a plethora of homopentameric or heteropentameric receptors.¹⁹ The $\alpha 9$ and $\alpha 10$ subunits (subfamily I) form homopentameric assembly by themselves or organize together to form heteropentamers ($\alpha 9\alpha 10$). Similarly, $\alpha 7$ and $\alpha 8$ (subfamily II) create homopentamers by self-organisation or heteropentamers with each other ($\alpha 7\alpha 8$). The set of $\alpha 2$ - $\alpha 6$ and $\beta 2$ - $\beta 4$ subunits (subfamily III) forms an intricate assortment of heteropentameric neuronal nAChRs located in the central and peripheral nervous system.^{4, 34} Eventually, the muscle nAChRs, found at the neuromuscular junction for transmitting nerve impulse to the muscles, are heteromeric in arrangement and constituted with $\alpha 1$, $\beta 1$, γ , δ and ϵ subunits (subfamily IV) (**Fig. 1.11**).⁷

As explained before, the ligand binding site is positioned at the interface of two subunits, where one subunit is called the positive (+) or principal side and the adjacent subunit is termed as the negative (-) or complementary side. Apart from muscle nAChRs, in neuronal receptors, the principal side subunit will be an α subunit (except $\alpha 5$), while the complementary side subunit could be either an α subunit or a β subunit (except $\beta 3$). Therefore, depending on the subunit composition, the number of binding sites have been found to vary between a minimum of two to a maximum of five sites per receptor. Since, the homopentameric receptors contain α subunits, they harbour five (maximum) binding sites that are formed at all the α subunit interfaces (e.g. $\alpha 7$ nAChRs). The heteropentameric receptors are composed of α and β subunits in varying proportions, therefore, have a limited

number of α (+) interfaces available to form the binding sites. Mostly, heteropentamers have two binding sites formed at the α - β interface, but sometimes three sites are also found with the additional site formed at the α - α interface. The classical example is $\alpha 4\beta 2$ nAChRs which is found in the nervous system in two alternate stoichiometries; $(\alpha 4)_2(\beta 2)_3$ and $(\alpha 4)_3(\beta 2)_2$. The $(\alpha 4)_2(\beta 2)_3$ possess only two binding sites positioned at the $\alpha 4$ - $\beta 2$ interface, whereas the $(\alpha 4)_3(\beta 2)_2$ have an additional 3rd binding site located at the $\alpha 4$ - $\alpha 4$ interface. The homomeric $\alpha 7$ and heteromeric $\alpha 4\beta 2$ nAChRs are the most common subtypes found in the nervous system.^{6, 7} The high diversity of nAChRs inclines it to several neurological disorders, but also classifies it as an attractive target for drug design, especially the $\alpha 4\beta 2$ nAChRs, which contain two structurally and functionally distinct α - β and α - α interfaces that can assist in developing subtype selective ligands.

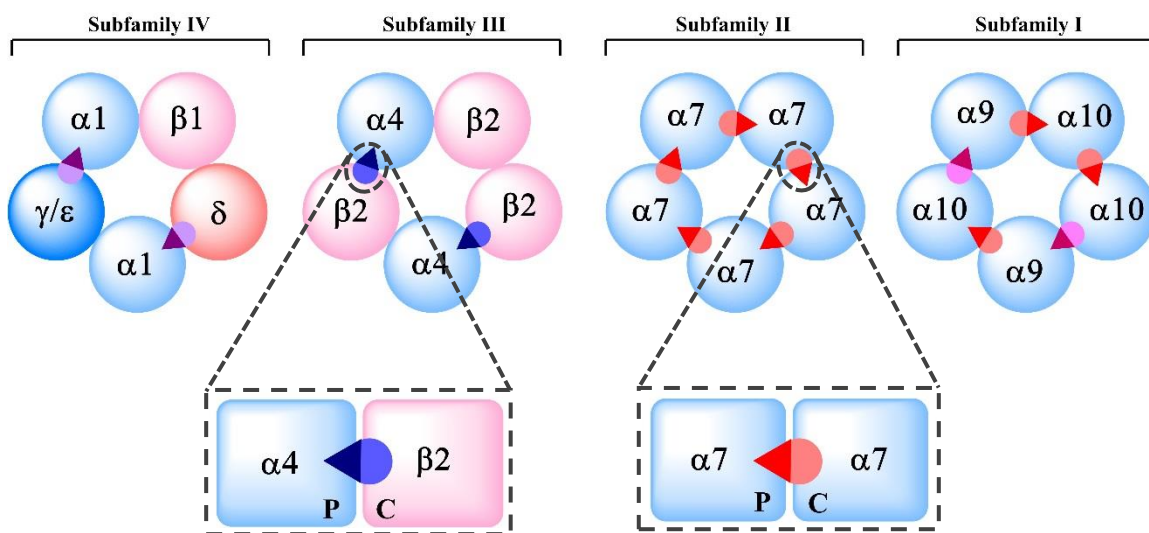


Fig. 1.11: Representative receptor subtypes of all the four subfamilies in different pentameric combinations. Triangles show principal (P) side and semi-circles show complementary (C) side of the ligand binding site.⁶

1.1.3. FUNCTIONAL AND KINETIC CHARACTERISTICS

The nAChRs are an intricate set of allosteric membrane proteins, with each receptor subtype displaying different functional and biophysical characteristics due to complex subunit compositions. The allosteric nature of nAChRs is best described through the Monod-Wyman-Changeux (MWC) model,³⁵ which explains receptor behaviour and response to ligands.¹⁹ But generations of research, enriched through technological advancement in electrophysiology and kinetic studies, have amended the MWC model into a sophisticated construct, suggesting multiple functional states from receptor activation to deactivation.³⁶

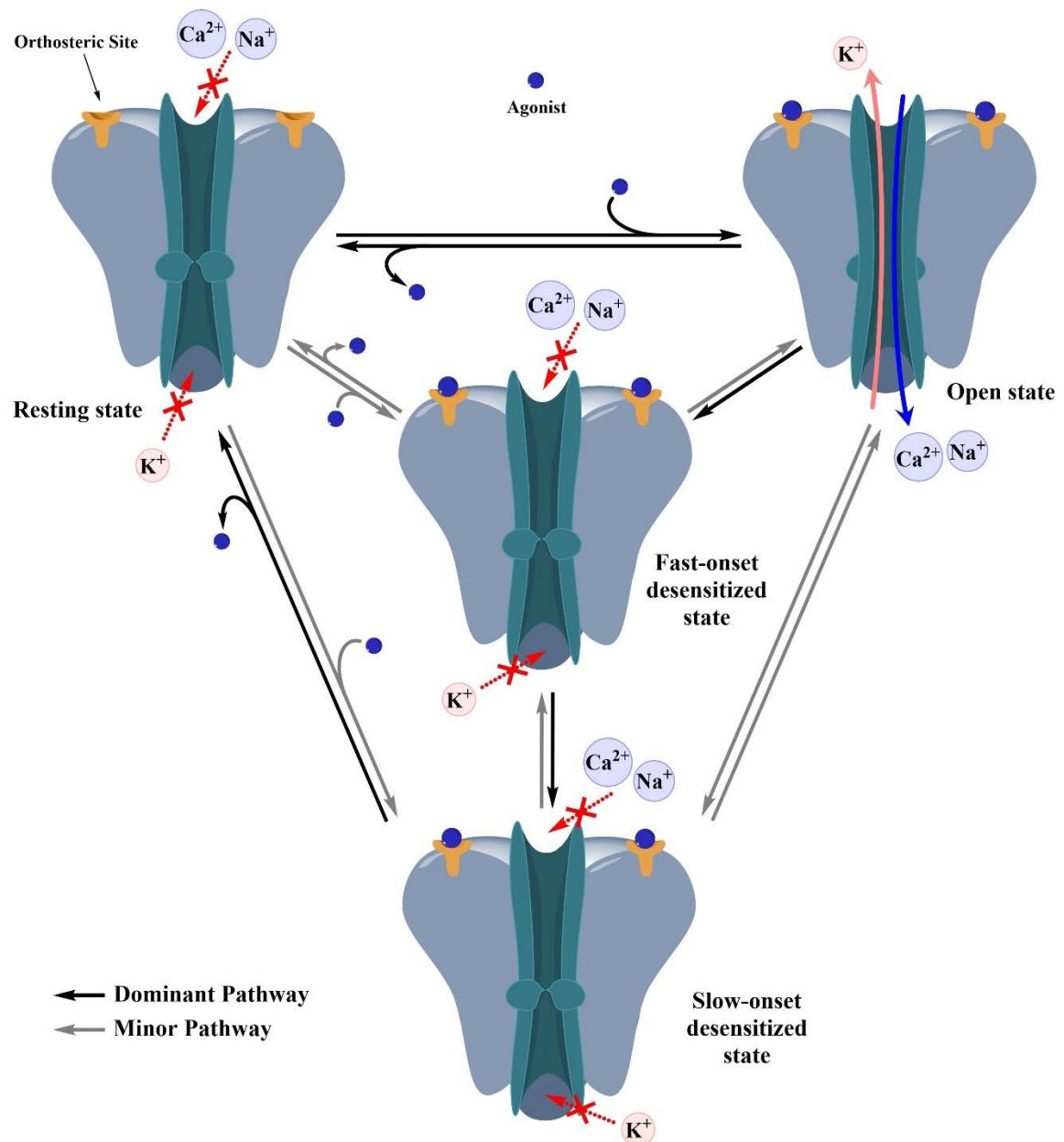


Fig. 1.12: General MWC Model depicting 3 functional states of nAChRs: Resting, open and fast- or slow-onset desensitized states. It describes receptor activation-deactivation, while the equilibrium between states is governed by the nature and influence of the ligand.^{7, 8}

According to MWC model, the nAChR functions through three states: resting/closed state, active/open state, and either fast- or slow-onset desensitized states.³⁵ In the absence of an agonist, the receptor exists predominantly in a resting state, showing no signs of ionic flow. Agonist binding to the orthosteric site favours quaternary conformational changes in the receptor, switching it from closed to open state and facilitating cation exchange (mainly Na^+ , K^+ or Ca^{2+}) through the channel.¹⁹ Within a few milliseconds, ionic conduction is terminated and receptor reverts to its original resting state, either by fast- or slow-onset

desensitisation (**Fig. 1.12**). There have been several instances where a ligand has been found to favour the desensitised state over the open state or vice versa.^{1,7} Hence, the equilibrium shifts between different states depending on the nature and influence of the ligand.

The nicotinic receptors, similar to other members of the LGIC superfamily, display a low affinity for the endogenous ligands like ACh, which is essential for the rapid and high-intensity signalling between neurons. Once the neurotransmitter reaches saturation concentration after its release from the pre-synaptic neurons, it binds to the receptors and rapidly shifts the equilibrium from closed to open state. However, after a quick drop in ACh concentration due to its reuptake by neurons or enzymatic degradation, the ligand immediately dissociates from the binding site due to its low affinity. This allows the receptor to revert to the closed state without shifting the equilibrium towards the desensitised state from open state.⁷

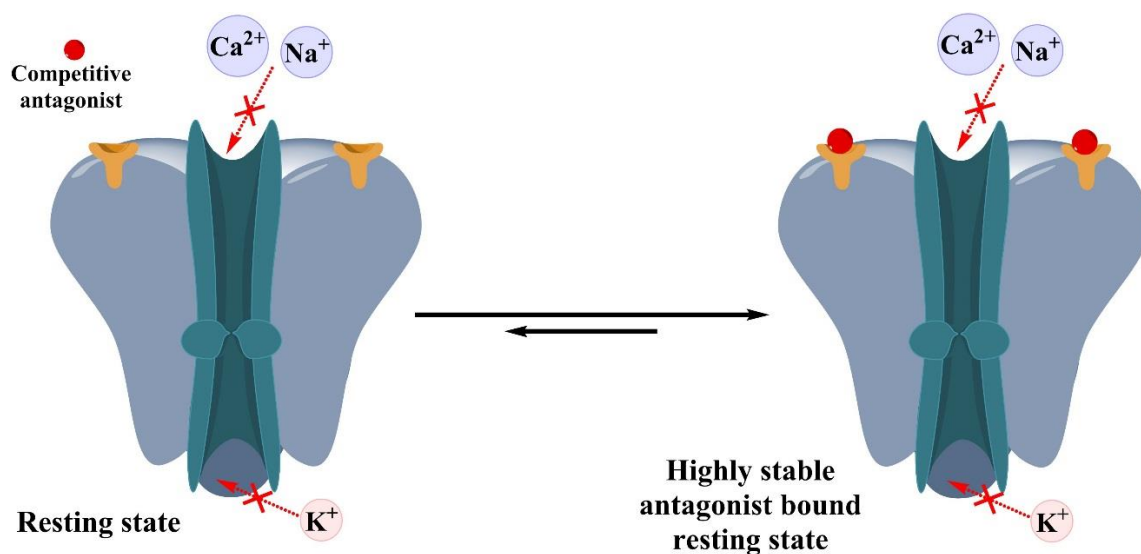


Fig. 1.13: Resting state gets further stabilised by a competitive antagonist.⁷

Generally, receptors exist in a stable, non-conducting, and ligand-free closed state, which is known to be further stabilised by competitive antagonists i.e., ligands that do not have any intrinsic activity and compete with an agonist for the same binding site (**Fig. 1.13**). But the blockade is ‘surmountable’ and can be reversed on increasing the agonist concentration. On the contrary, an agonist typically has a higher affinity for the metastable open state compared to the closed state. Based on its affinity and exposure, the receptor switches itself to another metastable fast or slow onset-desensitised state, which is then the most stable state under ligand-bound condition.^{1,7} The natural mechanism is to maintain the equilibrium

between the open and closed states via fast-onset desensitised state for rapid signalling. But this situation gets modified under elevated concentrations or continuous exposure of high affinity agonist to the active site, thereby, shifting the equilibrium more towards slow-onset desensitised state. This results in a prolonged state of desensitisation with ligand bound to the orthosteric site, which reduces the rate of receptor transition to a closed state and thus, decelerates synaptic signalling.^{1, 37}

The desensitisation equilibrium is also affected by the subunit type and composition, or by phosphorylation and de-phosphorylation of residues present in the cytoplasmic domain.³⁸ The rate of transitioning between each state depends upon various factors, but it can also be altered by allosteric sites present in the vicinity of the orthosteric site. Depending on its effect and chemical nature, an allosteric modulator can shift the equilibrium to either side, thereby, becoming an intriguing target for study and drug research in recent years.^{7, 37}

1.2. NICOTINIC ACETYLCHOLINE RECEPTOR LIGANDS

The understanding of structural and functional complexity within nAChRs, has triggered a cascade development of potential ligands for the treatment of associated neurological and psychiatric disorders. Regardless of the extensive research conducted in the past five decades, translation of potential to actual drugs has been limited, apart from value addition to the nicotinic pharmacopeia.⁸ Varenicline, a partial agonist of $\alpha 4\beta 2$ used as a smoking cessation aid, is the only nAChR drug granted (2006), since the first approval of anti-hypertensive drug mecamylamine in the 1950s, a nAChR antagonist.¹ The multifarious nature of neuronal nAChR subunits and their composition hinders drug discovery programs in developing subtype-selective ligands. Furthermore, some compounds in recent times have shown selectivity in terms of binding affinity amongst different subtypes, though the major challenge lies in translating binding into functional selectivity.⁷ As the ligand-bound receptor favours desensitised state in determining binding affinities, the functional potency can be very different, reflecting binding with the open state of the receptors. Thus, generally ligands, in most cases agonists, which display high subtype-selective binding and affinity, often show low functional preference over others or do not display any potency at all.^{7, 8}

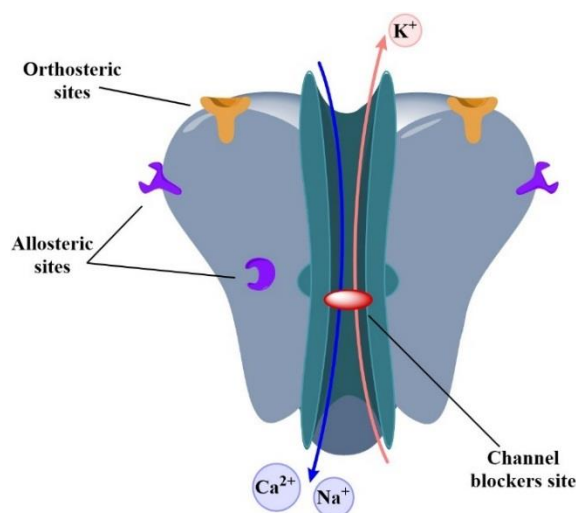


Fig. 1.14: Different binding sites present in a receptor: Orthosteric sites (agonist and competitive antagonist – orange), Allosteric sites (allosteric modulators – purple), and channel blockers site (non-competitive antagonist – red).⁸

The nAChRs activity can be affected, either positively or negatively, by three major classes of ligands: agonists, antagonists (competitive and non-competitive), and allosteric modulators. Apart from the orthosteric ligand binding site, to which mainly agonists and

competitive antagonists bind, there are additional sites present in the receptor (**Fig. 1.14**).⁷ The non-competitive antagonists may serve as channel blockers and interact with sites in transmembrane domain delineating the pore, while allosteric modulators bind to the sites present in proximity to the orthosteric sites and the transmembrane domain.⁸ Structurally and chemically, diverse sets of ligands obtained from synthetic,⁷ semi-synthetic, and natural sources,³⁹ provide a wide range of nAChR ligands. The reported compounds have helped in formulating structure-activity relationships and augmenting the design of potent and subtype-selective ligands. Some important nicotinic ligands are discussed below while more detailed accounts can be found in literature reviews.^{7, 8, 40}

1.2.1. AGONISTS

An agonist on binding to the orthosteric sites induces conformational changes in the receptor, leading to channel gating and passage of ions. When an agonist at full concentration achieves complete occupation of all the available binding sites, leading to maximal receptor activation, it is called as a full agonist. For example, epibatidine elicits close to 100% of the total current generated by the endogenous agonist ACh. However, an agonist that simultaneously induces fractional activation and competitive antagonism, i.e. the current elicited by its activation is less than the full agonist, then it is termed as a partial agonist. Varenicline is a partial agonist at $\alpha 4\beta 2$ nAChRs and elicits ~45% of the total current that ACh does on the same receptor subtype.^{1, 8} Biological and crystallographic studies reveal that both full and partial agonists bind at the same orthosteric site but elicit dissimilar responses. It is also evident that one agonist seldom behaves identically with different subtypes, signifying each subtype-agonist interaction as the basis for the intrinsic activity rather than being an inherent property of an agonist alone.¹

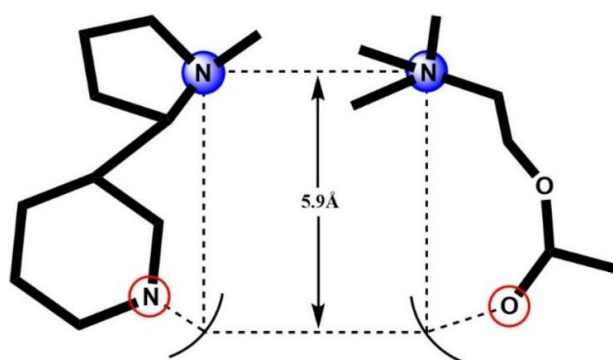
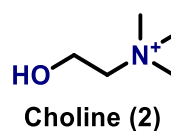


Fig. 1.15: Beers and Reich pharmacophore model of (*S*)-Nicotine and ACh, with 5.9 Å separation between cationic centre (blue) and hydrogen bond acceptor atom (red).⁴¹

Most of the nAChRs agonists are based on the common pharmacophoric features derived from natural agonists, like nicotine. Basically, a pharmacophore is a set of features present in a molecule that determines its bioactivity at a specific receptor. Identification of pharmacophore from the structure-activity relationship of several ligands on a specific receptor is a vital strategy used in ligand-based drug design. The general pharmacophore model for nAChRs agonists, as exemplified by Beers and Reich,⁴¹ necessitates two key structural features to be present in a ligand to function as an agonist (**Fig. 1.15**). First, an ammonium cation which forms the π -cation bridge with Trp143 in the aromatic cage, as previously explained and second, a hydrogen bond acceptor separated by a distance of 5.9 Å from the cationic centre.⁴¹ The recent models, as discussed by Nicolotti *et al.*,⁴² add a new pharmacophoric feature as a hydrophobic centre formed by aliphatic rings. Moreover, it suggests hydrogen bonding between binding site residues and the ammonium ion, apart from the critical π -cation interactions. It also implies that the lone pair interact as a hydrogen bond acceptor, which could be associated with either pyridyl nitrogen or certain carbonyl oxygen atoms. Some agonists, both synthetic and natural, with their pharmacological profile, are discussed below in detail.

Acetylcholine and Analogues

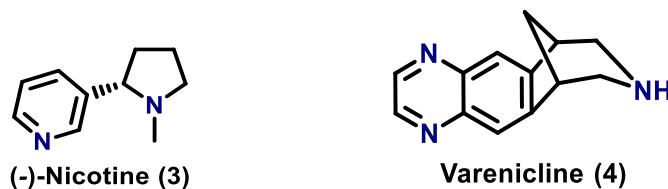


Acetylcholine **1** (ACh), an endogenous neurotransmitter, functions as a full agonist at all muscarinic (mAChRs) and nicotinic acetylcholine receptors subtypes. During neurotransmission, the presynaptic neurons releases the pre-synthesised ACh present in the vesicles of nerve terminals. Upon release, when ACh achieves saturation concentration, it binds to postsynaptic receptors to generate action potential via cation exchange, and further transmits nerve impulse to succeeding neurons. Subsequently, ACh present in the extracellular space gets hydrolysed into acetic acid and choline **2** by acetylcholinesterase (AChE) enzyme followed by choline reuptake.³

ACh exhibits a high binding affinity (K_i) and functional potency (EC_{50}) for the $\alpha 4\beta 2$ subtype ($K_i = 6.8$ nM, $EC_{50} = 0.48$ μ M) relative to the $\alpha 7$ subtype ($K_i = 4.0$ μ M, $EC_{50} = 79$ μ M).⁴³ Being a full agonist, it is generally used in various electrophysiology experiments, but due to non-selectivity against mAChRs and hydrolysis by AChE, the use of this agonist in more

complex biological systems is limited. In biological studies, either AChE inhibitors or the muscarinic antagonist (atropine) are co-applied with ACh to overcome these limitations.⁸

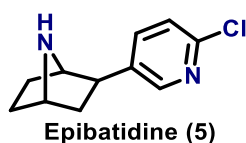
Nicotine and Smoking Cessation



The naturally occurring pyrrolidine alkaloid (-)-nicotine **3**, isolated from the tobacco plant *Nicotiana tabacum*,³⁹ is the eponymous nAChR agonist for all subtypes but an antagonist at homomeric $\alpha 9$ and heteromeric $\alpha 9\alpha 10$ receptors.⁴⁴ Nicotine possess a high selectivity for the $\alpha 4\beta 2$ subtype ($K_i \sim 1.0$ nM, $EC_{50} \sim 1.0$ μ M) but almost 1000-fold reduced affinity for $\alpha 7$ receptors with low potency ($EC_{50} \sim 500$ μ M).⁴⁰ Chronic intake of nicotine, as in case of tobacco smoking and chewing, results in upregulation of $\alpha 4\beta 2$ receptors due to altered post-translational modifications. Recent reports suggest nicotine also acts as a pharmacological chaperone and thus, amplifies folding and assembly of mature subunits in $\alpha 4\beta 2$ nAChRs.⁴⁵

Varenicline **4**, developed by Pfizer and sold under the brand name ChantixTM, is approved as a smoking cessation aid.⁴⁶ It is a full agonist at $\alpha 7$ ($EC_{50} = 18$ μ M) but is believed to target the $\alpha 4\beta 2$ subtype to treat nicotine addiction. It exhibits a partial agonistic activity of $\sim 45\%$ relative to ACh and $EC_{50} = 2$ μ M at the $\alpha 4\beta 2$ nAChRs.⁴⁷ Nicotine activates nAChRs on the dopaminergic reward pathway in the mesolimbic system of the brain to stimulate the release of dopamine, which may be responsible for the reinforcement and dependency of nicotine in chronic smokers. It has been proposed that varenicline inhibits nicotine-induced dopaminergic pathway by blocking the action of nicotine in a dose-dependent manner and thus, reverses the reward effect due to dopamine.⁴⁸

Epibatidine



Epibatidine **5**, an azabicycloheptane linked to chloropyridine, isolated from the skin of an Amazonian frog *Epipedobates tricolor*, is the most potent natural nAChRs agonist to date.³⁹

Both enantiomers of epibatidine display an extraordinarily high binding affinity and functional potency for different subtypes: $\alpha 4\beta 2$ nAChRs ($K_i = 19$ pM, $EC_{50} = 4.0$ nM); $\alpha 3\beta 2$ nAChRs ($K_i = 230$ pM, $EC_{50} = 22-130$ nM); $\alpha 3\beta 4$ nAChRs ($K_i = 380$ pM, $EC_{50} = 21-73$ nM); and $\alpha 7$ nAChRs ($K_i = 3.1-9.8$ nM, $EC_{50} \sim 1.1$ μ M). The major characteristic of epibatidine, a non-opioid ligand, is its potent analgesic activity, which suggested its role for the treatment of neuropathic pain.⁴⁹

1.2.2. ANTAGONISTS

A ligand that binds to the receptor, either at the orthosteric site or elsewhere in the receptor and does not display any intrinsic activity but serves to prevent agonist binding or ionic conductance, is termed as an antagonist.⁵⁰ Based on the mode of action and binding sites, antagonists can be subdivided into competitive and non-competitive antagonists.

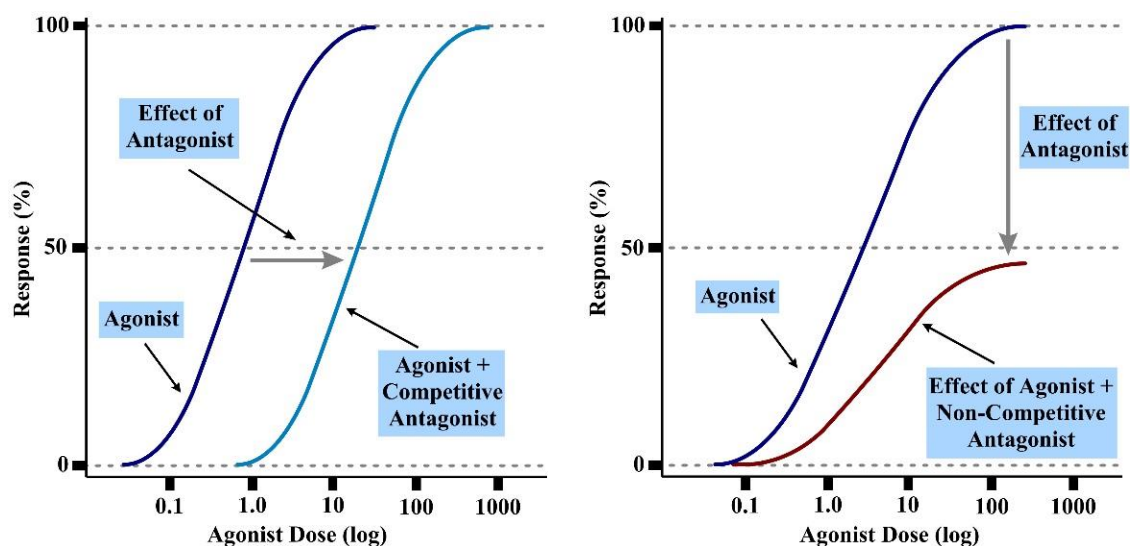


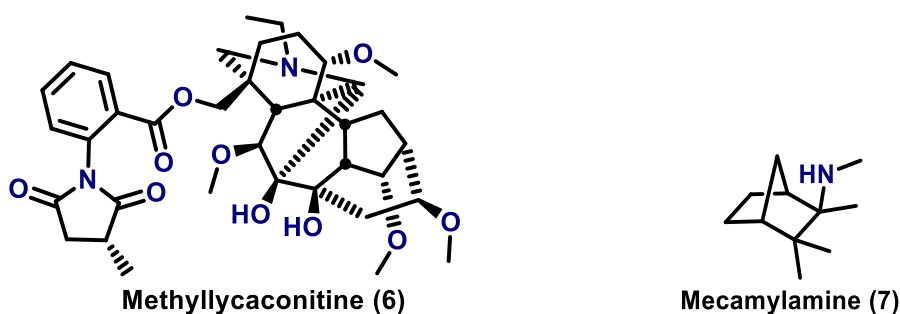
Fig. 1.16: Effect of competitive (left) and non-competitive (right) antagonist binding to the dose-response curve on increasing the concentration of agonist.^{51, 52}

A competitive antagonist competes for the orthosteric site reversibly, wherein the antagonist can be displaced from its binding site by increasing the concentration of agonist, which is demonstrated in the shift of the dose-response curve to the right.⁵¹ The competitive antagonists favour binding to a different quaternary state compared to agonists, and their binding result in stabilisation of the closed or resting state to prevent allosteric transition by agonists.^{40, 50} The non-competitive antagonist mostly interact with channel residues and physically block the ion exchange, though multiple sites and modes of action have been reported. Thus, increasing the agonist concentration will not reverse or reduce the

antagonistic effect, rather it reduces the efficacy by exhibiting a downward shift of dose-response curve (DRC) (**Fig. 1.16**).⁵²

Predominantly, antagonists are derived from natural sources in the form of toxins, and the number of potent compounds is few. They are largely used as tools to define structural and functional characteristics of nAChRs as well as develop animal models with cognitive deficits to study neurodegenerative disorders.⁸ The complex composition of nAChRs subunits and subtle differences amongst subtypes hamper the design of selective ligands. Ill-defined structure-activity relationships and pharmacophore modelling with underutilised high-throughput screening, are other major issues linked with antagonist development.⁵⁰ Some known antagonists with their associated activities, are discussed below.

Methyllycaconitine (MLA) and Mecamylamine



Methyllycaconitine **6** is a selective and reversible $\alpha 7$ antagonist, isolated as a tertiary diterpenoid alkaloid from *Delphinium brownii* plant seeds. MLA is highly potent non-peptide $\alpha 7$ antagonist ($K_i = 1$ nM, $IC_{50} = 100$ -600 pM),⁵³ generally used as a radioligand to examine $\alpha 7$ subtypes. The tertiary nitrogen-containing E-ring exhibits similar affinity to the $\alpha 7$ binding site as proven by SAR evaluations. The intrinsic activity of MLA resides in the side chain methylsuccinimidobenzoyl structure and any variation in benzoyl, methyl, or methylsuccinimide moiety results in reduced affinity (20-2000 times) for the $\alpha 7$ nAChRs.⁵⁰ Thus, methylsuccinimidobenzoyl motif and E-ring have been exploited of late, to construct synthetic analogues of MLA and use them as probes for nAChRs exploration studies.⁵⁴ Overall, MLA is a selective but not a specific inhibitor for $\alpha 7$ nAChRs and displays higher affinity over the muscle ($IC_{50} = 40$ μ M) and other neuronal receptors ($IC_{50} \sim 0.2$ μ M).⁸

Mecamylamine **7**, originally used as an anti-hypertensive agent via ganglionic blockade, is a conventional tool employed in various biological studies concerning neuronal nAChRs analysis and as a drug lead for psychiatric disorders.⁸ As evidenced in various docking and

modelling studies, the charged secondary amine enters channel pore similarly to other cationic species, but rather blocks the channel in a non-surmountable manner by interacting with the lumen residues.⁵⁵ It non-competitively inhibits muscle ($IC_{50} = 1-10 \mu M$) and binds reversibly with various neuronal nAChRs in sub-micromolar ranges ($IC_{50} = 0.1-5 \mu M$) but has a slightly higher affinity for $\alpha 3\beta 4$ subtype.⁸

1.2.3. ALLOSTERIC MODULATORS

Ligands which bind to the receptors without activating them but modulate the efficacy or potency of other ligands, are termed as allosteric modulators. Allosteric modulators don't compete for the orthosteric binding site, as they interact with different sites on the receptor to exert their effects.⁵ They are a novel class of ligands which has drawn attention in recent times as a promising pharmacological tool for the treatment of varied neurodegenerative and psychiatric disorders. As discussed, the allosteric modulators don't elicit a response, they alter the free energy levels during allosteric transitions between functional states of the receptor. This results in increased/decreased potency or efficacy of both endogenous and exogenous ligands like ACh or nicotine (**Fig. 1.17**).⁴ Based on its effect on the agonist response, allosteric modulators are further sectioned into positive and negative modulators.

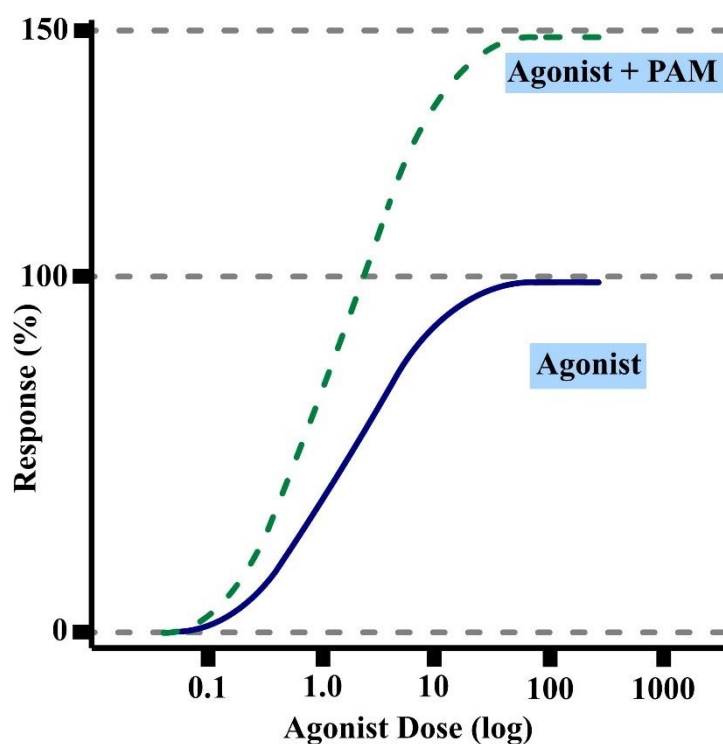


Fig. 1.17: Effect of positive (green curve) allosteric modulators relative to an agonist, increasing the efficacy of agonist.¹

Currently, positive allosteric modulators (PAMs) are the most explored class of ligands in this category due to their potentiation effect on the agonist efficacy, for example, the anthelmintic ivermectin which is an $\alpha 7$ PAM. The mechanism of action associated with PAMs can be classified into three main types (**Fig. 1.18**, green dash curve):^{5, 8}

- firstly, by reducing the energy barrier between the closed and open states without affecting the receptor response kinetics between the open and desensitised state, also known as Type I PAMs;
- secondly, by increasing the energy barrier between the open and desensitised states which slows the allosteric transition and thus, amplifies the period of channel opening, also known as Type II PAMs; and
- thirdly, by destabilising the desensitised state through induction of conformational changes in the quaternary structure of protein.

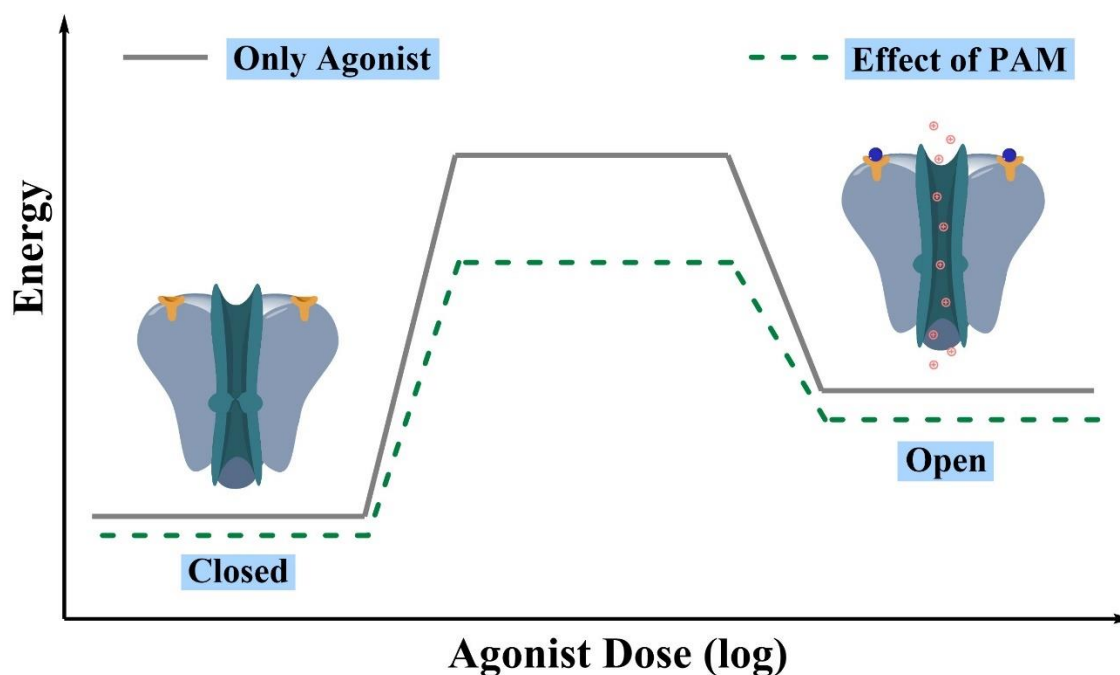


Fig. 1.18: Effect of positive (green curve) allosteric modulators on the energy barrier in presence of an agonist, during the allosteric transition between closed and open state.¹

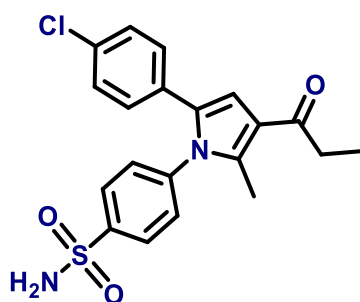
Consequently, PAMs have emerged as a valuable class of compounds over agonists and antagonists to enhance the neuronal therapeutic pharmacopoeia. This can be attributed to the fact that though PAMs don't directly elicit the response, they potentiate the agonist efficacy. Additionally, allosteric sites show a higher structural variability compared to

orthosteric sites, which have been preserved through various evolutionary changes to retain responses for the endogenous agonists. Hence, the structural diversity of allosteric sites could be exploited to develop subtype-selective PAMs. Moreover, repeated binding of PAMs will not increase the frequency of receptor desensitisation, which is a major limitation of agonists. If designed appropriately, a non-selective agonist could have a distinctive effect on the specific receptor subtype, or a potent response with less efficacious agonist, in presence of a subtype-selective PAM.⁵⁶

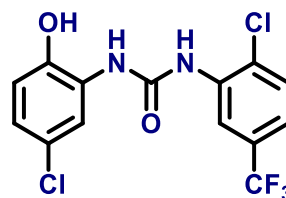
On the contrary, negative allosteric modulators (NAMs) produce an opposite effect compared to PAMs, i.e. they reduce the agonist efficacy/potency via modulation at allosteric sites. This can be achieved, either by heightening the energy barrier between the closed to open state transition or by favouring the desensitised state transition from the open state.¹ This preference to desensitised state could be due to lowering of the energy barrier between open and desensitised state or by inducing conformational changes to shift the equilibrium towards desensitised state. A classical example of NAM is steroidal hormone progesterone, which minimises the efficacy of agonists on $\alpha 4\beta 2$ nAChRs.⁵

Structurally similar compounds with minor variations in the substituents could act as either PAM or NAM at the same nAChR.⁵⁷ The following paragraphs focus mostly on PAMs, as despite failures during the clinical stage, they have been the mainstay for developing novel therapies for numerous neurodegenerative and psychiatric disorders in recent years.

Homomeric Allosteric Modulators



A867744 (8)



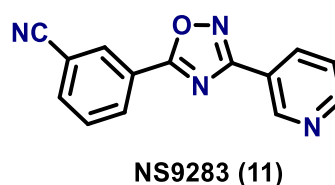
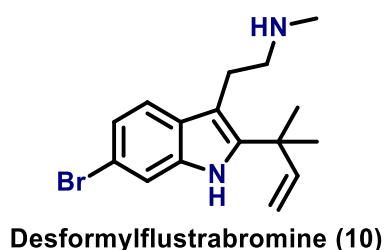
NS1738 (9)

The A867744 molecule **8** is a Type II $\alpha 7$ selective PAM ($EC_{50} \sim 1.0 \mu M$) that potentiates the agonist effect and shifts DRC to left. Subsequently, this prolongs the period of channel opening and slows allosteric transition from open to desensitised state under continued agonist presence. A867744 favours open and closed states as it acts by destabilising the

desensitised state. It doesn't potentiate other nAChRs or Cys-loop receptors, but it has demonstrated inhibition of $\alpha 4\beta 2$ and $\alpha 3\beta 4$ receptors.^{8, 58}

Similarly, NS1738 compound **9** also displays $\alpha 4\beta 2$ and $\alpha 3\beta 4$ receptor blockade ($IC_{50} > 10.0 \mu M$) without potentiating other Cys-loop receptors. However, it is a Type I PAM at $\alpha 7$ subtype ($EC_{50} = 1.6 \mu M$) and increases the receptor response in presence of an agonist, but it neither blocks receptor desensitisation nor destabilises the desensitised state.^{5, 8}

Heteromeric Allosteric Modulators



Desformylflustrabromine **10** is a PAM for heteromeric nAChRs, which potentiate and inhibits both $\alpha 4\beta 2$ ($EC_{50} = 120 \text{ nM}$ and $IC_{50} > 10 \mu M$, respectively) and $\alpha 2\beta 2$ ($EC_{50} = 446 \text{ nM}$ and $IC_{50} = 11 \mu M$, respectively) subtypes at variable concentrations. The potentiation effect occurs by increasing the agonist-induced response while inhibition is due to the physical blockade of channel in the transmembrane domain. It also happens to be an $\alpha 7$ nAChRs inhibitor ($IC_{50} = 2\text{-}44 \mu M$) as reported by recent studies.^{5, 59}

The NS9283 molecule **11** is an $\alpha 4\beta 2$ nAChRs selective PAM, which exhibits an exceptional property of interacting with the unique $\alpha 4\text{-}\alpha 4$ agonist binding site rather than allosteric sites present in the receptor. The $\alpha 4\beta 2$ subtype exists in two different stoichiometries, i.e. $(\alpha 4)_2(\beta 2)_3$ and $(\alpha 4)_3(\beta 2)_2$, but NS9283 exclusively binds to the $(\alpha 4)_3(\beta 2)_2$ stoichiometry ($EC_{50} = 0.99\text{-}4 \mu M$). It is effective only in the presence of an agonist and increases the agonist's potency without affecting its efficacy.^{5, 60} NS9283 has become a gold standard in an effort to develop $\alpha 4\beta 2$ selective PAMs.

A comprehensive discussion is covered in the forthcoming chapters on $\alpha 4\beta 2$ nAChRs, the different stoichiometries, NS9283 and other PAMs as lead molecules for drug design and development to treat various disorders linked to $\alpha 4\beta 2$ nAChRs.

CHAPTER 2

2. DESIGN OF SELECTIVE AGONISTS FOR $\alpha 4$ - $\alpha 4$ BINDING SITE

This chapter establishes a detailed discussion on the ubiquitous $\alpha 4\beta 2$ nAChRs and its two stoichiometries, followed by the design and development of novel hybrids as selective agonists for the $\alpha 4$ - $\alpha 4$ binding site.

2.1. THE $\alpha 4\beta 2$ NICOTINIC ACETYLCHOLINE RECEPTORS

The most abundant $\alpha 4\beta 2$ nAChR subtype in the brain, is a heteropentameric arrangement of $\alpha 4$ and $\beta 2$ subunits, formed around a symmetrical axis traversing the lipid membrane. Mostly found on presynaptic and postsynaptic neurons, the $\alpha 4\beta 2$ nAChRs are known to play a prominent role in memory, reward, cognition and analgesia (**Fig. 2.1**), thus, they are targeted as treatments in many associated neurodegenerative and psychiatric disorders.^{7, 56}

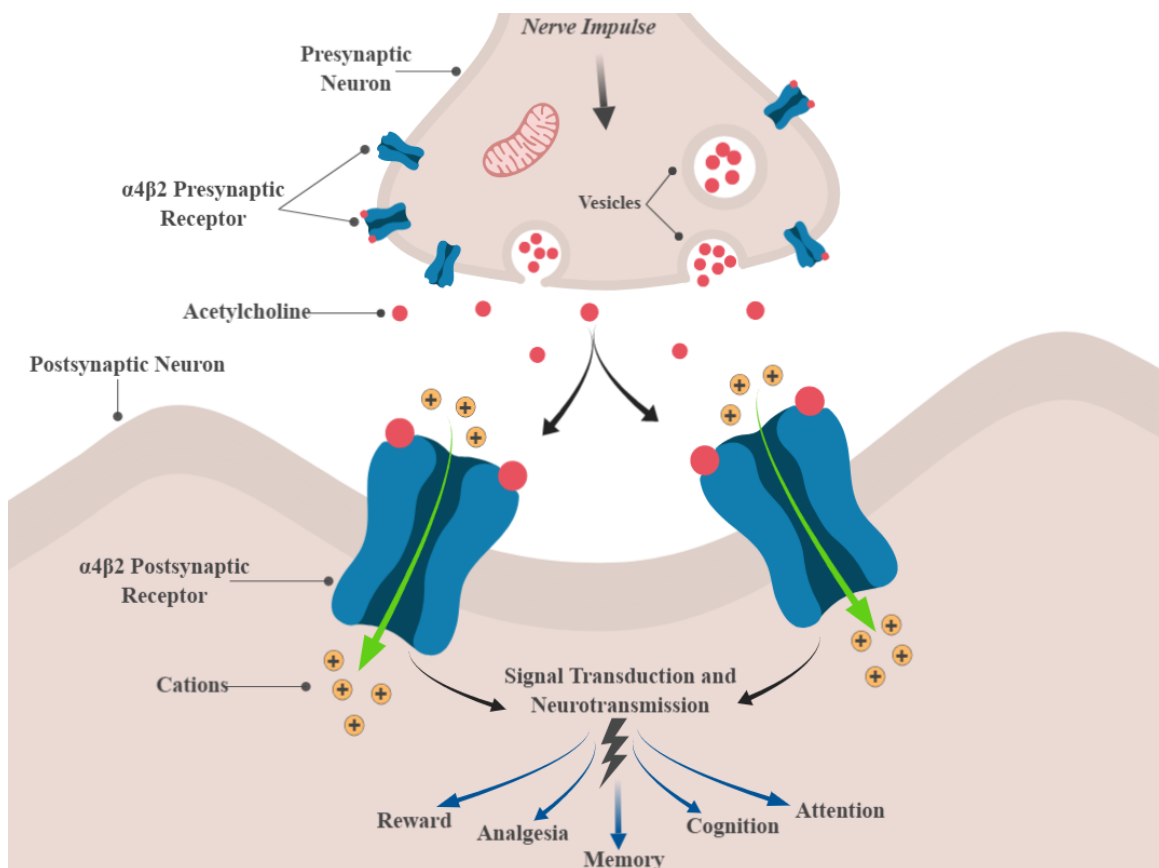


Fig. 2.1: Graphic illustration of $\alpha 4\beta 2$ nAChR on nerve cells, dispensing their physiological effects through receptor activation and signalling (Created with BioRender.com).⁵⁶

The momentous electron microscopic studies of *Torpedo* nAChR by Unwin² and crystallographic analysis of soluble acetylcholine-binding protein¹⁸, ascertained the

structure of nicotinic receptors and its ligand binding domain, respectively. Further, the binding proteins were engineered to generate $\alpha 4\beta 2$ nAChR models, suitable for devising novel ligands to treat the related disorders. Despite years of intense effort, few clinical studies reported positive results, as data obtained from using engineered models did not always reflect the behaviour observed for native receptors.⁷

2.1.1. X-RAY CRYSTAL STRUCTURE OF HUMAN $\alpha 4\beta 2$ RECEPTORS

Of late, numerous high-resolution structures of homopentameric nAChRs have been reported propelling the discovery of several selective ligands, especially for $\alpha 7$ receptors. The extensive structural and interface differences between homomeric and heteromeric receptors did not allow these available assemblies to be utilized further as models to develop selective ligands for heteromeric nAChRs. However, a recently published X-ray crystal structure of the human $\alpha 4\beta 2$ nAChR by Hibbs *et al* (**Fig. 2.2**),⁶¹ would positively solve this decade old problem. This archetypal structure of the most abundant receptor in the brain affords a more detailed understanding of receptor structure, subunit assembly, ligand interactions and cation exchange for heteropentameric nAChRs.

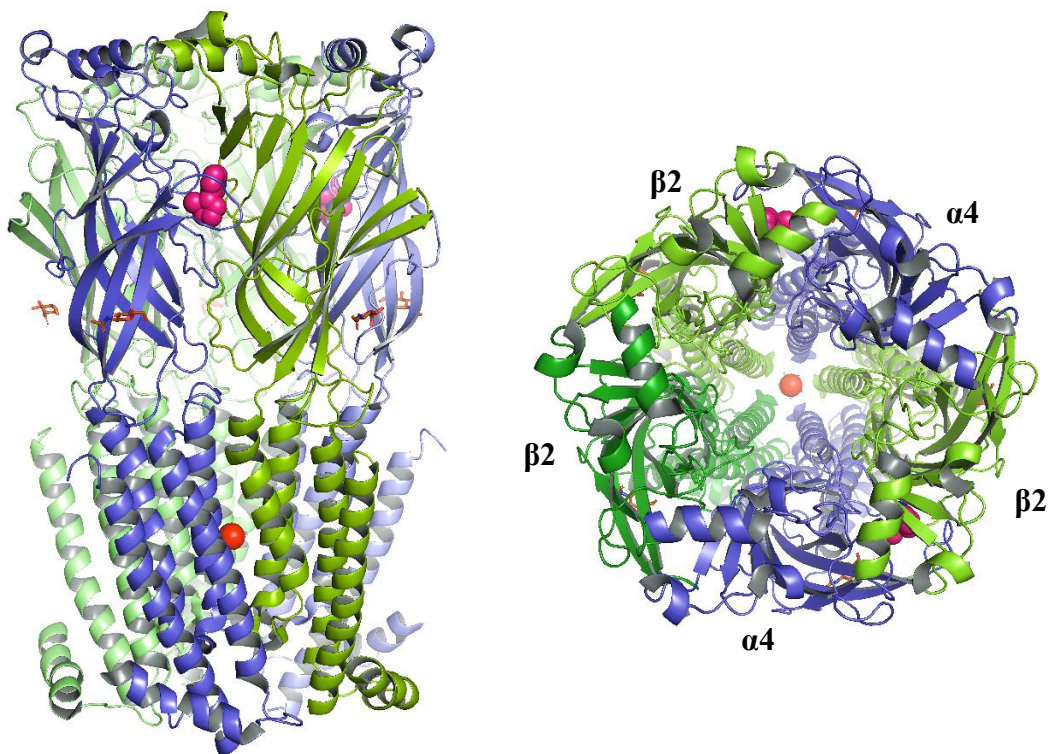


Fig. 2.2: Lateral (left) and top view (right) of X-ray crystal structure of human $\alpha 4\beta 2$ nAChR (PDB 5KXI). $\alpha 4$ (blue) and $\beta 2$ (green) subunits are shown as ribbons with nicotine (hot pink) and sodium ion (red) as spheres, and N-linked glycans (brown) as sticks.⁶¹

The crystal structure is similar to other members of Cys-loop family, unveiling a pentameric arrangement of α - β - β - α - β subunits in a ring formation around pseudo-symmetrical channel axis and embodies a cylindrical shape traversing the lipid membrane. The 59% sequence identity between $\alpha 4$ and $\beta 2$ subunits amino acids, suggests a similar conformation is adopted during allosteric transitions to different functional states, akin to homomeric nAChRs. The receptor was crystallised in the desensitised state with nicotine bound to the two α - β interfaces and a hydrated sodium ion residing in the channel pore. The observed conformation of $\alpha 4\beta 2$ nAChRs was closely related to GABA_A receptors,⁶² also crystallised in the non-conducting and desensitised state, but the overall quaternary structure of both receptors was distinct.

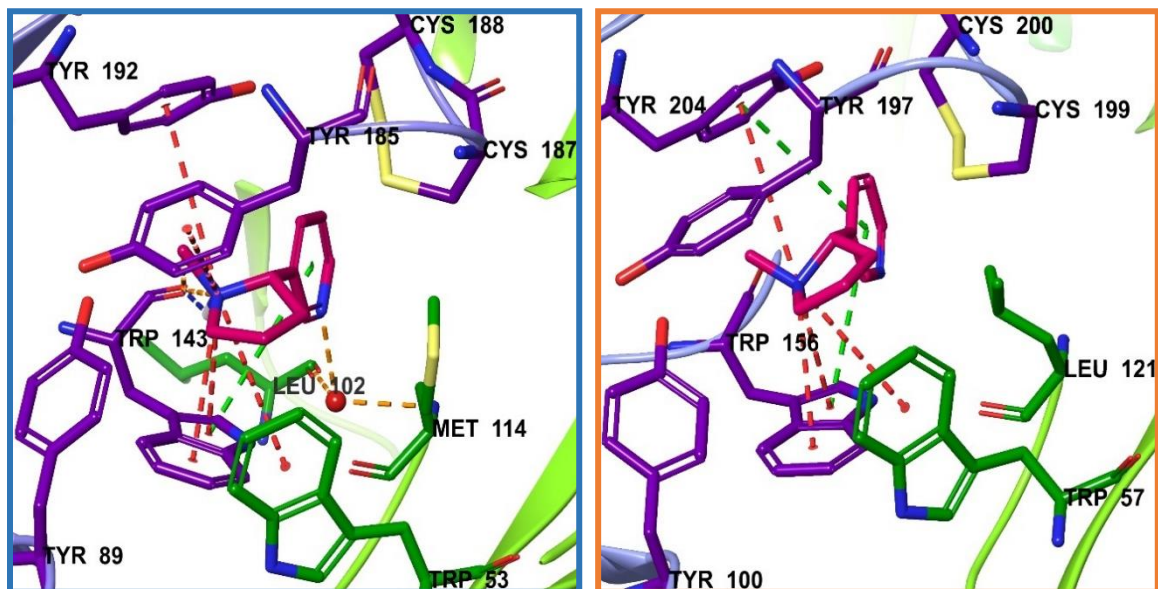


Fig. 2.3: Comparison of X-ray crystal structure of AChBP (left, PDB 1UW6) and human $\alpha 4\beta 2$ nAChR (right, PDB 5KXI) interacting with nicotine (hot pink-sticks) in the binding site. Water (red-sphere) is shown forming a bridge with side chain residues and nicotine in AChBP binding site but is missing in human $\alpha 4\beta 2$ receptor.^{18, 23, 61}

The nicotine binding in the extracellular domain of the $\alpha 4\beta 2$ receptor displays a high similarity with the ligand binding at the orthosteric site of AChBP. The conserved aromatic residues and cysteine pair forms a cage-like structure that encloses nicotine and stabilizes it through various interactions, analogous to the AChBP. The major difference in ligand interaction between AChBP and human $\alpha 4\beta 2$ receptor is the presence of a water molecule in the agonist binding site of AChBP (**Fig. 2.3**). Water forms a bridge via hydrogen bonding with the pyridine nitrogen of nicotine and side chain residues Leu102 and Met114,²³ to

provide further ligand stabilisation in the binding domain. Whereas, the crystal structure of the human $\alpha 4\beta 2$ nAChR exhibits no water bridging between the nicotine's pyridine nitrogen atom and side chain residues in the agonist binding site.

The human $\alpha 4\beta 2$ nAChR crystal structure provides insight into features of the non-canonical interfaces between β - β and β - α subunits, which do not bind to nicotine. Besides lacking adjacent cysteines in loop C, they exhibit rearrangement of conserved aromatic residues, contrary to the orientation in the conventional agonist binding site. In case of $\beta 2$ forming the principal (+) side, due to the absence of a tyrosine residue on loop C, Tyr196 (loop C) and Tyr 95 (loop A) rotate towards the centre of the supposed binding site and pushes Trp151 out of the interface. Another residue Arg149 (Gly154 in $\alpha 4$), adjacent to Trp151, inserts itself in between Tyr196 and Tyr95 to form a sandwiched structure. The guanidinium nitrogen of Arg149 forms π -cation interactions with the stacked tyrosine residues, analogous to nicotine's pyrrolidine nitrogen in the agonist binding site, as well as hydrogen bonding with Asp198 (**Fig. 2.4**). Consequently, hindering agonist binding at β - β and β - α interfaces, both sterically and electrostatically. This rearrangement in the principal side is preserved with all non-canonical interfaces between β - β and β - α subunits.

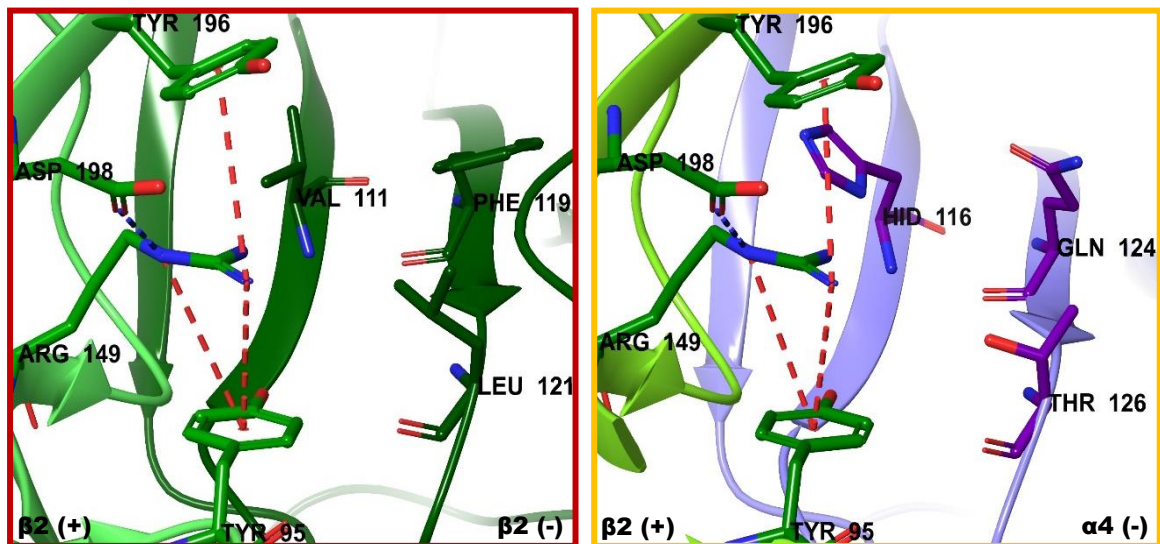


Fig. 2.4: β - β (left, green-green) and β - α (right, green-purple) interfaces in X-ray crystal structure of human $\alpha 4\beta 2$ nAChR (PDB 5KXI).⁶¹

The complementary (-) side formed by $\alpha 4$ subunit in the β - α interface, displays three crucial amino acid changes contrary to the $\beta 2$ side in α - β interface of the binding site. The hydrophobic Val111, Phe119 and Leu121 residues of the $\beta 2$ (-) side are replaced with the

polar His116, Gln124 and Thr126 residues of $\alpha 4$ (-) side (**Fig. 2.4**). However, homomeric $\alpha 7$ receptors demonstrate only one hydrophobic residue replacement, thus, illustrating a reduced affinity for nicotine at the $\alpha 7$ nAChRs. These changes can also explain the observed nicotine binding at the $\alpha 4$ - $\alpha 4$ interface of $(\alpha 4)_3(\beta 2)_2$ stoichiometry (discussed next).

2.1.2. THE TWO $\alpha 4\beta 2$ NICOTINIC RECEPTOR STOICHIOMETRIES

The $\alpha 4\beta 2$ nicotinic receptor diverges into two pharmacologically distinct functional stoichiometries: $(\alpha 4)_2(\beta 2)_3$ and $(\alpha 4)_3(\beta 2)_2$. Both assemblies display similar nicotine binding to the orthosteric site but different activation sensitivities, as $2\alpha:3\beta$ demonstrates high sensitivity while $3\alpha:2\beta$ shows low sensitivity.⁶³ The inherent complexity due to receptor heterogeneity requires an in-depth study to understand the fundamentals behind differences in structural and biophysical behaviour of both assemblies.

High and Low sensitivity $\alpha 4\beta 2$ Stoichiometries

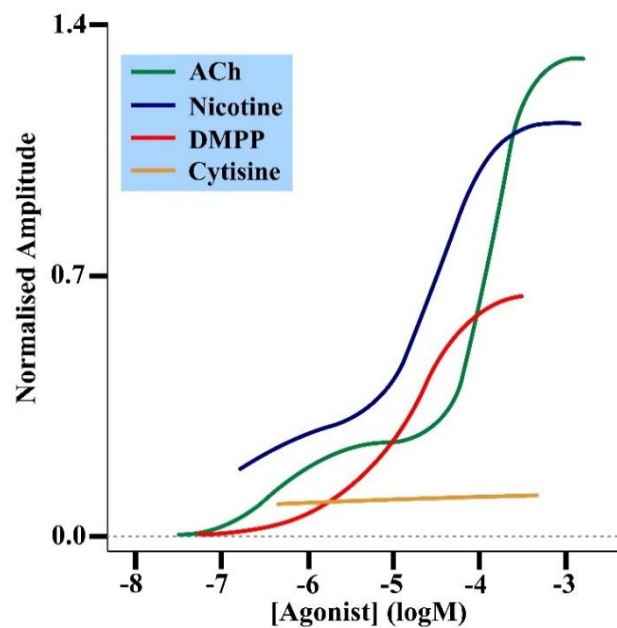


Fig. 2.5: Effect of ACh, nicotine, DMPP and cytisine on HEK $\alpha 4\beta 2$ nAChRs is shown in the dose-response curve. Agonist efficacy of ACh ($EC_{50} = 0.7$ and $74 \mu M$) and nicotine ($EC_{50} = 0.3$ and $18 \mu M$) was 100%, while it was 50% for DMPP and 5% for cytisine.⁶⁴

In two separate studies carried out by Anand *et al*⁶⁵ and Cooper *et al*⁶⁶, it was shown that only $(\alpha 4)_2(\beta 2)_3$ nicotinic receptors are present in chicks when its $\alpha 4$ and $\beta 2$ cDNAs were injected with 1:1 ratios and expressed in the oocytes of *Xenopus laevis*. On the contrary, when Zwart and Vijverberg⁶⁷ expressed the $\alpha 4$ and $\beta 2$ cDNAs of rat $\alpha 4\beta 2$ nAChRs in varied

ratios, the oocytes expressed two functional stoichiometries. Injection of $\alpha 4$ and $\beta 2$ cDNAs in 1:9 ratio formed a high sensitivity isoform of nAChRs with ACh as an agonist, while a 1:1 or 9:1 ratio formed nAChRs with low sensitivity. This suggested the presence of a different isoform with variable sensitivity in mammals besides the classical $2\alpha:3\beta$ assembly.

In another research, Nelson *et al*⁶⁴ permanently transfected human embryonic kidney (HEK) cells with 1:1 ratio of human $\alpha 4$ and $\beta 2$ cDNAs, to express two alternate stoichiometries of $\alpha 4\beta 2$ nicotinic receptors. The whole-cell electrophysiology study using various agonists, like ACh, demonstrated the presence of two functional assemblies (**Fig. 2.5**). Most of the HEK transfected $\alpha 4\beta 2$ nAChRs (82%) on ACh activation, displayed a low sensitivity ($EC_{50} = 74 \mu M$) biphasic dose-response curve (DRC) with a rapid desensitisation, when compared with the rest 18% of the receptor population, showing a high sensitivity ($EC_{50} = 0.7 \mu M$) monophasic DRC with slow desensitisation. The macroscopic current properties of the high sensitivity population correlated well with the similar research conducted by Kuryatov *et al*⁶⁸ on *Xenopus* oocytes expressing $(\alpha 4)_2(\beta 2)_3$ nAChRs (ACh, $EC_{50} = 2.2 \mu M$). Single-channel analysis also exhibited two-channel conductance in the transfected cell line with the majority displaying large channel conductance, owing to the high population of $3\alpha:2\beta$ stoichiometry. The [³⁵S]-methionine metabolic labelling of $\alpha 4$ and $\beta 2$ subunits in the HEK cell line, established that 82% of the expressed $\alpha 4\beta 2$ nAChRs population have a unique $(\alpha 4)_3(\beta 2)_2$ functional assembly.⁶⁴

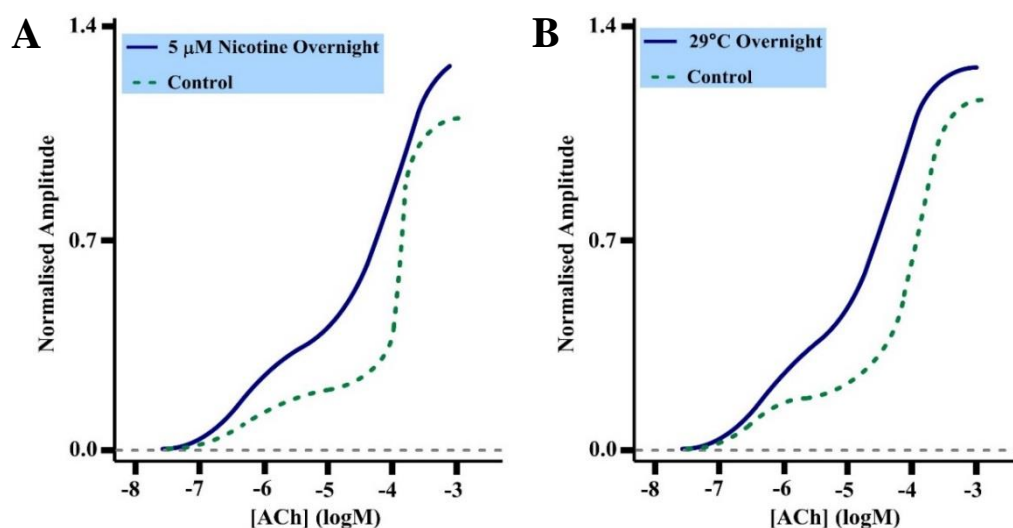


Fig. 2.6: Alteration in $\alpha 4\beta 2$ stoichiometries is visible from the dose-response curve (DRC), when HEK cell lines are incubated overnight; **A-** with $5 \mu M$ nicotine or **B-** at $29^\circ C$.⁶⁴

When equal ratios of $\alpha 4$ and $\beta 2$ cDNAs were transfected at 37 °C, the HEK cells primarily expressed $(\alpha 4)_3(\beta 2)_2$ over $(\alpha 4)_2(\beta 2)_3$ functional assembly. This could arise either due to favoured organisation of $\alpha 4$ subunits during receptor assembly, or due to rapid degradation of unassembled $\beta 2$ subunits relative to $\alpha 4$ subunits. However, transient transfection of $\alpha 4\beta 2$ expressing HEK cell line with $\beta 2$ cDNA resulted in an increased population of high sensitivity $(\alpha 4)_2(\beta 2)_3$ nAChRs, probably due to increased $\beta 2$ expression and incorporation during the construction of new receptor assemblies.⁶⁴ It was observed that incubation of transfected HEK cells with low concentrations of nicotine (0.5 or 5.0 μM) led to an increased population of the $(\alpha 4)_2(\beta 2)_3$ isoform, as also reported by Buisson and Bertrand.⁶⁹ A similar inference was drawn from culturing the transfected HEK cells at 29 °C, plausibly explaining the rationale behind the expression of mostly 2 α :3 β assembly in *Xenopus* oocytes as it is too incubated at lower temperatures (**Fig. 2.6**). Nicotine-induced upregulation of 2 α :3 β stoichiometry could be linked to addiction, as chronic exposure with a required concentration of nicotine is easily achieved in smokers.⁶⁴

It has now been established that difference in agonist sensitivities is due to two alternate stoichiometries, but it is also essential to determine whether both the high and low sensitivity component of a biphasic response arises only due to $(\alpha 4)_3(\beta 2)_2$ isoform or produced by a mixed population of stoichiometries.

Additional Binding Site at the $\alpha 4$ - $\alpha 4$ Interface of $(\alpha 4)_3(\beta 2)_2$ nAChRs

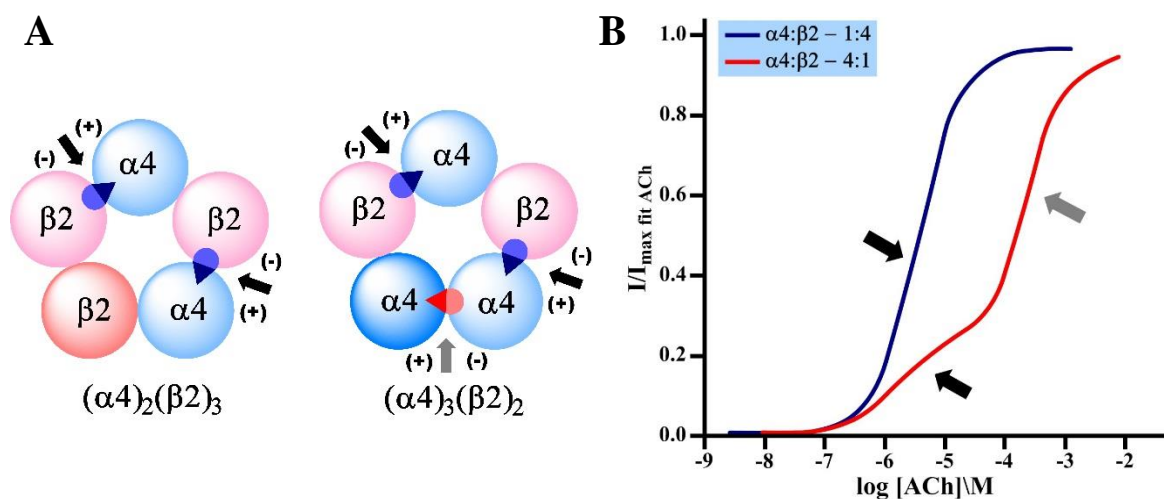


Fig. 2.7: A- $(\alpha 4)_2(\beta 2)_3$ shows two high sensitivity binding sites (black arrows) and $(\alpha 4)_3(\beta 2)_2$ shows an additional low sensitivity binding site (grey arrow). B- ACh dose response curves exhibited by wild type $\alpha 4\beta 2$ receptors expressed in 1:4 and 4:1 ratios.⁶³

Assembly of $\alpha 4\beta 2$ nAChRs in two different stoichiometries exhibiting altered functional properties necessitates further investigation to ascertain the differentiating factors behind distinct agonist sensitivities. Both the isoforms contain two $\alpha 4$ - $\beta 2$ interfaces to which an agonist binds for receptor activation, but the altered sensitivities could be due to the presence of a unique $\alpha 4$ - $\alpha 4$ interface in the $3\alpha 4:2\beta 2$ isoform. In two separate studies, Harpsøe *et al*⁶³ and Mazzaferro *et al*⁷⁰ were the first to identify $\alpha 4$ - $\alpha 4$ interface as the 3rd binding site which is responsible for the low sensitivity of the $(\alpha 4)_3(\beta 2)_2$ stoichiometry (**Fig. 2.7**). Their research also proved that biphasic response is an inherent property of the $(\alpha 4)_3(\beta 2)_2$ assembly and doesn't arise due to a mixed population of both isoforms.

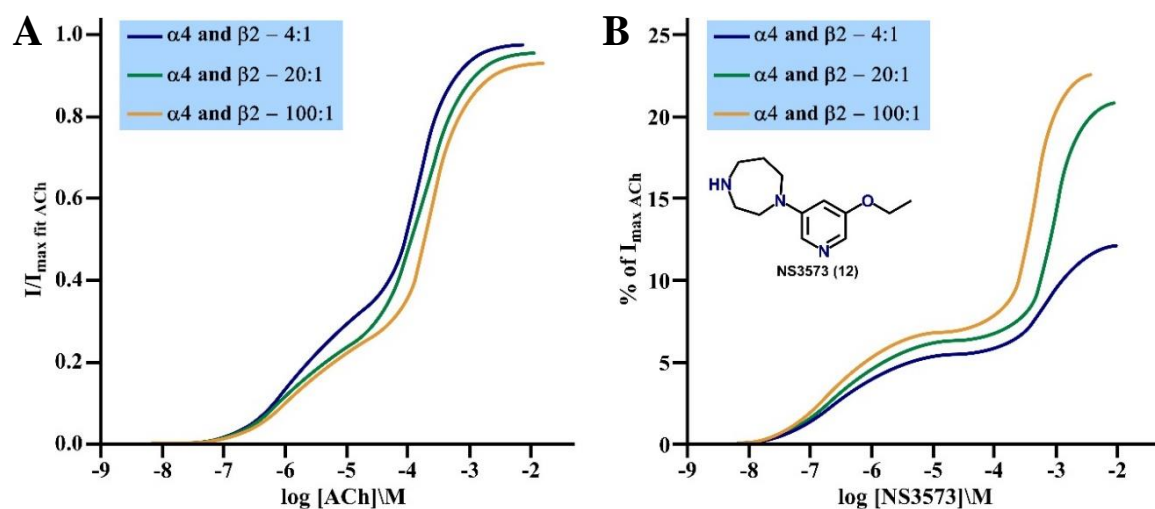


Fig. 2.8: ACh (**A**) and NS3573 (**B**) displayed a biphasic dose response curve from $(\alpha 4)_3(\beta 2)_2$ receptors expressed with higher subunit ratios of $\alpha 4:\beta 2$.⁶³

Expression of wild-type $(\alpha 4)_3(\beta 2)_2$ and $(\alpha 4)_2(\beta 2)_3$ receptors in oocytes, using varied ratios of $\alpha 4:\beta 2$ cRNAs, was fruitful to validate the biphasic response from $(\alpha 4)_3(\beta 2)_2$ isoform as its intrinsic property. The $(\alpha 4)_3(\beta 2)_2$ and $(\alpha 4)_2(\beta 2)_3$ isoforms were obtained through the expression of 4:1 and 1:4 cRNA ratios of $\alpha 4$ and $\beta 2$ subunits in oocytes. The oocytes with higher $\beta 2$ subunit ratio produced a monophasic response with ACh and NS3573, a pyridine-diazepane compound **12**. The potency of ACh and NS3573 as well as their dose-response curves matched well with the high-sensitivity response observed from $(\alpha 4)_2(\beta 2)_3$ receptors. The oocytes with higher $\alpha 4$ subunits resulted in biphasic ACh and NS3573 responses (**Fig. 2.8**).⁶³ Some researchers have suggested that the biphasic response could be due to a mixed population of both stoichiometries.⁷¹ So, if this theory holds, a higher ratio of $\alpha 4:\beta 2$ subunits should result in a reduced high sensitivity component from the biphasic DRC and may exhibit a monophasic response with only low sensitivity fraction. But, on increasing the

$\alpha 4:\beta 2$ ratio from 4:1 to 20:1 and 100:1, the receptors still generated biphasic responses of ACh and NS3573, i.e. the high sensitivity component did not diminish. Thus, it was suggested that a biphasic response is an intrinsic property of the $(\alpha 4)_3(\beta 2)_2$ receptors and its expression with a 4:1 ratio of $\alpha 4:\beta 2$ subunits in oocytes is uniform.⁶³

The homology modelling studies of $\alpha 4-\beta 2$ and $\alpha 4-\alpha 4$ dimers using nicotine co-crystallised structures with AChBP¹⁷ and *Torpedo*² receptor as templates identified the difference of only three amino acid residues in the agonist binding site between both the interfaces (**Fig. 2.9**). Presence of polar residues His142, Gln150 and Thr142 in the $\alpha 4$ (-) side compared to hydrophobic residues Val136, Phe144 and Leu146 in the $\beta 2$ (-) side, could be responsible for different agonist interactions at the $\alpha 4-\alpha 4$ interface. This was established through the binding affinities of ACh and NS3573, which seem to be high for the $\alpha 4-\beta 2$ site and low for the $\alpha 4-\alpha 4$ site. Site-directed mutagenesis of three residues in $(\alpha 4)_3(\beta 2)_2$ isoform to convert the $\alpha 4-\beta 2$ site into $\alpha 4-\alpha 4$ like site and vice versa, was imperative in establishing the role of $\alpha 4-\alpha 4$ interface as a low sensitivity site of $(\alpha 4)_3(\beta 2)_2$ stoichiometry.⁶³

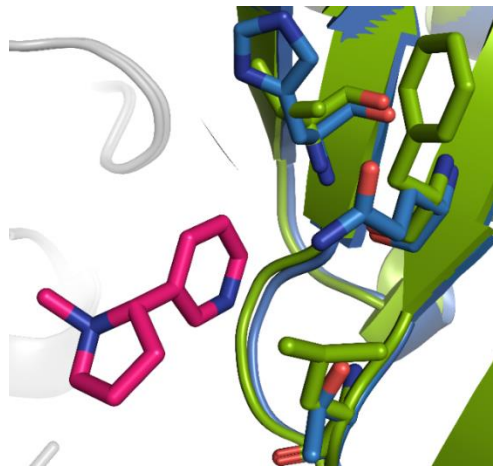


Fig. 2.9: Comparison of structural differences between the $\alpha 4-\beta 2$ and the $\alpha 4-\alpha 4$ binding interface. Nicotine (hotpink) and dissimilar residues are shown in sticks. The $\alpha 4$ (+) sides of both interfaces are in white, while $\beta 2$ (-) side residues; Val136, Phe144 and Leu146 are shown in green, and $\alpha 4$ (-) side residues; His142, Gln150 and Thr142 are shown in blue.⁶³

The mutated receptors were expressed in oocytes to study the macroscopic currents developed during electrophysiology using ACh and NS3573. Firstly, by altering the residues in the $\alpha 4-\alpha 4$ site to resemble it as $\alpha 4-\beta 2$ site, the currents generated by mutated $(\alpha 4^m)_3(\beta 2)_2$ receptors resulted in a monophasic DRC, similar to the high sensitivity DRC produced by wild-type $(\alpha 4)_2(\beta 2)_3$ isoform (**Fig. 2.10**). Potencies of ACh ($EC_{50} = 0.97 \mu M$)

and NS3573 ($EC_{50} = 20$ nM) were almost equivalent to those observed with the wild-type $(\alpha 4)_2(\beta 2)_3$. The most plausible explanation to this is the absence of a low sensitivity $\alpha 4$ - $\alpha 4$ site and its conversion to $\alpha 4$ - $\beta 2$ like site, ensuing receptor activation due to agonist binding at up to three high sensitivity $\alpha 4$ - $\beta 2$ sites. Secondly, amino acid mutations in the $\alpha 4$ - $\beta 2$ site to resemble the $\alpha 4$ - $\alpha 4$ site expressed as $(\alpha 4)_3(\beta 2^m)_2$ receptors in the oocytes. The current generated during electrophysiology was again monophasic but contained only the low sensitivity component of biphasic DRC, akin to the low sensitivity response observed with wild-type $(\alpha 4)_3(\beta 2)_2$ (**Fig. 2.10**). Here, potencies of ACh ($EC_{50} = 140$ μ M) and NS3573 ($EC_{50} = 23$ μ M) were close to the low potencies observed with wild-type $(\alpha 4)_3(\beta 2)_2$. This could be possible due to the conversion of all $\beta 2$ into $\alpha 4$ -like subunits, which gives rise to three low sensitivity $\alpha 4$ - $\alpha 4$ like binding sites requiring high agonist concentrations to elicit the response.⁶³ Thus, it validates the $\alpha 4$ - $\alpha 4$ interface as the 3rd binding site with a low sensitivity and the $\alpha 4$ - $\beta 2$ as two high sensitivity binding sites in the $(\alpha 4)_3(\beta 2)_2$ isoform.

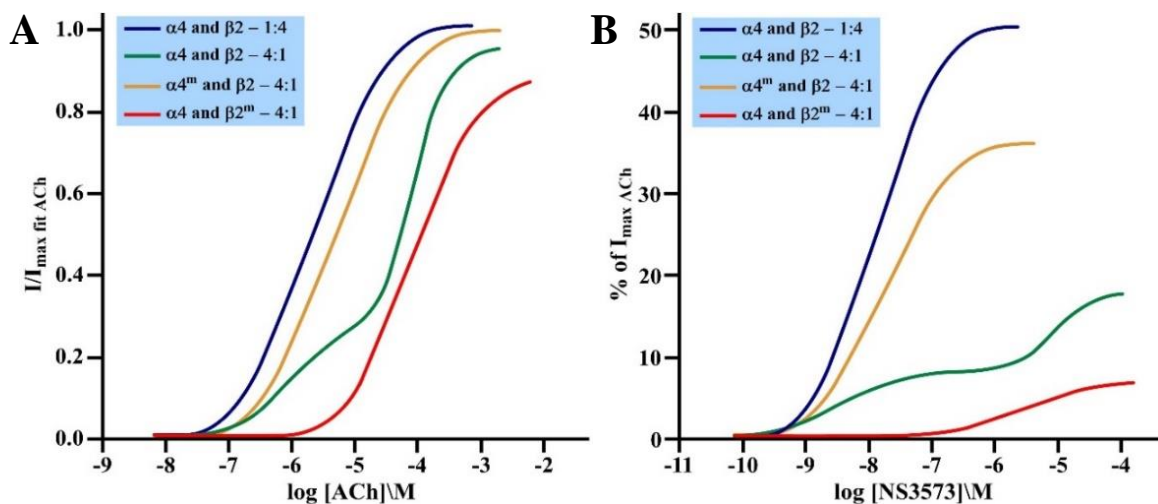


Fig. 2.10: ACh (A) and NS3573 (B) dose response curves on wild type and mutated $(\alpha 4)_3(\beta 2)_2$ receptors expressed in oocytes.⁶³

Recognition of the 3rd agonist binding site at the unique $\alpha 4$ - $\alpha 4$ interface is of great interest in drug discovery. Theoretically, any ligand specific for the $\alpha 4$ - $\alpha 4$ binding site will act as an allosteric modulator for the $(\alpha 4)_3(\beta 2)_2$ stoichiometry, owing to its absence of efficacy at the $\alpha 4$ - $\beta 2$ binding site, since maximal receptor activation could only be achieved when all the three binding sites of $(\alpha 4)_3(\beta 2)_2$ isoform are occupied. The structurally different $\alpha 4$ - $\alpha 4$ binding site offers an opportunity to exploit the variations using structure-based drug design and develop selective ligands for the $\alpha 4$ - $\alpha 4$ site of $(\alpha 4)_3(\beta 2)_2$ stoichiometry.

*Cryo-Electron Microscopy Structure of Two $\alpha 4\beta 2$ Nicotinic Receptor Stoichiometries*⁷²

The large hydrophobic surface of membrane proteins such as nicotinic receptors, with unstable and flexible domains, pose major challenges in purification and crystallisation to obtain high-resolution structures. To study the effects of various ligands binding to different stoichiometries of the $\alpha 4\beta 2$ receptors, AChBP was engineered to mimic specific receptor assemblies. Mutation of three amino acid residues in the receptor binding site, essential for ligand interaction and stabilization, generated models simulating the different binding sites of $\alpha 4\beta 2$ nAChRs.⁶³ Engineered receptors have proved their worth in various biological studies as models and give plausible but not absolute evidence of the principles governing the unique biophysical properties of both interfaces.

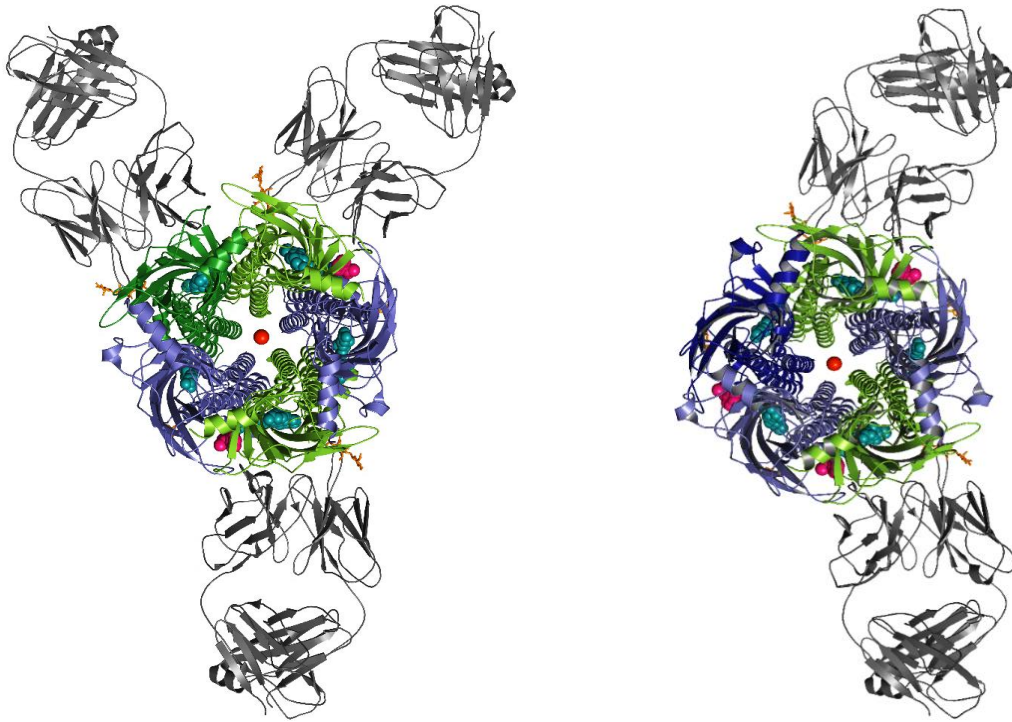


Fig. 2.11: *Fab-receptor complex resolves the 2 α :3 β (left) and the 3 α :2 β (right) stoichiometries in the cryo-EM structure of nicotine (hotpink) bound human $\alpha 4\beta 2$ nAChR (PDB 6CNJ and 6CNK). Fab fragments (grey) are linked to the $\beta 2$ subunits (green), while cholesterol molecules (teal-spheres) bind to all five subunits including $\alpha 4$ subunits (blue).⁷²*

Crystal structure of $\alpha 4\beta 2$ nAChRs by Hibbs *et al* (**Fig. 2.2**), provides a clear insight into the receptor but only for the 2 α :3 β isoform. However, recent cryo-electron microscopy (cryo-EM) study from the same group delivers more detail on the assembly and principal determinants responsible for their distinguishing properties of both the stoichiometries. Apart from aforesaid limitations, heterogeneity and high architectural similarity between

the secondary structures of $\alpha 4$ and $\beta 2$ subunits, renders the stoichiometry identical at low resolution. Antigen-binding fragments (Fab) specific to the $\beta 2$ subunits were used for targeting and as a tool to distinguish between the $2\alpha:3\beta$ and $3\alpha:2\beta$ isoform. The cryo-EM image (**Fig. 2.11**) reveals two distinct receptor assemblies, where three Fab bound complex relate to the $2\alpha:3\beta$ isoform, while two Fab bound complex match to the $3\alpha:2\beta$ stoichiometry.

Hypothetically, more $\alpha 4\beta 2$ stoichiometries could be possible, but only two assemblies are found in the nervous system. To rationalise the observed pentamer formations, free energies for different interfaces were determined. Based on free energy calculations, the following order is preferred during assembly: α - β (most favoured), β - α , α - α and β - β (least favoured). This suggests that during the pentamer construction, first the 2α and 2β subunits assemble to form the α - β and β - α interfaces, followed by integration of fifth α/β subunit to form either α - α or β - β interface. Formation of the β - β interface is least favoured due to the instability added by the conformational diversity of the $\beta 2$ subunit. Yet, to establish clear reasoning behind the formation of only two stoichiometries, different putative assemblies were designed and studied, containing the α - α , β - β or α - β interfaces.

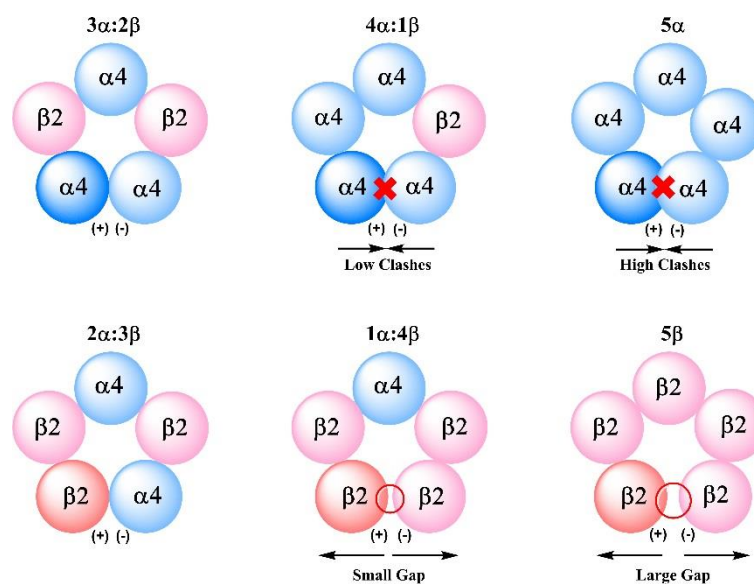


Fig. 2.12: Representation of observed ($3\alpha:2\beta$ and $2\alpha:3\beta$) and theoretical (5α , $4\alpha:1\beta$, $1\alpha:4\beta$ and, 5β) pentamers, showing overlap (red cross - top) and gaps (red circle - below) between subunit interfaces due to an increased composition of $\alpha 4$ and $\beta 2$ subunits, respectively.⁷²

Four theoretical pentamers were computationally analysed by increasing the $\alpha 4$ and $\beta 2$ subunit composition in respective $(\alpha 4)_3(\beta 2)_2$ and $(\alpha 4)_2(\beta 2)_3$ isoforms. The following describe the probable factors behind the observation of only two stoichiometries (**Fig. 2.12**):

1. 5α homopentamer arranges compactly resulting in subunit overlap and residue clashes, thus, deeming it unfit for pentamer formation;
2. 5β homopentamer organises in a relaxed manner, therefore, leaving a gap between β - β interface and making it ineffective to form the pentamer;
3. $4\alpha:1\beta$ exhibited reduced overlapping, while $1\alpha:4\beta$ displayed decreased gap, but were still unsuitable for pentamer formation.

Hence, the inference drawn from computational experiments corroborates previous studies^{64, 72} on the existence of only two stoichiometries, as the pentamer assembly can only be favoured in the presence of either, one α - α or β - β interface. The imbalance between the ratios of two stoichiometries is implicated in genetically linked neurological disorders as well as addiction. It has been observed in various cell culture studies⁶⁴ that nicotine causes overexpression of the $2\alpha:3\beta$ isoform compared to $3\alpha:2\beta$ assembly.

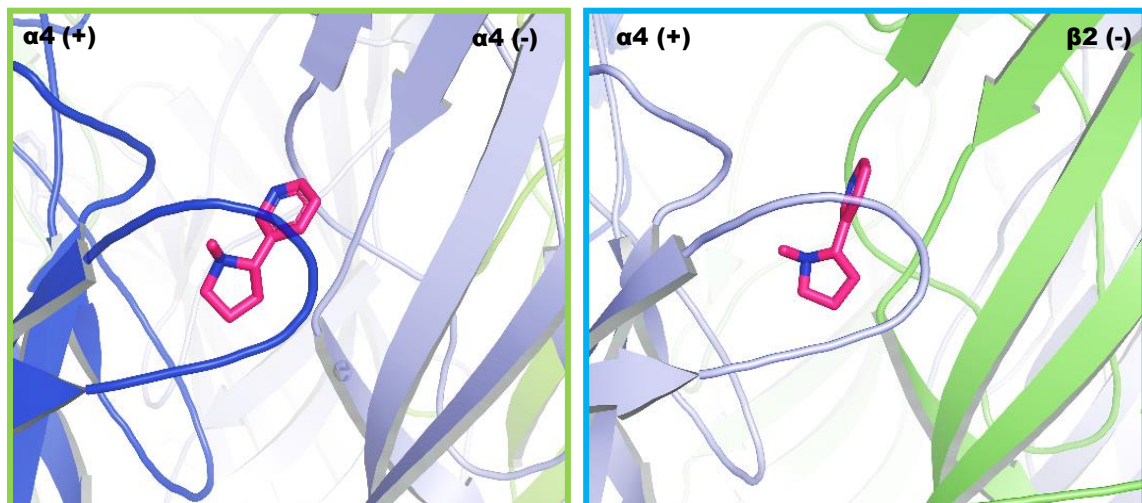


Fig. 2.13: Nicotine orientation (hotpink – stick) in α - α (left: blue-purple ribbons) and α - β (right: blue-green ribbons) interface of $3\alpha:2\beta$ and $2\alpha:3\beta$ stoichiometries, respectively.⁷²

The EC_{50} of agonists such as nicotine is ~ 100 times higher for the $(\alpha 4)_3(\beta 2)_2$ stoichiometry than the typical $(\alpha 4)_2(\beta 2)_3$ assembly. Both isoforms have two α - β interfaces forming the classical binding site, but the $3\alpha:2\beta$ stoichiometry harbours an additional binding site at the unique α - α interface, activation of which is essential for a full receptor response. The α - β and α - α interfaces contribute distinctively, providing a considerable difference in the sensitivities between two observed assemblies. As per the electron microscopy image, both the interface binding sites accommodate and orient nicotine discretely, with slightly variable ligand stabilising interactions. In the α - β interface, the pyridine ring of nicotine is

placed away from the lipid bilayer and close to the pore axis, with the whole molecule positioned parallelly to the central axis of channel lumen. In the α - α binding site, nicotine is marginally tilted off the channel axis, while the pyridine ring sits close to the membrane but points towards the channel (**Fig. 2.13**). Hence, the cryo-EM image corroborates the orientation of nicotine as described in earlier reports involving engineered receptors.

The variation in site residues in the α - α interface is responsible for contrasting sensitivities between the high sensitivity α - β and the low sensitivity α - α binding sites, in addition to distinct nicotine orientation. The residues present in the principal side are equivalent in both ligand binding sites, however, the difference arises from the residues in the complementary side of the interfaces. Three hydrophobic residues from $\beta 2$ (-) side; Val111, Phe119 and Leu121 are replaced in the $\alpha 4$ (-) side with polar amino acids; His116, Gln124 and Thr126, resulting in an altered interaction (**Fig. 2.14**). The large surface of van der Waals forces due to Phe119 and Leu121 in the α - β interface, positions nicotine compactly in the aromatic pocket, placing it parallel to the channel axis. But, the short hydrophilic side chain of Gln124 and Thr126 in the $\alpha 4$ (-) side disrupts van der Waals forces, offering more flexibility and polar surface for nicotine binding, leading to different orientation and sensitivity.

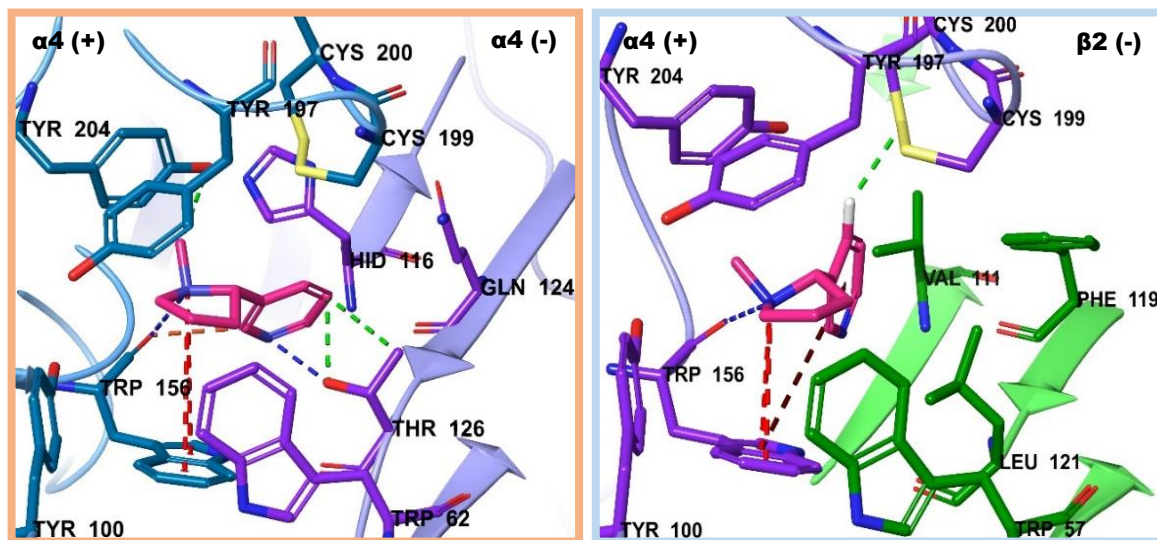


Fig. 2.14: Nicotine (hot pink) interacting with residues in the $\alpha 4$ - $\alpha 4$ (left: blue-purple) and $\alpha 4$ - $\beta 2$ (right: purple-green) interface of $3\alpha:2\beta$ and $2\alpha:3\beta$ stoichiometries, respectively.⁷²

Both the assemblies not only have different sensitivities but also have diverse permeability for cation exchange. The unique $(\alpha 4)_3(\beta 2)_2$ stoichiometry has a higher single-channel conductance and three times higher calcium permeation than the typical $(\alpha 4)_2(\beta 2)_3$ assembly. Though, both the isoforms display cation selectivity due to negatively charged

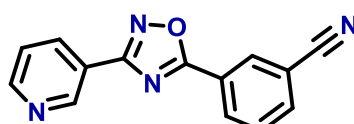
residues lining the channel lumen, however, $3\alpha:2\beta$ assembly exhibits a stronger negative potential which drives the calcium inflow. The differentiating factor between both stoichiometries is the presence of an acidic Glu268 in $3\alpha:2\beta$ compared to basic Lys264 in $2\alpha:3\beta$ at 20' position, guarding the entrance to the ion channel at the ECD-TMD junction. Mutational studies have also shown that the presence of an acidic amino acid at 20' position is imperative for calcium permeability and channel conductance, as the increase in negative charge is directly proportional to high calcium influx.

The unique $(\alpha 4)_3(\beta 2)_2$ isoform constitutes 70-80% of the stoichiometric population of the $\alpha 4\beta 2$ receptors expressed in the mammalian rat brain,⁷³ which makes it an attractive target for drug discovery programmes. This could be effectively done by designing the ligands that selectively bind at the $\alpha 4$ - $\alpha 4$ interface. Ligands targeting the specific stoichiometric population of $\alpha 4\beta 2$ receptors could prove valuable in developing a new class of therapeutics for psychiatric and neurodegenerative disorders as well as smoking cessation aids.

2.1.3. LIGANDS TARGETING $(\alpha 4)_3(\beta 2)_2$ NICOTINIC RECEPTORS

The $\alpha 4\beta 2$ receptors, as mentioned in introduction, are known to play a role in memory, cognition, analgesia, attention and their linked disorders. The high sequence similarity of the classical agonist binding sites amongst different nAChRs has impeded the development of $\alpha 4\beta 2$ subtype-selective agonists. However, since the recognition that $\alpha 4\beta 2$ receptors exist as two different stoichiometries with distinct pharmacological profiles, a newfound interest has developed in the design of ligands targeting specific stoichiometries. Moreover, the recent discovery of a 3rd agonist binding site at the unique $\alpha 4$ - $\alpha 4$ interface in the $(\alpha 4)_3(\beta 2)_2$ isoform has made it an attractive target for highly selective ligand design. Despite various attempts, only a few ligands have been found to be active and selective for the $\alpha 4$ - $\alpha 4$ binding site. Two such compounds, overlapping with the current research will be discussed.

NS9283: Pyridine-Oxadiazole compound



NS9283 (11)

A pyridine-oxadiazole compound NS9283 (**11**) developed by Neurosearch A/S,^{60, 74} acts selectively at the distinctive $\alpha 4$ - $\alpha 4$ binding site in the $(\alpha 4)_3(\beta 2)_2$ isoform without any

apparent effect on the $\alpha 4$ - $\beta 2$ sites. It does not activate the receptor itself but when co-administered with an agonist; it potentiates their action. Early reports found NS9283 to enhance the poor analgesic effect of ABT-594, an $\alpha 4\beta 2$ agonist, in several rat models.^{74, 75} Further studies, using various *in vivo* assays on rodents showed NS9283 improved cognition and attention^{60, 76} as well as reduces nicotine self-administration albeit with an increased reward effect.^{77, 78} It also displays augmentation of the discriminative-stimulus effects of nicotinic agonists.⁷⁹ The high site-selectivity of NS9283 has facilitated the detection of $(\alpha 4)_3(\beta 2)_2$ and $(\alpha 4)_2(\beta 2)_3$ stoichiometries in the brain.⁶⁰ Initially, NS9283 was categorised as a positive allosteric modulator (PAM) for $(\alpha 4)_3(\beta 2)_2$ receptors, due to its ability to modulate the action of agonists binding to the $3\alpha:2\beta$ isoform without showing any intrinsic activity. The DRC of ACh-elicited currents obtained from oocytes expressing both stoichiometries revealed the selective modulation of $(\alpha 4)_3(\beta 2)_2$ receptor by NS9283 ($EC_{50} = 3.3 \mu M$) with no effect at $(\alpha 4)_2(\beta 2)_3$ isoform.⁶⁰

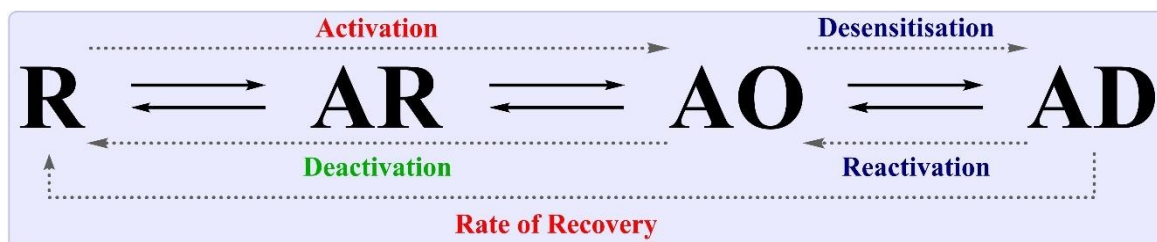


Fig. 2.15: Modulatory effect of NS9283 (green-positive, red-negative and blue-no effect) on the kinetic parameters (grey-dash arrows) of ACh-elicited currents in human $\alpha 4\beta 2$ nAChRs. R-resting state, O-open state, D-desensitised state and A-agonist bound to respective states.

Grupe *et al*⁸⁰ provided detailed insights into the mechanistic properties of NS9283 on ACh activated human $\alpha 4\beta 2$ receptors expressed in HEK cells (**Fig. 2.15**). In the whole cell electrophysiology, when applied alone, NS9283 did not elicit currents while ACh alone gave a biphasic response. However, the ACh DRC underwent a left shift (~ 60 fold) with a maximal concentration of NS9283, but intriguingly, there was no effect on the amplitude of peak currents and the response observed was monophasic (**Fig. 2.16A**). Thus, NS9283 only increased the potency of ACh on $\alpha 4\beta 2$ receptors with no effect on ACh efficacy. The EC_{50} value of $4.0 \mu M$ was identified for the NS9283 potentiation of ACh stimulated currents in $\alpha 4\beta 2$ nAChRs. Moreover, NS9283 slowed down the macroscopic current decay, i.e. rate of deactivation, by extending the period of agonist-bound open state, which was assumed as the primary reason for its modulation of ACh response. However, it moderately affected

the rate of receptor activation by slightly increasing the time to achieve maximal currents. On the contrary, NS9283 neither reduced the rate of desensitisation, nor increased the reactivation rate of desensitised receptors as displayed by some nAChR PAMs,^{81, 82} rather it slowed the rate of receptor recovery from the desensitised state. Therefore, with respect to the functional activity of other reported PAMs where they have more effect on the desensitisation state of receptors, the modulatory effect of NS9283 is unique. The monophasic DRC produced by ACh-elicited currents in presence of NS9283 had close resemblance with the response generated by ACh activation of the $\alpha 4$ - $\beta 2$ binding sites alone. Since NS9283 only acts on the $3\alpha:2\beta$ stoichiometry, it was suggested to associate with the $\alpha 4$ - $\alpha 4$ interface present only in $(\alpha 4)_3(\beta 2)_2$ receptors. The modulatory effects could be either due to increasing the ACh potency at the $\alpha 4$ - $\alpha 4$ binding site or NS9283 binding itself to ACh site in $\alpha 4$ - $\alpha 4$ interface.⁸⁰

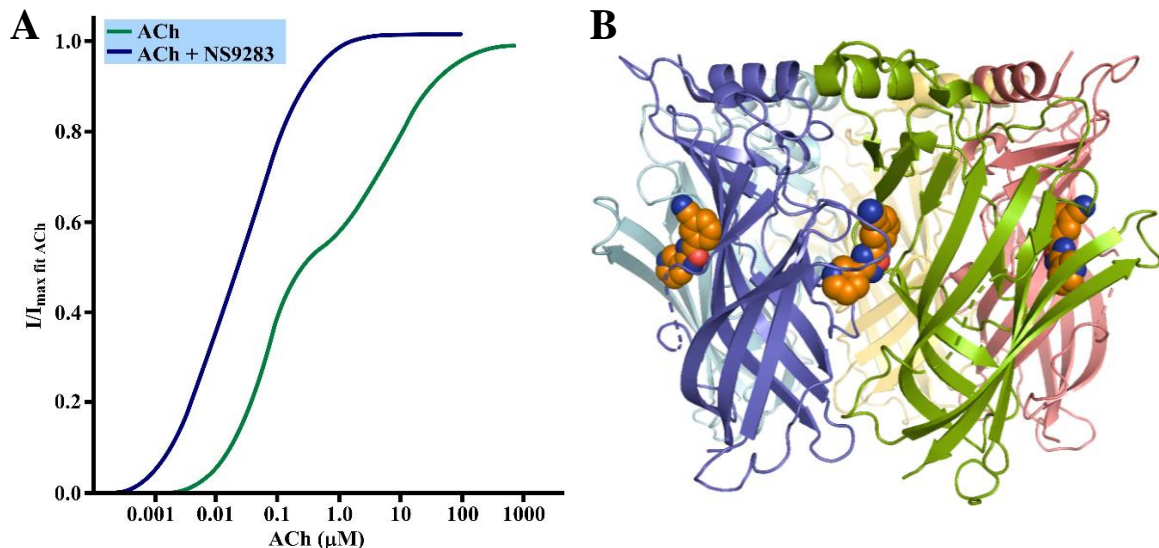


Fig. 2.16: A, DRC of ACh with and without NS9283.⁸⁰ B, X-ray structure of *Lymnaea stagnalis* AChBP co-crystallised with NS9283 shown as orange spheres (PDB 4NZB).⁸³

The X-ray co-crystal structure of *Lymnaea* AChBP with NS9283 (**Fig. 2.16B**, PDB 4NZB) and study of its structural and functional properties, as reported by Olsen *et al.*,⁸³ provided major insight into the mode of action and binding of NS9283 at the $(\alpha 4)_3(\beta 2)_2$ receptors. In the crystal structure, NS9283 was shown to mainly interact with the conserved aromatic residues and bind in the ACh binding site, similar to the ACh or nicotine (**Fig. 2.17**). On the principal side, pyridine ring of NS9283 exhibited π - π stacking with Tyr89, while pyridyl nitrogen as well as nitrile was stabilised by hydrogen bonding with Tyr185 and Tyr192, respectively. Interestingly, the oxadiazole motif was found to form weak contacts with

Trp143 carbonyl oxygen. Quantum mechanics established that a positive electrostatic potential was developed on C-5 of oxadiazole and C-3 of benzonitrile due to the deshielding effect of electron-withdrawing nitrile group. As a result, the partial positive character formed on C-5 and C-3 allowed interactions with the carbonyl oxygen lone pairs. Since, NS9283 didn't form any key π -cation interactions with Trp143 due to lack of charged amine nitrogen, the contact between oxadiazole and carbonyl of Trp143 was believed to be imperative in stabilising NS9283 in the binding site. Likewise, the oxadiazole N2 nitrogen formed similar interactions with the complementary side's Trp53 aromatic ring.

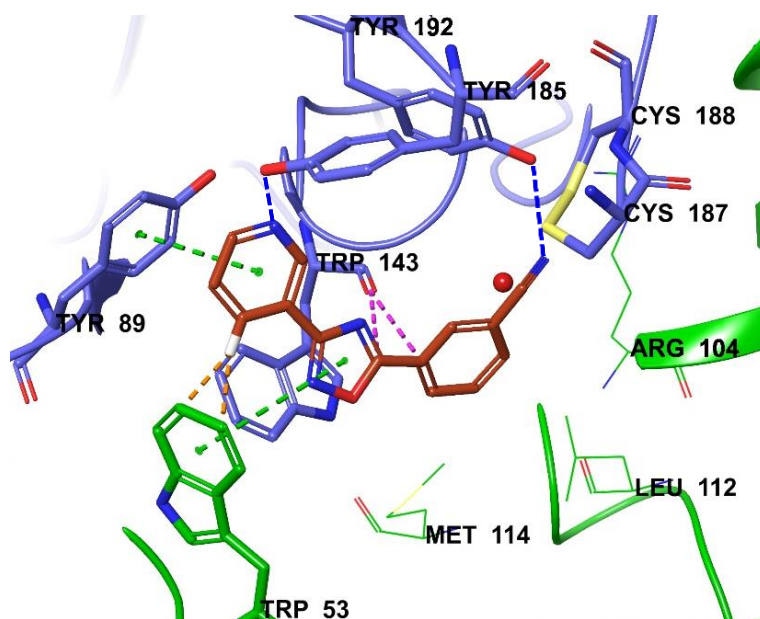


Fig. 2.17: NS9283 binding (sticks-brown) in the *Ls*-AChBP binding site (principal side-blue and complementary side-green). Residues of *Ls*-AChBP conserved in the $\alpha 4$ - $\alpha 4$ site are shown as sticks while the non-conserved residues are shown as lines.⁸³

The aromatic residues and adjacent cysteines from the principal side, and Trp53 (Trp60 - $\alpha 4$ subunit) from the complementary side, are conserved in both *Ls*-AChBP and the $\alpha 4$ - $\alpha 4$ binding site. However, the complementary side of the *Ls*-AChBP binding site is lined with hydrophobic residues, equivalent to $\beta 2$ (-) subunit, and differs from the hydrophilic residues present in the $\alpha 4$ (-) subunit. Homology modelling studies using X-Ray crystal structure as a template identified the following residues: Arg84, His114, Phe116, Gln122 and Thr124, crucial for NS9283 stabilisation in the $\alpha 4$ - $\alpha 4$ binding site. In the model, His114 was shown to be sandwiched between Arg84 and Phe116, protecting the residue from surrounding solvent. It was suggested that shielding of His114 may allow it to interact with the nitrile group of NS9283 via hydrogen bonding. Thereby, NS9283 may facilitate the formation of

an inter-subunit bridge between Tyr202 from $\alpha 4$ (+) side and His114 from $\alpha 4$ (-) side (**Fig. 2.18**), which could be essential for the activity of NS9283 in the $\alpha 4$ - $\alpha 4$ binding site.⁸³

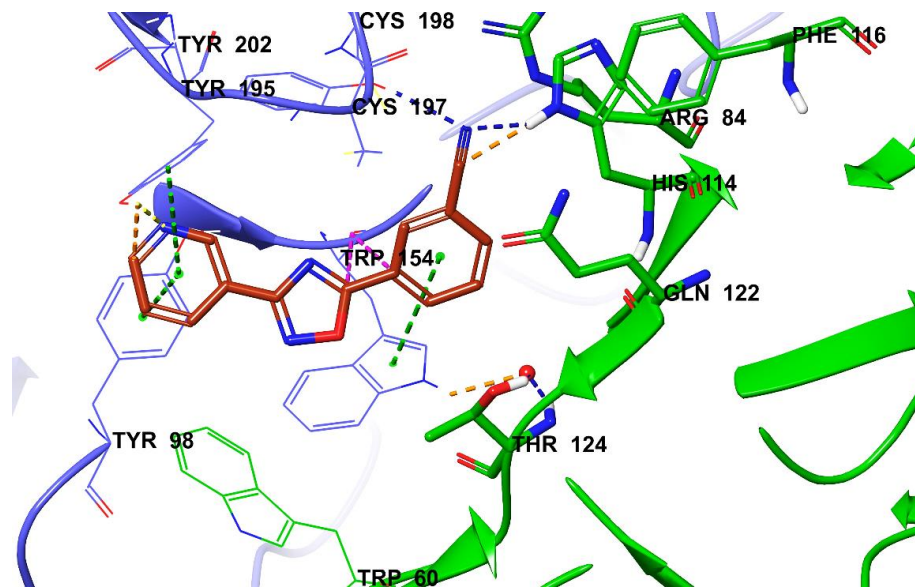


Fig. 2.18: Nitrile group of NS9283 (sticks-brown) shows an inter-subunit bridge formation in the $\alpha 4$ - $\alpha 4$ homology model (principal side-blue and complementary side-green). Conserved residues are shown as lines while the non-conserved residues as sticks.⁸³

The $\alpha 4$ - $\alpha 4$ homology model had only one conserved complementary residue Trp60, whose point mutation to alanine or phenylalanine reduced the functional potency of NS9283, but its replacement with a longer chain arginine completely obliterated the activity. Similar effects were observed on ACh potency, suggesting that NS9283 interacts with tryptophan residue in the $\alpha 4$ - $\alpha 4$ site similar to agonists, with a binding mode equivalent to that observed in the *Ls*-AChBP crystal structure. Likewise, three non-conserved residues; His114, Gln122 and Thr124, present in the complementary side of the $\alpha 4$ - $\alpha 4$ interface, were proposed to be responsible for the activity of NS9283 via direct contacts.

On wild-type (WT) $\alpha 4\beta 2$ nAChRs, NS9283 displayed similar potency as reported before,^{60, 80} but individual and collective mutation of three residues in the $\alpha 4$ (-) side of WT receptors showed altered activity (**Fig. 2.19**). Conversion of $\alpha 4$ (-) to $\beta 2$ (-) side by mutating H114V, Q122F and T124L, completely abolished the activity of NS9283 on the mutated WT receptors. Single point mutation of Q112F and T124L lowered the EC_{50} value of NS9283 by two and three times, respectively. Similarly, substitution of histidine to alanine reduced the potency by ~10 fold, but replacement with valine entirely obliterated the effect of NS9283. This signifies that bulky and branched valine prevents binding of NS9283 in the

$\alpha 4$ - $\beta 2$ interface due to steric hindrance, while histidine interacts directly with NS9283. Hence, histidine was suggested as the principal factor in determining the $\alpha 4$ - $\alpha 4$ selectivity of NS9283 and adds to the possibility of forming an inter-subunit bridge, which anchors the ligand in the binding site and thus, further substantiates its binding mode.⁸³

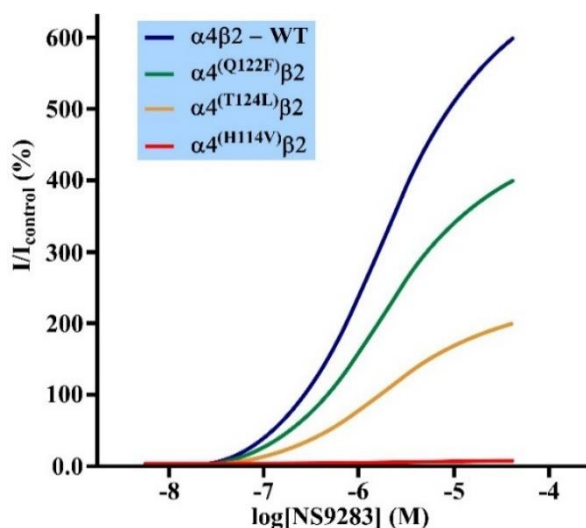
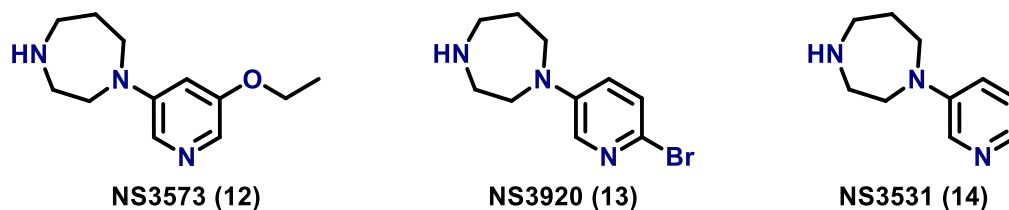


Fig. 2.19: DRC of NS9283 modulation of ACh evoked-currents on WT and single point mutated $\alpha 4\beta 2$ nAChRs expressed in *Xenopus oocytes*.⁸³

Compared to known agonists, the structurally distinct NS9283 was proposed to interact with the $\alpha 4$ - $\alpha 4$ binding site residues in a similar manner. However, even with equivalent contacts, NS9283 is only known to potentiate the agonist response at $(\alpha 4)_3(\beta 2)_2$ nAChRs rather than activating the receptor itself, plausibly due to its high selectivity for the $\alpha 4$ - $\alpha 4$ site. The ability of NS9283 to bind only at the $\alpha 4$ - $\alpha 4$ site may not be sufficient for channel gating and receptor activation, because at least two binding sites must be occupied for submaximal and three for maximal response. This theory was probed using mutated $(\alpha 4)_3(\beta 2)_2$ nAChRs expressed on *Xenopus oocytes*, where three mutations were induced: V136H, F144Q and L146T, converting $\beta 2$ (-) to $\alpha 4$ (-) side. The triple mutant $(\alpha 4)_3(\beta 2^m)_2$ receptor formed three $\alpha 4$ - $\alpha 4$ like interfaces, with one real and two engineered $\alpha 4$ - $\alpha 4$ binding sites. Interestingly, NS9283 exhibited activity at the mutated receptor and elicited currents, which were on par with the ACh-induced response. Thus, mechanistically NS9283 is an agonist for the $\alpha 4$ - $\alpha 4$ site, but pharmacologically, it acts as modulator which increases the potency of an agonist on the $(\alpha 4)_3(\beta 2)_2$ nAChRs without affecting its efficacy.^{83, 84}

Taken together, the activity profile and available structural information suggested NS9283 as a template for the design molecules, targeting the $\alpha 4$ - $\alpha 4$ agonist binding site.

NS3920 (35): Pyridine-Diazepane compound



Developed by Neurosearch A/S,⁸⁵ NS3920 is a pyridine-diazepane compound **13**, which acts as a full agonist at both the $\alpha 4\beta 2$ stoichiometries, with a low preferential selectivity between the two isoforms. Similar to many agonists from drug discovery programs, NS3920 was designed to resemble the structural features of nicotine. A pyridine ring linked to another nitrogen-containing ring system with the ability to generate a protonated form at physiological pH, is a common structural construct of nicotine like agonists. However, when compared to other pyridine-diazepane compounds, such as NS3573 (**12**) and NS3531 (**14**), the bromo-substituted NS3920 displayed some interesting characteristics that suggested its use as a primary template to design compounds discussed in this chapter. As reported by Rohde *et al.*,⁸⁶ bromine substituted compounds showed ~2 times higher affinities compared to the non-brominated analogues. The affinity of NS3920 ($K_i = 0.32$ nM and 1.3 nM) was greater than NS3531 ($K_i = 0.72$ nM and 3.1 nM) and NS3573 ($K_i = 0.62$ nM and 2.2 nM) at the $\alpha 4\beta 2$ nAChRs and *Ls*-AChBP, respectively. A similar gain was observed in terms of efficacy for concatenated $(\alpha 4)_2(\beta 2)_3$ receptors, increasing from 41% to 62% on adding a bromine substituent in the pyridine ring.

The binding of NS3920 determined on a mixed population of $\alpha 4\beta 2$ nAChRs doesn't exhibit any difference arising from distinct $\alpha 4\beta 2$ and $\alpha 4\alpha 4$ sites. This could be attributed to low affinity and a small fraction of $\alpha 4\alpha 4$ sites (1/3 of all sites) available for binding compared to $\alpha 4\beta 2$ sites. As previously described by Olsen *et al.*,⁸³ mutated $\alpha 4\beta 2^{\text{HQT}}$ nAChRs comprises of three $\alpha 4\alpha 4$ -like sites that may provide a reliable measure of NS3920 binding and correlates this binding with its functional profile.⁸⁷ Contrary to two times enhancement at WT $\alpha 4\beta 2$ receptors reflecting binding at $\alpha 4\beta 2$ sites,⁸⁶ the binding affinity of NS3920 ($K_i = 13$ μM) at $\alpha 4\beta 2^{\text{HQT}}$ nAChRs had a 15 and 75 fold difference to NS3531 ($K_i = 190$ μM) and NS3573 ($K_i = 960$ μM), respectively. Interestingly, a correlation was observed in functional responses of NS3920 at $(\alpha 4)_3(\beta 2)_2$ and $\alpha 4\beta 2^{\text{HQT}}$ nAChRs expressed in oocytes. At the $(\alpha 4)_3(\beta 2)_2$ isoform, a characteristic biphasic response was exhibited by both NS3531 and NS3573, but NS3920 displayed a monophasic DRC (**Fig. 2.20A**). This suggests that

NS3920 activates $\alpha 4$ - $\alpha 4$ and $\alpha 4$ - $\beta 2$ sites with similar potency, as indicated by the small difference in affinity. On the other hand, NS3920 showed a 10-50 fold higher functional potency and efficacy at the $\alpha 4\beta 2^{\text{HQT}}$ nAChRs than NS3531 and NS3573. Hence, a minor substituent variation in an agonist could cause large differences in its binding and functional activity between $\alpha 4$ - $\alpha 4$ and $\alpha 4$ - $\beta 2$ sites.⁸⁷

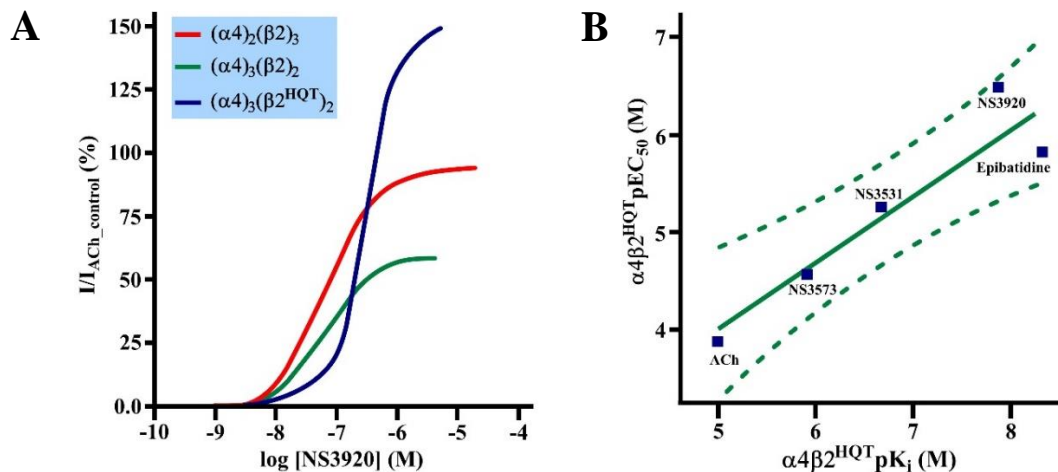


Fig. 2.20: **A**, Monophasic DRC of NS3920 elicited currents at two WT $\alpha 4\beta 2$ and a mutated $\alpha 4\beta 2^{\text{HQT}}$ receptors, expressed in *Xenopus oocytes*. **B**, Correlation curve of potency vs affinity of various agonists tested on $\alpha 4\beta 2^{\text{HQT}}$ nAChRs. Plain line- linear correlation and dotted lines- 90% confidence bands. ACh and Epibatidine discussed in the literature.⁸⁷

The binding affinities and functional potencies obtained from $\alpha 4\beta 2^{\text{HQT}}$ receptors correlated well for all the three compounds, as well as ACh and epibatidine; not discussed here (**Fig. 2.20B**). Further, their functional potencies at $\alpha 4\beta 2^{\text{HQT}}$ nAChRs obtained from monophasic responses were analogous to the second component of the biphasic DRC acquired from the $(\alpha 4)_3(\beta 2)_2$ isoform. As a result, the binding affinities obtained from $\alpha 4\beta 2^{\text{HQT}}$ receptors corresponded with the functional potencies resulting from WT $(\alpha 4)_3(\beta 2)_2$ isoform. Therefore, as concluded in the research by Ahring *et al*,⁸⁷ the $\alpha 4\beta 2^{\text{HQT}}$ construct provided an acceptable model for determining the binding affinity of NS3920 at the $\alpha 4$ - $\alpha 4$ sites, which also related well with its functional potency at WT $(\alpha 4)_3(\beta 2)_2$ receptor.

The interactions governing the different activity profile of NS3920 over NS3531 and NS3573 at the $\alpha 4\beta 2$ receptors was studied in detail using its co-crystal structure with *Ls*-AChBP and *Ls*-AChBP^{HQT} proteins.^{86, 88} Both contained five conserved aromatic residues, but the difference arises from the hydrophobic residues in the complementary side of *Ls*-AChBP, as it resembles closely to the $\alpha 4$ - $\beta 2$ site rather than the $\alpha 4$ - $\alpha 4$ interface. Since polar

residues are present in the $\alpha 4\text{-}\alpha 4$ site, point mutations were induced in the *Ls*-AChBP at three positions to install the signature hydrophilic residues: R104H, L112Q, M114T. Both the co-crystals exhibit common contacts with NS3920, but only *Ls*-AChBP^{HQT} is discussed here, as it revealed critical additional interactions (**Fig. 2.21**, PDB 4UM3).

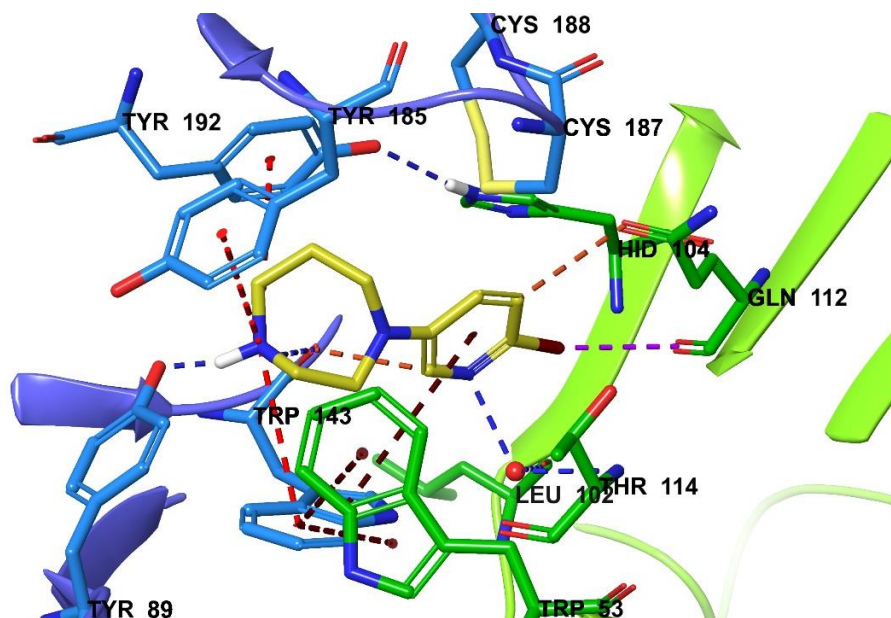


Fig. 2.21: NS3920 interactions (sticks-yellow) in the *Ls*-AChBP^{HQT} binding site. NS3920 exhibits three π -cation and two hydrogen bonds with the principal side (blue), and water-mediated bridge and halogen bond with the complementary side (green) (PDB 4UM3).⁸⁸

The *N4* secondary amine nitrogen of diazepane ring possess positive charge, resulting in the formation of an important secondary ammonium pharmacophore. Typically, nicotine like agonists are known to form only one π -cation contact with the Trp143 residue present at the bottom of aromatic box. However, a recent report suggests that secondary charged nitrogen possess more positive electrostatic potential than the tertiary ammonium.⁸⁹ Therefore, it could form dual π -cation contacts with the nearby residues; one with Trp143 which is well known and another with Tyr185 or Tyr192, depending on its distance from the cationic centre. Notably, with NS3920, Trp143 (3.3 Å), Tyr185 (3.8 Å) and Tyr192 (3.4 Å) from the principal side were almost equidistant from the cationic centre, due to the compact packing of secondary nitrogen compared to bulkier quaternary (ACh) or tertiary ammonium (nicotine) cation.⁸⁹ Hence, the secondary ammonium cation plausibly established not two but three π -cation contacts with the residues (**Fig. 2.21**). Besides π -cation interactions, it also formed hydrogen bonding with the hydroxyl of Tyr89 and the peptidic carbonyl oxygen of Trp143. Moreover, cysteine pair Cys187-Cys188 and Trp143

further stabilised the ligand via van der Waals forces along with π - π stacking of pyridine ring with Trp143, allowing a full closure of loop-C. On the complementary side, a water molecule present in the binding pocket acts as a bridge, which mediates hydrogen bonding between the backbone carbonyl oxygen of Leu102, the peptidic nitrogen of Thr114 (Met114 in *Ls*-AChBP) and pyridine nitrogen of NS3920. Apart from these contacts; Trp53, His104, Gln112 and Thr114 interact with NS3920 through van der Waals forces and stacking of pyridine ring with His104 (absent in *Ls*-AChBP).^{86, 88}

In the crystal structure, compared to NS3531, a ~ 0.5 Å shift in the binding pose of pyridine ring of NS3920 was observed, to accommodate the bulky bromo group. The proximal position of bromine to the peptidic carbonyl oxygen of Gln112 from the complementary side was much closer than simple van der Waals contacts. As indicated from quantum mechanical calculations, the electron-withdrawing pyridine ring results in polarisation of electron density at bromine, allowing it to develop a minor positive charge on its tip. Along with the positive character and bromine proximity, its directional vector is also in line with the electron-rich π -system of carbonyl oxygen, which establishes an electrostatic contact as a halogen bond (**Fig. 2.21**). Also, the carbonyl oxygen of Gln112 forms an interaction with the partially positive carbon adjacent to the bromine substituent. Thus, bromine provides added stability to the ligand by anchoring it with complementary side, which explains the increase in efficacy of bromo-substituted compounds over non-bromo compounds.^{86, 88}

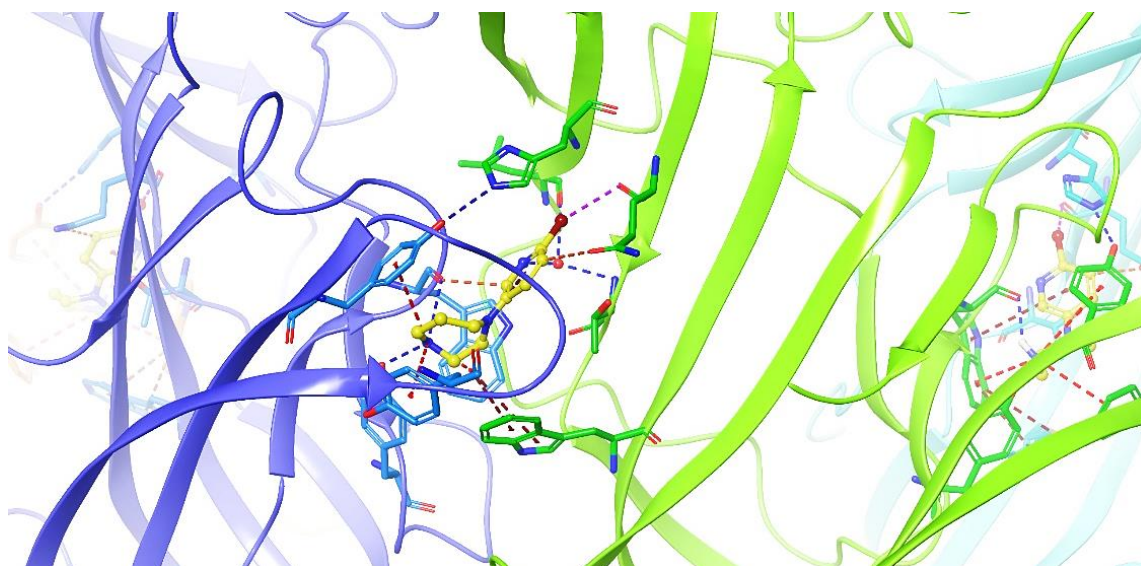


Fig. 2.22: Formation of an inter-subunit bridge via NS3920 (yellow) mediated interactions between principal (blue) and complementary (green) sides at the interface (PDB 4UM3).⁸⁸

As described in the EM studies of *Torpedo* nAChRs,^{2, 28} agonist binding at the interface of two subunits initiates a global quaternary twist mechanism in the protein structure of the pentamer, steering it to channel gating. However, an agonist that stabilises this allosteric transition by facilitating contacts between the residues of principal and complementary sides, could arguably prolong the duration of channel opening. For NS3920, the π -cation interactions and hydrogen bonding between secondary ammonium nitrogen of diazepane and four conserved aromatic residues; Tyr89, Trp143, Tyr185 and Tyr192, lock the ligand from the principal side. Similarly, van der Waals forces, water-mediated hydrogen bonding and especially halogen bonding, between the pyridine ring and residues from complementary sides, stabilises the ligand in the binding pocket. In this way, NS3920 anchors the principal and complementary side, which behaves like an inter-subunit bridge providing an extra stability and prolonged channel gating (**Fig. 2.22**). The ligand-mediated contacts were further strengthened through hydrogen bonding between Tyr192 and His104, causing firmer capping of loop-C than exhibited in *Ls*-AChBP co-crystal structure.⁸⁶ The stacking of the pyridine ring of NS3920 with His104 facilitated rearrangement of residue in a conformation that positioned it in hydrogen bonding distance with Tyr192. So, agonists like NS3920 mediate a crucial and strong interplay between the interfacial residues of two subunits and a stronger loop-C closure, explaining their greater efficacy and affinity.^{86, 88}

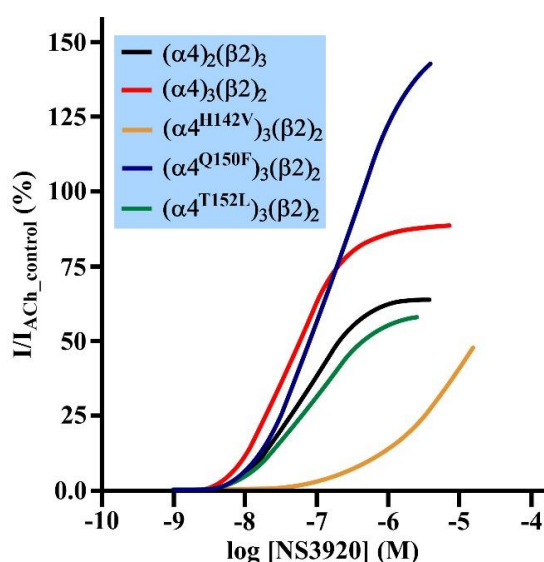


Fig. 2.23: DRC of NS3920 elicited currents at WT and mutated $\alpha 4\beta 2$ receptors, expressed in *Xenopus oocytes* for electrophysiology studies.⁸⁶

The literature report⁸⁸ corroborated that the binding affinity of NS3920 at the *Ls*-AChBP^{HQT} ($K_i = 29 \mu\text{M}$) corresponds with the $\alpha 4\beta 2^{\text{HQT}}$ nAChRs ($K_i = 13 \mu\text{M}$). Therefore, alteration in

any of the three residues present in the $(\alpha 4)_3(\beta 2)_2$ isoform could result in the varied functional profile of NS3920. The distinguishing interactions leading to a higher efficacy of NS3920 at the $\alpha 4$ - $\alpha 4$ binding site were distorted by mutating the signature residues on the complementary side in the $(\alpha 4)_3(\beta 2)_2$ receptors (**Fig. 2.23**). Point mutation of H142V (His104 in *Ls*-AChBP^{HQT}) was significant, as it disrupted the π - π stacking of the pyridine ring with His142, causing hydrogen bond with tyrosine to break. This destroyed the inter-subunit bridge formed between the principal and complementary sides which kept the tight closure of loop-C. As mentioned before, stronger loop-C capping leads to improved channel gating, thereby, resulting in a reduced efficacy of NS3920 from 82% to 54% along with a ~50 fold loss in potency due to this mutation. However, a single point mutation of Q150F slightly increased the efficacy, while T152L mutation lowered it similar to the H142V modification. Thus, these signature residues play an essential role in refining the agonist activity, but His142 is imperative for the ligands displaying high efficacy as well as selectivity at the $\alpha 4$ - $\alpha 4$ binding site.⁸⁸

Both NS9283 and NS3920 harbour interesting structural features that attract further research on using them as templates to design new agonists that can exhibit better selectivity than NS3920, combined with higher potency and efficacy than NS9283 in one or many analogues. Efforts to design improved $\alpha 4$ - $\alpha 4$ agonists is discussed in the next section, along with its synthesis and biological evaluation.

2.2. DESIGN AND SYNTHESSES OF NS9283-NS3920 HYBRIDS

2.2.1. PROJECT AIMS

New agonists targeting $\alpha 4\beta 2$ nAChRs may be useful to treat neurological and psychiatric disorders as well as nicotine addiction in smokers. The major challenge lies in overcoming structural similarities in the binding site to achieve receptor selectivity. This can be accomplished through recently discovered 3rd agonist binding site at the $\alpha 4$ - $\alpha 4$ interface in the $(\alpha 4)_3(\beta 2)_2$ isoform, which offers a novel approach for activating $\alpha 4\beta 2$ receptors only. The selective targeting of the $\alpha 4$ - $\alpha 4$ site not only has the potential to improve subtype selectivity, but will also activate a pharmacologically important stoichiometry that has a higher abundance and larger conductance than the $(\alpha 4)_2(\beta 2)_3$ isoform.⁶⁴

By exploiting the biophysical differences between two isoforms, our major aim was to design potent agonists that displayed higher selectivity and efficacy at the $\alpha 4$ - $\alpha 4$ binding site. Enthused by the distinct pharmacological profile of NS9283 and NS3920 at the $\alpha 4$ - $\alpha 4$ site, these compounds were used as templates to design analogues. Our collaborator, Dr. Thomas Balle from the University of Sydney, provided us with structural models based on the *Ls*-AChBP and *Ls*-AChBP^{HQT} co-crystal structures of both ligands. Analysing the binding modes overlay of both ligands (**Fig. 2.24**), we decided to develop hybrids that possess the shared structural features of a modulator and an agonist.

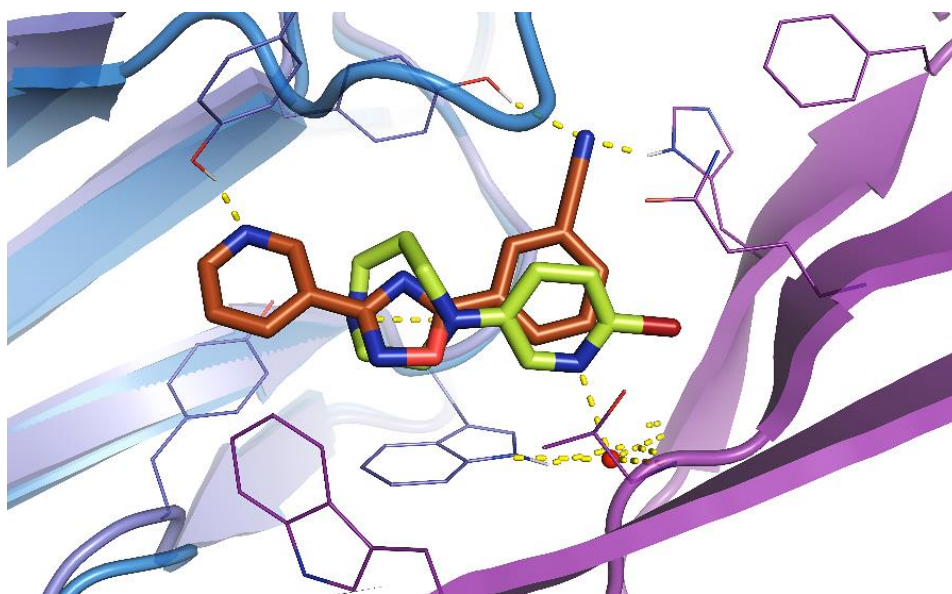


Fig. 2.24: Binding mode overlap of co-crystal structures of NS9283 (brown) and NS3920 (light green) with the *Ls*-AChBP^{HQT}.

As described previously, NS9283 is a PAM for the $(\alpha 4)_3(\beta 2)_2$ isoform, but mechanistically acts as an agonist with high selectivity for the $\alpha 4$ - $\alpha 4$ site. Activation of a single binding site doesn't evoke currents but potentiates ACh response with a low functional potency, $EC_{50} = 4.0 \mu\text{M}$. Alternatively, NS3920 is a classical $\alpha 4\beta 2$ nAChR agonist which without preference, potently activates both the isoforms with a strong binding affinity. However, NS3920 has high potency ($EC_{50} = 56 \text{ nM}$) but low efficacy ($I_{\text{max}} = 62\%$) at the $2\alpha:3\beta$ isoform, while it shows moderate potency ($EC_{50} = 220 \text{ nM}$) but high efficacy ($I_{\text{max}} = 151\%$) at the $3\alpha:2\beta$ isoform. Hence, the following structural hybrids were designed (**Fig. 2.25**) with the goal of achieving the selectivity of NS9283 with the efficacy and potency of NS3920.

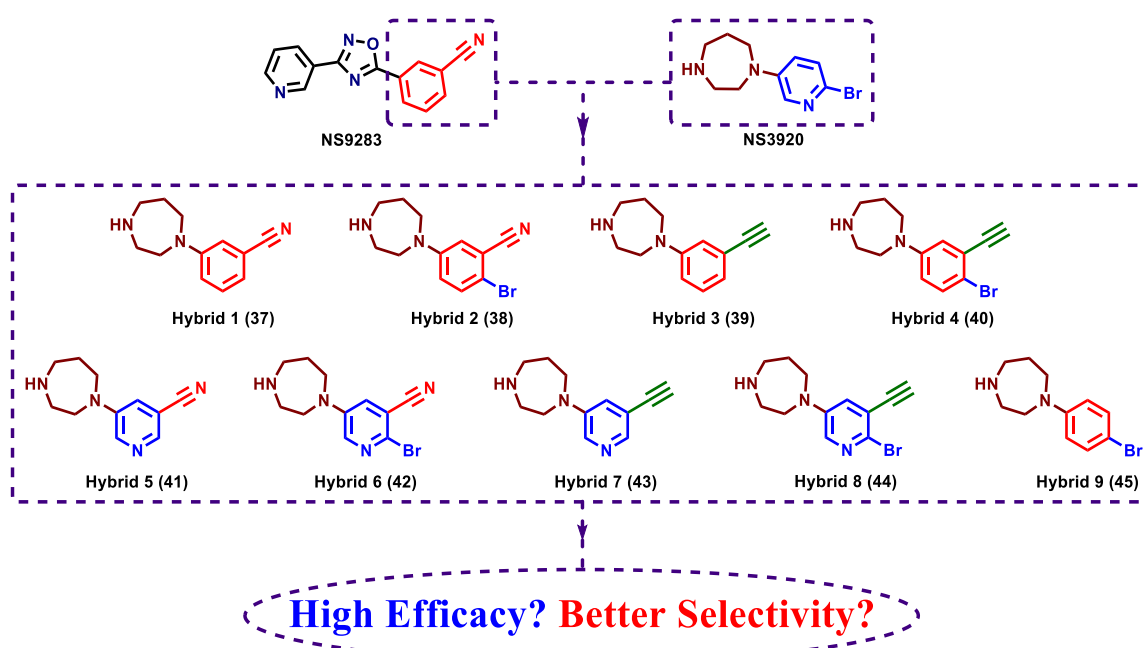


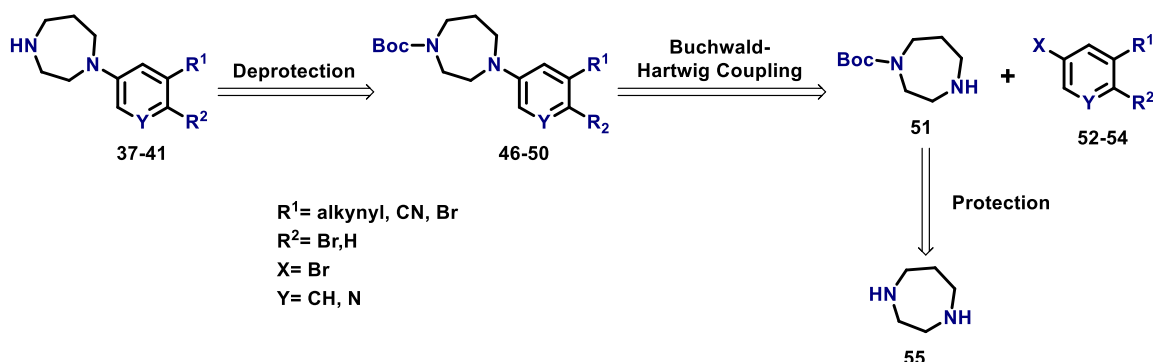
Fig. 2.25: Design of hybrids based on the shared structural features of NS9283 and NS3920.

The homopiperazine ring of NS3920 remains common in all hybrids (**Fig. 2.25**) as it has a secondary nitrogen that forms the crucial ammonium pharmacophore responsible for stabilisation via π -cation contacts and hydrogen bonding with the conserved aromatic residues. Variation of pyridine with the phenyl ring of NS9283 in hybrids 1-4 and 9, is for probing its effect on efficacy and potency as well as to explore differences in the binding mode of the ligand in AChBP and $\alpha 4\beta 2$ nAChR due to disruption of water-mediated bridge present in AChBP. Merging nitrile and bromo substitutions in one molecule could have an additive effect on the selectivity and efficacy, as both will facilitate the formation of ligand-mediated inter-subunit bridges. Replacement of nitrile with acetylene is to explore the role of the nitrile in arbitrating inter-subunit bridge formation.

The syntheses of phenyl and pyridyl analogues are explained in the next section along with the retrosynthetic scheme to achieve the target compounds. Since hybrids 6-9 were synthesised by a former co-worker (discussed briefly), the focus will be on describing challenges faced for syntheses of hybrids 1-5. Once the syntheses of all analogues were completed, they were shared with our collaborators at the University of Sydney for radioligand binding assay and two-electrode voltage clamp electrophysiology assay on $(\alpha 4)_2(\beta 2)_3$ and $(\alpha 4)_3(\beta 2)_2$ nAChRs, expressed in *Xenopus laevis* oocytes. Results of the biological evaluation are discussed following the synthesis of hybrids.

2.2.2. RETROSYNTHETIC ANALYSIS

As described in the retrosynthesis (**Scheme 1**), the target hybrids 1-5 (**37-41**) could be achieved by deprotection of Boc-group from compounds **46-50**, which were accessible through the palladium catalysed Buchwald-Hartwig coupling of substituted pyridyl and phenyl halides **52-54** with the Boc protected homopiperazine **51**. One of the free secondary amines in homopiperazine was selectively mono-protected with the Boc-group to prevent bis-substitution and allow Buchwald-Hartwig coupling only at the available amine.^{85, 90, 91}



Scheme 1: General retrosynthetic approach to synthesise phenyl and pyridyl hybrids 1-5.

The relevant starting materials and intermediates to achieve target hybrids were commercially available, while some intermediates were synthesised in the lab. For syntheses of hybrids 2-4 (**38-40**), additional substitution and coupling reactions were needed. Bromination of the nitrile substituted coupled product was required to generate hybrid 2, whereas Sonogashira coupling was envisioned to install the acetylene group on halide-substituted intermediates for producing hybrids 3 and 4. Optimisation of reactions, especially Buchwald-Hartwig and Sonogashira coupling, is discussed in detail in the following sections, along with other approaches to generate target compounds.

2.2.3. SYNTHESIS OF HYBRIDS

Since its emergence, palladium catalysed couplings have become the mainstay in synthetic schemes of various drug discoveries and total synthesis projects. Buchwald and Hartwig utilised palladium as a catalyst to form C-N bond between amines and aryl or heteroaryl halides.⁹¹⁻⁹⁴ Generally, a Pd(0) catalyst complexed with phosphine ligands is used for coupling aryl or heteroaryl bromides or iodides with amines in the presence of a strong base, such as an alkoxide. Mostly, the base is employed in stoichiometric amounts and the heating of reaction mixture generates the coupled product in good yield.⁹⁵ Therefore, similar conditions were used but with different combinations of ligands, base and solvent to yield the desired pyridyl and phenyl halide coupled homopiperazine products.

The Buchwald-Hartwig cross-coupling procedure optimised previously in the group was mostly followed, although, necessary modifications in the combination of reagents or their equivalents were introduced, whenever needed. The choice of palladium catalyst, as well as ligand used for activation of palladium catalyst, is crucial as it affects the efficiency and rate of reaction. In the current project, Pd₂(dba)₃ was used rather than the usual Pd(OAc)₂ to avoid an additional step of palladium reduction. The Pd₂(dba)₃ is an air-stable Pd(0) catalyst complexed with the bidentate ligand dibenzylideneacetone that can be used with other chelating agents in diverse reaction conditions. In this case, Pd₂(dba)₃ was complexed with XPhos, a dialkylbiaryl phosphine ligand, to reinforce the formation of a highly reactive [L₁Pd(0)] complex over [L₂Pd(0)] species. The structural properties of XPhos affecting the efficiency of Pd₂(dba)₃ catalyst are explained in the image below (Fig. 2.26).^{94, 96}

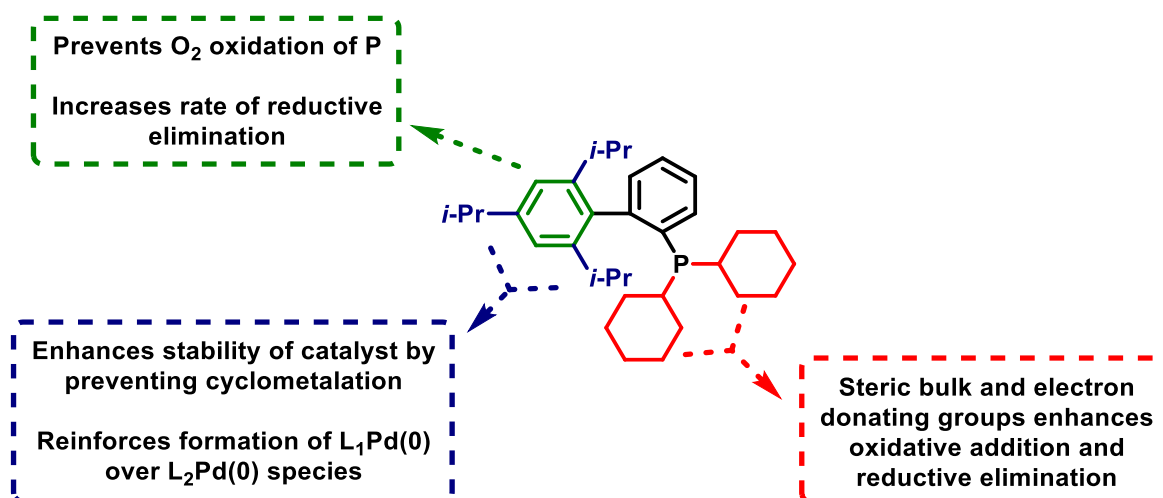
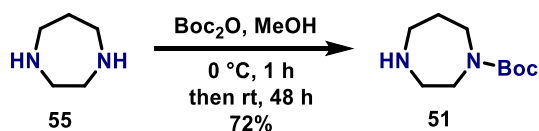


Fig. 2.26: Structural features of XPhos affecting reaction efficiency.⁹⁴

Boc-Homopiperazine

Scheme 2: Synthesis of *N*-Boc homopiperazine **55** from homopiperazine **51**.

The *N*-Boc mono-protected derivative of homopiperazine **51** was achieved from the commercially available homopiperazine **55** (Scheme 2), using a literature procedure.⁹⁷ Since two secondary amines were available for protection, di-*tert*-butyl dicarbonate (Boc) was slowly added as a limiting reagent to a diluted solution of homopiperazine present in excess. Here, homopiperazine serves as the base itself to facilitate the protection. Once the mono derivative is formed, the Boc-group spatially hinders the reactivity at the nearby secondary amine (Fig. 2.27). The reduced reactivity is also due to the presence of diamine in excess amounts and the electronic effects of Boc-substitution, as it makes the nearby secondary amine less nucleophilic for further reaction. Thus, the rate of formation of the di-protected derivative is low, and the reaction generates mono *N*-Boc derivative in high yield.

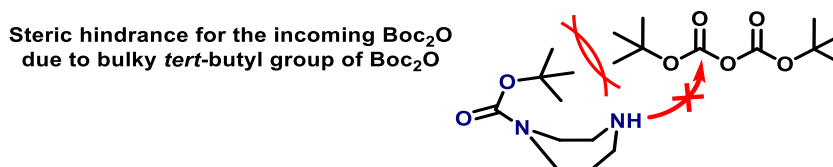


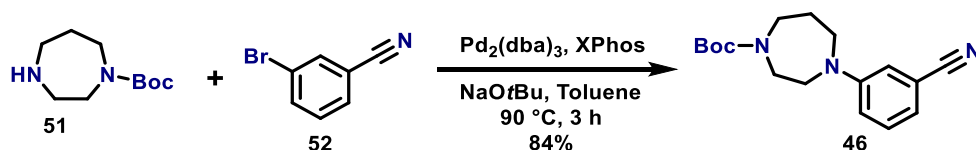
Fig. 2.27: Steric effect of bulky *tert*-butyl group hinders Boc protection at the free 2° amine.

Boc protection of the secondary amine was confirmed from ¹H NMR, showing a singlet at 1.46 ppm for the nine methyl protons of *tert*-butyl group. The broad singlet of free amine proton was observed at 1.95 ppm, validating the formation of mono-protected *N*-Boc derivative of homopiperazine. The obtained spectra matched well with the literature data.⁹⁷

*Hybrid 1***Step 1: Buchwald-Hartwig cross coupling**

Buchwald-Hartwig cross coupling of *N*-Boc homopiperazine **51** with commercially available 3-bromobenzonitrile **52** in toluene, yielded the intermediate **46** in 84% yield after flash chromatography (Scheme 3). The sequence of catalyst and ligand addition was the

key step responsible for high reaction efficiency. Both, $\text{Pd}_2(\text{dba})_3$ and XPhos, were added in catalytic amounts to form a stirring solution in dry toluene. The purpose of adding catalyst and ligand first is to form the highly active $[\text{L}_1\text{Pd}(0)]$ complex over $[\text{L}_2\text{Pd}(0)]$ species. This is followed by the addition of 3-bromobenzonitrile and stoichiometric amounts of sodium *tert*-butoxide (NaOtBu) to initiate the catalytic cycle.⁹⁴ Finally, on addition of *N*-Boc homopiperazine, NaOtBu deprotonates the secondary amine and facilitates coupling with the carbon-bromine bond of benzonitrile, forming a C-N bond to generate coupled product.



Scheme 3: Buchwald-Hartwig cross coupling to synthesise compound 46.

The formation of Buchwald-Hartwig cross-coupled product was characterised through ^1H and ^{13}C NMR. Two multiplets in the aromatic region around 7.22-7.16 and 6.88-6.78 ppm were observed for the four aromatic protons. Four peaks spread over the aliphatic region of ^1H NMR were consistent with 10 protons of the diazepane ring. The typical singlet for nine methyl protons of the Boc-group was split into two peaks at 1.35 and 1.26 ppm. This was due to the Boc-rotamers, which also resulted in broadened peaks of aromatic and diazepane protons. The rotamers are conformational isomers, which arise due to the hindered rotation around the single bond of amide carbon of the Boc group attached to diazepane nitrogen (Fig. 2.28). The bulky *tert*-butyl group and the amide carbonyl generates hindered rotation, resulting in additional peaks in the NMR spectrum.

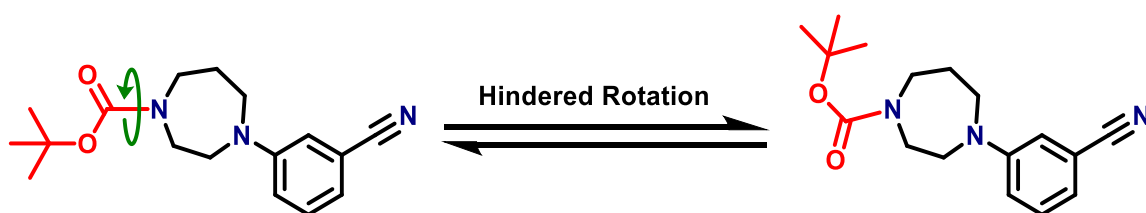
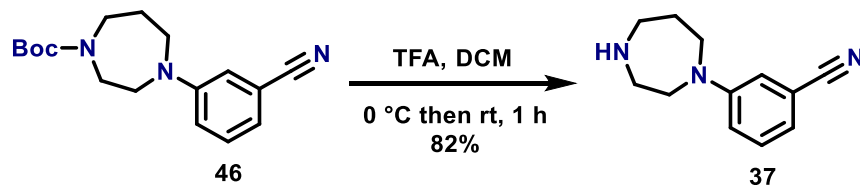


Fig. 2.28: Boc-rotamers formed due to hindered rotation around the amide bond.

A similar pattern was observed in ^{13}C NMR, where additional carbon peaks were present in the aromatic and unsaturated regions. The characteristic signals of carbonyl carbon and three methyl carbons of the Boc-group were visible at 155.19 and 28.47 ppm, along with two additional peaks at 154.80 and 28.27 ppm due to the Boc-rotamers. The IR spectrum

further confirmed the formation of cross-coupled product, as nitrile (2227.14 cm^{-1}) and phenyl CH (2973.53 cm^{-1}) stretching were evident as sharp peaks.

Step 2: Removal of Boc-group



Scheme 4: Synthesis of Hybrid 1 (37) after Boc-deprotection of cross coupled product.

The conditions for Boc deprotection were followed as described in the literature,^{85,90} where trifluoroacetic acid (TFA) in stoichiometric amounts under low temperature was added to a stirring solution of cross-coupled product **46** in dichloromethane (DCM). This resulted in Hybrid 1 (**37**) with 82% yield after flash chromatography (**Scheme 4**). The acidic silica gel was neutralised with triethylamine to carry out smooth purification of basic compound **37**.

Deprotection of cross-coupled product to afford Hybrid 1 was confirmed with the absence of peaks arising from *tert*-butyl protons and carbons in ^1H and ^{13}C NMR. Both the NMR spectra had no additional peaks after the removal of Boc-group, which also resulted in the observation of sharp peaks in the aromatic and aliphatic regions. Presence of broad singlet at 1.62 ppm in the ^1H NMR was consistent with the amine proton, while broad stretching at 3336.8 cm^{-1} in the IR spectrum for amino group further confirmed Boc-deprotection.

Mechanism of Buchwald-Hartwig Cross-Coupling

Synthesis of compound **46** is presented here as an example to explain the cross-coupling mechanism and therefore, was also represented in the image below (**Fig. 2.29**). Since $\text{Pd}_2(\text{dba})_3$ is an air-stable Pd(0) catalyst, it doesn't undergo reduction and directly enters the catalytic cycle on coordination with XPhos ligand. In the first step of the catalytic cycle, after the complexation of $\text{Pd}_2(\text{dba})_3$ with XPhos ligand, the XPhosPd(0) species undergoes oxidative addition with the aryl halide (ArX) **52**, 3-bromobenzonitrile to form XPhosPd(II)-(Ar)X complex. The second step is binding of *N*-Boc homopiperazine (NR^1R^2) with the formed complex. This is followed by deprotonation of the secondary amine with NaOtBu and formation of XPhosPd(II)-(Ar)[NR^1R^2] complex via displacement of bromine. Finally, XPhosPd(II)-aryl amide species undergoes reductive elimination to form the C-N bond

between benzonitrile and homopiperazine to form the cross-coupled product **46** and regenerate the initially formed XPhosPd(0) complex.^{94, 95}

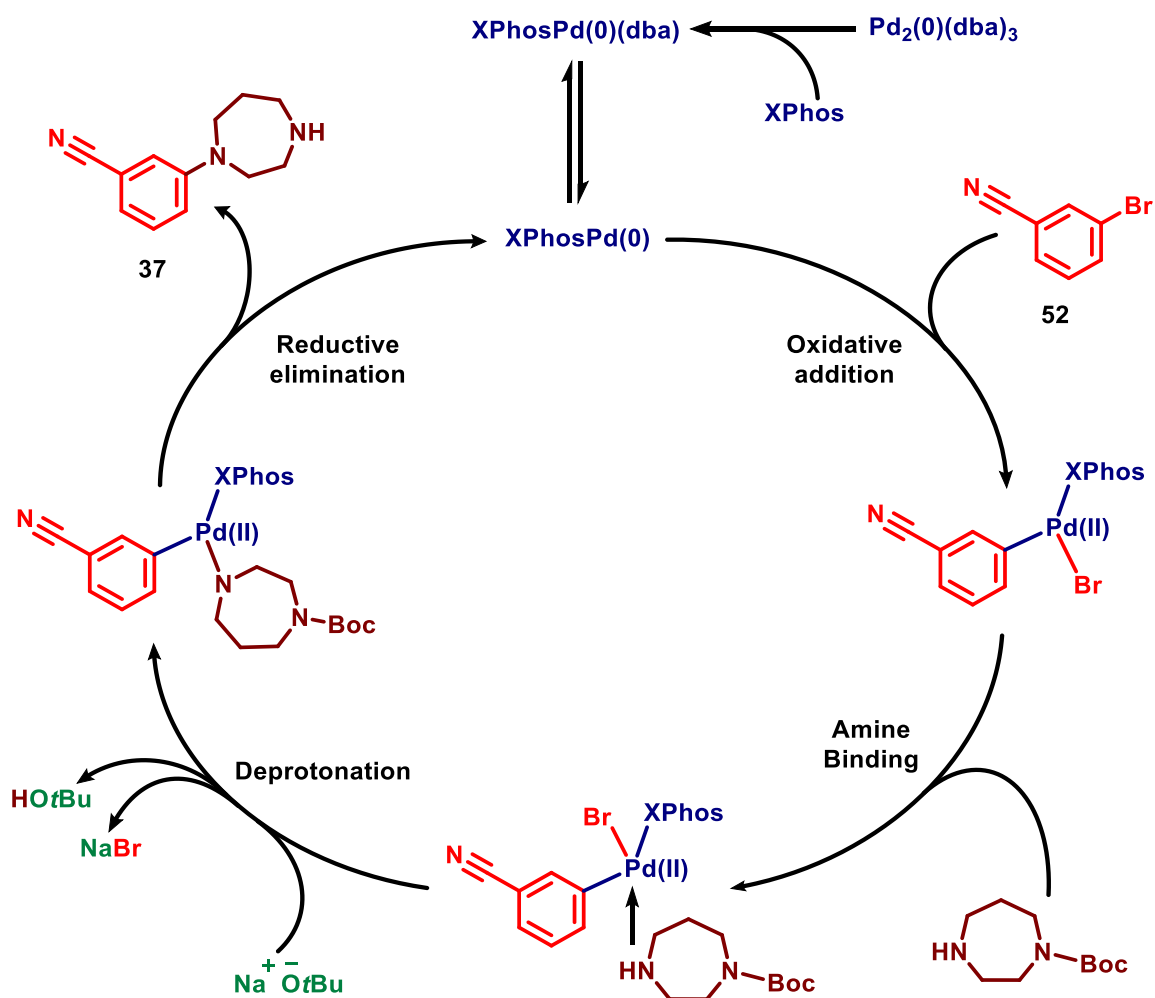
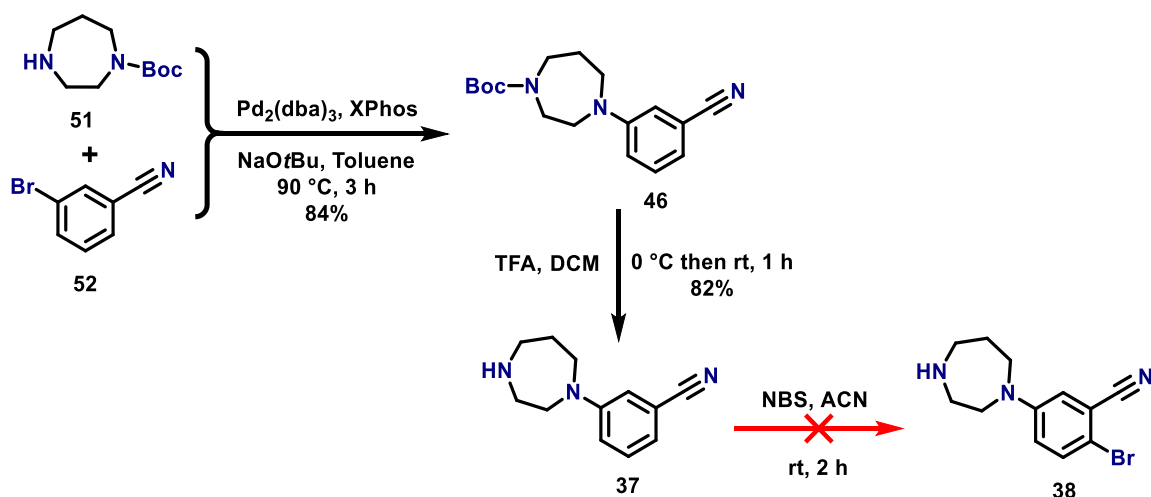


Fig. 2.29: Mechanism of Pd-catalysed Buchwald-Hartwig cross-coupling amination.^{94, 95}

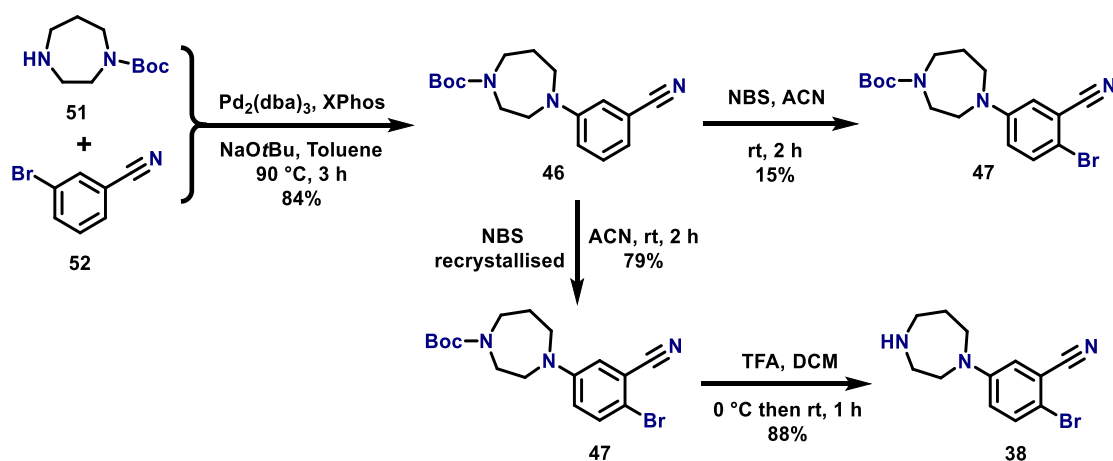
Hybrid 2

Synthesis of compound **38** (Hybrid 2) was carried out similar to the synthesis of compound **37**. However, an additional step of bromination of phenyl ring, *para* to diazepane substitution, was included after the Buchwald-Hartwig cross-coupling to generate the brominated analogue of compound **37**. The *N*-Bromosuccinimide (NBS) bromination was first trialled after the Boc deprotection of compound **37**⁸⁵ but the reaction failed (**Scheme 5**). Plausibly, the failure was due to the high reactivity of homopiperazine over the *para*-position of phenyl ring. The electron-rich secondary amine possibly traps the generated bromonium electrophile (Br^+) species from NBS, thus, might not allow it to undergo electrophilic aromatic bromination at the less electron-rich *para*-position of the phenyl ring.



Scheme 5: First trial for synthesis of compound **38** from **37**.

Consequently, Boc-protected compound **46** was subjected to similar conditions (**Scheme 6**), but brominated compound **47** was obtained in low yield, while most of the starting material remained unreacted, as observed from the TLC and chromatographic isolation. The reason for this was attributed to the impure NBS reagent, which could also be an added cause of failure in the first trial with compound **37**. On recrystallisation of NBS in water and used under similar conditions in acetonitrile (ACN),⁹⁸ the brominated intermediate **47** was achieved in 79% yield after flash chromatography. This was followed by deprotection of Boc-group using previously mentioned procedure to produce compound **38** in 88% yield.



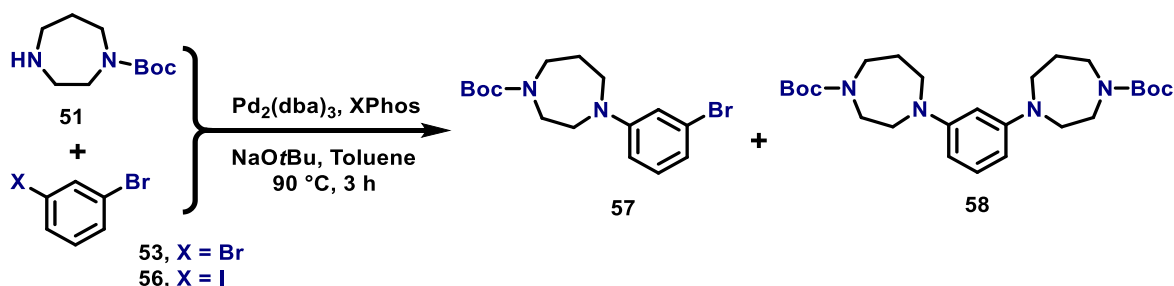
Scheme 6: Synthesis of Hybrid 2 (**38**) from bromination of cross-coupled product **47** using recrystallised *N*-Bromosuccinimide.

Bromination step was confirmed from the observation of two molecular ion peaks $[M+H]^+$ at 402 and 404 in both LRMS and HRMS spectra, owing to the two isotopes of bromine.

Three distinct signals at 7.44, 6.91 and 6.78 ppm in the aromatic region were consistent with the three phenyl protons. Multiple peaks arising due to Boc-rotamers were evident in both ^1H and ^{13}C NMR. Formation of Hybrid 2 after Boc-deprotection was established by the absence of signal from Boc protons as well as additional peaks observed due to Boc-rotamers. The amine proton was not seen in ^1H NMR.

Hybrid 3

Step 1: Buchwald-Hartwig cross-coupling



Scheme 7: Buchwald-Hartwig cross-coupling of aryl halides **53** and **56** yielded a mixture of two products, monosubstituted **57** and an unwanted disubstituted **58**.

Hybrid 3 (**39**) could be accessed from dihalogenated phenyls, which on Buchwald-Hartwig reaction delivers the precursor to install acetylene at the *meta*-position to diazepane via Sonogashira cross-coupling. The major challenge posed by dihalogenated phenyls is the preferential formation of the disubstituted product **58** over monosubstituted **57** (**Scheme 7**). Thus, variation in equivalents (eq.) of reagents and catalyst were trialled with two different aryl halides, 1,3-dibromobenzene **53** and 1-bromo-3-iodobenzene **56**, to achieve the desired **57** in higher yields over **58** (**Table 1**). In these reactions, *N*-Boc homopiperazine was the limiting reagent (1 eq.) and was added slowly over a period of 3 h to reduce the formation of unwanted side product **58**.

Previously, optimised Buchwald-Hartwig conditions predictably, gave low yields perhaps due to the similar reactivity of both bromo-groups (**Table 1: entry 1**). Reducing the catalyst-ligand loading or the temperature to lower the reactivity, further lessened the yield of **57** (**Table 1: entry 2 and 3**). However, on increasing the amount of **53** from 1.0 to 1.5 and 2.0 eq., an increment in the overall yield of **57** was observed over **58** (**Table 1: entry 4 and 5**). It was probably due to the presence of *N*-Boc-homopiperazine in a limited quantity for which the excess aryl halide competes to form the cross-coupled product. However, an

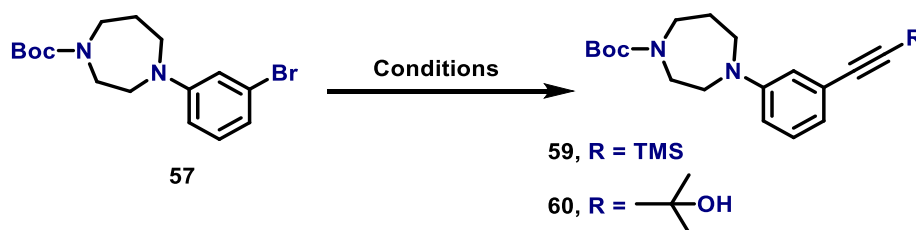
additional 1 eq. of aryl halide **53** didn't show much effect on the overall yield (**Table 1: entry 6**). Similar conditions (**Table 1: entry 7 and 8**) were employed for 1-bromo-3-iodobenzene **56**, as it may offer differential reactivity relative to the dibromobenzene. However, extremely low yields were observed which may be due to the high reactivity of both iodo- and bromo-group. Therefore, the conditions mentioned above (**Table 1: entry 5**) were used to synthesise precursor **57** for installation of the acetylene group via Sonogashira cross-coupling, even though the overall yield was only 35%.

Table 1: Optimisation of Buchwald-Hartwig cross-coupling to achieve a higher yield of compound **57** over undesirable disubstituted compound **58**.

S. No.	Aryl Halide	Pd ₂ (dba) ₃ /XPhos (mol%)	NaOtBu	Temp.	Time	Yield of 57
1.	53 (1 eq.)	0.02/0.06	1.5 eq.	90 °C	3 h	19%
2.	53 (1 eq.)	0.01/0.03	1.5 eq.	90 °C	3 h	6%
3.	53 (1 eq.)	0.02/0.06	1.5 eq.	65 °C	3 h	13%
4.	53 (1.5 eq.)	0.02/0.06	1.5 eq.	90 °C	3 h	25%
5.	53 (2 eq.)	0.02/0.06	1.5 eq.	90 °C	3 h	35%
6.	53 (3 eq.)	0.02/0.06	1.5 eq.	90 °C	3 h	36%
7.	56 (2 eq.)	0.02/0.06	1.5 eq.	90 °C	3 h	7%
8.	56 (3 eq.)	0.02/0.06	1.5 eq.	90 °C	3 h	9%

Both monosubstituted **57** and disubstituted **58** compounds displayed an equal number of signals in the ¹H NMR. However, four signals in the aliphatic region for compound **58** were integrated to 20 protons, 10 from each diazepane ring, while the two peaks at 1.44 and 1.40 ppm were equivalent to 18 protons, nine from each Boc-group. The mass spectra of compound **57** showed two molecular ion peaks [M+H]⁺ at 377 and 379, consistent with the presence of bromine isotopes, while compound **58** had a single molecular ion peak at 497.

Step 2: Sonogashira cross-coupling

**Scheme 8:** Sonogashira cross-coupling to access alkyne coupled product.

Different palladium catalysts and acetylene sources, as mentioned in **Table 2**, were used for the synthesis of alkyne substituted compounds in high yields through Sonogashira cross-coupling (**Scheme 8**). All the reactions were carried out after thorough deoxygenation of solvents and bases by freeze-pump thaw process.

Table 2: Sonogashira cross coupling optimisation to access alkyne substituted compound.

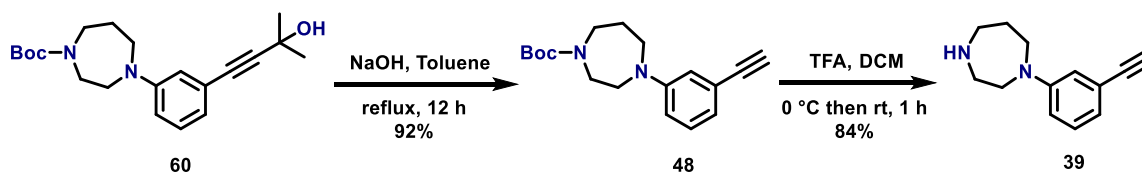
S. No.	Conditions (Pd catalyst-CuI in mol%)	Conversion	Product (NMR Yield)
1.	TMS acetylene (3 eq.)\ Pd(PPh ₃) ₂ Cl ₂ (0.05)\ CuI (0.1)\ (<i>i</i> -Pr) ₂ NH-THF (1:1)\ 3 h - 60 °C	Incomplete	59 (7%)
2.	TMS acetylene (3 eq.)\ Pd(PPh ₃) ₂ Cl ₂ (0.06)\ CuI (0.12)\ (<i>i</i> -Pr) ₂ NH\ 3 h - 60 °C	Incomplete	59 (16%)
3.	TMS acetylene (3 eq.)\ Pd(OAc) ₂ (0.06)\ CuI (0.12)\ PPh ₃ (3 eq.)\ (<i>i</i> -Pr) ₂ NH\ 3 h - 60 °C	Incomplete	59 (27%)
4.	TMS acetylene (3 eq.)\ Pd(PPh ₃) ₄ (0.06)\ CuI (0.12)\ (<i>i</i> -Pr) ₂ NH\ 3 h - 60 °C	Incomplete	59 (37%)
5.	2-methylbut-3-yn-2-ol (3 eq.)\ Pd(PPh ₃) ₄ (0.06)\ CuI (0.12)\ (<i>i</i> -Pr) ₂ NH\ 6 h - 60 °C	Incomplete	60 (54% isolated)
6.	2-methylbut-3-yn-2-ol (3 eq.)\ Pd(PPh₃)₄ (0.06)\ CuI (0.12)\ (<i>i</i>-Pr)₂NH\ 12 h - 60 °C	Complete	60 (96% isolated)

Initially, Pd(II) catalysts; Pd(PPh₃)₂Cl₂ and Pd(OAc)₂, were used to obtain TMS protected acetylene at the 3rd position in the phenyl ring **59**.^{99, 100} Even after using base as the solvent,

incomplete conversion of starting material **57** leading to low yields of alkyne substituted **59** along with their close ranging R_f values, were the two major problems that needed to be addressed (**Table 2: entry 1-3**). Incomplete conversion could be due to the use of inactivated Pd(II) catalysts. Hence, taking a cue from Pd(OAc)₂-PPh₃ combination that generates Pd(0) catalyst *in situ* but is more prone to oxidation, Pd(PPh₃)₄ was directly used in the reaction. The increase in yield was evident from NMR but the conversion was still incomplete, while the chromatographic isolation remained problematic (**Table 2: entry 4**). To address both the issues together, 2-methylbut-3-yn-2-ol was used,^{100, 101} resulting in alkyne substituted compound **60** with higher yields though with incomplete conversion (**Table 2: entry 5**). The tertiary alcohol provided the essential difference in the polarity between starting material and product that was visible from R_f values, thus, making the product isolable by chromatography. On advice from co-workers, adding an alkyne once the reaction temperature reaches 60 °C followed by stirring for 12 h, led to complete conversion of **57** into alkyne substituted **60** in high yields (**Table 2: entry 6**).

The alkynylation via Sonogashira cross-coupling was supported by the spectroscopic data. The presence of singlet at 1.62 ppm in the ¹H NMR was equivalent to the six protons of two methyl groups attached to the alkyne protecting group. In ¹³C NMR, the two methyl carbons were observed as a single peak at 31.20 ppm, while the signals for two quaternary alkyne carbons were observed at 83.08 and 92.86 ppm. The IR spectrum showed a broad, strong absorption at 3386.64 cm⁻¹ for the hydroxyl group.

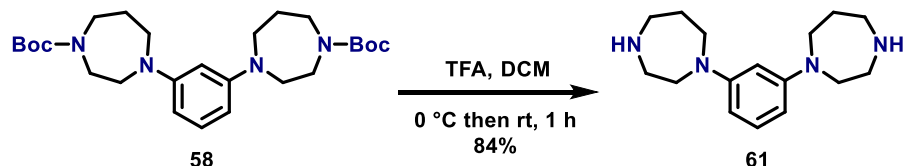
Step 3 and 4: Removal of protecting groups



Scheme 9: Removal of protecting groups to achieve Hybrid 3 (**39**).

Acetylene containing compound **48** was attained in 92% yield, after the removal of tertiary alcohol via its elimination of acetone under strong basic conditions in toluene reflux (**Scheme 9**).¹⁰¹ Deprotection to give terminal alkyne was confirmed from the absence of signals for the methyl protons and carbons. Presence of a singlet at 3.01 ppm in the ¹H NMR was consistent with the CH proton of acetylene, whereas, in the ¹³C NMR spectrum, the terminal carbon signal was observed at 79.57 ppm. The significant upfield shift of terminal

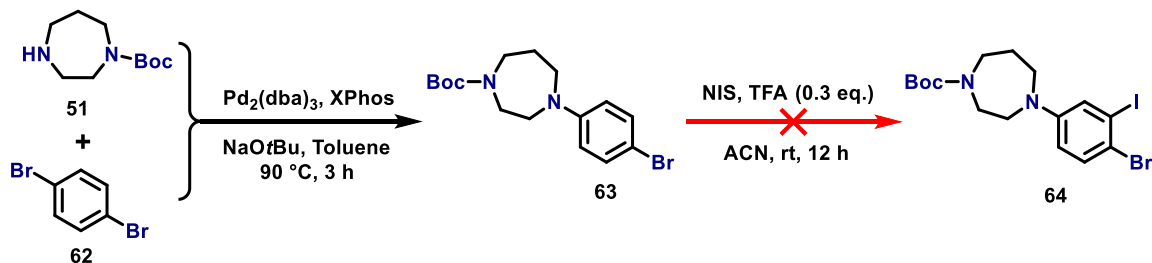
acetylene carbon from 92.86 to 79.57 ppm was attributed to the lack of deshielding effect due to the removal of electron-withdrawing hydroxyl group. A strong absorption band at 3286.61 cm^{-1} for the CH-group of acetylene further confirmed deprotection.



Scheme 10: Deprotection of the Boc-group gave disubstituted compound **61**.

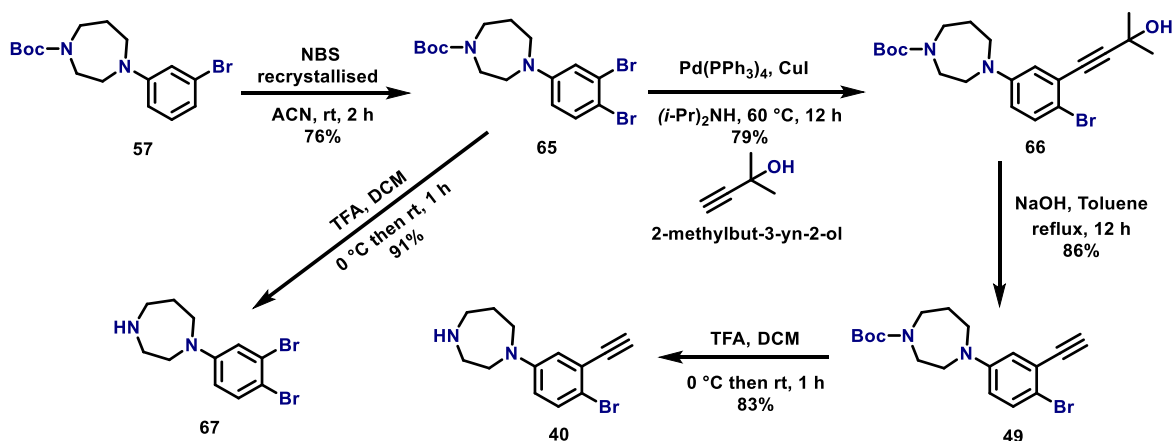
Alkyne deprotection was followed by deprotection of Boc-group (**Scheme 9**) using TFA to yield **39** (Hybrid 3). Since disubstituted compound **58** was formed as a by-product of the earlier Buchwald-Hartwig cross-coupling reaction to probe its interaction with the binding site, it was also deprotected to yield compound **61** (**Scheme 10**). The deprotection step leading to formation of Hybrid 3 (**39**) and disubstituted compound **61** was confirmed from the absence of Boc-group protons and carbons in their respective ^1H and ^{13}C NMR spectra.

Hybrid 4



Scheme 11: Attempted NIS iodination at the meta-position to diazepane in compound **63**.

Synthesis of Hybrid 4 (**40**) was procured in similar ways to Hybrid 3 but with an additional bromination step. In the first attempt, installation of the iodo-group at the third position of 1,4-dibromobenzene **63** was trialled, but no conversion of starting material was observed (**Scheme 11**). *N*-Iodosuccinimide (NIS) under acidic conditions was used in an attempt to access the iodo-group, but this could have resulted in Boc deprotection, thus, capturing the generated iodonium electrophile, as described previously.¹⁰² Also, trapping of iodonium ion further reduced the probability of iodinating the less-electrophilic *meta*-position.



Scheme 12: Synthesis of Hybrid 4 (**40**) via regioselective Sonogashira cross-coupling.

In the literature, 3,4-dibromoaniline is observed to undergo regioselective ethynylation at the *meta*-bromine.¹⁰³ The electron-donating amine increases electron density at the *para*-bromine, leaving the adjacent *meta*-bromine more electrophilic towards the Sonogashira reaction. A similar principle could be applied to the dibromo compound **65** obtained from the bromination of **57**. Using previously optimised Sonogashira conditions, the dibromo derivative **65** did undergo regioselective ethynylation at the *meta*-position to install alkyne **66** in high yields. Hybrid 4 (**40**) was then accessed after the removal of both protecting groups (**Scheme 12**).

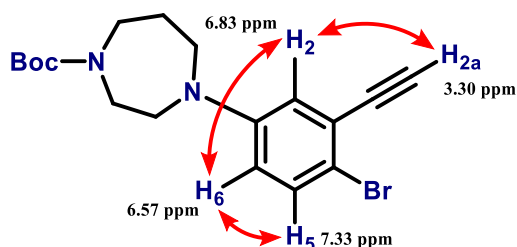


Fig. 2.30: Key *nOe* interactions (red arrows) confirms alkynylation at the 3rd position.

Regioselective ethynylation was confirmed from 2D NMR and 1D *nOe* experiments. In HMBC, a strong correlation was visible between H₂ and C_{1a} as well as H_{2a} and C₂, while a moderate correlation between H₅ and C_{1a} was observed. The 1D NOE experiment displayed interactions between acetylenic and aromatic protons that were consistent with the proposed regioselective substitution (**Fig. 2.30**). Interactions between protons H_{2a} and H₂, H₂ and H₆ as well as H₆ and H₅ were observed, confirming acetylene at more electrophilic C₃ position.

Additionally, dibromo derivative **67** was obtained after deprotection of compound **65** (Scheme 12) and submitted for bioactivity to explore its interaction with the binding site.

Mechanism of Sonogashira Cross-Coupling

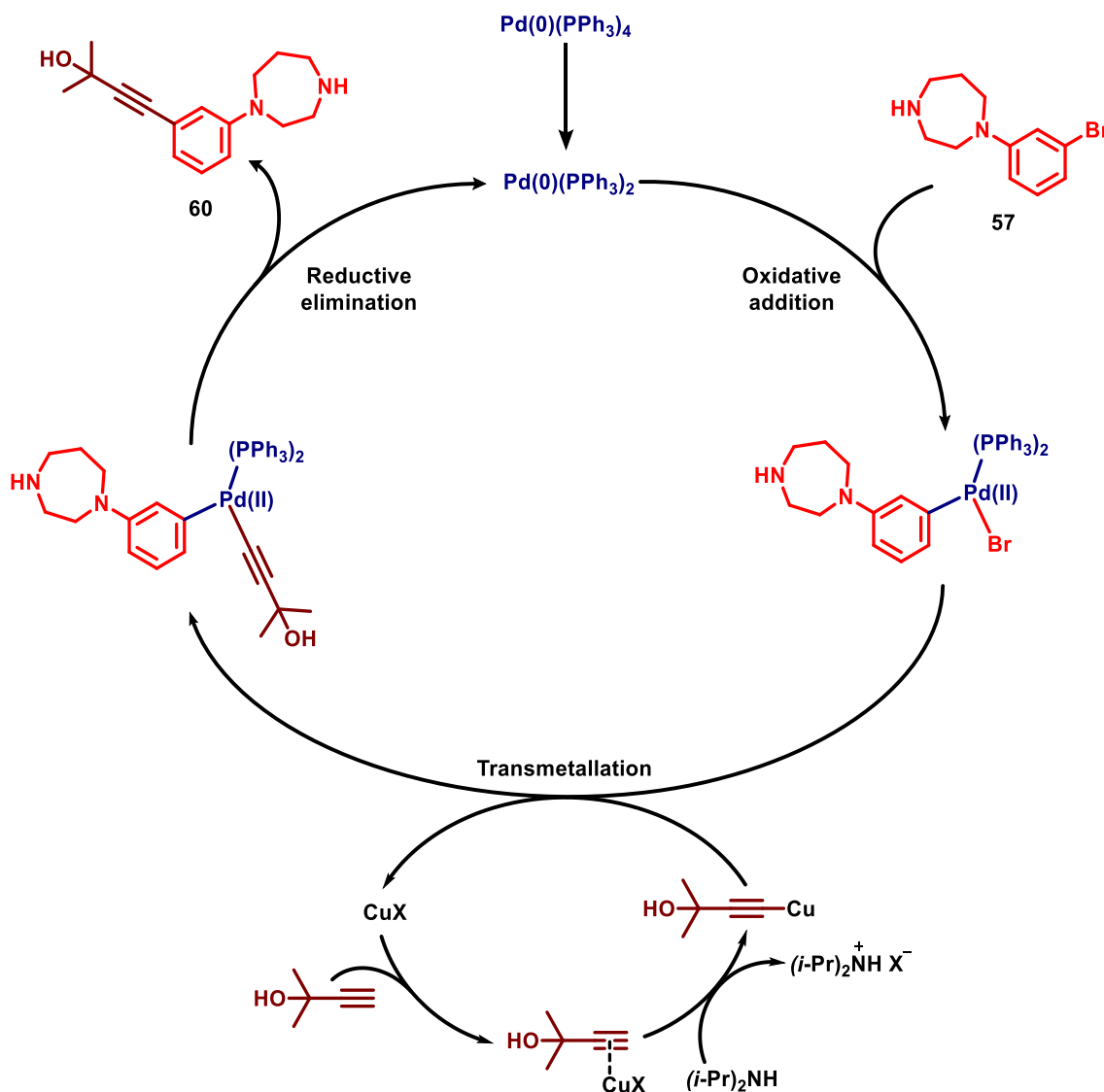
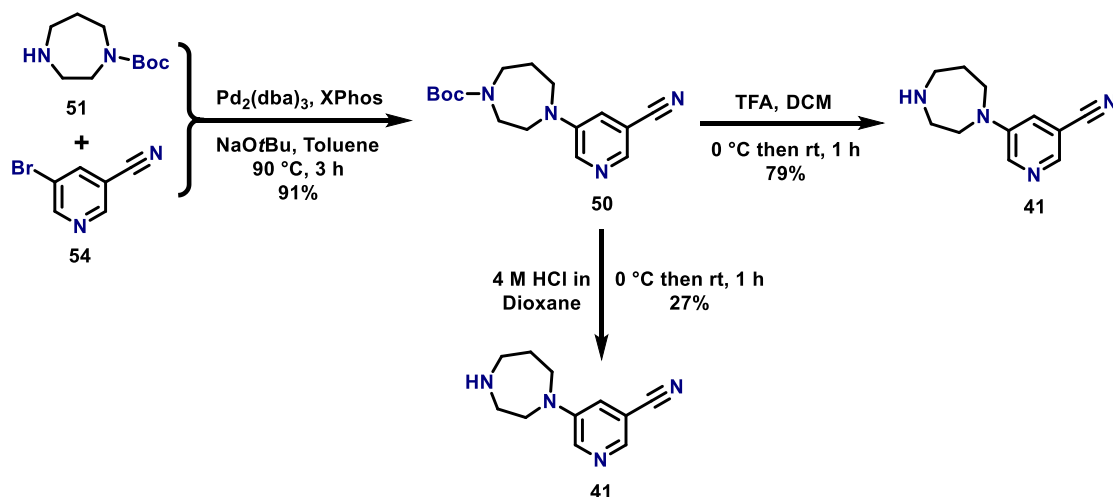


Fig. 2.31: Mechanism of Pd-CuI catalyzed Sonogashira cross-coupling, $X = \text{I or Br}$.⁹⁵

To describe the cross-coupling mechanism, the synthesis of compound **46** is taken here as an example and represented in the image above (Fig. 2.31). The $\text{Pd(PPh}_3)_4$ is an active Pd(0) catalyst and directly enters the catalytic cycle. In the first step, the $\text{Pd(0)(PPh}_3)_2$ species undergoes oxidative addition with the aryl halide (ArX) **56** to form $\text{Ar(X)-Pd(II)(PPh}_3)_2$ complex. Transmetalation with copper-acetylide complex, which is produced by deprotonation of alkyne by diisopropylamine [$(i\text{-Pr})_2\text{NH}$] base, generates the $\text{(Ar)[Acetylide]-Pd(II)(PPh}_3)_2$ species. Finally, $\text{Pd(II)(PPh}_3)_2$ -aryl acetylide complex

undergoes reductive elimination to form the C(sp²)-C(sp) bond between phenyl of **56** and alkyne to yield the cross-coupled product **60** and regenerates the initially formed Pd(0)(PPh₃)₂ complex.^{95, 100}

Hybrid 5



Scheme 13: Synthesis of Hybrid 5 (**41**) via Buchwald-Hartwig cross-coupling.

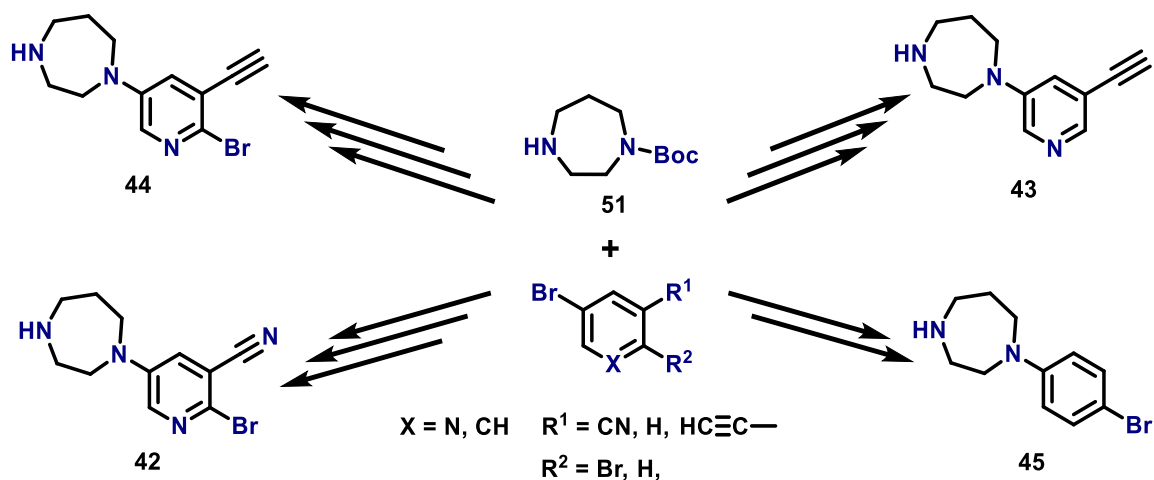
Finally, Hybrid 5 (**41**) was achieved using the same procedure as described during the synthesis of hybrid 1 (**37**). However, it was the first hybrid to be synthesised at the start of this project, so two different procedures were employed for the Boc deprotection (**Scheme 13**). In the first trial, 4 M HCl in dioxane was used in stoichiometric amounts to remove the Boc-group. However, the formation of water-soluble pyridine salts made the extraction process difficult, leading to lowered yields. Finally, a trial with TFA didn't form any water-soluble salts with pyridine, thus, high yields of the final compound **41** were isolated.

Three distinct signals at 8.29, 8.16 and 7.11 ppm in the ¹H NMR were consistent with three pyridine protons and five signals in the aliphatic region which were equivalent to 10 protons of diazepane of Hybrid 5. A signal observed at 117.74 ppm in ¹³C NMR was consistent with the presence of nitrile group at 3rd position, which was further confirmed by sharp stretching at 2231.30 cm⁻¹ in the IR spectrum.

Hybrids 6-9

Since, the synthesis of Hybrids 6-9 (**42-45**) was carried out by a co-worker, only a brief outline has been provided (**Scheme 14**). All the four compounds were synthesised in similar

ways as discussed previously for Hybrids 1-5 (**37-41**). Optimised Buchwald-Hartwig conditions were employed for the coupling of *N*-Boc homopiperazine **51** with substituted aryl halides, followed by acid-mediated deprotection of Boc-group to give title compounds. Bromination of compound **42** and **44** was carried out using *N*-Bromosuccinimide. Similarly, acetylene moiety on compound **43** and **44** were installed via an additional step of pre-optimised Sonogashira coupling conditions. Intermediate and final compounds (**42-45**) were purified through flash chromatography and confirmed using ^1H and ^{13}C NMR, FTIR and mass spectrometry techniques.



Scheme 14: Concise synthetic scheme of Hybrids 6-9 (**42-45**).

All the synthesised hybrids and miscellaneous compounds were then tested for biological activity. The results and experimental process are discussed in the next section along with the effect of different substitutions.

2.2.4. BIOLOGICAL EVALUATION OF HYBRIDS

Radioligand Binding Assay

Ligands possessing a high affinity for the receptors are radiolabelled with isotopes such as tritium (^3H) and are later used as radioligands to determine the binding affinity of the experimental compounds. The binding affinity of a radioligand is determined by a saturation assay, in which a radioligand in varying concentrations is incubated until equilibration, after which the total bound ligand is separated and analysed. Similarly, non-specific binding is obtained by incubating an excess of unlabelled ligand, such as nicotine. The results are compared, and the difference between the total binding and non-specific gives the specific binding of radioligand. This leads to the determination of affinity of test compounds by a competition assay, in which the displacement of a fixed concentration of radioligand is measured by varying concentrations of unlabelled test compounds.⁸⁸

Functional Assay

Ligands, whether they are agonists (full or partial) or antagonists at specific receptors, are determined by two-electrode voltage clamp (TEVC) electrophysiology. This determines the efficacy and potency of ligands by measuring the amount of current generated on binding of the ligand to the receptors expressed on a large cell surface. Generally, *Xenopus laevis* oocytes are injected with varied ratios of $\alpha 4:\beta 2$ subunit cRNA. to express receptors on its cell surface. Two electrodes are clamped to the cell surface in a customised recording chamber. One electrode is coupled to the cell at a given membrane potential while the other measures the amount of current generated due to passage of ions when the receptors are activated on ligand application.⁸⁸

Results and Discussion

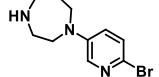
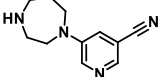
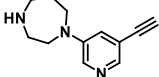
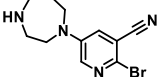
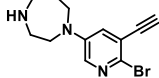
The synthesised compounds were tested by our collaborator Dr. Thomas Balle at the University of Sydney. Both the assays were conducted on three different receptor constructs expressed on the *Xenopus* oocytes: $2\alpha:3\beta$, $3\alpha:2\beta$ and $2\alpha:3\beta^{(\text{HQT})}$ receptors. However, the results for $\alpha 4\beta 2^{(\text{HQT})}$ receptors were incomplete, thus, they have not been included as part of the discussion. The main intention of the biological testing was to determine whether increased selectivity or high efficacy and potency at the $(\alpha 4)_3(\beta 2)_2$ receptors was achieved by constructing the hybrids with shared structural features of NS9283 and NS3920.

Both the tables (**Table 3 and 4**) displaying biological activity of hybrid compounds at $2\alpha:3\beta$ and $3\alpha:2\beta$ receptors, are discussed on three parameters. The first parameter K_i defines the binding affinity of hybrid compounds at both the receptor isoforms. The other two parameters, EC_{50} and I_{max} , describe the functional profile of the compounds i.e., potency and efficacy, respectively. The last column discusses the selectivity of hybrids at 3:2 or 2:3 by determining the ratio of potency at the two isoforms.

Pyridyl Hybrids:

The pyridyl hybrids displayed slightly higher potency at 2:3 receptors compared to the standard NS3920 compound, but an opposite trend was observed at 3:2 isoforms, since a decrease in potency was observed for all the compounds. However, the brominated compounds demonstrated slightly better potency at the $(\alpha_4)_3(\beta_2)_2$ receptors than their non-brominated analogues. In terms of selectivity, none of the pyridine compounds showed greater potency ratio value than NS3920 with 0.429, thus, the compounds showed no preference for 3:2 isoforms over 2:3.

Table 3: Binding and functional assay of pyridyl hybrids, K_i = binding affinity, EC_{50} = potency and I_{max} = efficacy.

Hybrid No.	Compounds	$\alpha_4\beta_2$ (2:3)			$\alpha_4\beta_2$ (3:2)			2:3/3:2 (EC_{50})
		K_i (μ M)	EC_{50} (μ M)	I_{max} (%)	K_i (μ M)	EC_{50} (μ M)	I_{max} (%)	
NS3920		3.66E-05	0.06	62	0.06408	0.14	151	0.429
5		3.50E-05	0.025	31	3.34	9.5	76	0.003
7		1.84E-05	0.014	41	2.11	1.00	30	0.014
6		1.53E-05	0.01	64		0.44	168	0.023
8		0.0241	0.042	96		0.78	100	0.054

Similarly, an overall decline in the efficacy was observed for all the compounds at both 2:3 and 3:2 receptors. The only exception was the bromonitrile hybrid 6 that showed slightly better efficacy than standard NS3920 and other pyridyl compounds at 3:2 isoform. Parallel to potency data, the brominated compounds exhibited better efficacy than non-brominated

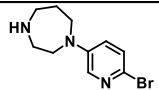
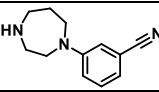
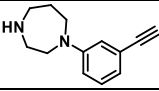
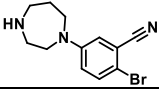
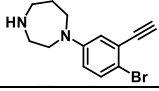
hybrids, at both the $3\alpha:2\beta$ and $2\alpha:3\beta$ receptors. The incomplete binding data for $(\alpha 4)_3(\beta 2)_2$ receptors rendered it difficult to interpret. Although, the binding values for all hybrids except hybrid 8, were found to be better than the standard NS3920 compound at the $2\alpha:3\beta$ receptors.

An interesting observation was made on comparing the efficacy data of acetylene and nitrile containing hybrids at both the isoforms. At the 2:3 receptor, acetylene substituted compounds displayed slightly higher efficacy than the nitrile derivatives. On the contrary, nitrile compounds expressed better efficacy than their acetylene analogues at $3\alpha:2\beta$ receptors. This suggests that presence of polar substituents at 5th position could hold the key towards achieving better selectivity at $(\alpha 4)_3(\beta 2)_2$ receptors over their 2:3 isoform.

Phenyl Hybrids:

The replacement of pyridyl to phenyl ring had a detrimental effect on the functional profile of phenyl hybrids. The compounds demonstrated poor potency at both the 2:3 and $3\alpha:2\beta$ receptors when compared to standard NS3920. Even in terms of efficacy, none of the compounds displayed a better profile at the two isoforms. Overall, the selectivity displayed by phenyl hybrids at the 3:2 over 2:3 receptors was still low, except for the bromonitrile derivative which had almost equal potency at both isoforms but greater selectivity profile than NS3920, while the efficacy was better at the $3\alpha:2\beta$ isoform than $2\alpha:3\beta$ receptors.

Table 4: Binding and functional assay of phenyl hybrids, K_i = binding affinity, EC_{50} = potency and I_{max} = efficacy.

Hybrid No.	Compounds	$\alpha 4\beta 2$ (2:3)			$\alpha 4\beta 2$ (3:2)			2:3/3:2 (EC_{50})
		K_i (μ M)	EC_{50} (μ M)	I_{max} (%)	K_i (μ M)	EC_{50} (μ M)	I_{max} (%)	
NS3920		3.66E-05	0.06	62	0.06408	0.14	151	0.429
1		8.71E-03	1.5	11	44.93	6.8	17	0.221
3		8.58E-02	4.7	2.3	61.36	12	1.5	0.392
2		1.61E-02	7.4	11	5.879	8.1	44	0.914
4		0.1654			17.32			

The binding data was also not encouraging, and all the compounds had a low binding affinity for the 2:3 receptors and even poorer trends for the 3:2 isoform. Nonetheless, an interesting pattern was inferred between the brominated and non-brominated analogues. The brominated hybrids exhibited a better affinity for the $(\alpha 4)_3(\beta 2)_2$ receptors than the non-brominated derivatives, while vice-versa was true for the 2:3 receptors. Similarly, nitrile substituted compounds had better affinity for both the isoforms over the acetylene hybrids.

Overall, the binding and functional data obtained for all the hybrids showed that none of the analogues demonstrated better potency or selectivity profile than NS3920. This suggests that the structural features derived from the overlay of NS9283 and NS3920 could not have translated well in the hybrids and the interactions we were expecting, may not have been established. This could perhaps be due to the incorrect binding pose for NS9283 as well as NS3920 compounds because the crystal structures were obtained from *Ls*-AChBP and not the $\alpha 4\beta 2$ receptors or its two stoichiometries. As discussed before, the water molecule present in the crystal structure of *Ls*-AChBP which mediates the bridge between complementary side residues and ligand, is absent in the orthosteric site of $\alpha 4\beta 2$ receptors as observed from its crystal structure. Therefore, the exact binding mode of both the compounds and their interactions with the binding site residues may not be correct and thus, led to the inaccurate hybrid design and poor biological profiles.

2.3. DESIGN OF SUBSTITUTED PYRIDINES

2.3.1. PROJECT AIMS

In the available literature and the work carried out previously in the group, several substituted pyridine-diazepane compounds have been synthesised, displaying variable activity at the $(\alpha_4)_3(\beta_2)_2$ receptors. Generally, mono 5- and 6-substitutions as well as di-substitutions at the pyridine ring have shown a promising biological activity, but good tolerance is only exhibited with smaller groups like halogens, nitro, amine, small chain alkyl, ethers and others. The substituents at the 6th position are known to affect the efficacy and potency, while groups at the 5th position affect the binding affinity of agonists.^{85,90} The lack of correlation between biological activities of previously evaluated agonists to establish a precise structure-activity relationship, led to the design of the following pyridine-diazepane compounds **68-70**. According to the unpublished evaluation carried out formerly in the group, trifluoromethyl analogue of **68** and ethoxy derivative of **70** showed only 3-6 fold potency difference at $2\alpha:3\beta$ over $3\alpha:2\beta$ isoform. This directed the design of structures **68** and **70**, which was completed with assistance from a summer scholar. Dihalogenated compound **69** was carryover research from a previous co-worker to complete the list of halogenated pyridines and establish their effect on biological activity (Fig. 2.32).

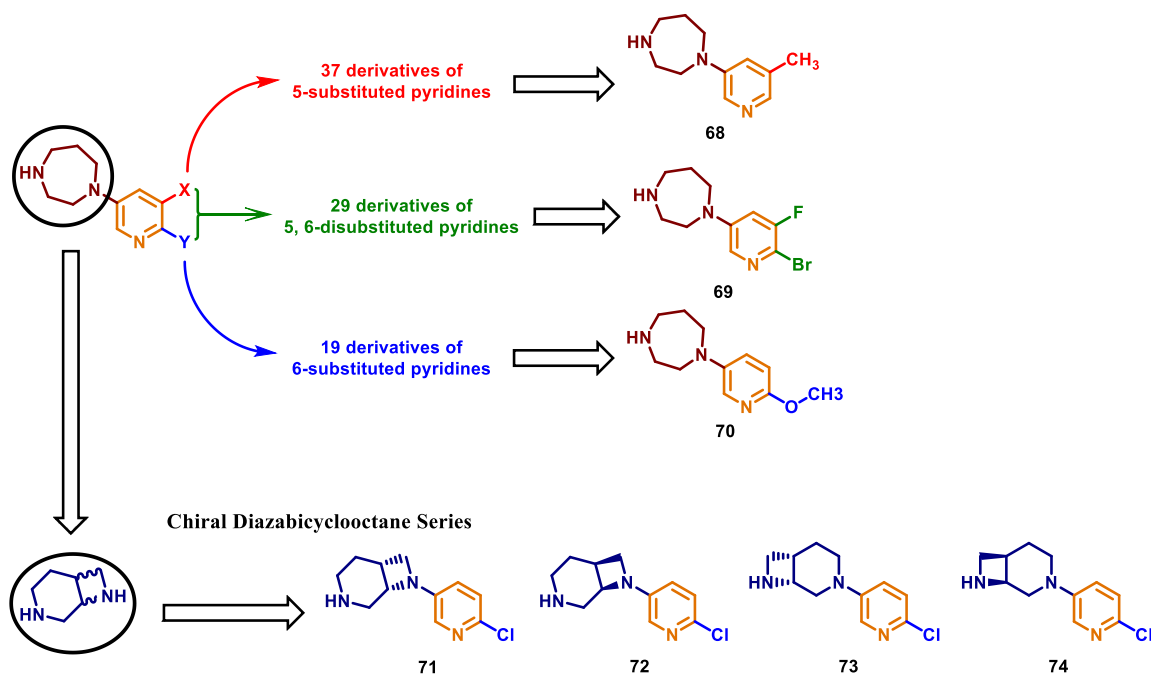
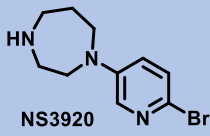
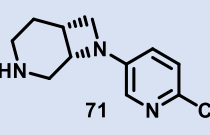
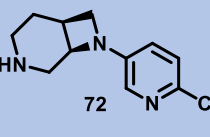
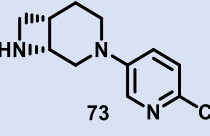
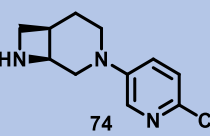


Fig. 2.32: Design of mono- and di-substituted pyridines linked with either, diazepam or chiral diazabicyclooctane ring.

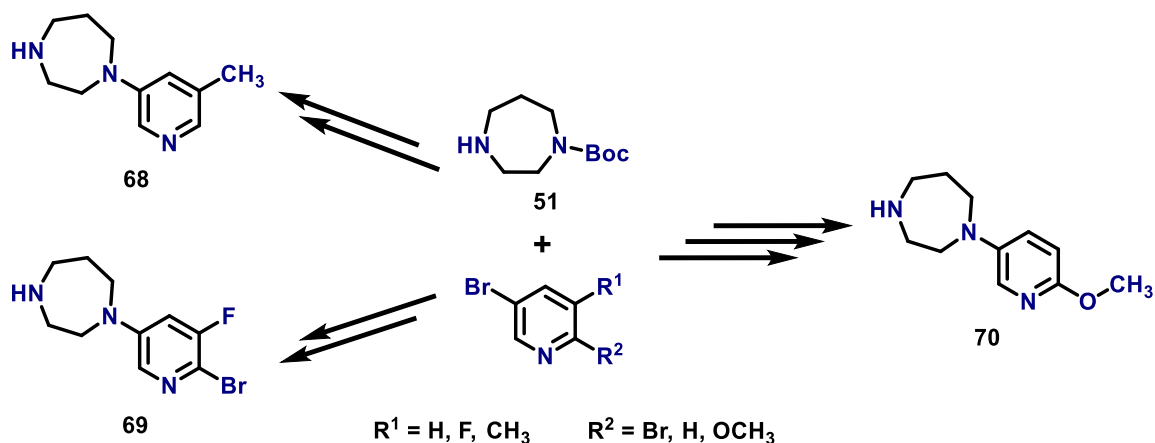
The rigidified chiral 3,8-diazabicyclo[4.2.0]octane substituted compounds were identified by a former student during the literature search to design novel compounds with close resemblance to known agonists.¹⁰⁴ The diazabicyclooctane ring possessed two well-defined structural features, a secondary nitrogen forming the crucial ammonium pharmacophore and an amine-containing ring that was larger than nicotine. The increased ring size is known to afford strong binding affinities, like NS3920. However, diazabicycloheptane¹⁰⁵ and spirocyclic diamines¹⁰⁶ were also examined for replacing diazepane ring, but the stereochemically rich and strained diazabicyclooctane ring linked to substituted pyridine showed a remarkable activity at the mixed population of $\alpha 4\beta 2$ receptors (**Table 5**). This prompted us to synthesise their chloropyridyl analogues (**Fig. 2.32**) as they may possess functional preference at $(\alpha 4)_3(\beta 2)_2$ receptors over $(\alpha 4)_3(\beta 2)_2$ isoform.

Table 5: Comparison of binding affinities, functional potencies and efficacies of NS3920¹⁰⁷ and four isomers of 3,8-diazabicyclo[4.2.0]octane substituted chloropyridyl analogues¹⁰⁴ at the mixed $\alpha 4\beta 2$ receptor population, as reported in the literature.

S. No.	Compound	K _i (nM)	EC ₅₀ (nM)	I _{max} (%)
1.	 NS3920	1.0	64.57	88
2.	 71	0.80	216	102
3.	 72	0.12	37.4	94
4.	 73	0.032	24	130
5.	 74	0.019	13	114

Since no biological data was received for both series of compounds, their syntheses have been discussed briefly, as it has been completely replicated based on the available literature.

Synthesis of Compounds 68-70



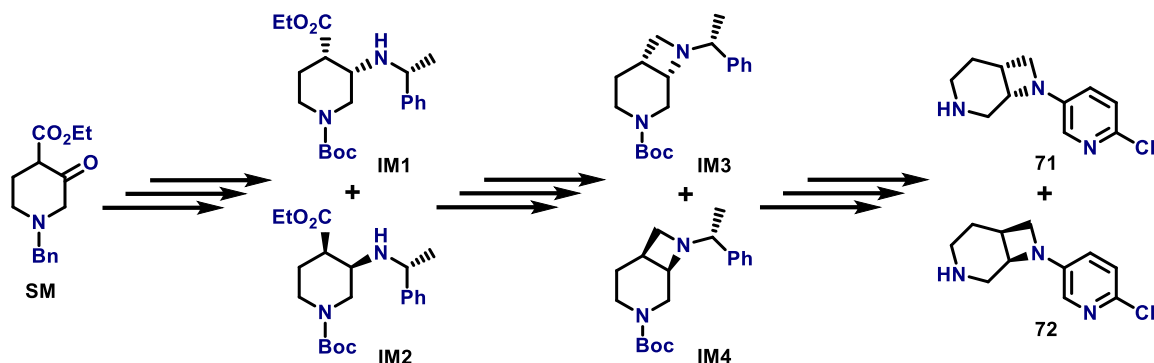
Scheme 15: Concise synthetic scheme of Compounds 68-70.

The core pyridine-diazepane moiety for all the three compounds was synthesised by using the previously optimised Buchwald-Hartwig protocol (**Scheme 15**). Compound **69** required an additional bromination step using NBS under cold conditions to selectively install bromine at the 6th position. Similarly, methoxylation was carried out using sodium methoxide to obtain methoxy substituent at the 6th position for compound **70**. Intermediate and final compounds (**68-70**) were purified through flash chromatography and confirmed using ¹H and ¹³C NMR, FTIR and mass spectrometry techniques.

Synthesis of Chiral Diazabicyclooctane Series (71-72)

The syntheses of target compounds goes via the construction of the integral 3,8-diazabicyclo-[4.2.0]octane core. The four chiral isomers of the bicyclic diamine compounds were accessed through the approach presented in the literature by Frost *et al.*¹⁰⁴ The synthesis has been discussed briefly and a concise scheme has been mentioned below (**Scheme 16**). The starting material (**SM**) oxopiperidine was firstly Boc-protected, following debenzoylation using hydrogenolysis. Subsequently, the chiral ester intermediates (**IM1-2**) were achieved as 1.5:1 mixture through the NaBH(OAc)₃ reduction of enamine double bonds, formed between benzylamine and Boc-oxopiperidine. The protected chiral diazabicyclooctane core (**IM3-4**) was accessed via the LiAlH reduction of esters (**IM1-2**) followed by cyclisation to four-membered azetidine ring via mesylation. The final chiral analogues **71-72** were obtained using the previously optimised Buchwald-Hartwig conditions, employing suitable protection and deprotection steps. Intermediates (**IM1-4**)

and final chiral analogues (**71-72**) were purified through flash chromatography and confirmed using ^1H and ^{13}C NMR, FTIR and mass spectrometry techniques, while optical rotations were determined using polarimetry. The obtained analytical data matched well with the literature data.¹⁰⁴



Scheme 16: Concise synthetic scheme of chiral diazabicyclooctane series **71-72**.

All the synthesised analogues were then sent to the University of Sydney for their biological evaluation.

2.4. CHAPTER CONCLUSION AND FUTURE WORK

This chapter dealt with the design and syntheses of potential agonists, by selectively targeting the $\alpha 4$ - $\alpha 4$ binding site present only in the $(\alpha 4)_3(\beta 2)_2$ nAChRs. The underlying principle towards the design of agonists was based upon exploiting the vital differences in the binding site construct of the $\alpha 4$ - $\alpha 4$ and $\alpha 4$ - $\beta 2$ interfaces and the distinct interactions demonstrated by ligands at both sites. After exhaustive literature review, as well as prior research carried out in the group, two major series of compounds were formulated preserving the essential pharmacophoric features required for agonistic activity (**Fig. 2.33**). The first series comprises the NS9283-NS3920 hybrids and the second series consists of substituted pyridines linked to either diazepane or chiral diazabicyclooctane ring. The common pathway to access both series of derivatives was through Palladium catalysed Buchwald-Hartwig cross-coupling amination followed by deprotection.

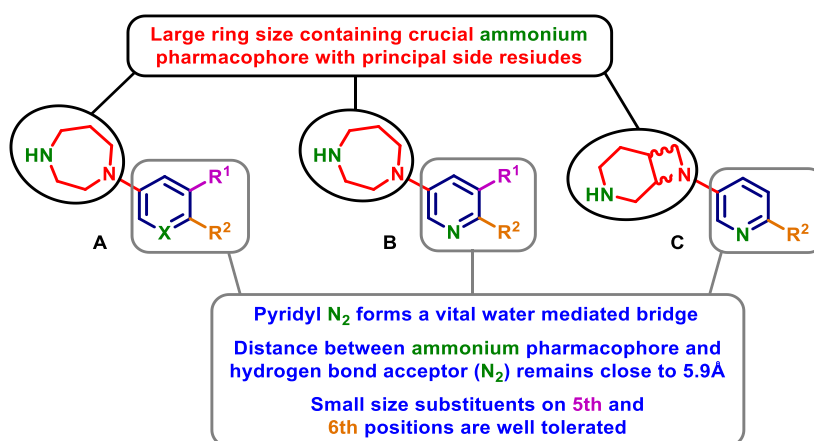


Fig. 2.33: Illustration of designed structures retaining important pharmacophoric features, A, NS9283-NS3920 hybrids ($X = N$ or CH), and substituted pyridines with either B, diazepane, or C, chiral diazabicyclooctane ring.

In total, nine hybrids **37-45** in the first series (**Fig. 2.34**), including four by a former student were designed based on the shared structural features of a modulator and an agonist, i.e. NS9283 and NS3920, respectively. Apart from the abovementioned steps, some target compounds (**38-40**) were achieved through additional steps like bromination and/or Sonogashira cross-coupling to install necessary substituents before the final deprotection step. After the careful choice of a palladium catalyst and alkyne source, Sonogashira cross-coupling was successfully optimised to access acetylene for completing four hybrids (**3-4** and **7-8**). Eventually, all the title compounds were generated in an overall yield of 79-88%.

Despite the incomplete results from electrophysiology and binding assays at three constructs; $2\alpha:3\beta$, $3\alpha:2\beta$ and $2\alpha:3\beta^{(HQT)}$, some key inferences were drawn from the available data that underscore the rationale behind the design of hybrids. Hydrogen bond acceptor such as pyridyl nitrogen, appeared key to overall better activity while small groups such as bromine, were well tolerated and augmented the overall agonist activity of the ligands at the $(\alpha4)_3(\beta2)_2$ nAChRs. The nitrile group at the *meta*-position imparted low functional selectivity at the $3\alpha:2\beta$ receptors, corroborating its ability to form an inter-subunit bridge in the $\alpha4$ - $\alpha4$ site as known for NS9283. Overall, the pyridyl hybrids were better than the phenyl hybrids, though, none showed preferential selectivity for the 3:2 receptor compared to the standard NS3920 compound.

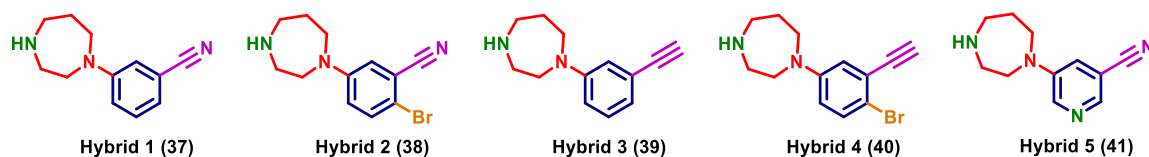


Fig. 2.34: Representation of the pharmacophoric features retained in the structure of hybrids 1-5 synthesised in this research.

In the second series, total of seven compounds were designed but the syntheses of only five derivatives were accomplished. In 1-(pyridin-3-yl)-1,4-diazepane series, the basis for designing compounds **68-70** (Fig. 2.35) was to establish a precise correlation with their structural variants synthesised by past co-workers. The structural variants demonstrated selectivity in terms of potency with minor differences between the two stoichiometries, thus, deeming them fit to develop related compounds and analyse their effect. For the three compounds synthesised, additional steps of methoxylation or bromination were included to install the target-specific substituents. In the synthesis of **69**, the high reactivity of fluoropyridine ring produced mono- as well as di-brominated compounds. However, on lowering the temperature, the strong *para*-directing effect of tertiary amine prevailed over fluorine, yielding only the mono-brominated target compound **69**.

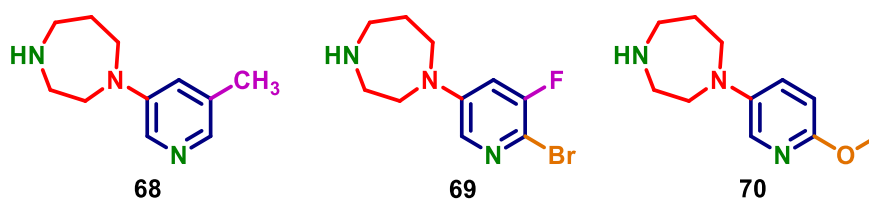


Fig. 2.35: Synthesised 1-(pyridin-3-yl)-1,4-diazepane series compounds.

A rigidified chiral diamine template was identified by a former student during the literature search. The template 3,8-diazabicyclo[4.2.0]octane possessed similar structural features as that of diazepane and was the ideal replacement to link with substituted pyridines. The published research inferred promising activity of 3-/8-(pyridin-3-yl)-3,8-diazabicyclo[4.2.0]octane compounds at the mixed population of $\alpha 4\beta 2$ nAChRs. It was anticipated that the rigidity as well as rich stereochemistry of the diamine ring could offer better selectivity at the $3\alpha:2\beta$ stoichiometry over diazepane. Initially, out of the four most active compounds, two were synthesised to explore their potential and interactions at the two isoforms of $\alpha 4\beta 2$ nAChRs (**Fig. 2.36**). The pre-existing literature procedure with necessary modifications was utilised towards the 8-step syntheses of enantiopure 8-(pyridin-3-yl)-3,8-diazabicyclo[4.2.0]octane compounds. The enantiopure target compounds were accessed from Buchwald-Hartwig cross-coupling followed by Boc-deprotection and have been submitted for biological evaluation.

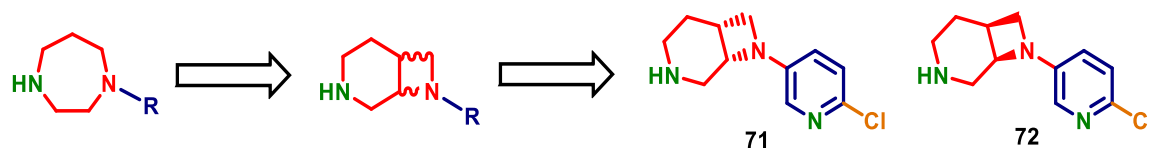


Fig. 2.36: Rationale behind replacing diazepane with diazabicyclooctane and structures of two target compounds synthesised.

Future work on diazepane linked compounds will be based on the complete assessment of biological activity. The results will help in establishing strong structure-activity relationships and accordingly, to make modifications for the development of new compounds. The pyridine ring can be replaced with other heteroaromatic systems, as hydrogen bond acceptor atom in the ring is important for high potency. Further variations with smaller substituents can be made on the aromatic ring, as large groups are generally not well tolerated. Based upon the biological activity mentioned in the literature, the diazabicyclooctane series has the potential to replace diazepane due to its common pharmacophoric features and therefore, should be further explored. The strained ring system with chirality may result in a specific spatial arrangement of ligand in the $\alpha 4-\alpha 4$ binding site and could lead to better selectivity and efficacy.

CHAPTER 3

3. DESIGN OF NOVEL POSITIVE ALLOSTERIC MODULATORS

This chapter focusses on the identification of a new pocket in the $\alpha 4$ - $\alpha 4$ binding site of $(\alpha 4)_3(\beta 2)_2$ nAChRs, followed by the design and development of a novel class of positive allosteric modulators targeting this newly identified site.

3.1. THE $(\alpha 4)_3(\beta 2)_2$ NICOTINIC ACETYLCHOLINE RECEPTOR

The $\alpha 4\beta 2$ nAChRs as discussed previously, is known to occur in two pharmacologically distinct stoichiometries, i.e., $(\alpha 4)_2(\beta 2)_3$ and $(\alpha 4)_3(\beta 2)_2$. Unlike the $2\alpha:3\beta$ receptor, the $3\alpha:2\beta$ stoichiometry possess an additional $\alpha 4$ - $\alpha 4$ binding site apart from the two classical $\alpha 4$ - $\beta 2$ binding sites. The macroscopic currents generated through $(\alpha 4)_2(\beta 2)_3$ receptors are high sensitivity single-phase currents produced at low ACh concentration. However, $(\alpha 4)_3(\beta 2)_2$ stoichiometry displays an intricate picture where, low ACh concentration generates a similar pattern of high sensitivity (HS) currents, while on the application of high ACh concentration, low sensitivity (LS) currents are produced but with higher macroscopic amplitude. Thus, giving rise to a unique biphasic dose-response curve (Fig. 3.1).

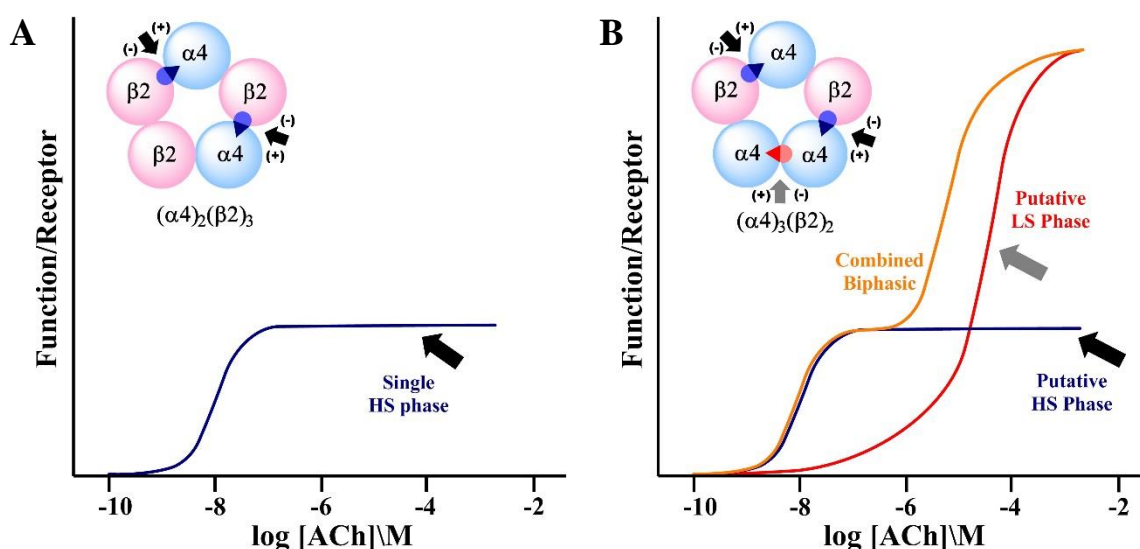


Fig. 3.1: Graphical illustration of $\alpha 4\beta 2$ nAChR stoichiometries. The $(\alpha 4)_2(\beta 2)_3$ isoform displays single HS phase currents (A) while, $(\alpha 4)_3(\beta 2)_2$ isoform displays two putative HS and LS phase currents (B), which combine to show a biphasic dose-response curve.¹⁰⁸

The $\alpha 4$ - $\alpha 4$ agonist binding site inherently influences the biphasic response of $(\alpha 4)_3(\beta 2)_2$ stoichiometry, generating functional differences between the two receptors. However, the unique $\alpha 4$ - $\alpha 4$ binding site in the $3\alpha:2\beta$ stoichiometry has remained largely unexplored in

drug discovery, attributed to the complexity associated with the ($\alpha 4$)₃($\beta 2$)₂ stoichiometry functions and its engagement with the ligands. Since the full therapeutic potential of ($\alpha 4$)₃($\beta 2$)₂ receptor still eludes the scientific community, it is imperative to first understand its distinct channel properties and how the $\alpha 4$ - $\alpha 4$ binding site affects function, to design and develop ligands targeting the LS isoform.

3.1.1. IDENTIFICATION OF NEW POCKET IN THE $\alpha 4$ - $\alpha 4$ SUBUNIT INTERFACE

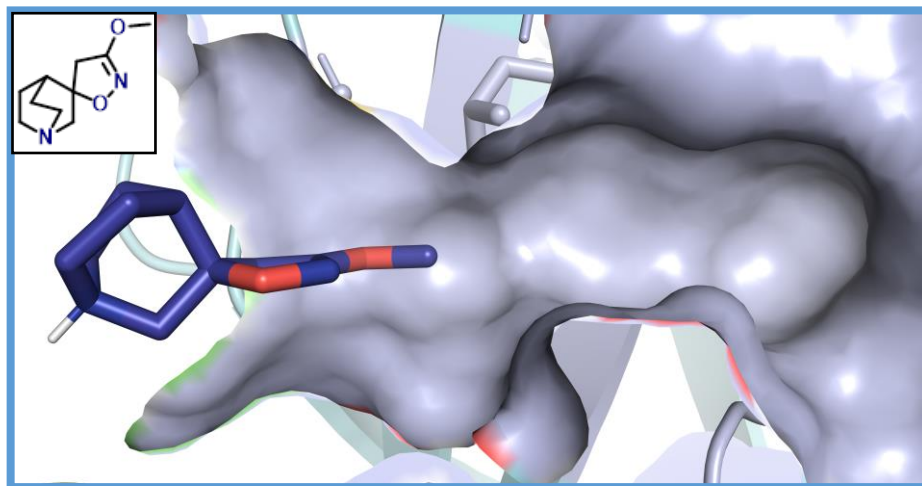


Fig. 3.2: Recognition of a new pocket (grey surface) in the $\alpha 4$ - $\alpha 4$ interface on analysing the ($\alpha 4$)₃($\beta 2$)₂ homology model derived from the *Ls*-AChBP^{HQT} receptor bound⁶³ with ICH3 ligand (deep blue, structure in box),¹⁰⁹ a spirocyclic quinuclidine-isoxazoline $\alpha 7$ agonist.

The research carried out by our collaborator Dr. Thomas Balle at the University of Sydney, in studying the biophysical differences between the two stoichiometries led to an enhanced understanding of the $\alpha 4$ - $\alpha 4$ binding site. The analysis of an ($\alpha 4$)₃($\beta 2$)₂ homology model derived from the *Ls*-AChBP^{HQT} binding protein⁶³ with the $\alpha 7$ nAChR agonist ICH3 bound, identified a novel pocket in proximity to the $\alpha 4$ - $\alpha 4$ binding site (**Fig. 3.2**). The *Ls*-AChBP^{HQT} binding protein was mutated to resemble the $\alpha 4$ - $\alpha 4$ interface, while the ICH3 ligand is a spirocyclic quinuclidine-isoxazoline $\alpha 7$ nAChR agonist.¹⁰⁹ The identification of this new pocket is an important revelation, as the identified pocket is absent in the $\alpha 4$ - $\beta 2$ binding site and therefore, any ligand interaction in the $\alpha 4$ - $\alpha 4$ site could result in energy transduction to the residues responsible for channel gating and opening. This will not only prove beneficial in our endeavour to design and develop selective $\alpha 4$ - $\alpha 4$ ligands but will also pave a way for mechanistic investigation of ($\alpha 4$)₃($\beta 2$)₂ receptor activation and understanding its unique functional properties.

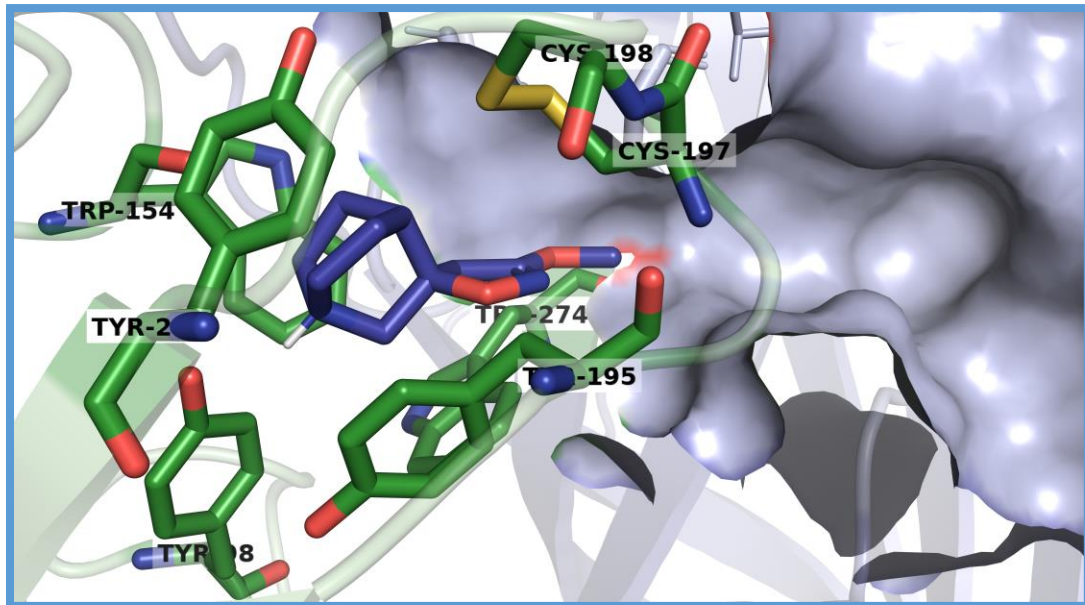


Fig. 3.3: The new pocket (grey, surface) in the $\alpha 4$ - $\alpha 4$ interface is in proximity to the binding site's conserved set of five 'aromatic cage' residues and the cysteine pair capping from the top (green, sticks), with ICH3 ligand¹⁰⁹ (deep blue, sticks) bound in the aromatic cage with isoxazoline directed towards the pocket.

The most intriguing detail associated with this finding is the location of a new pocket adjacent to the $\alpha 4$ - $\alpha 4$ binding site that forms a small void or extension of the typical orthosteric binding site. The amino acids lining the architectural construct of the new pocket are contributed from the $\alpha 4$ (-) side of the subunit interface, and are as follows: Glu196, Gly253, Leu254, Ser255, Trp274, Lys276, Thr338, Met380, His381, Arg383, Val384, Asp385 and Tyr421. The unique $\alpha 4$ - $\alpha 4$ binding site could be thus, envisaged as; a conserved set of five 'aromatic cage' residues with cysteine pair capping from the top and an assortment of amino acids arranging to form a 'hidden tunnel' like construct (**Fig. 3.3**). Therefore, a ligand that can bind with the 'aromatic cage' residues and further extends itself into the pocket, may result in selective binding to the $\alpha 4$ - $\alpha 4$ binding site to promote channel gating and opening, or may lead to a complete blockade of the binding site. However, it will be interesting to investigate whether the residues lining the pocket have any role in the overall conformational changes that occur on ligand binding to the receptor site, or they only act as a 'space to be filled' to achieve selectivity.

As discussed in previous chapters, the $(\alpha 4)_3(\beta 2)_2$ nAChRs harbour three binding sites; one low-affinity site at the $\alpha 4$ - $\alpha 4$ interface and two high-affinity sites at the $\alpha 4$ - $\beta 2$ interfaces. These binding sites hold the standard set of five conserved 'aromatic cage' residues and

cysteine pair capping, but the difference arises from the complementary (-) side of subunit interface, which may be exploited for the design of selective $\alpha 4$ - $\alpha 4$ ligands. The pocket described above in the $\alpha 4$ - $\alpha 4$ interface is not observed in the $\alpha 4$ - $\beta 2$ interface due to the presence of one amino acid; i.e., Met250 in the $\beta 2$ (-) side of the subunit interface (**Fig. 3.4**). The Met250 residue is positioned in a way that it acts to block the pocket in the $\alpha 4$ - $\beta 2$ interface and consequently, may not allow enough space for ligand interaction if it is large. Therefore, this intriguing difference between the two interfaces provides an attractive opportunity to develop ligands that can be accommodated into the pocket, leading to selective binding and interaction at the $\alpha 4$ - $\alpha 4$ interface site.

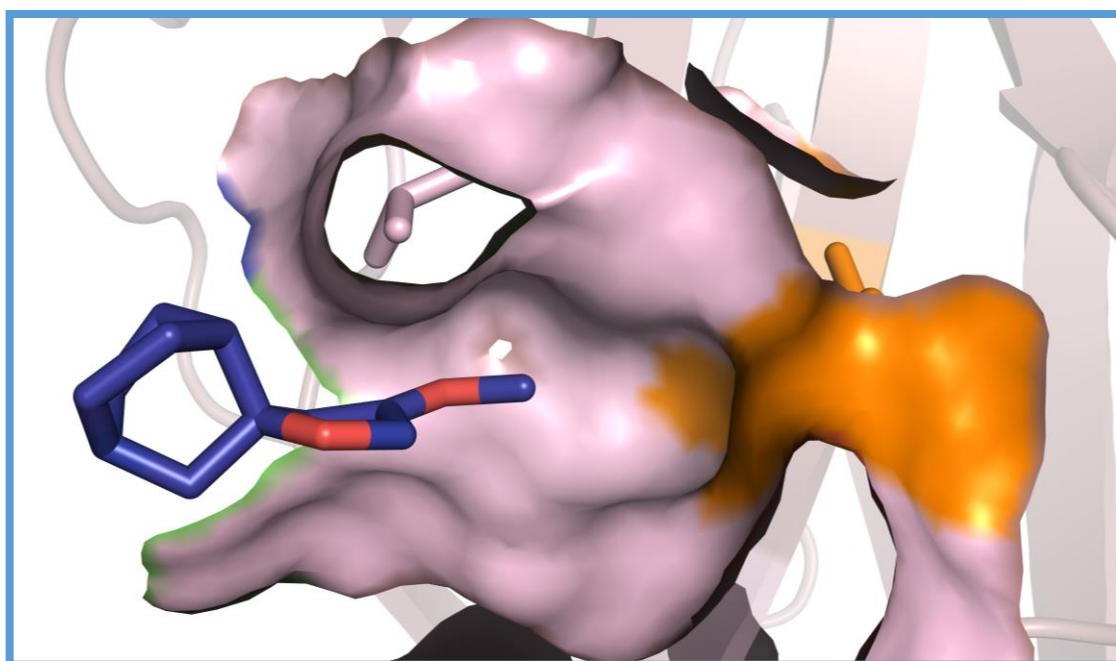


Fig. 3.4: No pocket (light pink, surface) is observed in the $\alpha 4$ - $\beta 2$ interface, as presence of Met250 (orange surface) residue practically blocks the space witnessed in the $\alpha 4$ - $\alpha 4$ interface and for larger ligand it is likely to disfavor ligand interaction.

Since homology modelling studies were done using the *Ls*-AChBP^{HQT} and not the ($\alpha 4$)₃($\beta 2$)₂ nAChR that harbours the original $\alpha 4$ - $\alpha 4$ interface, conclusions derived from analysing the identified pocket should be carefully assessed. Although, some extremely fascinating and encouraging details were deduced from the study that does provide further motivation and ideas to design site-selective ligands for the $\alpha 4$ - $\alpha 4$ interface.

3.1.2. TARGETING THE NEWLY RECOGNISED SITE IN THE $\alpha 4$ - $\alpha 4$ INTERFACE

The full response of $(\alpha 4)_3(\beta 2)_2$ nAChRs can only be achieved through ligand interaction at both $\alpha 4$ - $\beta 2$ and $\alpha 4$ - $\alpha 4$ binding sites. It has already been discussed that the $\alpha 4$ - $\beta 2$ site can be activated at low agonist concentration resulting in sub-maximal receptor response. However, maximal functional activity of 3:2 stoichiometry is only attained via simultaneous activation of the $\alpha 4$ - $\alpha 4$ binding site either by high agonist levels, or PAM binding to lower the required agonist threshold. The recognised pocket proximal to the $\alpha 4$ - $\alpha 4$ binding site in the subunit interface, is an attractive target for devising ligands that will selectively modulate the $(\alpha 4)_3(\beta 2)_2$ nAChRs.

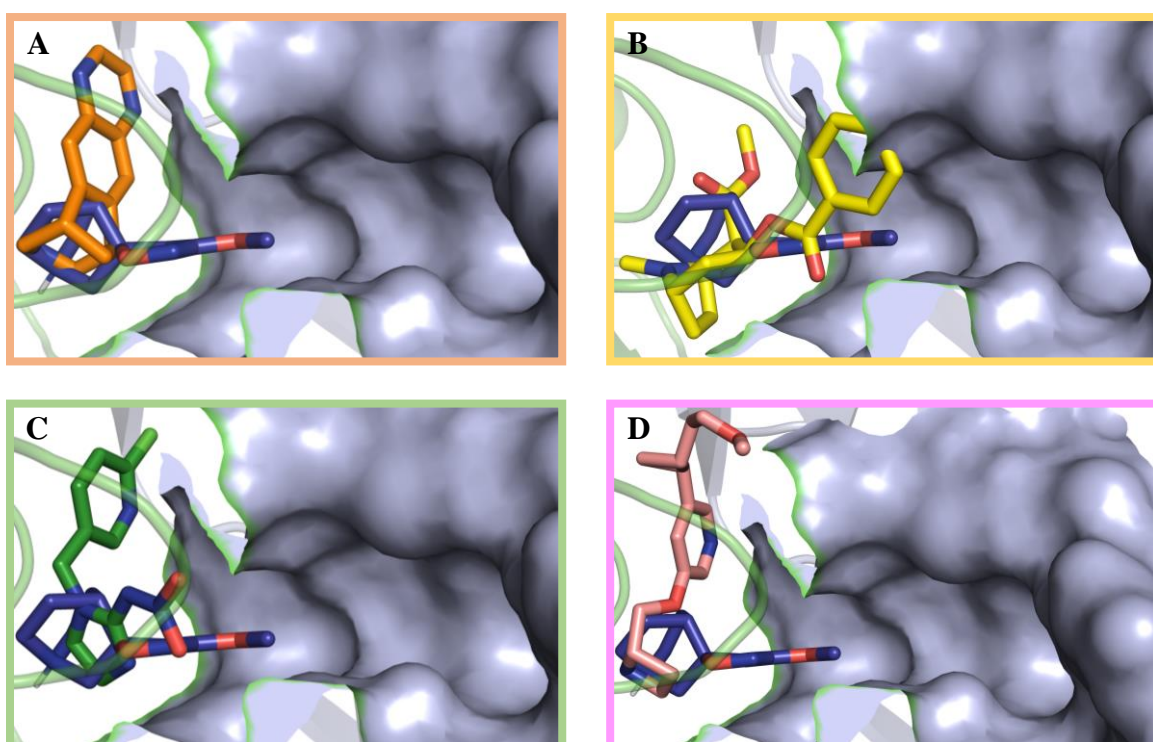


Fig. 3.5: Structural overlay of the $\alpha 4$ - $\alpha 4$ binding site homology model with co-crystallised ligands directing substituents towards the pocket. The ICH3 ligand¹⁰⁹ is shown overlapping with some selected eight ligands: **A-** Varenicline (PDB 4AFT),¹¹⁰ **B-** Cocaine (PDB 2PGZ),¹¹¹ **C-** Imidacloprid (PDB 2ZJU)¹¹² and **D-** Sazetididine analogue (PDB 4FRR)¹¹³.

To identify prospective templates for ligand development with a focus on designing PAM type molecules, several co-crystallised structures (>50) of diverse nAChR ligands were analysed by overlaying them with the $\alpha 4$ - $\alpha 4$ binding site homology model displaying the identified pocket. The co-crystal structures utilised for evaluation were bound to either $\alpha 4\beta 2/\alpha 7$ agonists, modulators or nicotinic insecticides. Out of numerous co-crystal ligands

that were superimposed with the homology model, eight best fits were selected for more detailed analysis after an initial screening. Orientation of ligands was the first condition for screening, as all the ligands (8) chosen had a bond vector directed towards the pocket similar to the ICH3 compound (**Fig. 3.5**). The reason for choosing known nAChR ligands was to utilise their activity and exploit the directed vector with different substitutions extending into the pocket to improve $\alpha 4$ - $\alpha 4$ site selectivity.

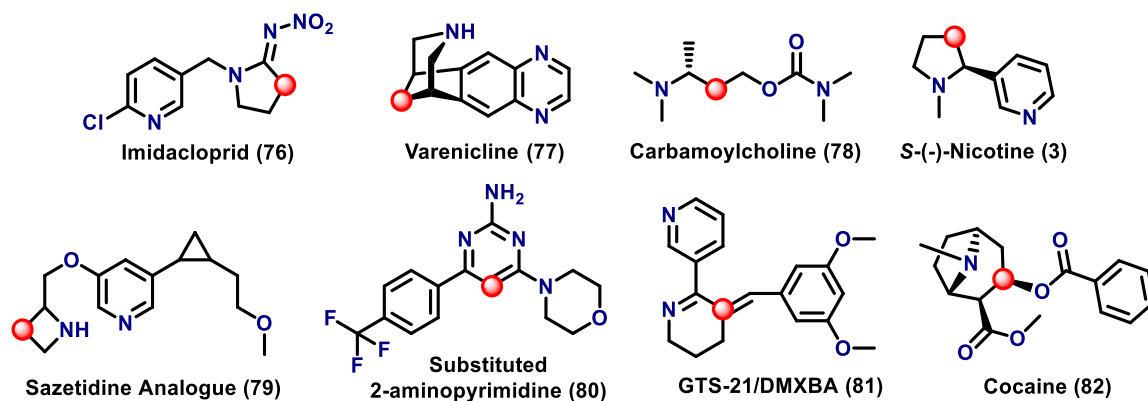


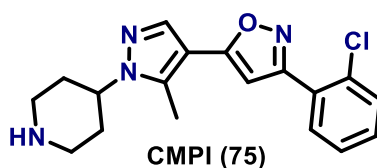
Fig. 3.6: Structure of ligands after initial screening, with red circle displaying their bond vector directed towards the identified pocket.^{17, 110-115}

The final eight ligands selected for a comprehensive study had some well-established molecules like nicotine, varenicline, and others as illustrated above (**Fig. 3.6**). Further screening from the chosen molecules was based upon the following three aspects: intrinsic activity of ligands, presence of secondary or tertiary nitrogen in the structure, and the extent as well as ease of substitutions which can be introduced at the vector position. Based on the above factors, two compounds, nicotine **3** and GTS-21 (DMXBA **81**), were selected as lead constructs for designing novel templates with an assortment of substitutions. The key aspect to consider here is the introduction of those substituents would provide the much required $\alpha 4$ - $\alpha 4$ selectivity by directly fitting into the pocket and interacting with the site residues for better receptor modulation.

Further investigation and detailed analysis of nicotine and GTS-21 is discussed in the subsequent section along with the rationale behind the design of their related analogues. Instead, CMPI is reviewed next, which is a unique ligand known for its potent $\alpha 4\beta 2$ PAM activity. CMPI is an $\alpha 4$ - $\alpha 4$ selective ligand, which on molecular docking exhibited a distinct binding mode in the receptor site compared to other agonists or PAMs.

CMPI – A ($\alpha 4$)₃($\beta 2$)₂ nAChR Selective PAM

The nAChR-selective PAMs are categorised as a novel class of ligands, which induces conformational changes in the receptor on binding to an allosteric site(s) and potentiates the response on ACh binding to the orthosteric sites. The known $\alpha 4\beta 2$ nAChR PAMs to date are CMPI,¹¹⁶ NS9283⁶⁰ and desformylflustrabromine (dFBr);⁵⁹ the latter two have already been discussed thoroughly in the preceding chapters. The effect of dFBr is to potentiate ACh induced response on both stoichiometries of the $\alpha 4\beta 2$ nAChRs, while NS9283 only enhances the response of ($\alpha 4$)₃($\beta 2$)₂ isoforms due to its selective binding at the $\alpha 4$ - $\alpha 4$ interface. On the other hand, CMPI was known to be an effective $\alpha 4\beta 2$ nAChR modulator, but until recently had not been investigated thoroughly for its isoform-specific functions, even though reported before NS9283. It was only recently that CMPI was identified as a potent and selective PAM for ($\alpha 4$)₃($\beta 2$)₂ stoichiometry, making it a suitable candidate to study its probable binding sites in the $\alpha 4$ - $\alpha 4$ interface.¹¹⁷



CMPI **75**, 3-(2-chlorophenyl)-5-(5-methyl-1-(piperidin-4-yl)-1H-pyrazol-4-yl)isoxazole, was designed and reported by Albrecht *et al* for its potentiating effects on the $\alpha 4\beta 2$ nAChRs, but with no reference to its isoform selectivity.¹¹⁶ It was Hamouda *et al* who carried out a detailed investigation on CMPI not only on $\alpha 4\beta 2$ nAChRs but also on the muscle type human and *Torpedo* nAChRs. This was fruitful in identifying its intrinsic photolabeling properties and isoform selectivity. The ($\alpha 4$)₃($\beta 2$)₂ and ($\alpha 4$)₂($\beta 2$)₃ isoforms along with human ($\alpha 2\beta\epsilon\delta$) and *Torpedo* ($\alpha 2\beta\gamma\delta$) nAChRs were expressed individually in the *Xenopus* oocytes to study the functional effects of CMPI using electrophysiology.¹¹⁷

Electrophysiology studies revealed the selectivity of CMPI in potentiating the ACh induced response of ($\alpha 4$)₃($\beta 2$)₂ nAChRs only, without affecting the ($\alpha 4$)₂($\beta 2$)₃ isoforms. The co-application of varied submicromolar concentrations of CMPI with 10 μ M ACh resulted in enhanced potentiation of ACh induced response of ($\alpha 4$)₃($\beta 2$)₂ nAChRs with $EC_{50} = 0.26$ μ M and $I_{max} = 314\%$. Similar injections of CMPI with ACh did not have any modulatory effect on the current generated by ($\alpha 4$)₂($\beta 2$)₃ isoforms, though, it significantly inhibited the response by $\sim 35\%$ on increasing the CMPI concentration to 10 μ M, indicating that it may

be an allosteric inhibitor of ($\alpha 4$)₂($\beta 2$)₃ receptors. When 1 μM of CMPI was co-applied with varied of ACh concentrations, a left shift was observed in the ACh DRC of ($\alpha 4$)₃($\beta 2$)₂ nAChRs, as maximal potentiation remained unaffected ($I_{\text{max}} = 97\%$) but the EC_{50} value of ACh reduced to 0.7 μM from 92 μM .¹¹⁷ Thus, inferring that CMPI acts as a selective potentiator amplifying the ACh potency on ($\alpha 4$)₃($\beta 2$)₂ nAChRs without altering its maximal response, an effect studied previously in case of NS9283.⁸³ On the basis of observed outcomes, it could be implied that the binding site for CMPI may be within in the $\alpha 4$ - $\alpha 4$ interface, although, further investigation was required to demonstrate this.

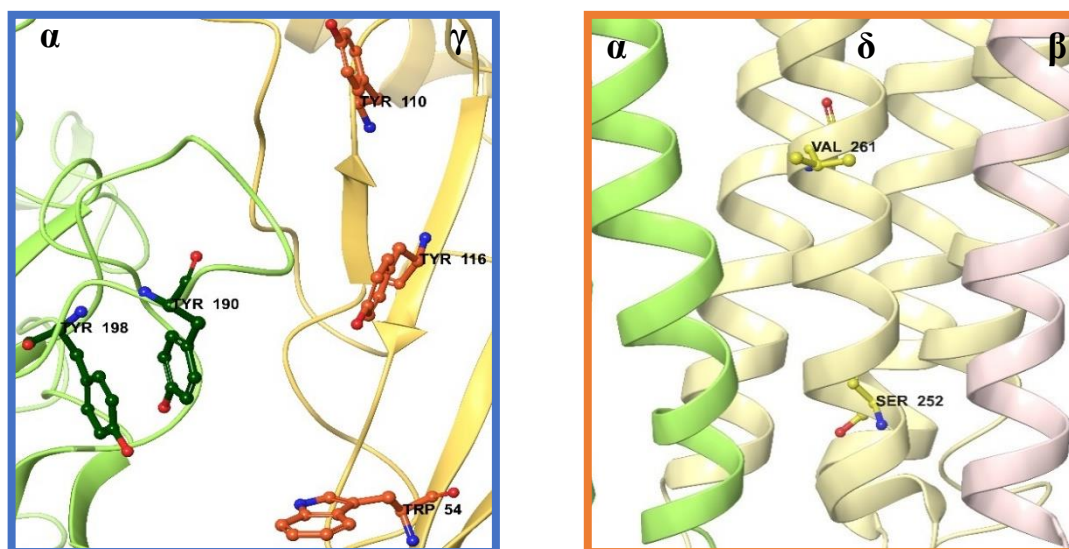


Fig. 3.7: Photolabeled amino acids (sticks) by [³H]CMPI in the ECD (left) and TMD (right) of *Torpedo* nAChRs (PDB 2BG9).^{2, 117}

On the human muscle and *Torpedo* nAChRs, CMPI inhibited the ACh-induced response of both receptors with $\text{IC}_{50} = 0.7 \mu\text{M}$ and $0.2 \mu\text{M}$, respectively. Further analysis of *Torpedo* nAChRs using [³H]ACh and an ion-channel blocker [³H]PCP revealed that increasing the concentrations of CMPI (up to 100 μM) competitively displaces the [³H]PCP from its binding site, while the same extent of displacement was not observed for [³H]ACh. A ~30 fold stronger affinity was observed for CMPI as an ion-channel blocker compared to its inhibition at the orthosteric sites of *Torpedo* nAChRs.¹¹⁷ The photoaffinity study of *Torpedo* nAChR with [³H]CMPI identified and confirmed the presence of two aforesaid binding sites in the ECD and ion-channel. [³H]CMPI displayed intrinsic photoreactivity, labelling the following residues: α Tyr190/Tyr198, γ Trp54/Tyr110/Tyr116 of the orthosteric binding site in the α - γ interface of ECD; and δ S252/V261 of TM2 helix in the ion-channel's TMD (**Fig. 3.7**). The photoreactivity of CMPI was implied by the formation of radical or electrophilic

intermediates after UV irradiation. CMPI molecule includes chlorobenzene and isoxazole which can undergo dehalogenation and azirine rearrangement, respectively, forming reactive species to interact with aromatic (tyrosine/tryptophan) or aliphatic (valine/serine) residues. This innate ability of CMPI to photo-incorporate an assortment of amino acids will be hugely useful for the recognising its binding site(s) in the $(\alpha 4)_3(\beta 2)_2$ isoforms.

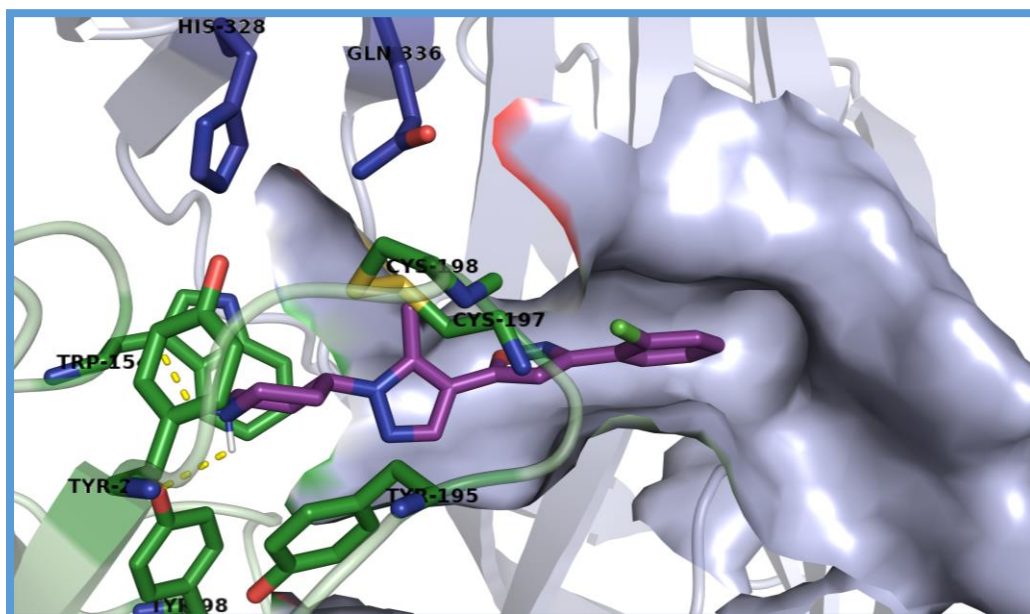


Fig. 3.8: CMPI Docking (purple, sticks) in the constructed $(\alpha 4)_3(\beta 2)_2$ nAChR homology model. CMPI is seen oriented towards the identified pocket (grey, surface) and demonstrates interaction with the $\alpha 4$ - $\alpha 4$ binding site residues (green and blue, sticks).

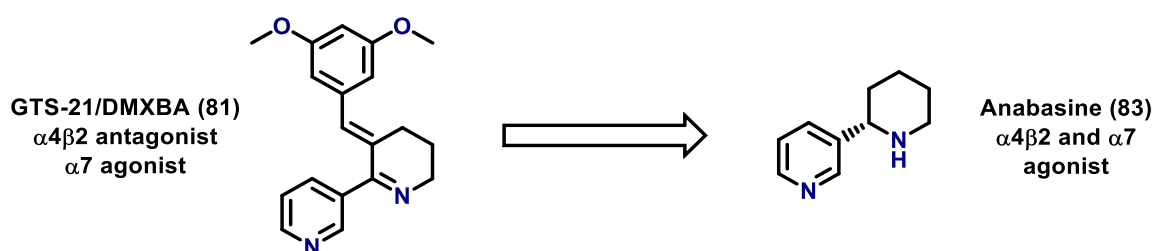
Determination of CMPI's binding site in the $(\alpha 4)_3(\beta 2)_2$ nAChRs was initially carried out through molecular modeling using the protein-ligand docking. Generally, crystallised protein structures are used for docking studies, but upon their unavailability such as the case with $(\alpha 4)_3(\beta 2)_2$ nAChRs, even proteins built through homology modeling can be utilised. Fortuitously, the docking of CMPI in the $(\alpha 4)_3(\beta 2)_2$ nAChR's homology model established its interaction with the residues of the orthosteric binding site and the newly identified pocket present in the $\alpha 4$ - $\alpha 4$ interface (**Fig. 3.8**). The CMPI ligand docked into the $\alpha 4$ - $\alpha 4$ binding site with its orientation towards the pocket, displaying strong interactions with the site residues. Thus, the docking studies facilitated in identifying CMPI's plausible binding site and demonstrated the prospective role of the new site in modulating the functional activity of $(\alpha 4)_3(\beta 2)_2$ nAChRs.

3.2. DESIGN OF ANABASINE AND NICOTINE ANALOGUES

The recognition of another pocket in the $\alpha 4$ - $\alpha 4$ binding site and proposed binding of CMPI within this pocket, are the two major motivators in our endeavour to design a novel class of $\alpha 4$ - $\alpha 4$ selective PAMs. After the analysis of *Ls*-AChBP^{HQT} co-crystal structures, nicotine and DMXBA were identified as the two strategic ligands that will serve as templates for the development of their analogues. But what makes them special over others and how their non-selectivity will be modified to achieve our main goal?

3.2.1. PROJECT AIMS

Both nicotine and DMXBA are known for their affinity towards the acetylcholine receptors, with a manifold higher binding affinity for the $\alpha 4\beta 2$ nAChRs over $\alpha 7$ receptors. Nicotine is a well-established agonist of both the receptor subtypes, with a high preference for the $\alpha 4\beta 2$ nAChRs ($K_i = 1.0$ nM, over 1600 nM for $\alpha 7$), while DMXBA displays partial agonism at the $\alpha 7$ receptors ($K_i = 650.0$ nM) but acts as an antagonist for $\alpha 4\beta 2$ receptors ($K_i = 20.0$ nM). However, DMXBA is an unsaturated benzylidene derivative of anabasine, a naturally occurring compound which is an agonist for $\alpha 4\beta 2$ and $\alpha 7$ nAChRs in high concentration, with a binding affinity of $K_i = 65.0$ and 38 nM, respectively.^{8, 39} Anabasine is a structural isomer of nicotine with a parallel chemical and pharmacological profile, though it is used as an insecticide.



The structural overlay of nicotine (PDB 1UW6)¹⁷ and DMXBA (PDB 2WNJ)¹¹⁴ with the $\alpha 4$ - $\alpha 4$ interface homology model exhibited some important reasons behind their selection to design and develop novel lead candidates as the $\alpha 4$ - $\alpha 4$ selective PAMs. Both ligands were positioned within the ‘aromatic cage’ of the $\alpha 4$ - $\alpha 4$ binding site, while the Cys-pair caps the entrance (Fig. 3.9 A and C). In case of DMXBA, Cys-pair capping was slightly distorted due to the bulky benzylidene group. Further validation of the ligands came from visualising their positioning towards the newly recognised pocket in the $\alpha 4$ - $\alpha 4$ interface. A bond vector in each ligand was directed towards the identified pocket in the binding site

(Fig. 3.9 B and D). Thus, the goal was to introduce wide-ranging modifications and substitutions at that position, allowing the extension of the developed ligands towards the pocket that could result in realizing the $\alpha 4$ - $\alpha 4$ site selectivity.

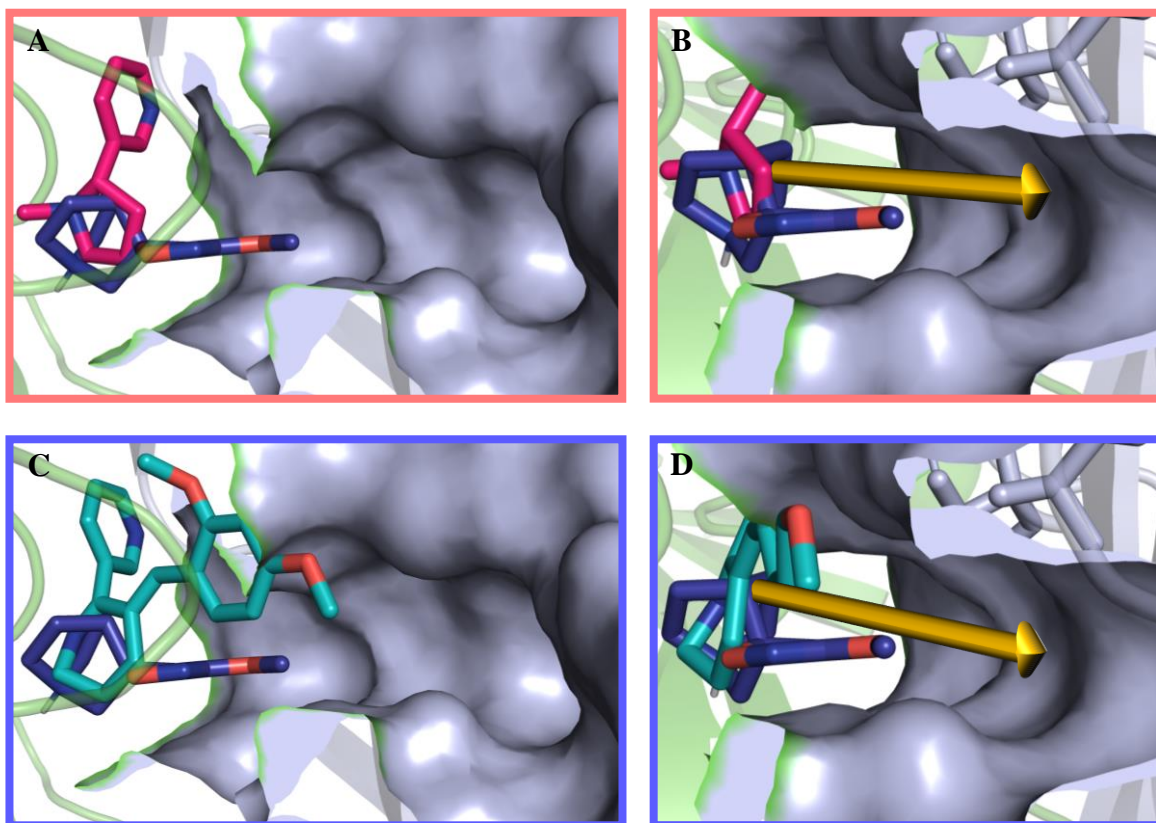


Fig. 3.9: A & C- Structural overlay of selected Nicotine (pink, PDB 1UW6)¹⁷ and DMXBA (teal, PDB 2WNJ)¹¹⁴ co-crystals in the $\alpha 4$ - $\alpha 4$ binding site with ICH3 ligand (blue). B & D- The pinpointed in-ring carbon atom vector (yellow arrow) is directed towards the newly identified pocket, something worthy of further exploration and modification.

Another significant aspect that was made in favour of nicotine and DMXBA, was their overlap with the key $(\alpha 4)_3(\beta 2)_2$ nAChR ligand NS3920. As discussed in the previous chapter, NS3920 was used as the foundation for designing selective $\alpha 4$ - $\alpha 4$ agonists by exploiting their key structural features and combining them into developed analogues. The pyridine ring of DMXBA and nicotine shows a complete overlap with the pyridine of NS3920 (Fig. 3.10). Since the pharmacophore is proximal to the NS3920 secondary amine, which stabilises the ligand through π -cation interactions, the same may also be observed with anabasine and nicotine (Fig. 3.10 A and B) Both, DMXBA and nicotine will occupy the same space and probably create parallel interactions with the binding site residues. Thus, preserving the closely related molecular structure of NS3920, with an extension in the

pocket where CMPI is proposed to bind, the ligands under development may possess the characteristics of $\alpha 4$ - $\alpha 4$ selective PAMs.

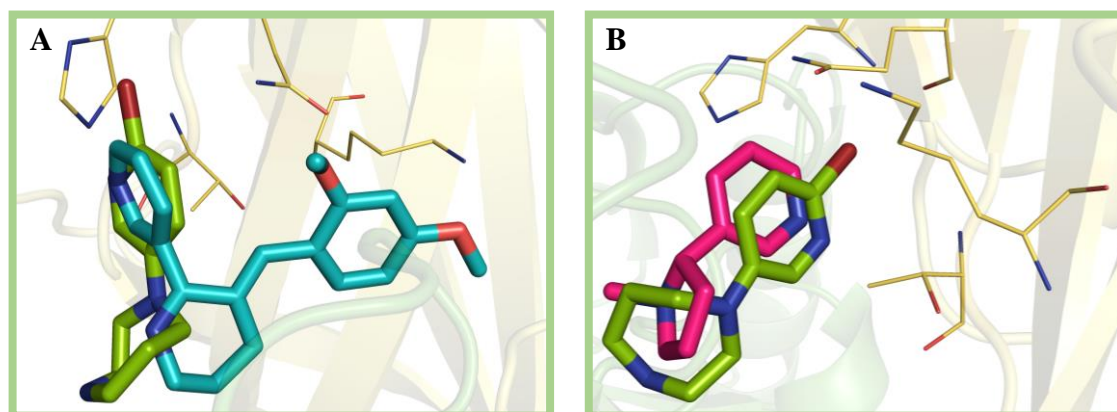


Fig. 3.10: Overlay of DMXBA (A- PDB 2WNJ)¹¹⁴ and Nicotine (B- PDB 1UW6)¹⁷ co-crystals with NS3920. Pyridine ring of selected ligands show good overlap with NS3920, while the aliphatic ring nitrogen is proximal to secondary ammonium pharmacophore of NS3920.

Based on the aspects studied below (**Fig. 3.11**), several modifications were considered towards design of nicotine and anabasine template, deduced from DMXBA. Introduction of short-chain aliphatic/aryl/heteroaryl substitutions at the position identified, with the bonding vector pointing towards the recognised pocket, should allow designed analogues to extend sidechain into the vacant space and possibly result in a $\alpha 4$ - $\alpha 4$ site selectivity.

The presence of secondary and tertiary amine in anabasine as well as nicotine, respectively, are of critical importance for ligand stabilisation, since under biological conditions, the amine nitrogen of both templates will be protonated to form the characteristic ammonium ion pharmacophore. The same entity has been found to establish π -cation interactions with the nearby aromatic residues. Maintaining a secondary nitrogen could prove beneficial as it has been evident with NS3920 that the secondary amine on protonation, formed two π -cation interactions, one with tryptophan (Trp156) while the other with nearby tyrosine (Tyr197).^{86, 88, 89} Hence, unsubstituted pyrrolidine and piperidine nitrogen should show strong binding to the receptor relative to their substituted counterparts. Variations could also be made with the pyridine ring of nicotine and anabasine, but with smaller substitutions like halogens, nitriles, methyl, etc or entirely replacing the ring with a phenyl moiety. This will help in exploiting NS3920 type interactions with HQT amino acids from the α (-) side of interface and help in forming similar inter-subunit bridge as observed with NS3920.⁸⁸

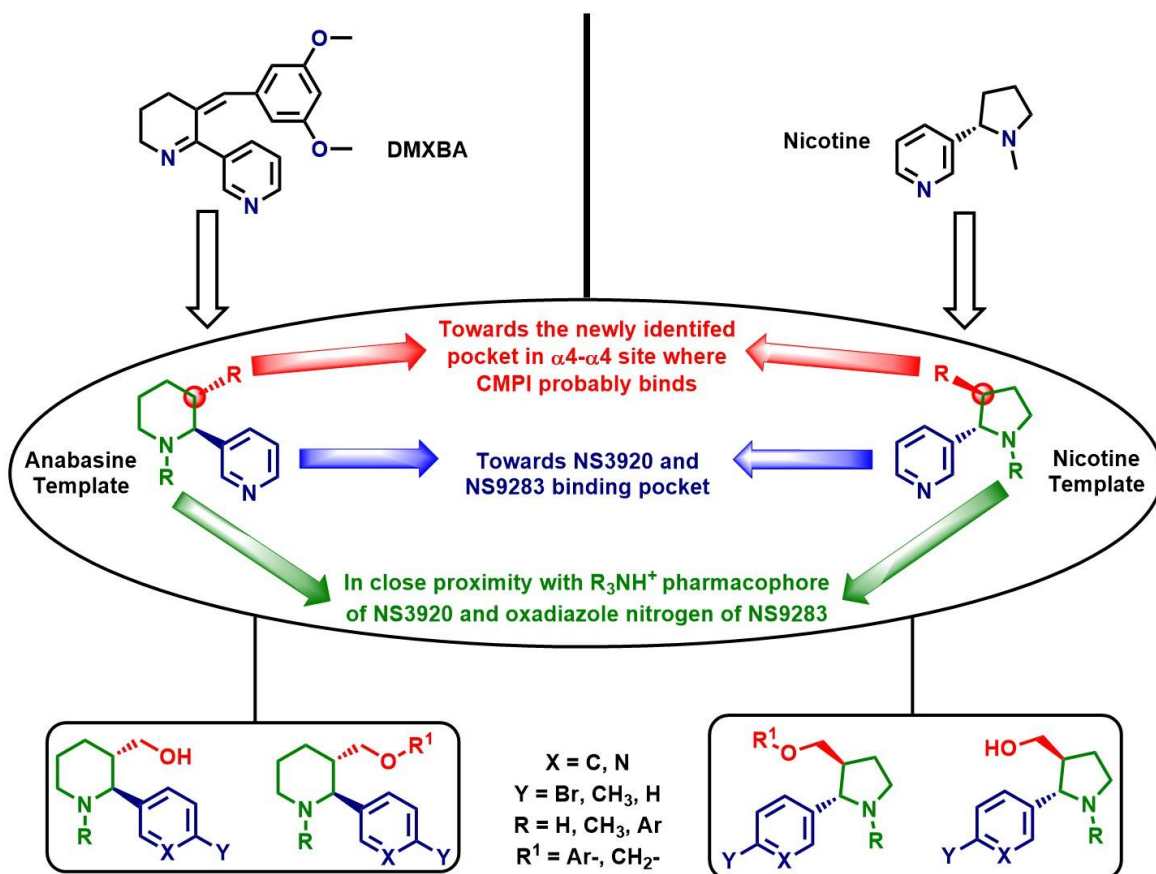


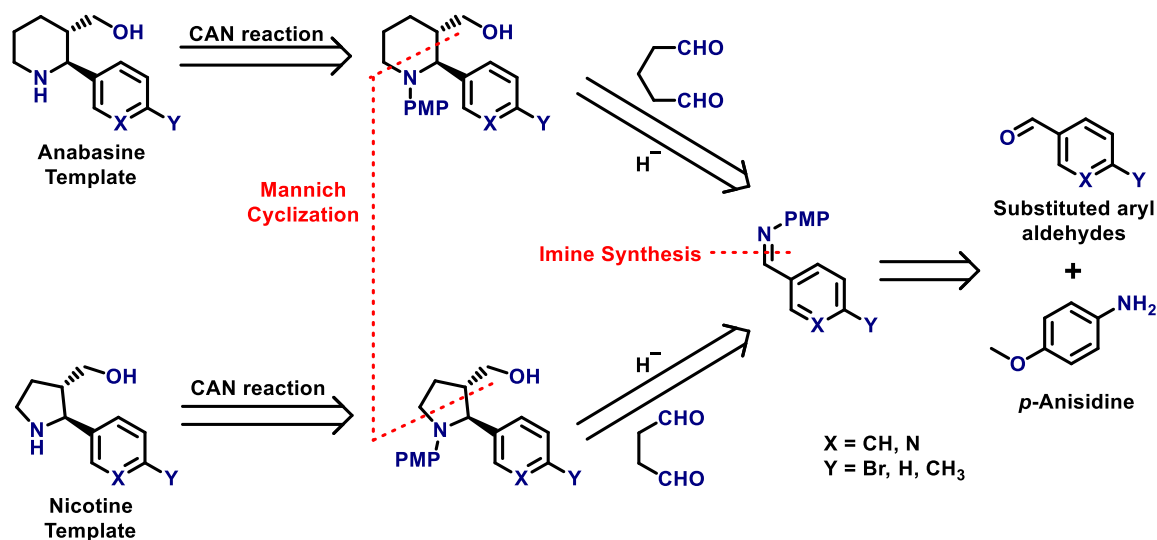
Fig. 3.11: Design and comparative analysis of nicotine and anabasine templates.

Syntheses of designed anabasine and nicotine templates as well as their analogues have been elaborated in the next section along with the synthetic strategy. A part of the next section also includes a brief discussion on generating CMPI-anabasine linked hybrids, since some CMPI related analogues designed by another co-worker gave promising results on the $\alpha 4$ - $\alpha 4$ selectivity. After syntheses, all the analogues were submitted for determination of their biological activity to our collaborator Dr. Balle at the University of Sydney. The bioactivity of synthesised compounds was assessed using the two-electrode voltage-clamp electrophysiology assay on $(\alpha 4)_3(\beta 2)_2$ nAChRs expressed in *Xenopus laevis* oocytes.

3.2.2. RETROSYNTHETIC ANALYSIS

As per the retrosynthetic approach described below (**Scheme 17**), the target anabasine and nicotine templates could be achieved from the ceric ammonium nitrate (CAN) mediated *p*-methoxy phenyl (PMP) deprotection^{118, 119} from the Mannich cyclised product. The anabasine pathway product was available via L-proline catalysed Mannich reaction and cyclisation of glutaraldehyde with substituted aromatic imines followed by reduction.¹²⁰

Similarly, the cyclised product for the nicotine pathway was accessible through L-proline catalysed Mannich addition and cyclisation of succinaldehyde with substituted aromatic imines followed by reduction.¹²¹ Condensation of substituted aromatic aldehydes with *p*-anisidine generated the aromatic imines for Mannich cyclisation.¹²²



Scheme 17: Retrosynthetic strategy to synthesise anabasine and nicotine templates.

Almost all the relevant starting materials and intermediates required for the target synthesis were commercially available, while others were synthesised in lab. Since succinaldehyde was not commercially available due to its instability and tendency to polymerize, it was synthesised in the lab before setting up the Mannich reaction for nicotine related analogues. The additional step of methylation at the pyrrolidine and piperidine ring nitrogen was needed for some of the designed analogues after the final PMP deprotection. Extension of the hydroxymethyl side chain, with short aliphatic/aromatic substitutions to introduce ether and ester functional groups required base catalysed as well as carbonyldiimidazole (CDI) promoted reactions. Several reactions, especially Mannich addition and cyclisations, were optimised for high yields and stereoselectivity, have been discussed with an attention to detail in the subsequent sections along with reaction mechanisms.

3.2.3. SYNTHESIS OF UNSUBSTITUTED ANABASINE AND NICOTINE ANALOGUES

Target analogues with pyridyl substitutions were expected to establish better interactions over the phenyl analogues, because the pyridyl nitrogen is predicted to maintain the same hydrogen bonding between the ligand and site residues via water-mediated bridge, as seen previously with NS3920 compounds. The replacement of the pyridyl with a phenyl ring

sought to observe the differences in ligand interaction and its influence on the bioactivity. Brominated ring systems such as in NS3920, have previously shown to initiate halogen bonding with the complementary residues in the binding site, therefore, their presence or absence may influence bioactivity.

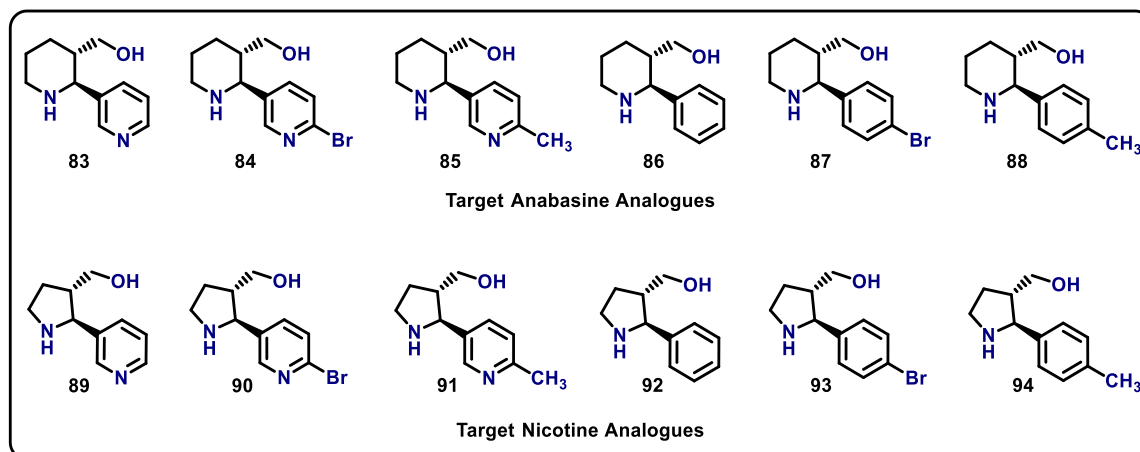
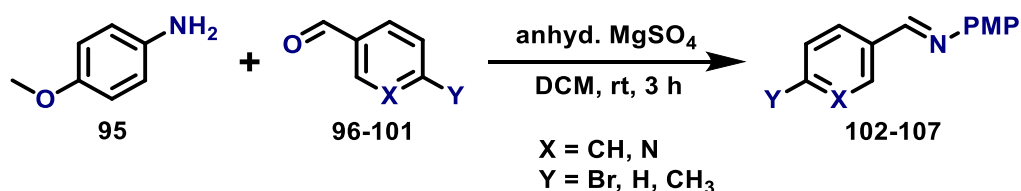


Fig. 3.12: Target anabasine and nicotine analogues designed for syntheses and bioactivity.

These are preliminary targets (**Fig. 3.12**) designed to establish bioactivity and select ligands for further substitutions at the hydroxymethyl position to extend it into the new pocket.

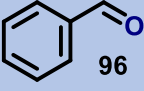
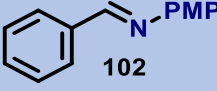
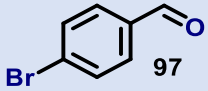
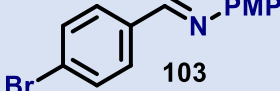
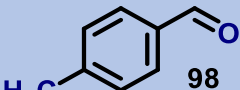
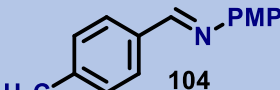
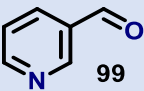
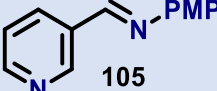
Synthesis of Substituted Aryl Imines



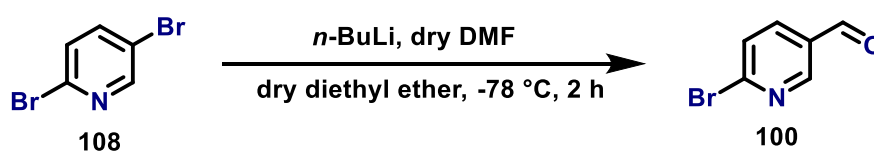
Scheme 18: Substituted imine **102-107** synthesis using *p*-anisidine **95** and substituted aldehydes **96-101** under anhydrous conditions.

The substituted imines **102-107** were synthesised (**Scheme 18**) using a literature procedure that involved condensation of equal equivalents of primary amine *p*-anisidine **95** and substituted aryl aldehydes **96-101** in dichloromethane.¹²² Water generated during the reaction was removed *in situ* using anhydrous magnesium sulfate as desiccant. Respective yields and substituted imines formed using commercially available aldehydes, are listed below (**Table 6**).

Table 6: Aryl aldehydes **96-99** with corresponding imines **102-105** and their %yields.

S. No.	Aryl Aldehydes	Substituted Imines	Yields (%)
1.			84
2.			88
3.			81
4.			92

Some aryl aldehydes were not commercially available, hence, 6-bromonicotinaldehyde **100** and 6-methylnicotinaldehyde **101**, were synthesised in the lab. The best approach for functionalised pyridine synthesis is from halopyridines via halogen-metal exchange, followed by electrophilic trapping to generate the required functional group. Amongst all the methods available, lithiation of halopyridines at low temperatures yields best results.¹²³ Based on this approach, synthesis of 6-bromonicotinaldehyde **100** and 6-methylnicotinaldehyde **101** was attempted, though, only the former product was achieved in good yields.

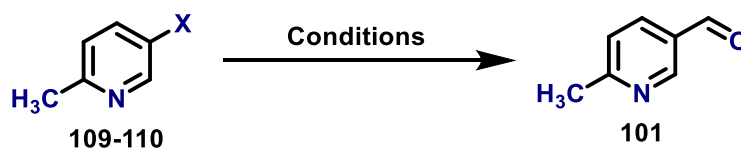
**Scheme 19:** Selective formylation of 2,5-dibromopyridine **108** using *n*-butyllithium.

Under anhydrous conditions at $-78\text{ }^{\circ}\text{C}$, *n*-butyllithium (*n*-BuLi) reacted with 2,5-dibromopyridine **108** in diethyl ether (DEE) as a solvent, leading to *in situ* generation of monolithiated species, which was trapped by adding a formyl electrophile in the form of dimethylformamide (DMF) to give high yields of 6-bromonicotinaldehyde **100** (**Scheme 19**, **Table 7**).¹²⁴ High *n*-butyllithium concentration, as well as cryogenic conditions, have been reported to kinetically favour the lithiation at the 5th position.¹²⁵

Table 7: Reaction optimisation for selective formylation of 2,5-dibromopyridine **108**.

S. No.	<i>n</i> -butyllithium eq.	Yield (%)
1.	1.0	-
2.	2.0	5
3.	3.0	27
4.	5.0	66
5.	7.5	87

Formation of 6-bromonicotinaldehyde **100** was confirmed from the ^1H NMR spectrum, as a sharp singlet corresponding to the aldehyde proton was observed at 10.09 ppm. Three peaks were also observed in the aromatic region, of which a small doublet at 8.83 ppm was consistent with the proton ortho to pyridyl nitrogen, while the two other peaks as doublets were equivalent to two other protons of the ring. The data obtained experimentally matched well with the literature data.¹²⁴

**Scheme 20:** Synthesis of 6-methylnicotinaldehyde **101** using substituted methylpyridines.

Several conditions were tried to synthesize 6-methylnicotinaldehyde **101**, though, all the approaches gave either no or low yields of the desired compound. Transmetalation (**Table 8: entry 1**) using *n*-BuLi and isopropyl magnesium bromide (*i*-PrMgCl),¹²² previously employed halogen-lithium exchange¹²⁴, (**Table 8: entry 2**) and diisobutylaluminium hydride (DIBAL) reduction of esters (**Table 8: entry 3**),¹²⁶ were the three unsuccessful methods used for the formylation of methylpyridine (**Scheme 20**).

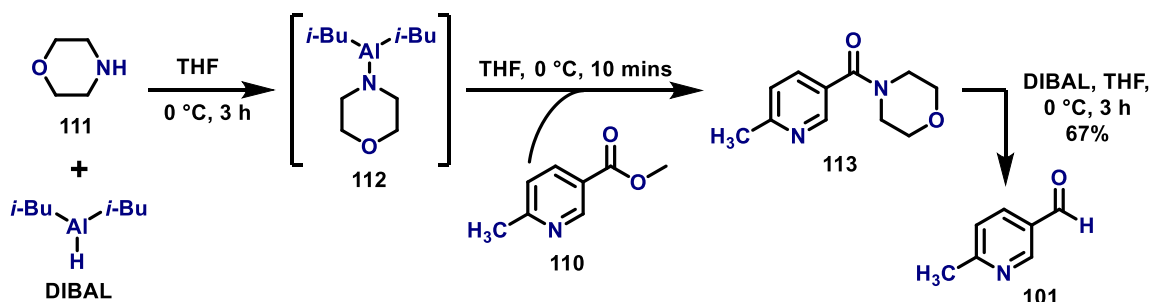
The synthesis of 6-methylnicotinaldehyde **101** was proposed via the formation of Weinreb amide using methyl 6-methylnicotinate **110** as the starting material. Weinreb amides, i.e., *N*-methoxy-*N*-methylamides, can be synthesised from *N,O*-dimethylhydroxylamine and activated carboxylate derivatives such as esters, under cold and strong basic conditions. It can be reduced further to aldehydes or ketones using large quantities of hydride reducing agents.⁹⁵ However, some articles have suggested the use of morpholine and pyrrolidine as amines to generate respective amides from activated carboxylate derivatives. In this case,

morpholine **111** was first treated with DIBAL to form diisobutyl(morpholino)aluminium intermediate **112** under cold conditions, and further reacted with methyl 6-methylnicotinate **110** to form the morpholine amide **113**. The *in-situ* generated tertiary amide was then treated with an excess of DIBAL as a hydride donor, followed by acid hydrolysis, to afford 6-methylnicotinaldehyde **101** in one-pot synthesis (Scheme 21).¹²⁷ The complete conversion of the ester to an amide was monitored with TLC, followed by addition of the second portion of DIBAL. Three trials were carried out for the reduction of amides to aldehyde using different equivalents of DIBAL (Table 8: entry 4-6), but none gave complete conversion. However, on adding an excess of DIBAL, the reaction proceeded to completion with full conversion and high yields (Table 8: entry 7).

Table 8: Reaction optimisation for synthesis of 6-methylnicotinaldehyde **101**.

S. No.	Conditions	X	Conversion, Yield
1.	<i>n</i> -BuLi/ <i>i</i> -PrMgCl/DMF/dry DEE/-78 °C/2 h	-Br (109)	Incomplete conversion, 8%
2.	<i>n</i> -BuLi/DMF/dry DEE/-78 °C/2 h	-Br (109)	No reaction
3.	DIBAL/dry DCM/-78 °C/2 h	-COOCH ₃ (110)	Alcohol formation
4.	DIBAL (1 eq.)/Morpholine/dry THF/0 °C/3 h	-COOCH ₃ (110)	Incomplete conversion, 17%
5.	DIBAL (3 eq.)/Morpholine/dry THF/0 °C/3 h	-COOCH ₃ (110)	Incomplete conversion, 29%
6.	DIBAL (7 eq.)/Morpholine/dry THF/0 °C/3 h	-COOCH ₃ (110)	Incomplete conversion, 42%
7.	DIBAL (10 eq.) /Morpholine/dry THF/0 °C/3 h	-COOCH₃ (110)	Complete conversion, 67%

Methyl 6-methylnicotinate **110** conversion to 6-methylnicotinaldehyde **101** was confirmed from the analysis of ¹H NMR spectrum. Characteristic singlets at 10.06 and 2.65 ppm were equivalent to the formyl as well as methyl protons, respectively. The three aromatic protons were observed as three individual doublets at 8.94, 8.04 and 7.33 ppm. Literature data matched well with the obtained experimental NMR spectra.¹²⁷



Scheme 21: Synthesis of 6-methylnicotinaldehyde **101** via *in situ* formation of Weinreb type morpholine amide **113** intermediate.

The mechanism proposed (Fig. 3.13)¹²⁸ for the functional group transformation of ester to aldehyde, primarily involved attack of the *in situ* generated morpholinide anion of intermediate **112** on the ester methyl 6-methylnicotinate **110**. This led to the formation of an intermediate **114**, where its morpholine oxygen was in co-ordination with the aluminium metal and stabilised as a seven-membered cyclic form. The morpholine amide **113** intermediate was formed on elimination of the methoxy-aluminium complex. Following treatment with DIBAL, the morpholine-amide stabilises as a seven-membered cyclic adduct **115** through aluminium coordination with the morpholine oxygen, which on hydrolysis yielded the desired 6-methylnicotinaldehyde **101**.¹²⁸

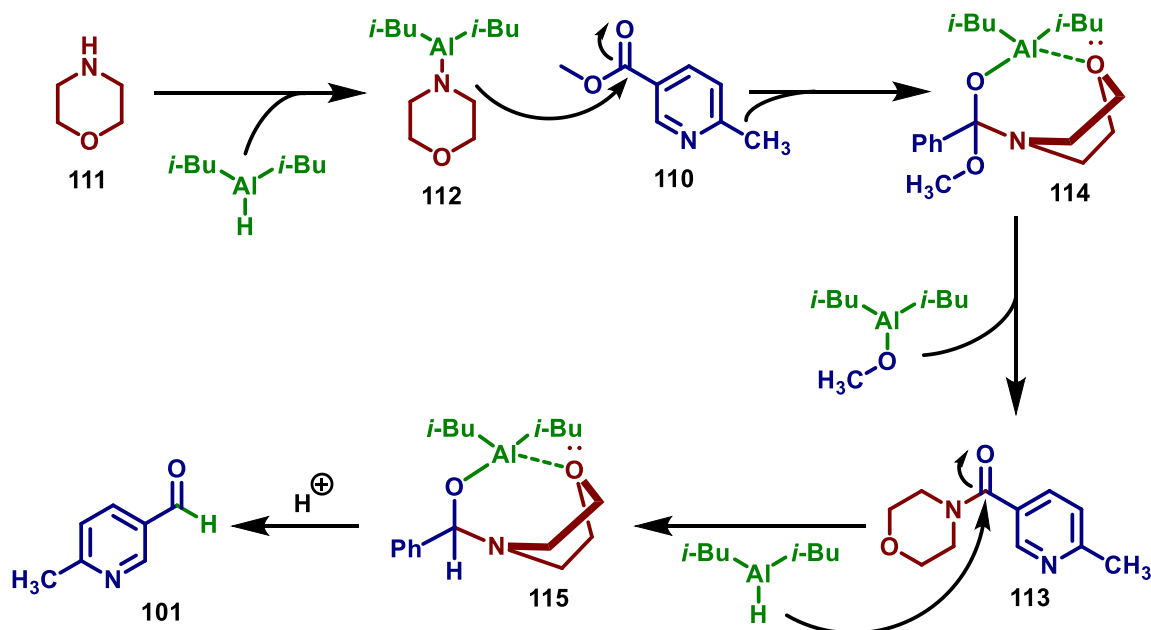
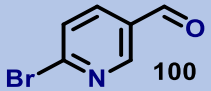
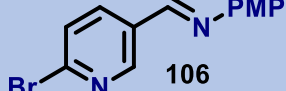
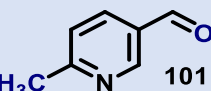
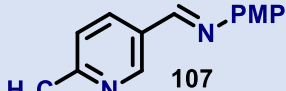


Fig. 3.13: Proposed mechanism for the conversion of ester to aldehyde via the formation of morpholine amide intermediate.¹²⁸

After synthesis of 6-bromonicotinaldehyde **100** and 6-methylnicotinaldehyde **101**, they were also subjected to similar conditions as described earlier for the substituted aryl imines synthesis and afforded respective imines **106-107** in high yields (Scheme 18, Table 9).

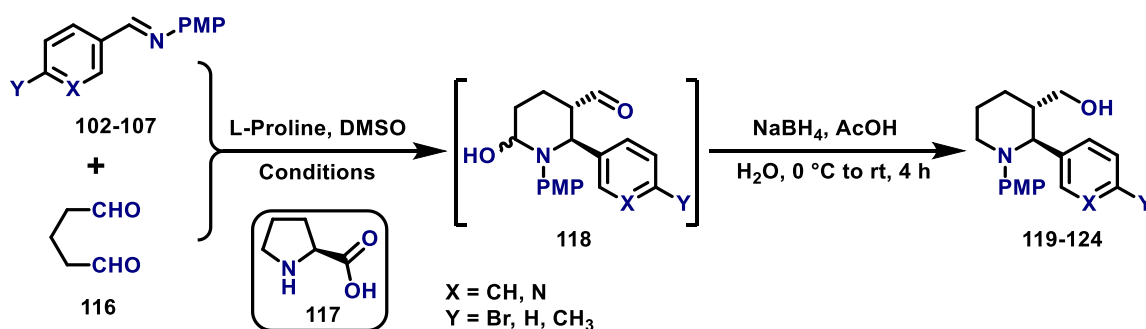
Table 9: Aryl aldehydes **96-99** with corresponding imines **102-105** and their % yields.

S. No.	Aryl Aldehydes	Substituted Imines	Yields (%)
1.			88
2.			80

Synthesis of Anabasine Analogues

The key step in the development of anabasine analogues is the synthesis of an optically enriched 2,3-disubstituted piperidine ring system, which was carried out on the basis of a recently reported literature procedure with minor modifications.¹²⁰ The synthetic approach involved L-proline catalysed one-pot Mannich reductive cyclisation cascade of aryl aldimines and glutaraldehyde. By definition, the Mannich reaction involves the addition of enolizable carbonyl nucleophiles at the α -carbon, to imines and their salts yielding β -amino carbonyl derivatives called as Mannich bases.⁹⁵ Here, the 1,5-dicarbonyl derivative glutaraldehyde *in situ* generates an enamine that undergoes direct Mannich reaction with the preformed PMP-protected aryl aldimines followed by cyclisation, after which the acid-mediated reduction yields substituted piperidine intermediates.¹²⁰

Step 1: L-Proline catalysed one-pot Mannich reductive [4+2] cyclisation cascade



Scheme 22: Synthesis of substituted piperidines **119-125** from PMP-protected aryl aldimines **102-107** via one pot Mannich reductive [4+2] annulation cascade.

The preformed substituted aldimines **102-107** were made to react with 25% aqueous solution of glutaraldehyde **116** in the presence of catalytic amount of L-proline **117** under cool conditions using dimethyl sulfoxide (DMSO) as solvent (**Scheme 22**). The reaction was monitored by TLC and once all the aldimine was converted to Mannich Base **118**, it was carried onto the next step in the same vessel. The reaction was cooled to 0 °C and sodium borohydride (NaBH₄) was added cautiously in several portions (excess) over a period of 30 mins, followed by cold water as a co-solvent to prevent elevation of reaction temperature. Subsequently, glacial acetic acid was added slowly in a dropwise manner until the effervescence stopped. The reaction was allowed to warm to room temperature and stirred till the Mannich base formed *in situ* disappeared from TLC. Care was taken during the addition of acetic acid, as it tended to make the reaction vigorously exothermic causing it to spill out of the vessel. The substituted piperidines **119-124** formed were purified by flash chromatography and characterised by various spectroscopic techniques.

Table 10: Optimisation of conditions for one-pot Mannich reductive cyclisation cascade, using PMP-protected aldimine **105** (1 eq.).

S. No.	116 (eq.)	L-proline (mol%)	Conditions	NaBH ₄ (eq.)	Yield (%)
1.	3	20	10 °C, 9 h	3	19
2.	4	20	10 °C, 9 h	3	26
3.	5	20	10 °C, 9 h	3	15
4.	4	30	10 °C, 9 h	3	31
5.	4	40	10 °C, 9 h	3	42
6.	4	40	10 °C, 7 h	6	55
7.	4	40	10 °C, 6 h	10	69
8.	4	40	10 °C, 4 h	10	39

Despite following the literature procedure,¹²⁰ the product yield and reactant to product conversion was low, in addition to some side product formation observed on TLC. Therefore, some modifications were introduced to optimise the method for better reaction efficiency. Initially, the reaction was carried out as per the procedure mentioned in the literature, however, much of aldimine **105** remained unreacted. Nonetheless, the NaBH₄ reduction of Mannich intermediate **118** was carried over, resulting in an extremely low yield

of 19% for piperidine **119** (Table 10: entry 1) along with several side products. To remedy this, glutaraldehyde **116** amount was increased from 3 eq. to 4 eq. that enhanced the aldimine to Mannich base conversion, as inferred from TLC and the yield increased slightly to 26% (Table 10: entry 2). Remarkably, on further increasing the glutaraldehyde equivalents, a major drop in aldimine conversion and overall yield was observed (Table 10: entry 3). Next, the catalyst loading of L-proline was raised from 20 to 30 and 40 mol% (Table 10: entry 4 and 5) which improved the overall yield of the final product as well as Mannich base conversion, although minor side products were still observed. Reducing the reaction time from 9 h to 7 h and then further to 6 h along with the use of excess NaBH₄, ensued a near to complete conversion of aldimine and consequently, higher overall yields (Table 10: entry 6 and 7). Although, a further drop in reaction time caused a lower than expected yield attributed to incomplete conversion of aldimine (Table 10: entry 8).

Hence, the aforesaid conditions (Table 10: entry 7) were employed for the synthesis of following optically enriched 2,3-disubstituted piperidines in good yields (Table 11) after purification from flash chromatography. All the synthesised compounds were characterised by various spectroscopic techniques.

Table 11: Respective yields as well as substitutions present in the synthesised PMP-protected piperidines **119-124**.

S. No.	Substitutions X, Y	Piperidine Yield (%)
1.	N, H (119)	69
2.	N, Br (120)	72
3.	N, CH ₃ (121)	42
4.	CH, H (122)	56
5.	CH, Br (123)	64
6.	CH, CH ₃ (124)	51

For easier understanding, spectral data of substituted piperidine **119** is used here as a representative for analysis and characterisation. In the ¹H NMR spectrum, four peaks spread between 8.43 ppm to 7.08 ppm of the aromatic region were equivalent to four protons of the pyridine ring. Further upfield, two doublet of triplets at 6.89 and 6.63 ppm were consistent with the four phenyl ring protons of PMP-protecting group, while its methoxy

protons were observed as a singlet at 3.66 ppm. Six peaks present in the aliphatic region between 3.95 ppm to 1.57 ppm correspond well with the 10 protons of piperidine ring and hydroxymethyl moiety, whereas the alcoholic proton was found to be overlapping with the multiplet at 1.87 ppm. Similarly, the ^{13}C NMR spectrum displayed nine peaks in the aromatic region that corresponds to the pyridine and phenyl carbons. Characteristic peaks at 64.48 ppm and 55.37 ppm corresponded to the two carbons of hydroxymethyl and methoxy motif, respectively. Also, five peaks in the aliphatic region overlap well with the five carbons of piperidine ring. The mass spectrum showed molecular ion peak $[\text{M}+\text{H}]^+$ at 299.3 and $[\text{M}+\text{Na}]^+$ peak at 321.2, corresponding to the mass of compound **119**. The IR data provided further validation, with broad absorption at 3293 cm^{-1} for hydroxyl group and medium absorption at 2933 cm^{-1} for alkane C-H stretching. The specific rotation of compound **119** was $[\alpha]_{\text{D}}^{25} = +11.2$, which was equivalent to the reported literature value.¹²⁰

Proposed Mechanism for Mannich Reduction [4+2] Cyclisation Cascade

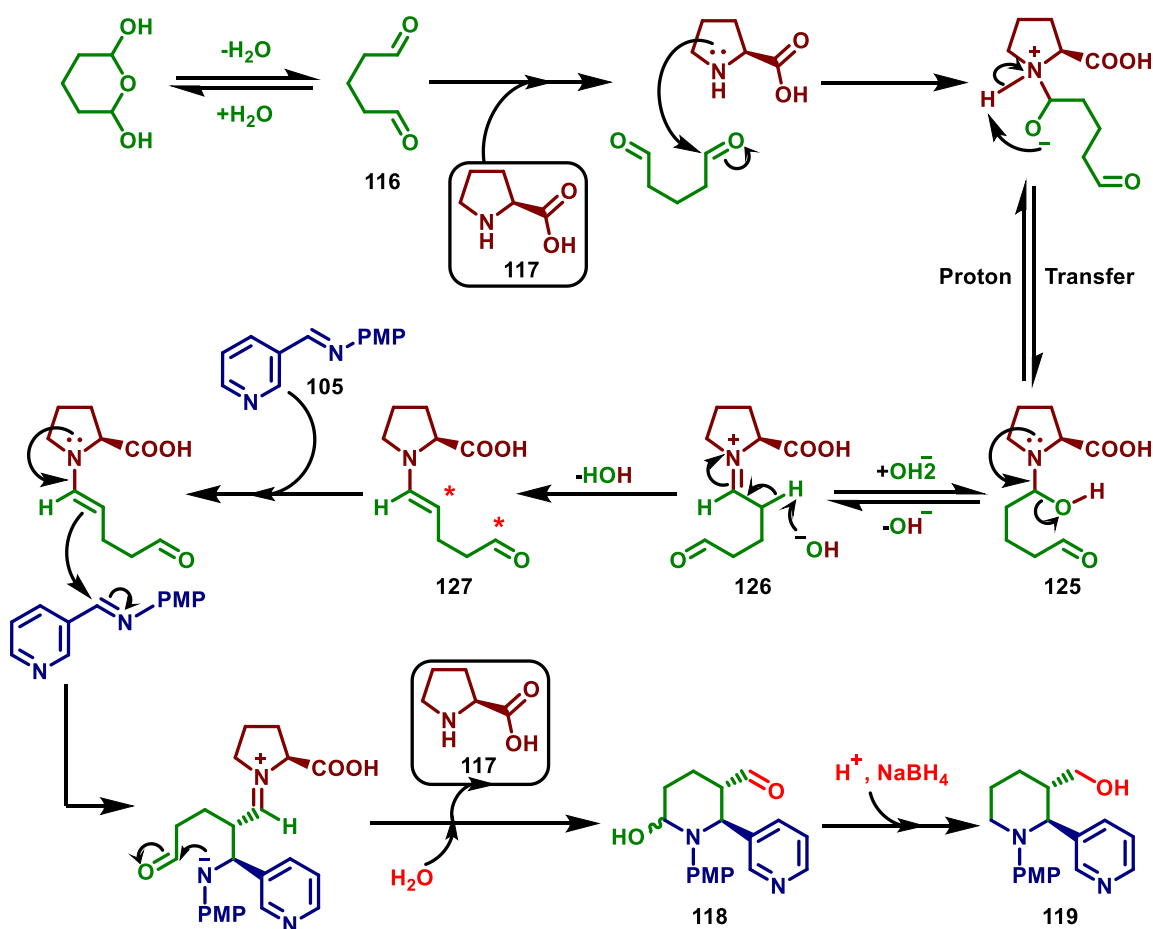
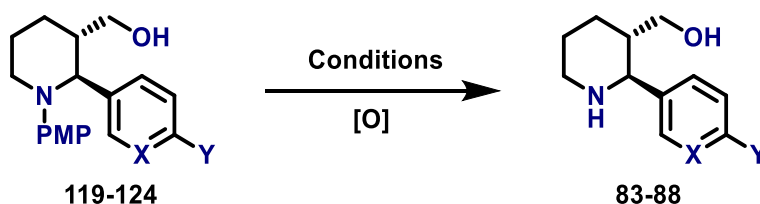


Fig. 3.14: Plausible mechanism for *L*-proline catalysed one-pot Mannich reductive [4+2] annulation cascade to form substituted chiral piperidines from achiral starting materials.¹²⁰

Synthesis of compound **119** is taken as a representative example to explain the L-proline catalysed Mannich reductive cyclisation cascade mechanism (**Fig. 3.14**). Glutaraldehyde **116** exists in two forms; the hydrated tetrahydropyran diol and the enolisable dialdehyde, formed on loss of water. The first step involves nucleophilic attack of the amine lone pair on one of the dialdehyde carbonyl carbons, followed by proton transfer to form hemiaminal **125**. This further undergoes delocalisation of amine's lone pair electrons, leading to the elimination of hydroxide, ensuring formation of an iminium ion **126**. The iminium species undergo deprotonation into the enamine **127**, which behaves as a nucleophile and reacts at its α -carbon position with the preformed non-enolizable PMP-pyridyl aldimine **105**. Both undergo an asymmetric *aldol*-type direct Mannich reaction followed by [4+2] cyclisation and hydrolytic cleavage of L-proline to yield the β -amino carbonyl intermediate, i.e., Mannich base **118**. The final step involves acid-catalysed borohydride reduction of aldehyde and iminal to give the chiral 2,3-substituted piperidine **119**.

Step 2: PMP-deprotection by Ceric Ammonium Nitrate

The cleavage of *p*-methoxy phenyl (PMP) protecting group has been reported using various oxidising agents (**Scheme 23**) such as, ceric ammonium nitrate (CAN), orthoperiodic-sulfuric acid, etc. However, reaction conditions required optimisation (**Table 12**), as several literature procedures resulted in either incomplete conversion, poor yields or degradation.



Scheme 23: Cleavage of PMP-protected piperidines **119-124** to yield free amines **83-88**.

The PMP-group deprotection of piperidine **119** to give first anabasine analogue **83** was initially attempted (**Table 12: entry 1**) with the procedure reported in previously used literature for piperidine synthesis,¹²⁰ though, incomplete conversion and poor yield was obtained. Also, on neutralising the reaction with potassium carbonate (K_2CO_3), solid lumps were observed that made the solution difficult to filter and purify. Another trial (**Table 12: entry 2**) was carried out utilising periodic acid (H_5IO_6) and sulfuric acid (H_2SO_4) mixture, which *in situ* generated an oxidising agent that removed the PMP-group.¹²⁹ However, this caused the product to degrade as visualised from the appearance of several spots on TLC,

yielding just 12% of the final product. Degradation could be due to the harsh conditions of two acid mixtures under reflux, therefore, CAN was utilised for further deprotection attempts, as it is the most common oxidising reagent used and comparatively milder than acid. In subsequent attempts, both 6 eq. and 3 eq. of CAN (**Table 12: entry 3-4**) resulted in product degradation as observed from numerous spots on TLC, but the latter proceeded with incomplete conversion.¹¹⁸ To prevent product degradation, two changes were made, firstly, the use of an increased amount of protic solvent (water) as it plays a direct role in assisting the CAN-mediated oxidative cleavage. Secondly, reducing the reaction time from 3 h to 30 mins,¹¹⁹ as continuous contact with the oxidising agent could also play a role in degradation. This ensured no product degradation as seen from clean TLC with a single spot, together with improved yield of 40% (**Table 12: entry 5**). However, further reduction in reaction time to 5 mins augmented the yield to 51% (**Table 12: entry 6**). Some loss of product was detected in the aqueous layer after extraction when spotted on TLC. Therefore, a final attempt (**Table 12: entry 7**) was made with similar conditions, except using chloroform (CHCl₃) and isopropanol (IprOH) mixture in a 3:1 ratio as a strong polar protic solvent for extraction. This ensured complete transfer of product to organic layer and boosted the yield to 72%, thus, generating the optimum conditions for deprotection of other related analogues.

Table 12: Optimisation of reaction conditions employed for deprotection of PMP-group, using PMP-piperidine **119**. Reaction time was kept at 3 h, unless mentioned otherwise.

S. No.	Reagent (eq.)	ACN:H ₂ O	Workup	Observation	Yield (%)
1.	CAN (6)	4:1	K ₂ CO ₃	Difficult to filter	35
2.	H ₅ IO ₆ (1) + H ₂ SO ₄ (1)	1:1 (reflux)	5M NaOH	Too many spots on TLC	12
3.	CAN (6)	4:1	NaHCO ₃	Too many spots on TLC	41
4.	CAN (3)	4:1	NaHCO ₃ + K ₂ CO ₃	Incomplete conversion and too many spots on TLC	32
5.	CAN (5)	1:1	1M NaOH	Clean TLC, work up in 30 mins	40
6.	CAN (5)	1:1	1M NaOH	Clean TLC, work up in 5 mins	51
7.	CAN (4)	1:1	5M NaOH	Clean TLC, work up in 5 mins and extracted with CHCl ₃ + IprOH (3:1)	72

Removal of PMP-group from piperidine was confirmed from the disappearance of two doublet of triplets at 6.89 ppm and 6.63 ppm in the aromatic region as well as the methoxy proton singlet at 3.66 ppm in the ^1H NMR spectrum. This also resulted in observation of sharp peaks in the aliphatic as well as aromatic region. Two doublet of doublets at 3.35 ppm and 3.23 ppm in the aliphatic region of ^1H NMR were equivalent to the pair of diastereotopic protons attached to hydroxymethyl group, thus, displaying two different chemical shifts. A broad singlet at 2.42 ppm was consistent with the piperidine ring's amine proton, while two overlapping broad absorptions at 3352 cm^{-1} and 3265 cm^{-1} were consistent with hydroxyl and secondary amino groups, respectively. Likewise, the absence of methoxy and phenyl carbon peaks in the ^{13}C NMR spectrum established the PMP-deprotection step. Its further validation was obtained from the mass spectrum with visualisation of a molecular ion peak $[\text{M}+\text{H}]^+$ at 193.13 corresponding to the mass of anabasine analogue **83**.¹²⁰

The conditions optimised (**Table 12: entry 7**) for the PMP-group removal were employed for the deprotection of all 2,3-disubstituted piperidines **119-124** to give final analogues **83-88** in good-to-moderate yields (**Table 13**) after purification from flash chromatography. The acidic silica gel was neutralised with aqueous ammonia to carry out smooth purification of free amine-containing basic compounds.

Table 13: Respective yields as well as substitutions present in the PMP-deprotected final anabasine analogues **83-88**.

S. No.	Substitutions X, Y	Analogue Yield (%)
1.	N, H (83)	72
2.	N, Br (84)	70
3.	N, CH ₃ (85)	47
4.	CH, H (86)	56
5.	CH, Br (87)	62
6.	CH, CH ₃ (88)	43

Plausible Mechanism for CAN-Mediated PMP Deprotection

Deprotection of PMP-group from substituted piperidine **119** to form the final anabasine analogue **83**, is taken as a representative example to explain the plausible mechanism behind CAN-mediated PMP-group removal (**Fig. 3.15**). First, ceric (Ce^{IV}) ion oxidises the electron-

rich phenyl ring system of PMP-group by abstracting an electron to form the radical-cation intermediate **128**, while simultaneously reducing itself to cerium (Ce^{III}) ion. This undergoes addition of water at the electron-deficient in-ring carbon attached to the methoxy group, ensuing the creation of radical-hemiketal intermediate **129**. Next, elimination of methanol to form the keto group is followed by second Ce^{IV} ion oxidation of the radical carbon that results in the formation of cationic intermediate **130**. As the final step, the carbocation adds water, which after proton transfer results in elimination of 1,4 benzoquinone moiety **131** and, frees the piperidine nitrogen to form the final anabasine analogue **83**.¹³⁰

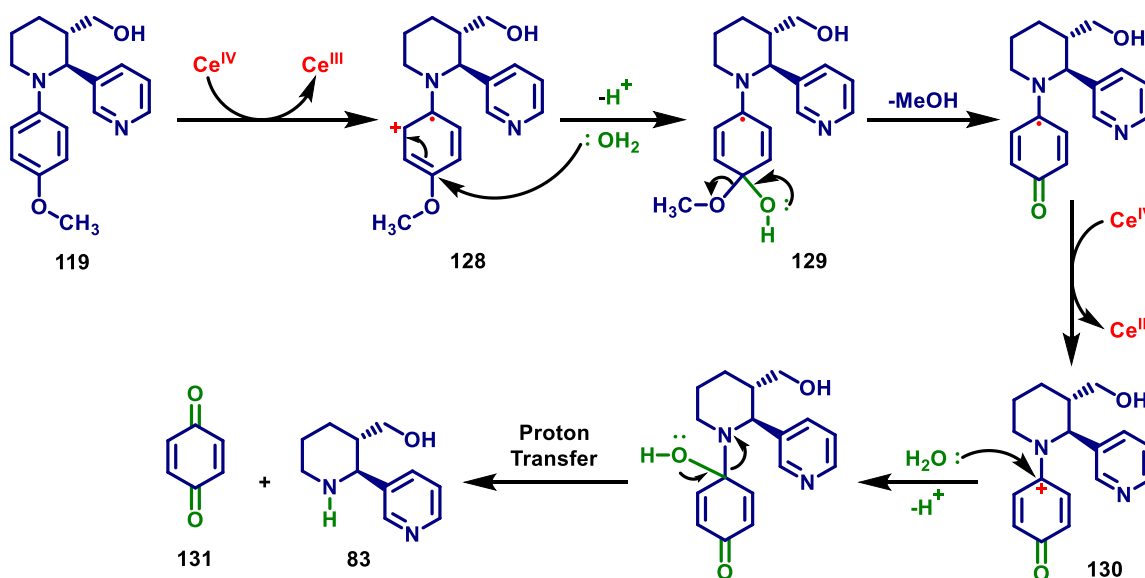


Fig. 3.15: Plausible mechanism for CAN-mediated deprotection of PMP-group from the substituted chiral piperidines to yield final anabasine analogues.¹³⁰

Synthesis of *N*-Methyl Anabasine Analogues

Both secondary and tertiary amines are important pharmacophoric features present in almost all known nAChRs ligands, as they form the crucial quaternary ammonium ion at physiological pH and establish π -cation interactions with the Trp156 residue in the agonist binding site of nAChRs. Since all the anabasine analogues had secondary amine, two bromo substituted analogues **84** and **87** were modified to their respective *N*-methyl compounds **132** and **133** for preliminary study (Fig. 3.16). This was done to determine any differences in the binding interactions and biological activity if found, between methylated and non-methylated compounds.

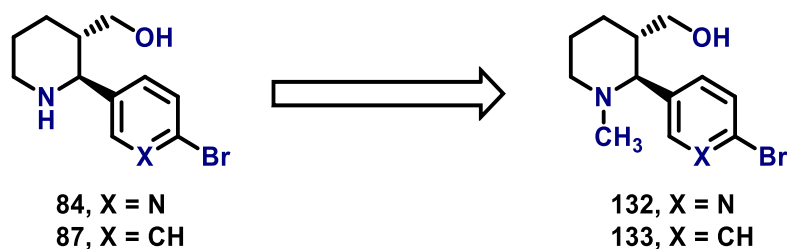
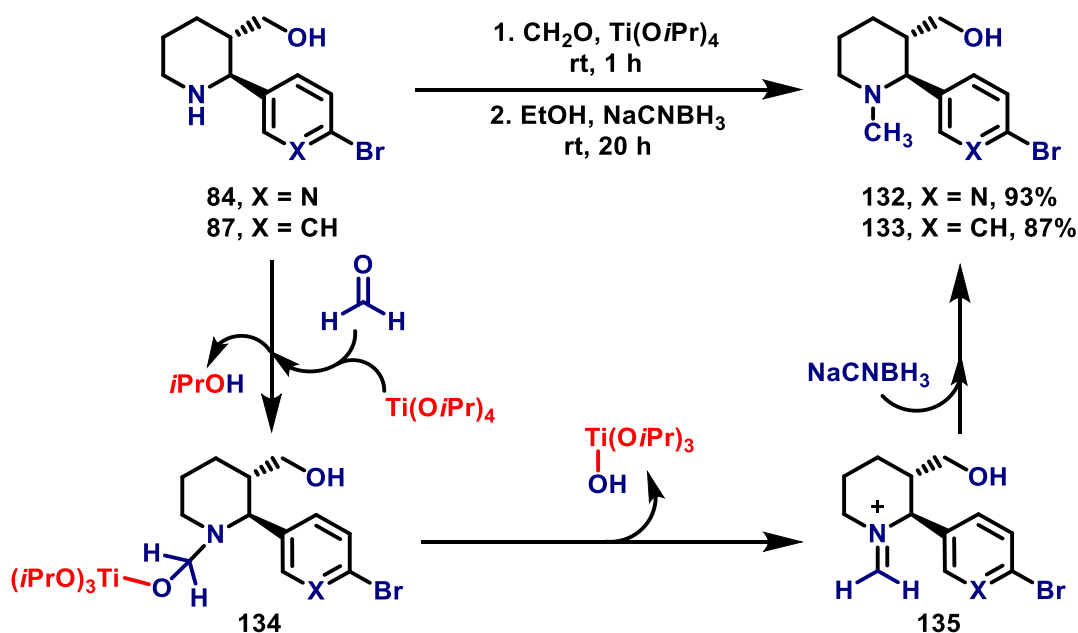


Fig. 3.16: Structural modification of anabasine analogues **84** and **87** from secondary to tertiary amine via introduction of *N*-methyl substituent.

The synthesis of *N*-methyl anabasine analogues **132** and **133** was carried out using the classical reductive alkylation of amines involving titanium(IV) isopropoxide ($Ti(OiPr)_4$), a mild Lewis acid, and sodium cyanoborohydride ($NaCNBH_3$) as the reducing agent.¹³¹ Excess of $Ti(OiPr)_4$ was used along with equal amounts of amine and formaldehyde, the alkylating agent, to plausibly form a stable aminal intermediate **134**. This was further subjected to $NaCNBH_3$ reduction, which has been proposed to proceed via generation and reduction of iminium species **135** to form the *N*-methyl products **132** and **133** (Scheme 24).



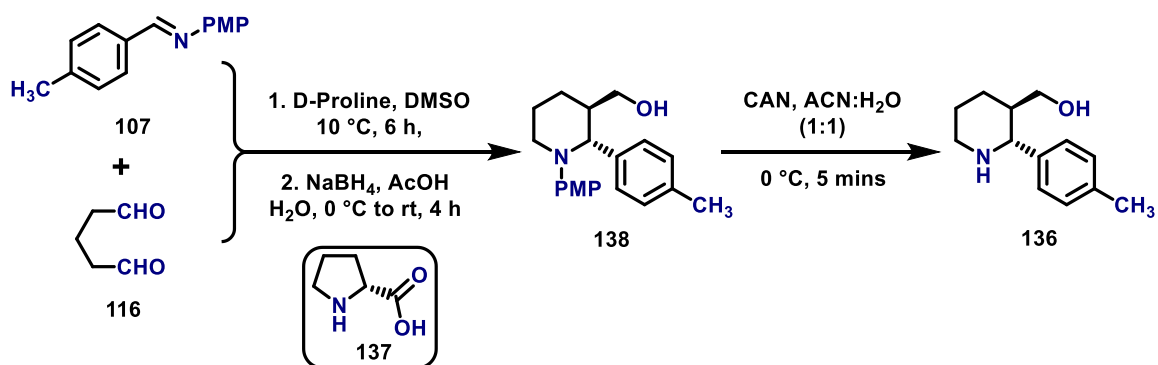
Scheme 24: Synthesis of *N*-methyl anabasine analogues **132** and **133** via formation of titanium **134** and iminium **135** species, followed by $NaCNBH_3$ reduction.¹³¹

Spectroscopic data of *N*-methyl anabasine **132** is used here as a representative for analysis and characterisation of the compound. In the 1H NMR spectrum, a singlet at 1.92 ppm was equivalent to the *N*-methyl protons, while its carbon peak appeared at 45.42 ppm in the ^{13}C

NMR spectrum. The mass spectral analysis showed two molecular ion peaks $[M+H]^+$ at 285.06 and 287.05 due to bromine isotopes, matching to the mass of compound **132**. The IR data further validated the product formation with a single broad absorption at 3368 cm^{-1} corresponding to the hydroxyl group.

Synthesis of (2*R*,3*R*)-Enantiomer of Anabasine Analogue

Since all the anabasine analogues synthesised using L-proline have 2*S*,3*S* configuration, where the 2*S*-position is equivalent to the only stereocentre present in the naturally occurring anabasine, and the 3*S*-position has been predicted to orient itself towards the targeted binding pocket. It was interesting to observe how the (2*R*,3*R*)-enantiomer of anabasine analogue **136** positions itself in the binding site and whether the orientation of the 3*R*-carbon vector towards the pocket will be better or worse compared to the (2*S*,3*S*)-enantiomer. Therefore, compound **88** was chosen for the enantiomer synthesis, as it was the last unsubstituted anabasine analogue synthesised.



Scheme 25: Synthesis of (2*R*,3*R*)-enantiomer **136** of anabasine analogue **88** via Mannich reductive cyclisation involving D-proline **137** as a catalyst.

The previously employed procedure for the one-pot Mannich reductive annulation cascade was utilised in the synthesis of piperidine core, using D-proline in place of L-proline as a catalyst, giving PMP-protected (2*R*,3*R*)-enantiomer **138** in 62% yield. The enantiomer stereochemistry was confirmed from the determination of its specific rotation and comparison with compound **124**. The compound **138** had $[\alpha]_D^{25} = -7.9$, which was equal to but opposite in sign-specific rotation of the compound **124**, i.e., $[\alpha]_D^{25} = +7.9$. The final analogue **136** was obtained in a moderate yield of 49% by applying previously optimised CAN oxidative cleavage conditions for PMP-group deprotection (**Scheme 25**). Both the

products, **138** and **136**, were characterised by various spectroscopic techniques and data obtained was the same as that for compounds **124** and **88**.

Synthesis of Nicotine Analogues

The nicotine analogues were structurally different compared to the anabasine series, as it had a pyrrolidine core rather than a piperidine ring (**Fig. 3.17**). The synthesis of pyrrolidine core utilises similar Mannich reductive cyclisation chemistry but involves an annulation cascade using succinaldehyde rather than glutaraldehyde and generates a 5-membered pyrrolidine ring. The analogue synthesis included an extra step of preparing succinaldehyde solution before every Mannich reaction, as it tends to polymerise if stored for longer periods.¹³² The preformed *N*-PMP protected aryl aldimines used previously, were exploited again for the synthesis of pyrrolidine core, employing a literature protocol after minor optimisation of reaction conditions.¹²¹

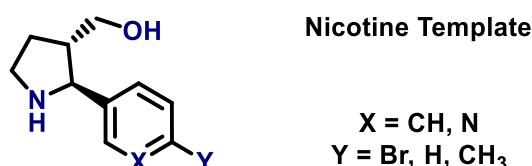
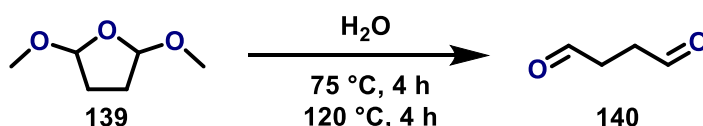


Fig. 3.17: The core nicotine template with probable substitutions for analogue synthesis.

Step 1: Synthesis of Succinaldehyde



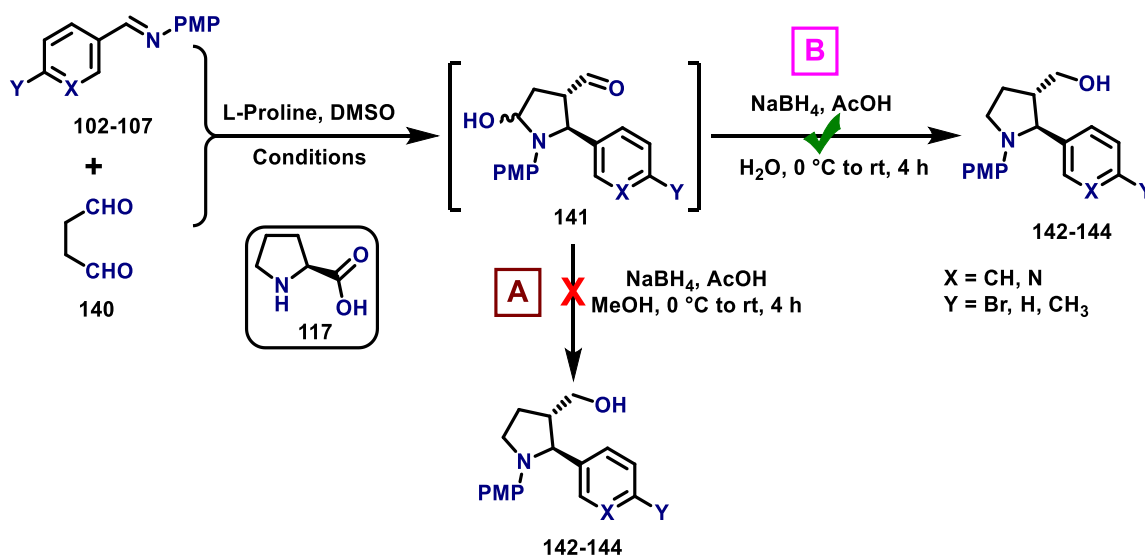
Scheme 26: Synthesis of succinaldehyde **140** from 2,5-dimethoxytetrahydrofuran **139**.¹³²

Succinaldehyde **140** was synthesised from 2,5-dimethoxytetrahydrofuran **139** (2,5-dimethoxyTHF) on gram scale using a literature procedure,¹³² a day before the Mannich reaction for generation pyrrolidine core. The aqueous solution of 2,5-dimethoxyTHF was first heated at 75 °C for 4 h to distil off the methanol formed during the process and subsequently, the reaction temperature was elevated to 120 °C to remove the excess water from the reaction mixture (**Scheme 26**). Since the rotary evaporation must be performed without heat to avoid acceleration of the polymerisation process to form the oligomer, extraction of formed succinaldehyde was carried out with the low boiling solvent DCM.

The succinaldehyde was stored at $-20\text{ }^{\circ}\text{C}$ as DCM extracts, and concentrated before the Mannich reaction. However, storing it in aqueous form for 2-3 days after extraction had no effect on the yield of proline catalysed reaction.

The succinaldehyde product formation was confirmed from the NMR spectroscopy, where two singlets in the ^1H NMR spectrum at 2.80 ppm and 9.82 ppm were equivalent to the four methylene protons and two aldehyde protons, respectively. Similarly, the ^{13}C NMR spectrum had two characteristic peaks at 36.14 ppm and 199.73 ppm corresponding to the two methylene and two aldehyde carbons. No oligomer formation was visible in both spectra and the analytical data was consistent with the literature values.¹³²

Step 2: L-Proline catalysed one-pot Mannich reductive cyclisation cascade with succinaldehyde



Scheme 27: Synthesis of substituted pyrrolidines **142-144** from PMP-protected aryl aldimines **102-107**. Reduction of Mannich Base **141** was attempted in two different ways; **A**- in separate reaction vessel using methanol as solvent, and **B**- one-pot Mannich reductive [3+2] cyclisation using previous conditions.

The general synthetic approach was to react preformed substituted aldimines **102-107** with an aqueous solution of succinaldehyde **140** using DMSO as a solvent and in the presence of a catalytic amount of L-proline **117** under cool conditions, leading to the formation of Mannich Base **141**. This was further reduced with NaBH_4 to yield *N*-PMP protected pyrrolidine compounds **142-144** (Scheme 27). The reduction was attempted in two different

ways; first, the literature procedure was followed, wherein Mannich Base **141** was isolated, and the crude product was reduced in a separate reaction vessel using methanol as a solvent (**Scheme 27A**). The yield of final product obtained was extremely low, along with several spots of the by-product observed on TLC. However, second trial of the reduction under one-pot operation employing similar protocol as used in anabasine series with water as the co-solvent gave slightly better yield with fewer by-products (**Scheme 27B**). Therefore, the latter was chosen for the reduction of Mannich Base, since the results obtained were slightly better, allowed one-pot operation bypassing the tedious process of removing DMSO from the reaction mixture, and eliminated two time-consuming workups.

Table 14: Optimisation of conditions for one-pot Mannich reductive cyclisation cascade, using PMP-protected aldimine **105** (1 eq.). ^ϕReduction was carried out in a separate vessel.

S. No.	140 (eq./xM)	L-proline (mol%)	Conditions	Co-solvent	Yield (%)
1.	3/3	20	10 °C, 9 h	Water	12
2.	3/3	20	10 °C, 9 h	MeOH ^ϕ	19
3.	4/3	20	10 °C, 9 h	Water	27
4.	5/3	20	10 °C, 9 h	Water	17
5.	4/3	30	10 °C, 9 h	Water	37
6.	4/4	30	10 °C, 7 h	Water	49
7.	4/4	40	10 °C, 6 h	Water	67
8.	4/4	40	10 °C, 6 h	MeOH ^ϕ	27

Next, the Mannich reaction was optimised to improve the product yield and reduce by-product formation. Synthesis of *N*-PMP protected 2,3-disubstituted pyrrolidine **142** has been used here as a representative example. The initial two trials (**Table 14: entry 1-2**) mentioned in the table below have already been discussed in the preceding paragraph. Increasing the succinaldehyde amount to 4 eq. improved the overall yield from 19% to 27% but dropped to 17% on using 5 eq. of the dialdehyde (**Table 14: entry 3-4**). Raising the amount of L-proline to 30 mol% gave a better yield of 37%, though, it was still accompanied by several by-products as observed on TLC (**Table 14: entry 5**). This issue was addressed when the concentration of succinaldehyde solution was increased to 4 M along with the shortening of reaction time from 9 h to 7 h, giving a 49% yield (**Table 14: entry 6**). Further reduction in the reaction time to 6 h while elevating the catalyst amount to 40 mol% afforded

the title compound **142** in 67% yield (**Table 14: entry 7**). The optimised protocol was attempted with the literature method using a separate vessel to carry out reduction with methanol as the solvent, though, the result achieved was not as per expectation and gave only 27% yield (**Table 14: entry 8**).

The aforementioned conditions (**Table 14: entry 7**) were employed for the synthesis of following optically enriched *N*-PMP protected 2,3-disubstituted pyrrolidines in good yields (**Table 15**) after purification from flash chromatography. All synthesised compounds pyrrolidines were characterised by various spectroscopic techniques. However, the time constraints along with the positive biological evaluation of substituted anabasine series (discussed later), restricted the synthesis of unsubstituted nicotine series, therefore, only three disubstituted pyrrolidines were generated.

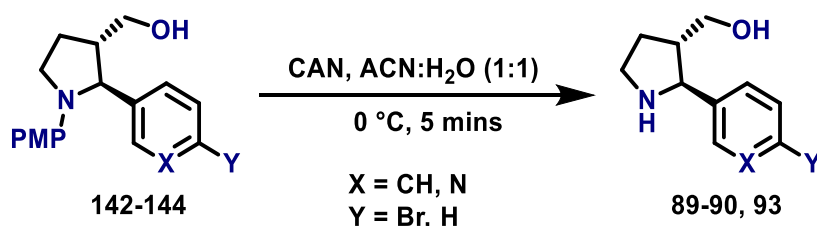
Table 15: Respective yields and substitutions present in the synthesised *N*-PMP protected piperidines **142-144**.

S. No.	Substitutions X, Y	Piperidine Yield (%)
1.	CH, Br (142)	67
2.	N, H (143)	65
3.	N, Br (144)	70

For easier understanding, spectral data of substituted pyrrolidine **142** is used here as a representative for the analysis and characterisation of these compounds. In the ^1H NMR spectrum, two peaks at 7.43 ppm and 6.76 ppm of the aromatic region were equivalent to four protons of the phenyl rings from the PMP group, while the methoxy protons were observed as a singlet at 3.71 ppm. The other two peaks at 7.15 ppm and 6.42 ppm were characteristic of the bromophenyl ring protons. Methylene protons of the hydroxymethyl group were observed as a doublet of doublet at 3.68 ppm. Five peaks present in the aliphatic region between 4.47 ppm to 1.89 ppm correspond well with the 6 protons of pyrrolidine ring. Similarly, the ^{13}C NMR spectrum displayed 8 peaks between 151.29 ppm and 113.45 ppm in the aromatic region that complemented with the six carbons at each of the two phenyl rings. Characteristic peaks at 64.31 ppm and 55.99 ppm were equivalent to the two carbons of hydroxymethyl and methoxy groups, respectively. Also, four peaks in the aliphatic region were consistent with the four carbons of the pyrrolidine ring. The mass spectral analysis showed molecular ion peaks $[\text{M}+\text{H}]^+$ at 362.1 and 364.2 as well as

$[M+Na]^+$ peaks at 384.2 and 386.0, corresponding to the mass of compound **142** with bromine isotopes. The IR data further validated the pyrrolidine synthesis with a broad absorption at 3410 cm^{-1} for hydroxyl group and a medium absorption at 2938 cm^{-1} for alkane C-H stretching. The experimental specific rotation of compound **142** was $[\alpha]_D^{25} = -43.2$ which was equivalent to the reported literature value.¹²¹

Step 3: PMP-deprotection by Ceric Ammonium Nitrate



Scheme 28: Cleavage of *N*-PMP pyrrolidines **142-144** to yield free amines **89-90, 93**.

The removal of the *N*-PMP protecting group from the pyrrolidine ring was carried out employing similar conditions optimised for the anabasine series (**Scheme 28**). The 2,3-disubstituted pyrrolidine compounds **142-144** were subjected to CAN oxidising conditions in a solvent mixture of ACN and water (1:1) at $0\text{ }^\circ\text{C}$. The reaction was neutralised within 5 mins of using sodium hydroxide (NaOH) and subsequently, extracted with a strong polar solvent mixture of CHCl_3 and IprOH (3:1). The crude extract was purified from the flash chromatography and afforded the final nicotine analogues **89-90** and **93** in moderate to high yields, as mentioned in the table below (**Table 16**).

Table 16: Respective yields as well as substitutions present in the final PMP-deprotected nicotine analogues **89-90** and **93**.

S. No.	Substitutions X, Y	Analogue Yield (%)
1.	N, H (89)	66
2.	N, Br (90)	73
3.	CH, Br (93)	69

Removal of the PMP-group from piperidine compound **142** to afford its corresponding analogue **93** was confirmed from the disappearance of two doublet of triplets at 7.43 ppm and 6.76 ppm in the aromatic region as well as the methoxy proton singlet at 3.71 ppm in

the ^1H NMR spectrum. The pair of diastereotopic protons attached to hydroxymethyl group was observed as a multiplet at 3.66 ppm in the aliphatic region, contrary to the two doublet of doublets observed in case of anabasine analogues. A broad singlet at 1.96 ppm was consistent with the piperidine ring's amine proton, while the two overlapping broad absorptions at 3310 cm^{-1} and 3250 cm^{-1} were consistent with the hydroxyl and secondary amino groups, respectively. Likewise, the absence of methoxy and phenyl carbons peaks in the ^{13}C NMR spectrum established the PMP-deprotection step. Further validation was obtained from the analysis of the mass spectrum, with visualisation of a molecular ion peak $[\text{M}+\text{H}]^+$ at 256.2 and 258.1, corresponding to the mass of nicotine analogue **93**.

3.2.4. SYNTHESIS OF SUBSTITUTED ANABASINE AND NICOTINE ANALOGUES

Once the synthesis of unsubstituted series of anabasine and nicotine analogues was complete, they were submitted for biological evaluation. From the anabasine series, non-methylated bromopyridyl anabasine analogue **84** showed some activity in the early stages of study, out of all the nine compounds submitted. Therefore, the substituted series was developed on the basis of bromopyridyl anabasine as a template. The other reason for selecting the bromopyridyl anabasine was its close resemblance to NS3920.

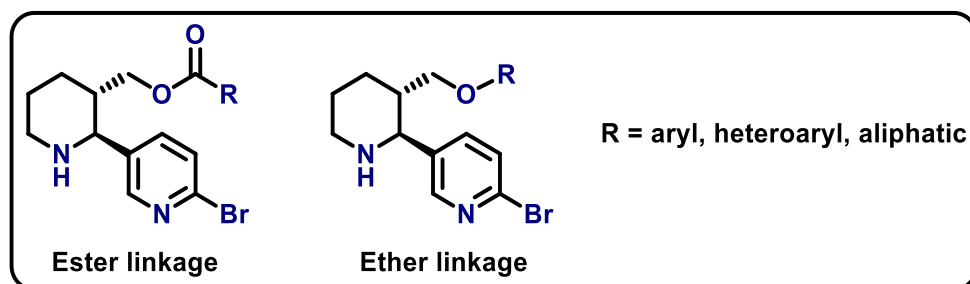


Fig. 3.18: Structural modification of anabasine template to introduce ester and ether linkages for side-chain substitutions with various aryl, heteroaryl or aliphatic moieties.

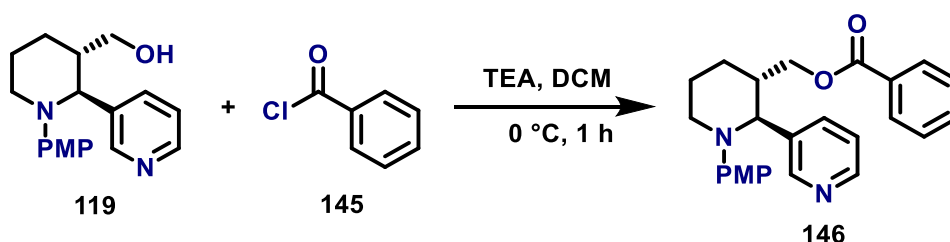
On finalising the template for side-chain extension, various substituents were chosen for introduction at the hydroxymethyl group, as it was predicted to be directed towards the newly identified pocket in the binding site. The two major aims were to, establish the extension of side chain into the pocket, and identifying different substituents that initiate some sort of interactions with the nearby amino acid residues. Since the reactive hydroxyl group attached to the methylene alcohol can easily undergo functional group interconversion, thus, it could provide linkage to the assorted substituents with the potential

to extend into the pocket and interact. In this research, the ether and ester linkages were initially explored, first, for their ability to initiate a donor-acceptor type interaction with the amino acid residues and second, by providing an inducible fit in the pocket via a single bond rotation. Entities like aromatic, heteroaromatic and aliphatic systems were planned for introduction as side-chain substituents linked to ester and ether moieties (**Fig. 3.18**). This will further assist in designing novel molecules that may display enhanced bioactivity and selectivity for the $\alpha 4$ - $\alpha 4$ binding site.

Synthesis of Ester Linked Substituted Anabasine Analogues

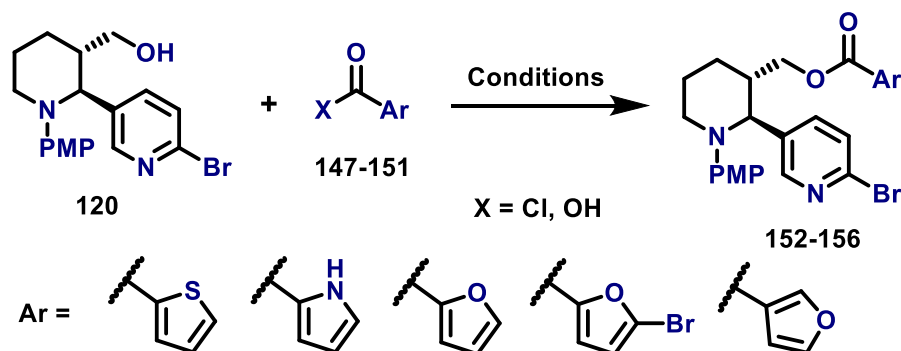
The key step towards synthesis of ester sidechains on the anabasine template was to modify the secondary alcohol to an ester functionality. Since the previously optimised reductive Mannich cyclisation cascade afforded the *N*-PMP bromopyridyl anabasine template **120**, the protected compound was used for further reaction to install ester moiety. The synthesis was carried out in two steps, starting with the esterification of alcohol followed by deprotection of the PMP-group utilising an optimised procedure mentioned in the preceding section. The esterification reaction is well known, and a handful of conditions were trialled, especially on the five-membered heterocyclic systems to provide the target compounds in high yields and purity.

Step 1: Esterification of Alcohol



Scheme 29: Esterification of compound **119** with benzoyl chloride **145** under cold basic conditions to afford ester **146**.¹³³

Firstly, the reaction was tried with benzoyl chloride and *N*-PMP pyridyl anabasine **119** rather than the bromopyridyl **120** to keep things simple. Benzoyl chloride **145** was reacted with compound **119** utilising triethylamine (TEA) in cold DCM as a solvent, affording the phenyl ester **146** in high yields of 77% (**Scheme 29**).¹³³



Scheme 30: Esterification of compound **120** with various heterocyclic acid or acyl chloride derivatives **147-151** to afford esters **152-156**.

Since the benzoyl esterification proceeded smoothly, the bromopyridyl compound **120** was used in further syntheses towards target compounds. To generate esters, five-membered heterocycles were chosen due to the easy availability or synthesis of their carbonyl derivatives (**Scheme 30**). As the reaction didn't proceed as expected, minor optimisation of conditions were carried out to obtain high yields (**Table 17**).

The first trial (**Table 17: entry 1**) involved the synthesis of thiophene-2-carbonyl chloride from its acid derivative **147** using thionyl chloride under reflux conditions.¹³⁴ The formed acyl chloride was carried onto the next step without purification and reacted with anabasine **120** using TEA as a base in cold DCM. Though the overall yield of 38% was too low compared to the previous esterification, it was observed that the thionyl chloride reaction itself afforded a low yield of acyl chloride. Hence, thionyl chloride was replaced with oxalyl chloride with catalytic amounts of dimethylformamide (DMF) using cold DCM.¹³⁵ This further resulted in a reduced overall yield to 26%, as the generation of acid chloride remained extremely poor (**Table 17: entry 2**). Therefore, a different approach was employed for the synthesis of ester linkage using carbodiimides, i.e. Steglich esterification reaction. Firstly, dicyclohexylcarbodiimide (DCC) was stirred with thiophene-2-carboxylic acid in DCM for an hour at room temperature to activate the carbonyl via formation of acylisourea intermediate. Subsequent addition of anabasine **120** with catalytic amounts of 4-dimethylamino pyridine (DMAP) to the stirring solution, yielded the final compound **152** in moderate yield of 44% (**Table 17: entry 3**).¹³⁶ Since the major disadvantage of using DCC is the formation of dicyclohexylurea, a water-insoluble product, therefore, the final product exhibited difficulty in purification as visible from an unclear NMR spectrum. The issue was rectified with the use of carbonyldiimidazole (CDI) as a carbonyl activator

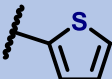
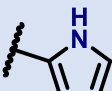
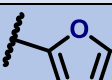
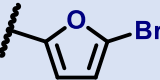
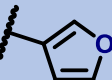
because it leads to the formation of a water-soluble imidazole as a by-product, which can be easily removed by simple aqueous work-up (**Table 17: entry 4**).¹³⁶ Thus, the esterification was mediated by CDI under strong basic conditions of 1,8-diazabicyclo[5.4.0]undec-7-ene (DBU) with catalytic amounts of DMAP in DMF, leading to moderately high yields of 68% for the final compound **152**.

Table 17: Optimisation of esterification conditions to obtain products in high yields.

S. No.	Reactants	Conditions	Yield of 152
1.	147 (1 eq.)	(A) SOCl ₂ , reflux, 1 h (B) 120 (1 eq.), TEA, DCM, 0 °C, 2 h	38%
2.	147 (1 eq.)	(A) (COCl) ₂ , DMF (cat.), DCM, 0 °C to rt, 5 h (B) 120 (1 eq.), TEA, DCM, 0 °C, 2 h	26%
3.	147 (2 eq.)	DCC, DCM, 1 h, 120 (1 eq.), DMAP, 36 h, rt	44%
4.	147 (3 eq.)	(A) CDI, DMF, 1 h, rt (B) 120 (1 eq.), DBU, DMAP, 24 h, rt	68%

The spectroscopic data of thiophene ester **152** is used as a representative for analysis and characterisation of the compound. In the ¹H NMR spectrum, three peaks at 8.20 ppm, 7.69 ppm and 7.23 ppm of the aromatic region were equivalent to the three pyridyl protons, while three peaks at 7.56 ppm, 7.43 ppm and 7.11 ppm matched well with the three thiophene ring protons. Similarly, two doublets at 6.90 ppm and 6.63 ppm corresponded to the phenyl ring protons of the PMP group, while the methoxy protons were observed as a singlet at 3.68 ppm. Methylene protons of the ester linkage were observed as a doublet of doublet at 3.92 ppm. Seven peaks present in the aliphatic region between 4.13 ppm and 1.47 ppm correspond well with the 8 protons of the piperidine ring. Similarly, the peak observed at 161.96 ppm in the ¹³C NMR spectrum was characteristic of the ester carbonyl carbon, while the four thiophene carbon peaks were observed at 138.59 ppm, 136.92 ppm, 133.40 ppm and 127.89 ppm. The peaks 66.66 ppm and 55.38 were consistent with the corresponding methylene and methoxy carbons of ester linkage and PMP group, respectively. Other carbon peaks complemented well with the peaks observed in the respective aromatic and aliphatic regions of the carbon spectrum. The analysis of mass spectrum showed molecular ion peaks [M+H]⁺ at 487.3 and 489.2 corresponding to the mass of compound **152** with bromine isotopes. The IR data further validated the esterification with a strong absorption at 1758 cm⁻¹ for the ester group.

Table 18: Respective yields and heterocyclic substitutions to yield ester-linked N-PMP protected piperidine compounds 152-156.

S. No.	Ester Substitutions	Yield (%)
1.	 152	68
2.	 153	55
3.	 154	51
4.	 155	57
5.	 156	45

The aforementioned CDI-mediated esterification conditions (**Table 17: entry 4**) were used for the synthesis of esters linked heterocyclic piperidine derivatives **153-156** in good to moderate yields (**Table 18**) after purification from flash chromatography. All synthesised compounds were characterised by various spectroscopic techniques, after which they were carried onto the next step of PMP-group deprotection.

Mechanism of CDI-mediated Esterification

Synthesis of thiophene ester-linked piperidine **152** is taken as the representative example to explain carbonyldiimidazole (CDI)-mediated esterification mechanism (**Fig. 3.19**).¹³⁷ A strong base such as 1,8-diazabicyclo[5.4.0]undec-7-ene (DBU) deprotonates thiophene-2-carboxylic acid **147** to generate the carboxylate anion **157**. The formed anion attacks at the carbonyl centre of CDI molecule which undergoes substitution to eliminate one of the two imidazoles. This results in the activation of carboxylic acid via the formation of a mixed anhydride intermediate **158** to which alcohol can be added to yield respective ester. Yet, the reaction can be sluggish as the acyl migration is slow, therefore, catalytic amounts of DMAP are crucial to drive the reaction towards completion. DMAP, being the stronger nucleophile than alcohol acts as an acyl transfer reagent that accelerates the rate by reacting with the anhydride **158** to produce a reactive acylpyridinium species **159**. This active intermediate reacts rapidly with the incoming piperidine alcohol **120** to yield ester **152**.

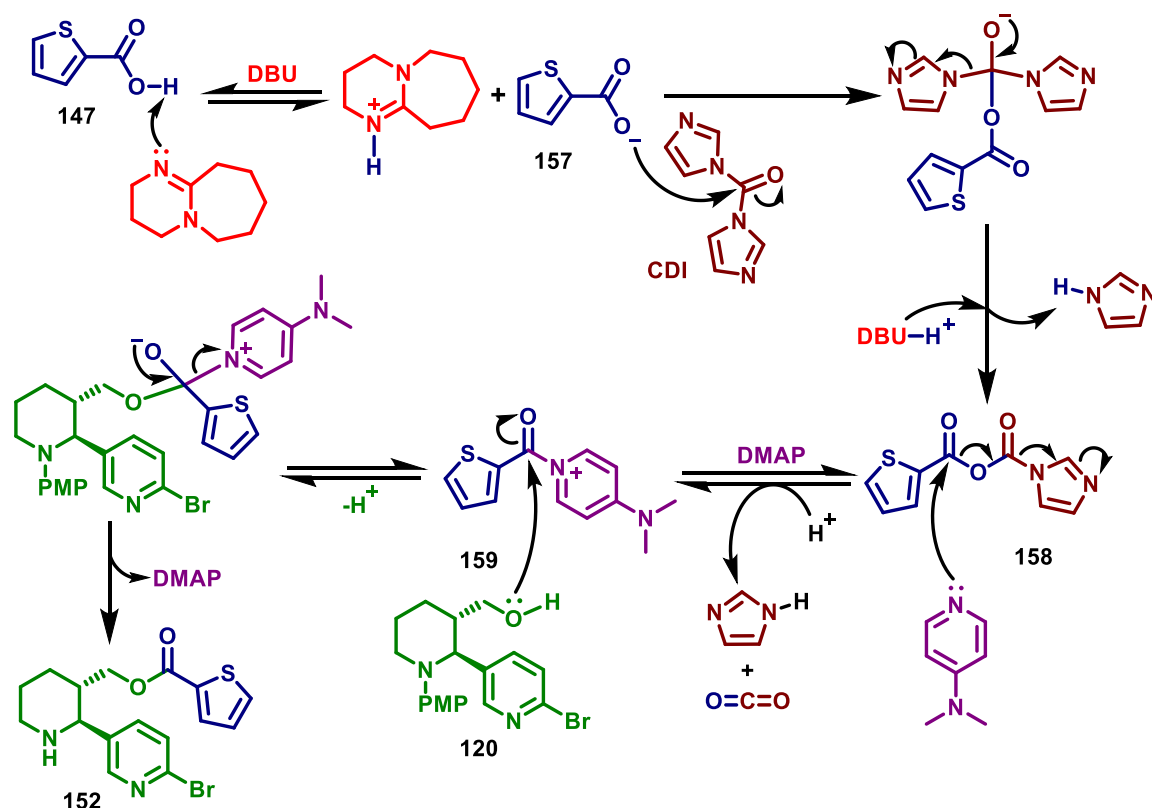
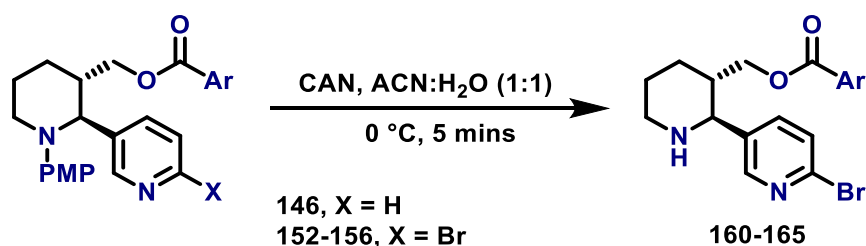


Fig. 3.19: Plausible mechanism for the CDI-mediated esterification.¹³⁷

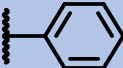
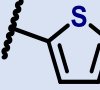
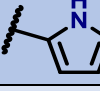
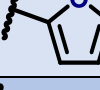
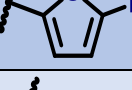

Step 2: PMP-deprotection by Ceric Ammonium Nitrate

Similar conditions were employed for the cleavage of the *N*-PMP protecting group from the piperidine ring that were optimised for the anabasine series (**Scheme 31**). The 2,3-disubstituted piperidine ester compounds **146**, **152-156** were subjected to CAN oxidising conditions in a solvent mixture of ACN and water (1:1) at 0 °C. The reaction was neutralised within 5 mins of using sodium hydroxide (NaOH) and subsequently, extracted with a strong polar solvent mixture of CHCl₃ and IprOH (3:1). The crude extract was purified from the flash chromatography and afforded the final piperidine ester analogues **160-165** in moderate to high yields, as mentioned in the table below (**Table 19**).



Scheme 31: Cleavage of PMP-piperidine esters **146**, **152-156** to yield free amines **160-164**.

Table 19: Respective yields and heterocyclic substitutions present in the final PMP-deprotected piperidine ester analogues **160-165**.

S. No.	Ester Substitutions	Yield (%)
1.	 160	66
2.	 161	75
3.	 162	63
4.	 163	69
5.	 164	72
6.	 165	61

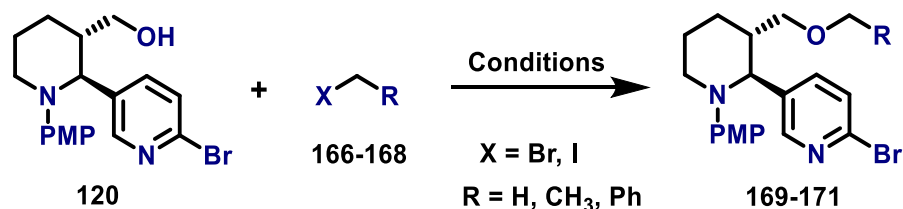
The PMP-group deprotection from piperidine ester **152** to afford its corresponding analogue **161** was confirmed by the disappearance of two doublet of triplets at 6.90 ppm and 6.63 ppm in the aromatic region as well as the methoxy proton singlet at 3.68 ppm in the ^1H NMR spectrum. This also resulted in the observation of sharp peaks in the aliphatic as well as aromatic region. Only five peaks were present between 8.38 ppm to 7.09 ppm, equivalent to the aromatic protons of pyridyl and thiophenyl rings. The appearance of two doublet of doublets at 4.05 ppm and 3.88 ppm in the aliphatic region were characteristic to the pair of diastereotopic protons attached to the hydroxymethyl group. A broad singlet merged with a multiplet between 2.06-1.96 ppm was consistent with the piperidine ring amine proton, while in the IR spectrum, it was observed as a broad absorption at 3342 cm^{-1} . Likewise, the absence of methoxy and phenyl carbons peaks in the ^{13}C NMR spectrum established the PMP-deprotection step. Its further validation was obtained from the mass spectral analysis with visualisation of molecular ion peaks $[\text{M}+\text{H}]^+$ at 381.6 and 383.1, corresponding to the mass of piperidine ester analogue **161** with bromine isotopes.

Synthesis of Ether Linked Substituted Anabasine Analogues

Formation of the key ether linkage to introduce sidechain substitutions on the secondary alcohol moiety was carried on the same pre-synthesised *N*-PMP bromopyridyl anabasine

template **120**. The first step involved the base promoted installation of substituents using various aryl, heteroaryl and aliphatic halides, followed by CAN-mediated oxidative cleavage of the PMP-group to release respective piperidine ethers. Minor optimisation was needed to achieve the formation of ether functionality in high yields.

Step 1: Synthesis of *N*-PMP protected Piperidine Ethers



Scheme 32: Synthesis of *N*-PMP protected piperidine ethers **169-171** from piperidine alcohol **120** using various halogenated compounds.¹³³

Due to time constraints, a total of three ether substituted piperidines were synthesised from halo-compounds (**Scheme 32**). For optimisation of reaction, benzyl bromide (BnBr) and *N*-PMP bromopyridyl anabasine **120** were employed to obtain the target piperidine ether compound **169** in a high yield.

Table 20: Optimisation of conditions to install ether-linked substituents.

S. No.	Reactant	Conditions	Result
1.	BnBr (1 eq.)	K ₂ CO ₃ , MeOH, rt, 3 h	Pyridinium-benzyl adduct
2.	BnBr (1 eq.)	NaH, DMF, 0 °C, rt, 1 h	Pyridinium-benzyl adduct
3.	BnBr (1 eq.)	NaH, THF, 0 °C, rt, 1 h	Major: Pyridinium-benzyl adduct Minor: Benzyl ether 169 (19%)
4.	BnBr (1 eq.)	NaH, THF, 0 °C, 12 h	Benzyl ether 169 (82%)

The first trial (**Table 20: entry 1**) was carried out using potassium carbonate in methanol at an ambient temperature that resulted in the formation of product. However, the product formed largely remained in the aqueous layer during work-up and was difficult to extract. Further analysis suggested that benzyl bromide reacted with pyridyl nitrogen to form pyridinium-benzyl adduct, rather than the expected benzyl ether. Since potassium carbonate is not strong enough as a base to completely abstract the proton from the alcohol, hence,

sodium hydride (NaH) was used with other aprotic polar solvents to achieve the ether formation. Similar result was obtained on using NaH in DMF (**Table 20: entry 2**), however, changing the solvent to THF resulted in the formation of benzyl ether, but in an extremely low yield of 19% along with major amounts of pyridinium-benzyl adduct (**Table 20: entry 3**). The issue was resolved by carrying out the reaction in cold conditions for 12 h, as it lowers the reactivity of pyridyl nitrogen and consequently, the target piperidine benzyl ether **169** was achieved in a high yield of 82% (**Table 20: entry 4**).

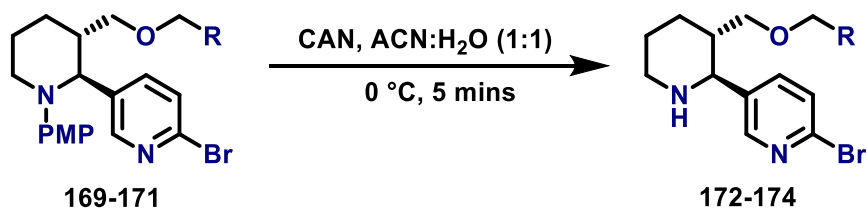
Spectroscopic data for the piperidine benzyl ether **169** is used as a representative for characterisation purpose. In the ^1H NMR spectrum, a multiplet overlapping with the CDCl_3 peak between 7.36 ppm to 7.21 ppm, was equivalent to the five protons of the phenyl ring linked to ether. The methylene protons attached to the phenyl ring were observed downfield as a singlet at 4.34 ppm due to the combined deshielding effect from phenyl ring and ether oxygen, while the diastereotopic methylene protons of the piperidine ring appeared upfield as multiplets between 3.23 ppm to 3.18 ppm. In the ^{13}C NMR spectrum, four peaks at 138.61 ppm, 128.51 ppm, 127.76 ppm and 127.66 ppm were equivalent to the six phenyl ring carbons attached via an ether linkage. Similar to ^1H NMR, in this instance too, the methylene carbon attached to the phenyl ring appeared slightly downfield at 73.35 ppm compared to the diastereotopic carbon at 71.96 ppm. The analysis of the mass spectrum showed molecular ion peaks $[\text{M}+\text{H}]^+$ at 467.1 and 469.6 corresponding to the mass of compound **169** with bromine isotopes.

Table 21: Respective yields and substitutions to yield *N*-PMP protected piperidine ether compounds **169-171**.

S. No.	Ether Substitutions	Yield (%)
1.	Benzyl (169)	82
2.	Methyl (170)	79
3.	Ethyl (171)	87

The previously optimised conditions (**Table 20: entry 4**) were used for the installation of ether linkage and synthesis of piperidine ethers **169-171** in high yields (**Table 21**) after purification from flash chromatography. All synthesised compounds were characterised by various spectroscopic techniques, after which they were carried onto the next step of PMP-group deprotection.

Step 2: PMP-deprotection by Ceric Ammonium Nitrate

**Scheme 33:** Cleavage of PMP-piperidine ethers **169-171** to yield free amines **172-174**.

As before, the 2,3-disubstituted piperidine ether compounds **169-171** were reacted with CAN oxidising conditions in a solvent mixture of ACN and water (1:1) at 0 °C for deprotection of the PMP-group (**Scheme 33**). The crude extract was purified from the flash chromatography and afforded the final piperidine ether analogues **172-174** in moderate to high yields, as mentioned in the table below (**Table 22**).

Table 22: Respective yields and substitutions in final piperidine ether analogues **172-174**.

S. No.	Ester Substitutions	Yield (%)
1.	Benzyl (172)	69
2.	Methyl (173)	71
3.	Ethyl (174)	62

The cleavage of PMP-group from the piperidine benzyl ether **169** to afford its corresponding analogue **172** was confirmed from the disappearance of two doublet of triplets at 6.88 ppm and 6.64 ppm in the aromatic region as well as the methoxy proton singlet at 3.68 ppm in the ^1H NMR spectrum. The broad singlet at 1.76 ppm was equivalent to the piperidine ring's amine proton, while in the IR spectrum, it was observed as a broad absorption at 3333 cm^{-1} . The absence of methoxy and phenyl carbons peaks in the ^{13}C NMR spectrum further confirmed the cleavage of PMP-group from piperidine. The mass spectrum showed molecular ion peaks $[\text{M}+\text{H}]^+$ at 361.8 and 363.5, corresponding to the mass of piperidine benzyl ether analogue **172** with bromine isotopes.

Synthesis of CMPI Linked Substituted Anabasine Analogues

It has been discussed in the preceding sections that CMPI is a selective and potent PAM for $(\alpha 4)_3(\beta 2)_2$ stoichiometry which can also be used in photoaffinity labelling experiments.

Since anabasine template displays complete overlap with NS3920 in the $\alpha 4$ - $\alpha 4$ binding site, while CMPI binds to the targeted pocket of the $\alpha 4$ - $\alpha 4$ site, hence, it will be interesting to assess the bioactivity of compounds that possess important structural determinants of both CMPI and anabasine.

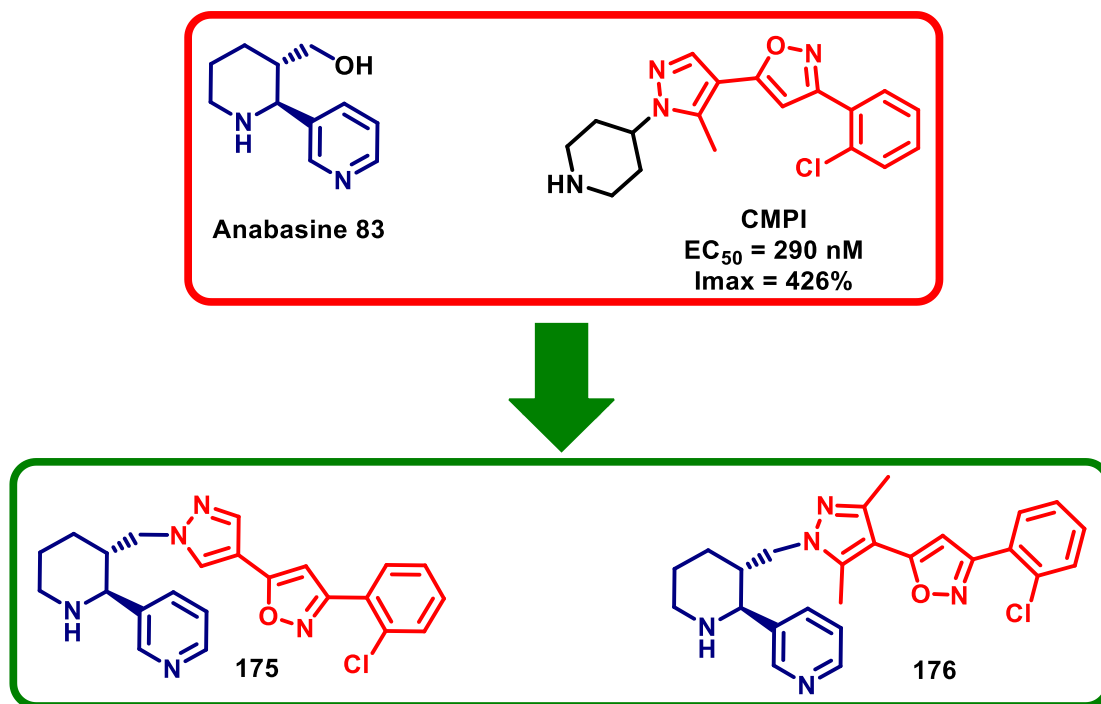
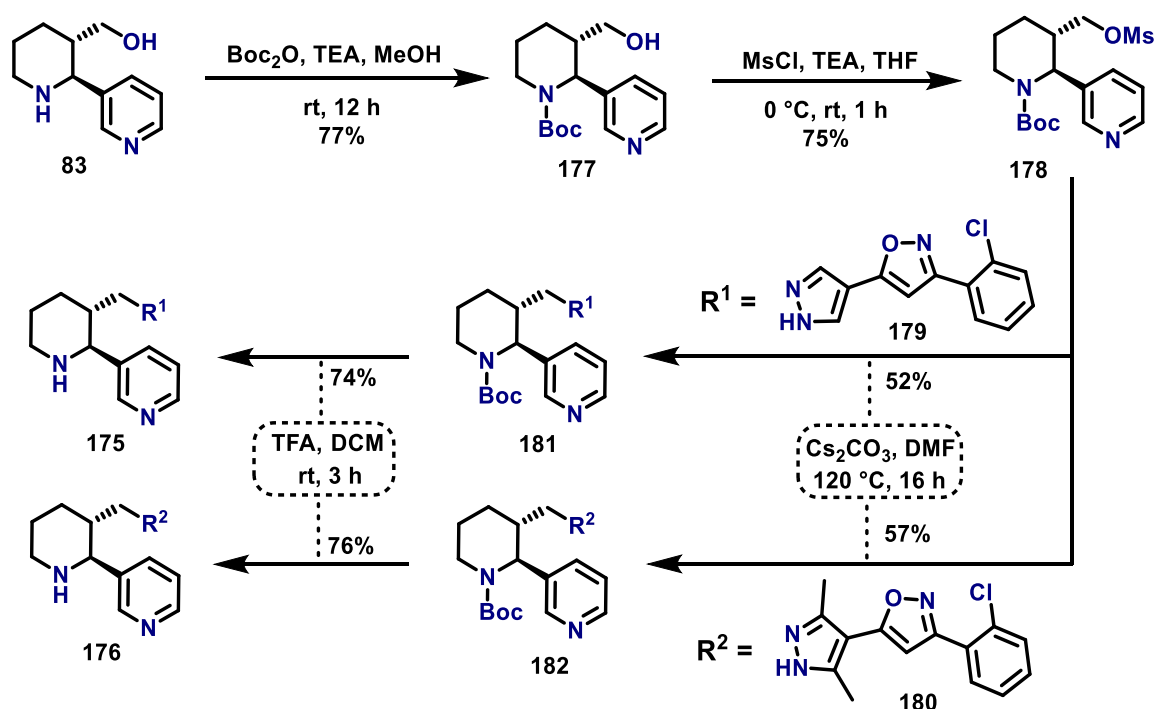


Fig. 3.20: CMPI linked anabasine analogues **175** and **176**.

As shown above (**Fig. 3.20**), the piperidine ring is a common structural feature present in both the compounds and replacing it in CMPI with anabasine, like a sidechain substitution, still maintains the basic architecture of both molecules. It was predicted that the anabasine part of the molecule will interact with the five ‘aromatic cage’ residues similar to NS3920, whereas, the CMPI backbone will extend into the pocket. This may not only provide better selectivity and modulatory activity but could also become an effective photolabeling tool to further identify and study amino acids present in the binding site as well as its pocket. For the design of analogues **175** and **176**, pyridyl piperidine **83** was chosen, because the synthesis was executed before the bioactivity results of anabasine series were obtained. The pyrazole-isoxazole backbone of the CMPI was already synthesised by a co-worker.

The synthesis of analogues **175** and **176** was carried out in four high yielding steps, as mentioned below (**Scheme 34**). Before extending the sidechain of piperidine **83** with the pyrazole-isoxazole backbone substituent, the free amine of piperidine **83** was protected with

Boc-group under basic conditions,¹⁰⁴ as it can undergo self-coupling. Once the Boc-protected compound **177** was obtained in 77% yield, confirmed by the appearance of Boc-singlet at 1.48ppm in the ¹H NMR, the alcohol was subjected to mesylation that installs a superior leaving group for easier and rapid substitution by the pyrazole nucleophile.¹⁰⁴ Piperidine alcohol **177** was reacted with mesyl chloride under cold basic conditions that functionalised the alcohol into mesylate **178** with 75% yield. Mesylation was established by the presence of methyl protons singlet at 3.08 ppm and methylene protons multiplet between 2.80 ppm to 2.72 ppm in the ¹H NMR spectrum. Subsequently, the mesylate **178** was reacted with two different pyrazole-isoxazole backbones **179** and **180**, under strong basic conditions of cesium carbonate in DMF at 120 °C,¹⁰⁴ to afford piperidine substituted pyrazoles **181** and **182** in 52% and 57% yield, respectively. This was followed by the removal of Boc-group using TFA which generated the final anabasine linked CMPI analogues **175** and **176** in 74% and 76% yield. The confirmation of pyrazole substitution was established by various spectroscopic techniques after chromatographic purification.



Scheme 34: Synthesis of CMPI linked anabasine analogues **175** and **176** from piperidine **83** and pyrazoles **179** and **180**.

Spectroscopic data for the anabasine-CMPI analogue **176** is used as a representative for characterisation purpose. In the ¹H NMR spectrum, the two sets of methyl protons attached to the pyrazole ring were observed as singlets at 2.56 ppm and 2.45 ppm, while the lone

isoxazole proton appeared as a singlet at 6.63 ppm. The two sets of doublet of doublets at 4.36 ppm and 4.11 ppm were consistent with the methylene sidechain of the piperidine ring. The absence of methyl and methylene protons peak of the mesyl group at 3.08 ppm and 2.80 ppm confirmed the substitution of pyrazole-isoxazole backbone to the anabasine, while the Boc-group cleavage was established from the disappearance of singlet at 1.48 ppm.

3.2.5. BIOLOGICAL EVALUATION OF ANABASINE AND NICOTINE ANALOGUES

All the 23 anabasine and nicotine analogues were sent to our collaborator Dr. Thomas Balle at the University of Sydney for biological evaluation using nAChR functional assay, i.e., two-electrode voltage clamp electrophysiology technique. Since the technique has been discussed in detail in the previous section, so the focus will be on assessing the biological results obtained for some analogues.

The representative dose-response curve (DRC) and electrophysiological trace of anabasine ester **164** have been illustrated below (Fig. 3.21). The magnitude of electrical response from the current generated over a time period by the *Xenopus* oocyte on the binding of analogue **164** is characterised as black peaks in the trace. Varied concentrations of the analogue were injected into the oocytes, with each being accompanied with a ‘wash out’ period demonstrated as a straight line, i.e., no compound was applied to prevent receptor desensitisation. The largest peak shown below is the maximum response generated by 3.16 mM ACh concentration which determines the maximal activation of the receptor achieved from complete occupancy of both the $\alpha 4$ - $\beta 2$ and $\alpha 4$ - $\alpha 4$ binding sites.

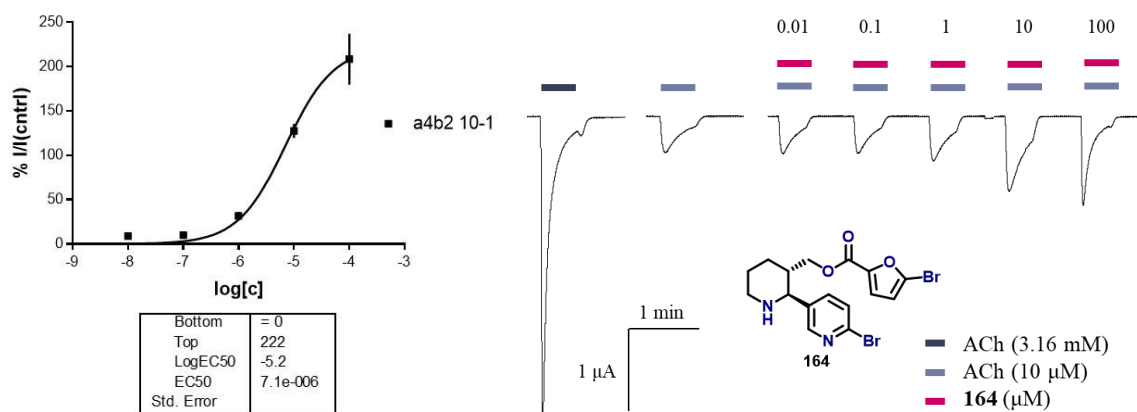


Fig. 3.21: Representative DRC and electrophysiological trace for analogue **164**.

To determine the efficacy and potency of the applied drug, the dose-response curve is plotted by fitting the EC_{50} data obtained from the electrophysiology assay, into a sigmoidal curve with $\%I_{max}$ value against the concentration of the applied compound. The $\%I_{max}$ of an applied drug is the improvement of maximal current generated and recorded (I_{max}) in terms of percentage relative to the EC_{10} concentration of ACh, which is equivalent to 0%. Thus, the $\%I_{max}$ value obtained measures the efficacy of an applied drug, while the halfway response to top of the curve (EC_{50}) is measured as its potency.

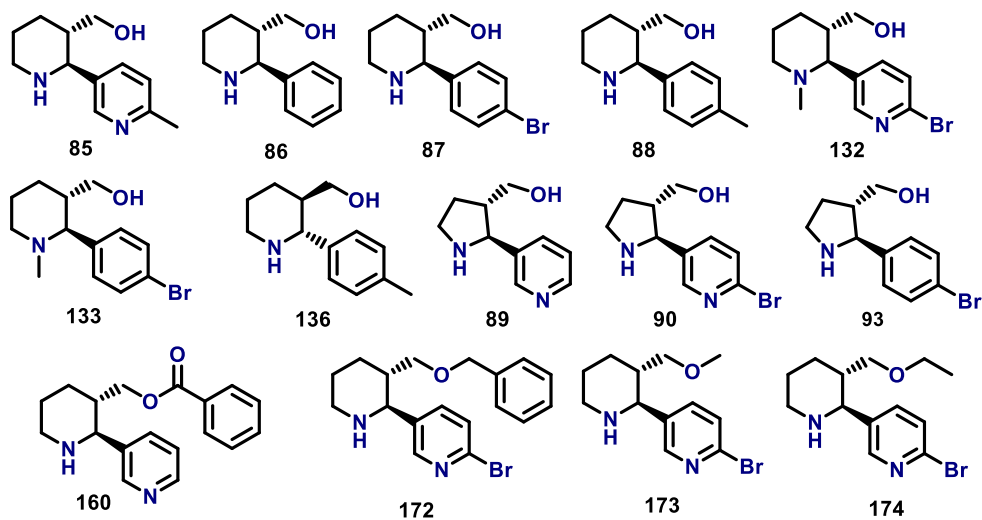


Fig. 3.22: 14 anabasine and nicotine analogues that remained untested.

The 14 analogues shown above were the compounds that remain untested during the preparation of this thesis (**Fig. 3.22**). However, the remaining 9 compounds were evaluated for their bioactivity, of which four compounds showed extremely promising activity (**Fig. 3.23**). The compounds that displayed no activity are shown in red, while the ones exhibiting bioactivity are shown in green. The CMPI molecule (blue) is shown as the standard molecule for comparing the obtained bioactivity of all the four analogues.

Five heterocyclic esters substituted anabasine analogues were synthesised, of which four displayed good biological activity, with the only exception of 3-furan ester that exhibited no activity (**Fig. 3.23**). It was interesting to observe that of all the three furan substituted esters, the 2-bromofuran ester displayed maximum efficacy, whereas 2-furan showed maximum potency. The difference in efficacy between the analogues **163** and **164** could be due to the presence of bromine next to the furan oxygen in analogue **164** that facilitates additional hydrogen bonding over compound **163**. Though, such a large difference in

potency between **163** and **164** could arise from the bulkiness of the bromine substitution in **164**. On the other hand, the plausible rationale behind no activity of 3-furan ester **165** was attributed to the disruption of any possible interaction with the nearby residues, which was observed in all other ester analogues that possessed a heteroatom like sulphur, oxygen or nitrogen at the 2nd position. It is also possible that carbonyl oxygen of ester in conjunction with a heteroatom at the 2nd position gets involved in some sort of intermolecular interaction with nearby residues, thus, facilitating receptor activation and channel opening. The CMPI-linked anabasine analogues **175** and **176** failed to display any activity, despite possessing the crucial pyrazole-isoxazole backbone. This could be attributed to the relatively large change in structure, such that the compounds were not able to fit in the binding site.

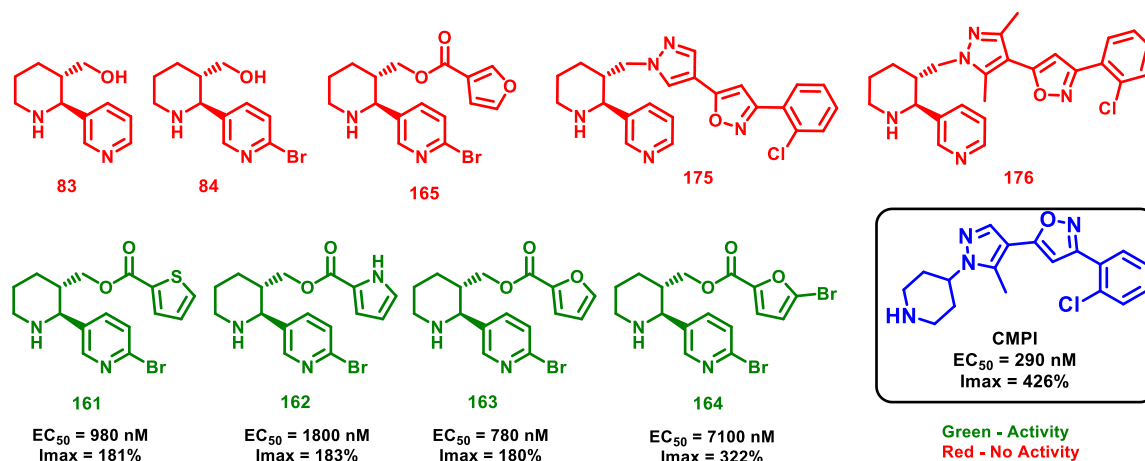


Fig. 3.23: Nine anabasine analogues that were tested. Five analogues (red) had no activity, four analogues (green) displayed some activity and CMPI (blue) is shown for comparison.

At present, it is difficult to interpret and determine the structure-activity relationship from the obtained biological study, as it still lacks considerable data from other synthesised anabasine and nicotine analogues. However, it is safe to say that the sidechain substitutions plausibly extend into the pocket present in the $\alpha 4$ - $\alpha 4$ binding site and display the possibility for potentiating the receptor through various interactions. The bioactivity of four ester analogues provide a great scope to exploit the sidechain substituents with a variety of other moieties, especially with electron-rich functionalities.

3.2.6. DETERMINATION OF ENANTIOMERS FROM CHIRAL HPLC

The L-proline catalysed Mannich reductive cyclisation for synthesis of anabasine and nicotine series of compounds was *syn*-selective, yielding desired products with a high

diastereoselectivity as confirmed from the ^1H NMR. However, presence of other enantiomers and determination of enantiomeric excess (ee) of the major enantiomer (2*S*,3*S*) was established from the chiral HPLC. Two PMP-protected enantiomers of tolyl-piperidines, (2*S*,3*S*)-**124** and (2*R*,3*R*)-**138** were synthesised using L- and D-proline, respectively. Therefore, the same two compounds were used for the enantiomeric purity determination and effectiveness of the employed Mannich reductive cyclisation to generate stereochemically rich compounds. For enantiomer separation, Waters UltraPerformance Convergence chromatography (UPC²) system was utilised with PDA detector. Based on the principles of supercritical fluid chromatography (SFC), a binary mobile phase containing compressed liquid CO₂ with methanol as a co-solvent were used for separation.

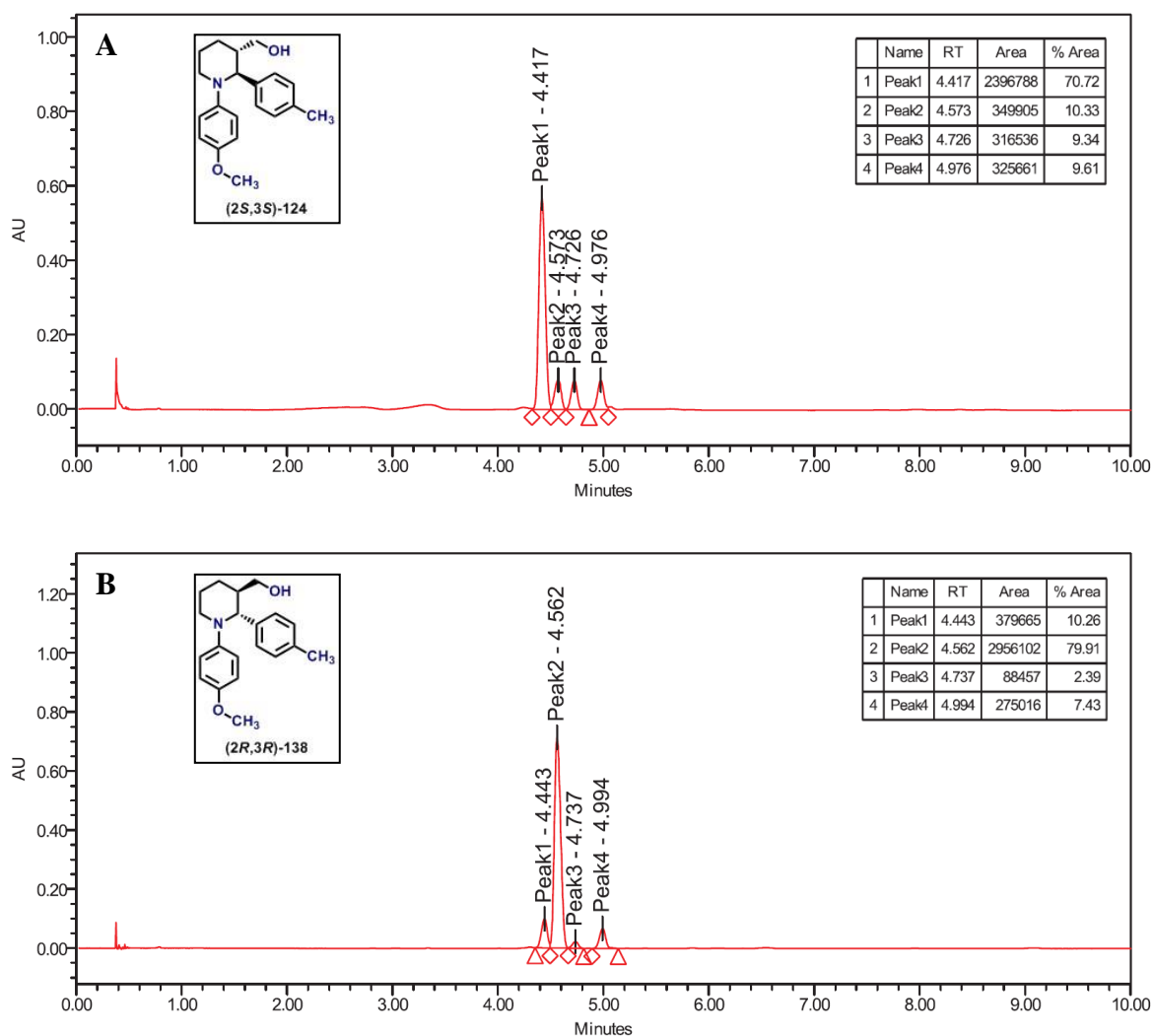


Fig. 3.24: Determination of enantiomeric excess of (2*S*,3*S*)-**124** (**A**) and (2*R*,3*R*)-**138** (**B**), using Waters UPC² supercritical fluid chromatography.

The chromatogram **A** was obtained from the analysis of the product afforded after L-proline catalysed Mannich reductive cyclisation, while chromatogram **B** was obtained from the product of D-proline catalysed Mannich reaction. As per the chromatograms obtained, peak 1 at 4.4 mins is for the enantiomer (2*S*,3*S*)-**124**, while peak 2 at 4.5 mins refers to the enantiomer (2*R*,3*R*)-**138**, as both were the expected major products from the respective reactions mentioned above. In chromatogram **A**, the relative peak area of enantiomer (2*S*,3*S*)-**124** was found to be 70.7%, whereas for (2*R*,3*R*)-**138** it was 10.3% (**Fig. 3.24A**). Similarly, in chromatogram **B**, relative peak area of enantiomer (2*R*,3*R*)-**138** was found to be 79.9%, while for (2*S*,3*S*)-**124** it was 10.3% (**Fig. 3.24B**). Hence, the (2*S*,3*S*)-**124** enantiomer obtained from L-proline catalysed reaction was in 60.4% ee, whereas the (2*R*,3*R*)-**138** enantiomer was afforded in 69.6% ee from D-proline catalysed reaction. Thus, validating the stereoselectivity of L-proline catalysed Mannich cyclisation to obtain designed (2*S*,3*S*)- anabasine and nicotine analogues. Since, chiral isomers (2*S*,3*S*)-**124** and (2*R*,3*R*)-**138** are novel compounds, therefore, no literature data was available to corroborate with the obtained experimental values.

Here, chiral determination of (2*S*,3*S*)-**124** and (2*R*,3*R*)-**138** was used as a representative for all the other chiral piperidine and pyrrolidine compounds, which were understood to have % ee values in similar range. However, the optical rotation of both novel and reported compounds were determined, where the values of reported molecules matched with the values available in the literature data.^{120, 121} The optical rotation values are mentioned in the experimental section under each synthesised compound.

3.3. CHAPTER CONCLUSION AND FUTURE WORK

Recognition of a new pocket in the $\alpha 4$ - $\alpha 4$ binding site has been identified as an attractive target to design compounds that bind at the $\alpha 4$ - $\alpha 4$ binding site. This could pave way to achieve the desired selectivity for the $(\alpha 4)_3(\beta 2)_2$ isoform by directly activating the $\alpha 4$ - $\alpha 4$ binding site. Several co-crystallised structures were overlaid with the homology model of the $\alpha 4$ - $\alpha 4$ binding site demonstrating the new pocket. Based on the vector directing towards the pocket as well as the extent of overlap with the NS3920, DMXBA and nicotine were chosen for designing the anabasine and nicotine template (**Fig. 3.25**). Since the identified pocket has remained relatively unexplored, thereby, it gives an opportunity to explore it with designed templates and install a number of substituents, especially at the 3rd position of the piperidine and pyrrolidine ring as it is directed towards the target site.

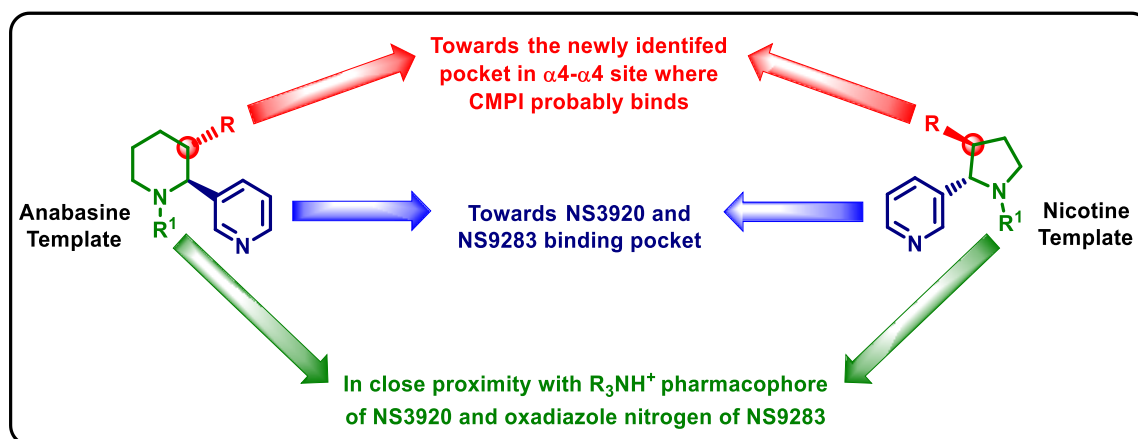


Fig. 3.25: Designed Anabasine and Nicotine templates with rationale for their selection.

The key step towards the synthesis of both templates was achieved through the reductive Mannich cyclisation cascade process catalysed by L-proline. This approach required optimisation for the synthesis of both anabasine and nicotine template. Several issues were also addressed during the cleavage of PMP-group from the respective piperidine and pyrrolidine ring systems, which were resolved after optimising the reaction conditions, and the reaction was completed within 5 mins, giving high yields of final analogues.

A total of 23 compounds were synthesised, of which, 12 were from the unsubstituted series of anabasine and nicotine analogues, while 11 were substituted at the 3rd position facing the target site. In the unsubstituted series, the aryl moiety was selected for different modifications and this led to the identification of bromopyridyl ring as a promising 2nd

position substituent based on the preliminary biological evaluation as well as the similarity in structural features with NS3920. Further, a number of ester and ether substitutions were installed at the 3rd position of bromopyridyl piperidine and pyrrolidine compounds. However, due to time constraints, only a limited number of nicotine analogues were synthesised. Apart from this, two CMPI linked anabasine analogues were also synthesised based on the CMPI's excellent PAM activity as well as high selectivity for the $(\alpha 4)_3(\beta 2)_2$ receptor stoichiometry, as it only activates the $\alpha 4$ - $\alpha 4$ binding site.

All the 23 compounds were submitted for the biological evaluation using two-electrode voltage clamp electrophysiology technique on the nAChRs expressed on *Xenopus* oocytes. This was done to determine the functional activity, i.e., efficacy and potency of the synthesised compounds. Only nine compounds were tested until the writing of this thesis, out of which four piperidine ester exhibited excellent promising bioactivity.

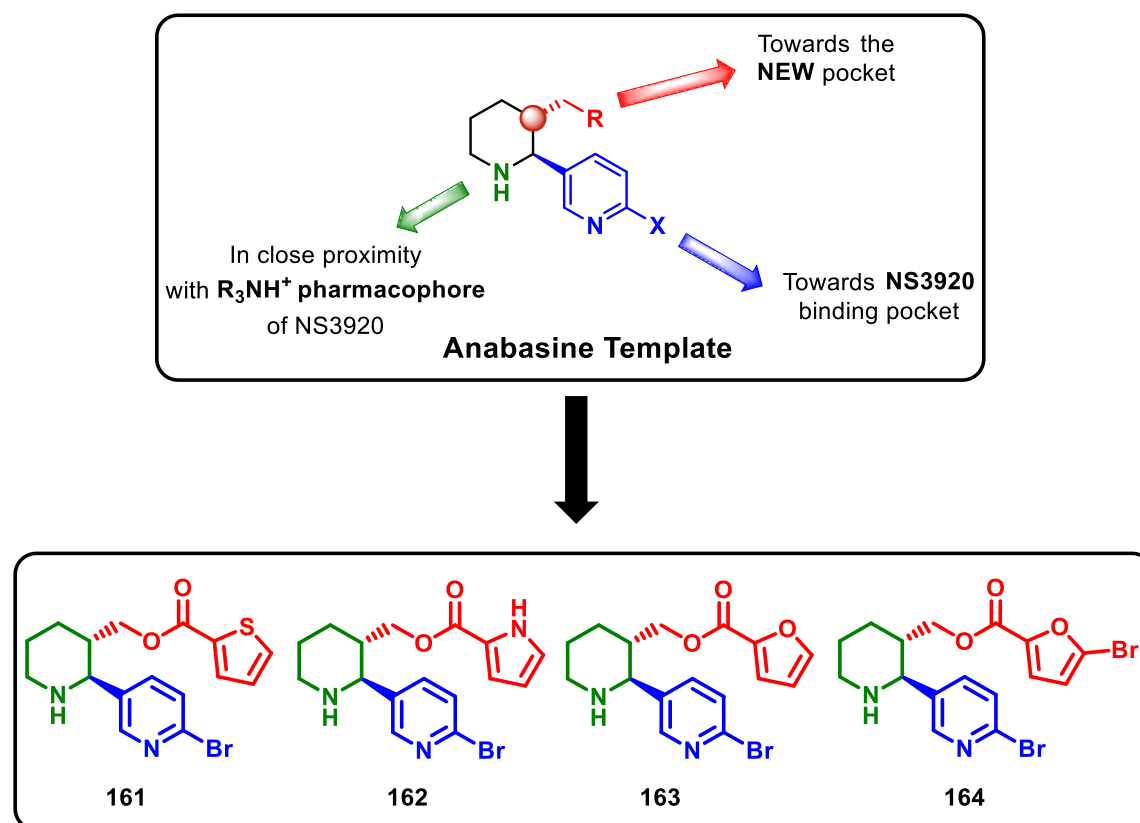


Fig. 3.26: Designed anabasine template and the four ester analogues found active.

Analogue **163** was found to be the most potent, while **164** was the most efficacious amongst all the four (**Fig. 3.26**). Despite the lack of biological data, some important structural features were identified from the results. First, sidechain should not be too long or bulky as

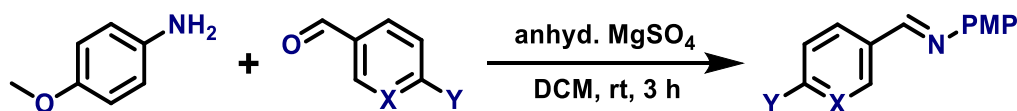
it may not allow the ligand to bind, and second, smaller and electron-rich systems should be installed as substituents to help achieve higher potency as well as efficacy.

Although, comprehensive research is still needed to exploit the full potential of the identified pocket, a variety of substituents as well as new templates could be designed that may lead to not only better efficacy and potency but also maintain a high selectivity for the $(\alpha 4)_3(\beta 2)_2$ receptor stoichiometry. Future work can be done to explore the nicotine template, as nicotine itself is an agonist for the $\alpha 4\beta 2$ nAChR and has the vector positioned directly towards the newly identified pocket.

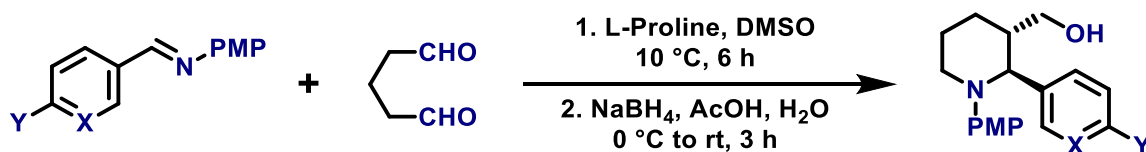
CHAPTER 4

4.2. EXPERIMENTAL FOR CHAPTER 3

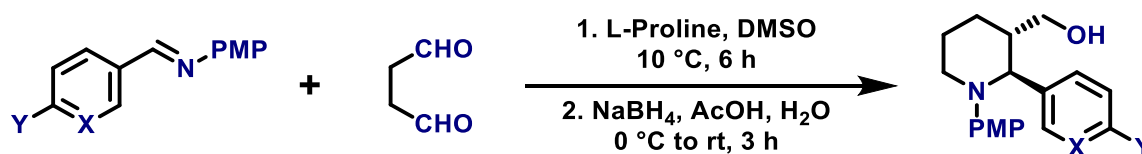
GENERAL PROCEDURES AND ANALYTICAL DATA

*Imine synthesis (A)*¹²²

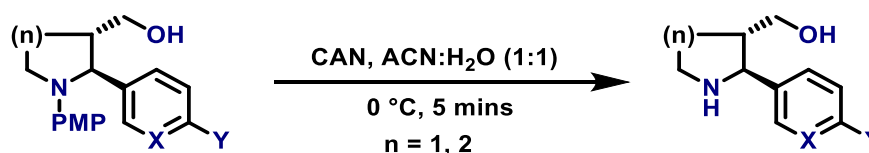
To a round bottom flask containing a solution of substituted aryl/heteroaryl aldehyde (1 mmol) and anhydrous MgSO_4 (4 mmol) in dry DCM, *p*-anisidine (1 mmol) was added at ambient temperature and stirred for 3 h. The solvent was concentrated under reduced pressure to obtain the desired imines as brown or yellow powder and carried forward to the next step without further purification.

*Piperidine Synthesis - Mannich Cyclization (B)*¹²⁰

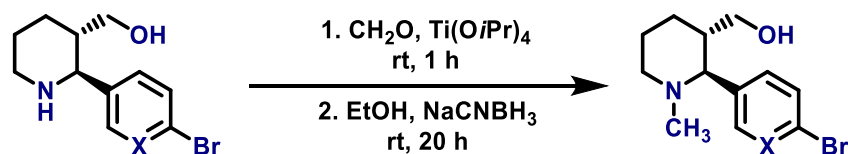
To a round bottom flask containing a solution of preformed *N*-PMP aldimine (1 mmol, 100 mg) and L-proline (0.4 mmol) in DMSO (3 ml), glutaraldehyde solution (25% in water, 5 mmol) was added at ambient temperature and cooled to 10 °C. The reaction mixture was stirred for 6 h at the same temperature and monitored by TLC until aldimine was consumed. The reaction temperature was further lowered to 0 °C, followed by the addition of cold water (2 ml) and NaBH_4 (10 mmol) to the stirring solution. To this, acetic acid (12 mmol) was added slowly and cautiously from the sides, as the mixture tends to react vigorously with effervescence. The reaction was warmed up to room temperature and stirred for 3 h. On completion, excess acid was neutralised by the slow addition of saturated NaHCO_3 solution and subsequently extracted with ethyl acetate (5 x 5 ml). The combined organic layer was washed with LiCl solution (5%, 5 ml) to remove residual DMSO. The organic extract was dried over Na_2SO_4 and concentrated under reduced pressure. The crude product was purified through column chromatography (EtOAc:Hex, 1:4 – 2:3) to afford the desired piperidines.

*Pyrrolidine Synthesis - Mannich Cyclization (C)*¹²¹

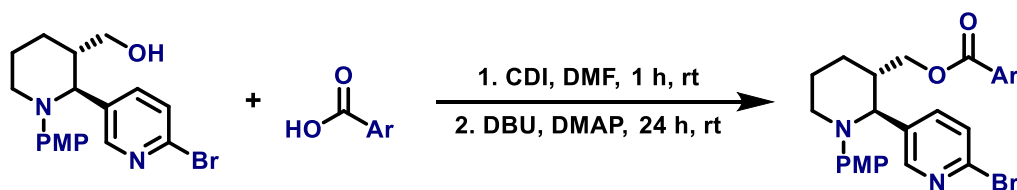
To a round bottom flask containing a solution of preformed *N*-PMP aldimine (1 mmol, 100 mg) and L-proline (0.4 mmol) in DMSO (3 ml), freshly prepared succinaldehyde solution (4 M aqueous solution, 4 mmol) was added at 5 °C. The reaction mixture was stirred for 6 h at the same temperature and monitored by TLC until aldimine was consumed. The reaction temperature was further lowered to 0 °C, followed by addition of cold water (2 ml) and NaBH₄ (10 mmol) to the stirring solution. To this, acetic acid (12 mmol) was added slowly and cautiously from the sides, as the mixture tends to react vigorously with effervescence. The reaction was warmed up to room temperature and stirred for 3 h. On completion, excess acid was neutralised by slow addition of saturated NaHCO₃ solution and subsequently extracted with ethyl acetate (5 x 5 ml). The combined organic layer was washed with LiCl solution (5%, 5 ml) to remove residual DMSO. The organic extract was dried over Na₂SO₄ and concentrated *in vacuo*. The crude product was purified through column chromatography (EtOAc:Hex, 1:4 – 2:3) to afford the desired pyrrolidines.

PMP deprotection (D)

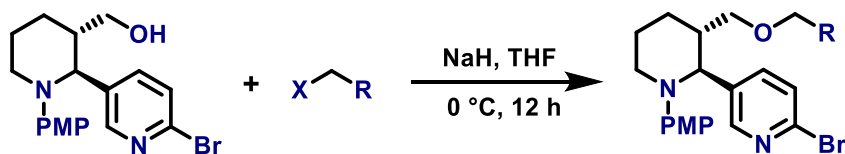
To a round bottom flask containing a solution of *N*-PMP piperidine [*n* = 2] or pyrrolidine [*n* = 1] (1 mmol, 100 mg) in a solvent mixture of ACN and Water (1:1, 10 ml), ceric ammonium nitrate (4 mmol) was added in portions at 0 °C and stirred for 5 mins. The reaction was quenched by the addition of 5M aq. NaOH solution (10 ml) and stirred for another 15 mins at room temperature. The suspension was filtered through a sintered funnel and the precipitate was washed with CHCl₃:*i*-PrOH solution (3:1, 2 x 5 ml) and subsequently extracted with CHCl₃:*i*-PrOH (3:1, 4 x 5 ml). Both organic solutions were combined, dried over Na₂SO₄, and concentrated *in vacuo*. The crude product was purified through column chromatography (DCM:MeOH, 9:1 – 4:1) to afford the desired product.

Reductive Amination (E)¹³¹

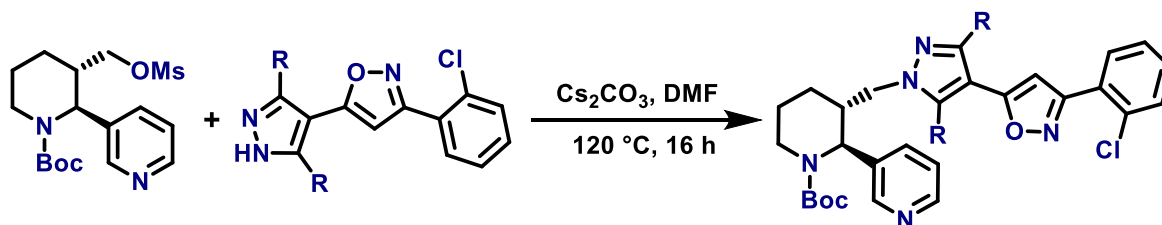
To a round bottom flask containing a suspension of paraformaldehyde (1 mmol) and amine (1 mmol, 100 mg), $\text{Ti}(\text{O}i\text{Pr})_4$ (1.3 mmol) was added and stirred for 1 h at ambient temperature. The viscous suspension was diluted with absolute ethanol (3 ml), followed by the addition of NaCNBH_3 (1 mmol) and stirred for 20 h at room temperature. The reaction mixture was diluted with water (1 ml) and the formed inorganic precipitate was filtered and washed with ethanol. The filtrate was concentrated under reduced pressure and redissolved in ethyl acetate, filtered again to remove the residual inorganic precipitate. The obtained organic filtrate was concentrated under reduced pressure and purified through column chromatography (EtOAc:Hex, 1:9 – 1:5) to afford desired products.

CDI-mediated Esterification (F)

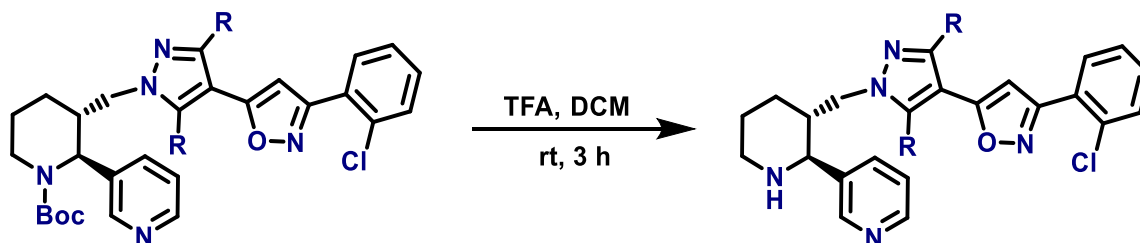
To a round bottom flask containing a solution of aryl/heteroaryl acid (3 mmol) and CDI (1 mmol) in dry DMF (3 mL) and stirred for 1 h at room temperature. To the stirring solution, piperidine alcohol (1 mmol, 100 mg), DBU (1.5 mmol) and DMAP (0.2 mmol) were added, and the reaction was stirred for 24 h under nitrogen atmosphere at room temperature. The mixture was diluted with ethyl acetate and washed with HCl (0.2 M), saturated NaHCO_3 solution, brine and then dried over Na_2SO_4 . The organic extract was concentrated under reduced pressure and the residue was purified by column chromatography (EtOAc:Hex, 1:5 – 1:4) to afford desired products.

Etherification of Piperidine Alcohol (G)

To a round bottom flask containing a stirring solution of piperidine alcohol (1 mmol) in dry THF at 0 °C, NaH (3 mmol) was added. The reaction was warmed to room temperature and stirred for 12 h. The mixture was diluted with ethyl acetate and washed with brine. The organic solvent was concentrated under reduced pressure and the residue was purified by column chromatography (EtOAc:Hex, 1:5) to afford desired products.

Piperidine Coupling with Isoxazole-Pyrazole Compound (H)

To a round bottom flask containing a solution of mesyl piperidine (1 mmol, 100 mg), pyrazole-isoxazole compound (1.3 mmol) in DMF (3 ml), Cs₂CO₃ (1.5 mmol) was added. The reaction was heated to 120 °C and stirred for 16 h. The mixture was cooled to ambient temperature, diluted with saturated NaHCO₃ solution, extracted with ethyl acetate (5 x 3 ml) and then dried over Na₂SO₄. The organic extract was concentrated *in vacuo* and purified by column chromatography (EtOAc:Hex, 1:5 – 3:7) to afford desired products.

Boc Deprotection (I)

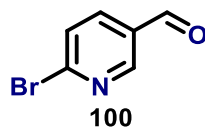
To a round bottom flask containing the *N*-Boc protected amine (1 mmol) in DCM was added TFA (15 mmol) at 0 °C. The reaction mixture was stirred at ambient temperature for 3 h.

The reaction mixture was concentrated under reduced pressure and purified by column chromatography (DCM:MeOH:NH₃, 9:1:0.1 – 1:4:0.1) to afford the desired products.

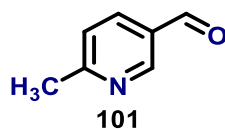
Determination of Enantiomeric Excess

Chiral HPLC analysis was undertaken using a Waters ACQUITY UPC² (Supercritical Fluid Chromatography) System coupled to with a PDA (UV) detector equipped with a Waters Trefoil cellulose-based chiral stationary phase column (CEL2 column, 2.5 μ m, 3.0 mm x 150 mm, Water Corporation) eluting with a gradient consisting of the following mobile phases, A: Liquified CO₂, B: Methanol (+10 mM ammonium formate and formic acid 0.01% v/v), gradient: 0-0.5 min A-B (98:2 v/v), 0.5-7 min A-B (98:2 v/v), 7-10 min, 5 min re-equilibration, flow rate 2 mL/min. Purities of the compounds were determined as AUC of UV absorbance at 256 nm.

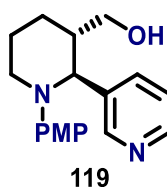
6-Bromonicotinaldehyde (**100**)¹²⁴



Procedure: To a round bottom flask containing a suspension of 2,5-dibromopyridine **108** (1 mmol, 1 g) in dry diethyl ether (50 ml) at -80 °C under a nitrogen atmosphere, *n*-BuLi (1.6 M in hexane, 7.5 mmol) was added and stirred for 1 h. To the mixture, dry DMF (1.1 mmol) was added and stirred for an additional hour at -80 °C and then warmed up to room temperature. Excess *n*-BuLi was neutralised with dilute HCl (1 M, 20 ml) while stirring the reaction mixture for 15 mins. The neutralised aqueous layer was extracted with diethyl ether (3 x 10 ml), washed with brine and then dried over Na₂SO₄. The combined organic extracts were concentrated under reduced pressure to yield 6-bromonicotinaldehyde **100** (690 mg) as a light yellow solid; Yield: 87%; ¹H NMR (400 MHz, CDCl₃) 10.09 (s, 1H), 8.83 (d, *J* = 2.3 Hz, 1H), 8.01 (dd, *J* = 8.4, 2.2 Hz, 1H), 7.70 (d, *J* = 8.2 Hz, 1H); LRMS (+ESI) *m/z* 185.6 ([M+H]⁺) and 187.9 ([M+H]⁺); HRMS (+ESI) *m/z* calcd for C₆H₄⁷⁹BrNO⁺ ([M]⁺) 184.9476, found 184.9481. ([M]⁺) and calcd for C₆H₄⁸¹BrNO⁺ ([M]⁺) 186.9456, found 184.9458. ([M]⁺). Data was consistent with the literature values.¹²⁴

6-Methylnicotinaldehyde (101)¹²³

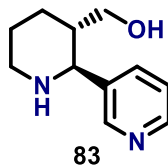
Procedure: To a round bottom flask containing a stirring solution of morpholine (2.1 mmol) in dry THF (50 mL) at 0 °C, DIBAL (1 M in hexane, 2 mmol) was added dropwise, and the mixture was stirred for 3 h at the same temperature. To the reaction mixture methyl 6-methylnicotinate **110** (1 mmol, 1 g) was added slowly and stirred for another 10 mins. This was followed by another addition of DIBAL (1 M in hexane, 8 mmol) further stirred for 10 mins. Excess DIBAL was neutralised with dilute HCl (1 M, 50 ml) while stirring the reaction mixture for 15 mins. The neutralised aqueous layer was extracted with diethyl ether (3 x 30 ml), washed with brine and then dried over Na₂SO₄. The combined organic extracts were concentrated under reduced pressure to yield 6-methylnicotinaldehyde **101** (540 mg) as a light brown solid; Yield: 67%; ¹H NMR (400 MHz, CDCl₃) δ 10.06 (s, 1H), 8.94 (d, *J* = 2.0 Hz, 1H), 8.04 (dd, *J* = 8.0, 2.0 Hz, 1H), 7.33 (d, *J* = 8.0 Hz, 1H), 2.65 (s, 3H); LRMS (+ESI) *m/z* 122.1 ([M+H]⁺); HRMS (+ESI) *m/z* calcd for C₇H₈NO⁺ ([M+H]⁺) 122.0610, found 122.0614 ([M+H]⁺). Data was consistent with the literature values.¹²³

((2*S*,3*S*)-1-(4-Methoxyphenyl)-2-(pyridin-3-yl)piperidin-3-yl)methanol (119)¹²⁰

Procedure: Prepared as per procedure B, using aldimine **105**; Yield: 69%, a dark brown oil; IR (neat) 3306 (br), 2937 (m), 1508 (s), 1240 (s), 802 (m), 715 (m); ¹H NMR (400 MHz, CDCl₃) δ 8.43 (d, *J* = 2.0 Hz, 1H), 8.27 (dd, *J* = 4.8, 1.2 Hz, 1H), 7.59 (d, *J* = 8.0 Hz, 1H), 7.11 – 7.04 (m, 1H), 6.89 (d, *J* = 8.9 Hz, 2H), 6.63 (d, *J* = 8.9 Hz, 2H), 3.94 (d, *J* = 9.2 Hz, 1H), 3.66 (s, 3H), 3.41 (dd, *J* = 10.7, 3.7 Hz, 1H), 3.32 – 3.20 (m, 2H), 2.93 – 2.79 (m, 1H), 1.95 – 1.82 (m, 5H, overlapping with OH brs), 1.65 – 1.49 (m, 1H); ¹³C NMR (101 MHz, CDCl₃) δ 155.82, 150.25, 148.09, 145.65, 138.05, 136.11, 125.78 (2C), 123.40, 114.05 (2C), 64.62, 64.48, 57.17, 55.37, 45.93, 27.53, 25.76; LRMS (+ESI) *m/z* 299.3 ([M+H]⁺), 321.2 ([M+Na]⁺); HRMS (+ESI) *m/z* calcd for C₁₈H₂₃N₂O₂⁺ ([M+H]⁺) 299.1760, found

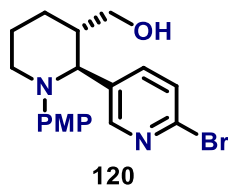
299.1761 ($[M+H]^+$); $[\alpha]_D^{25} = +11.2$ ($c = 1.0$, MeOH), lit. $[\alpha]_D^{25} = +11.1$ ($c = 1.0$, MeOH, 81% ee). Data was consistent with the literature values.¹²⁰

((2*S*,3*S*)-2-(Pyridin-3-yl)piperidin-3-yl)methanol (83)¹²⁰



Procedure: Prepared as per procedure D; Yield: 72%, a clear bright orange oil; IR (neat) 3481 (br), 3265 (w), 2929 (s), 2857 (s), 1427 (s), 804 (s), 715 (s); ^1H NMR (400 MHz, CDCl_3) δ 8.54 (d, $J = 1.8$ Hz, 1H), 8.48 (dd, $J = 4.8, 1.6$ Hz, 1H), 7.78 (d, $J = 7.9$ Hz, 1H), 7.29 – 7.22 (m, 1H), 3.54 (d, $J = 10.1$ Hz, 1H), 3.35 (dd, $J = 10.7, 3.5$ Hz, 1H), 3.23 (dd, $J = 10.6, 5.8$ Hz, 1H), 3.19 – 3.11 (m, 1H), 2.82 – 2.71 (m, 1H), 2.21 (brs, 1H, NH), 2.06 – 1.98 (m, 1H), 1.84 – 1.65 (m, 4H, overlapping with OH brs), 1.51 – 1.39 (m, 1H); ^{13}C NMR (101 MHz, CDCl_3) δ 149.57, 149.14, 138.59, 135.51, 123.84, 64.32, 61.96, 47.44, 44.95, 28.35, 25.85; LRMS (+ESI) m/z 193.2 ($[M+H]^+$); HRMS (+ESI) m/z calcd for $\text{C}_{11}\text{H}_{17}\text{N}_2\text{O}^+$ ($[M+H]^+$) 193.1341, found 193.1339 ($[M+H]^+$); $[\alpha]_D^{25} = +9.5$ ($c = 1.0$, MeOH), lit. $[\alpha]_D^{25} = +9.2$ ($c = 1.0$, MeOH). Data was consistent with the literature values.¹²⁰

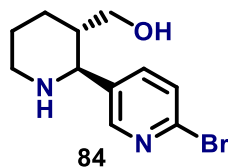
((2*S*,3*S*)-2-(6-Bromopyridin-3-yl)-1-(4-methoxyphenyl)piperidin-3-yl)methanol (120)



Procedure: Prepared as per procedure B, using aldimine **106**; Yield: 72%, a dark orange oil; IR (neat) 3312 (br), 2913 (m), 1524 (s), 1408 (s), 1240 (s); ^1H NMR (400 MHz, CDCl_3) δ 8.13 (s, 1H), 7.44 – 7.38 (m, 1H), 7.19 – 7.15 (m, 1H), 6.80 (d, $J = 8.2$ Hz, 2H), 6.58 (d, $J = 8.4$ Hz, 2H), 3.85 (d, $J = 9.3$ Hz, 1H), 3.61 (s, 3H), 3.35 (d, $J = 10.3$ Hz, 1H), 3.25 – 3.12 (m, 2H), 2.79 – 2.69 (m, 1H), 1.99 – 1.88 (m, 2H, overlapping with OH brs), 1.85 – 1.69 (m, 4H), 1.52 – 1.41 (m, 1H); ^{13}C NMR (101 MHz, CDCl_3) δ 156.05, 150.65, 145.38, 140.20, 138.67, 137.58, 127.79, 125.87 (2C), 114.21 (2C), 64.43, 63.83, 57.30, 55.39, 45.90, 27.49, 25.73; LRMS (+ESI) m/z 377.1 ($[M+H]^+$), 379.4 ($[M+H]^+$); HRMS (+ESI) m/z calcd for $\text{C}_{18}\text{H}_{22}^{79}\text{BrN}_2\text{O}_2^+$ ($[M+H]^+$) 377.0859, found 377.0860 ($[M+H]^+$) and calcd

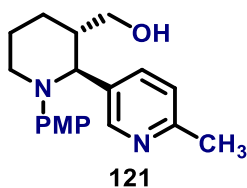
for $C_{18}H_{22}^{81}BrN_2O_2^+$ ($[M+H]^+$) 379.0839, found 379.0843 ($[M+H]^+$); $[\alpha]_D^{25} = +6.2$ ($c = 1.0$, MeOH).

((2S,3S)-2-(6-Bromopyridin-3-yl)piperidin-3-yl)methanol (84)



Procedure: Prepared as per procedure D; Yield: 70%, a bright red oil; IR (neat) 3457 (br), 3215 (w), 2988 (s), 1511 (s), 1473 (s), 818 (s); 1H NMR (400 MHz, $CDCl_3$) δ 8.34 (s, 1H), 7.62 (d, $J = 8.0$ Hz, 1H), 7.44 (d, $J = 8.1$ Hz, 1H), 3.49 (d, $J = 10.0$ Hz, 1H), 3.33 (dd, $J = 10.7, 3.3$ Hz, 1H), 3.22 (dd, $J = 10.7, 5.6$ Hz, 1H), 3.17 – 3.09 (m, 1H), 2.80 – 2.68 (m, 1H), 2.04 – 1.94 (m, 1H), 1.84 – 1.75 (m, 1H), 1.73 – 1.58 (m, 3H, overlapping with OH brs), 1.54 (brs, 1H, NH), 1.50 – 1.36 (m, 1H); ^{13}C NMR (101 MHz, $CDCl_3$) δ 149.93, 141.24, 138.39, 138.13, 128.22, 64.48, 61.23, 47.44, 45.14, 28.34, 25.91; LRMS (+ESI) m/z 293.3 ($[M+Na]^+$), 295.5 ($[M+Na]^+$); HRMS (+ESI) m/z calcd for $C_{11}H_{16}^{79}BrN_2O^+$ ($[M+H]^+$) 271.0441, found 271.0441 ($[M+H]^+$) and calcd for $C_{11}H_{16}^{81}BrN_2O^+$ ($[M+H]^+$) 273.0420, found 271.0423 ($[M+H]^+$); $[\alpha]_D^{25} = +8.2$ ($c = 1.0$, MeOH).

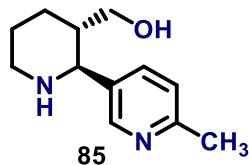
((2S,3S)-1-(4-Methoxyphenyl)-2-(6-methylpyridin-3-yl)piperidin-3-yl)methanol (121)



Procedure: Prepared as per procedure B, using aldimine **107**; Yield: 42%, a clear brown oil; IR (neat) 3331 (br), 2967 (m), 1501 (s), 1444 (s), 1283 (s); 1H NMR (400 MHz, $CDCl_3$) δ 8.29 (s, 1H), 7.47 (dd, $J = 8.0, 2.4$ Hz, 1H), 6.93 (d, $J = 8.1$ Hz, 1H), 6.89 (d, $J = 9.1$ Hz, 2H), 6.62 (d, $J = 8.9$ Hz, 2H), 3.90 (d, $J = 9.0$ Hz, 1H), 3.67 (s, 3H), 3.42 (dd, $J = 10.6, 3.7$ Hz, 1H), 3.31 – 3.21 (m, 2H), 2.89 – 2.75 (m, 1H), 2.40 (s, 3H), 2.04 – 1.98 (m, 2H, overlapping with OH brs), 1.90 – 1.83 (m, 3H), 1.57 – 1.50 (m, 1H); ^{13}C NMR (101 MHz, $CDCl_3$) δ 156.68, 155.74, 149.48, 145.83, 136.36, 134.83, 125.77 (2C), 123.08, 114.02 (2C), 64.36, 57.23, 55.37, 45.93, 32.53, 27.58, 25.79, 24.03; LRMS (+ESI) m/z 313.3

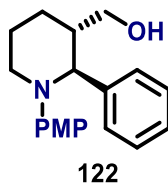
([M+H]⁺); HRMS (+ESI) m/z calcd for C₁₉H₂₅N₂O₂⁺ ([M+H]⁺) 313.1911, found 313.1912 ([M+H]⁺); $[\alpha]_D^{25} = +10.2$ (c = 1.0, MeOH).

((2S,3S)-2-(6-Methylpyridin-3-yl)piperidin-3-yl)methanol (85)



Procedure: Prepared as per procedure D; Yield: 47%, a pale-brown oil; IR (neat) 3453 (br), 3256 (w), 2934 (s), 1566 (s), 785 (s); ¹H NMR (400 MHz, CDCl₃) δ 8.29 (s, 1H), 7.87 (d, $J = 7.8$ Hz, 1H), 7.06 (d, $J = 8.3$ Hz, 1H), 3.68 (d, $J = 10.7$ Hz, 1H), 3.51 (dd, $J = 10.9, 3.6$ Hz, 1H), 3.43 (dd, $J = 10.3, 5.4$ Hz, 1H), 3.03 – 2.91 (m, 1H), 2.77 – 2.63 (m, 1H), 2.44 (s, 3H), 2.17 – 1.99 (m, 1H), 1.89 – 1.80 (m, 2H, overlapping with OH brs), 1.73 – 1.65 (m, 2H), 1.58 (brs, 1H, NH), 1.49 – 1.37 (m, 1H); ¹³C NMR (101 MHz, CDCl₃) δ 152.01, 143.66, 140.08, 134.37, 129.69, 65.22, 61.71, 46.19, 43.15, 28.51, 24.39, 22.87; LRMS (+ESI) m/z 207.9 ([M+Na]⁺), 229.5 ([M+Na]⁺); HRMS (+ESI) m/z calcd for C₁₂H₁₉N₂O⁺ ([M+H]⁺) 207.1492, found 207.1499 ([M+H]⁺); $[\alpha]_D^{25} = +16.4$ (c = 1.0, MeOH).

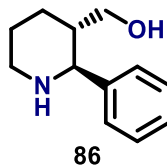
((2S,3S)-1-(4-Methoxyphenyl)-2-phenylpiperidin-3-yl)methanol (122)¹²⁰



Procedure: Prepared as per procedure B, using aldimine **102**; Yield: 56%, a clear yellow oil; IR (neat) 3374 (br), 3029 (w), 2932 (m), 2833 (w), 1508 (s), 1240 (s), 832 (m), 765 (m); ¹H NMR (400 MHz, CDCl₃) δ 7.26 – 7.21 (m, 2H), 7.17 – 7.12 (m, 2H), 7.10 – 7.04 (m, 1H), 6.89 (d, $J = 8.9$ Hz, 2H), 6.63 (d, $J = 8.9$ Hz, 2H), 3.82 (d, $J = 8.6$ Hz, 1H), 3.66 (s, 3H), 3.48 – 3.40 (m, 1H), 3.34 – 3.24 (m, 2H), 2.90 – 2.81 (m, 1H), 2.02 – 1.82 (m, 5H, overlapping with OH brs), 1.51 – 1.39 (m, 1H); ¹³C NMR (101 MHz, CDCl₃) δ 155.35, 146.21, 142.29, 128.62 (2C), 128.20 (2C), 126.89, 125.31 (2C), 113.80 (2C), 67.65, 65.50, 56.83, 55.36, 46.16, 27.62, 25.70; LRMS (+ESI) m/z 298.3 ([M+H]⁺), 299.3 ([M+2H]⁺), 320.2 ([M+Na]⁺); HRMS (+ESI) m/z calcd for C₁₉H₂₄NO₂⁺ ([M+H]⁺) 298.1807, found

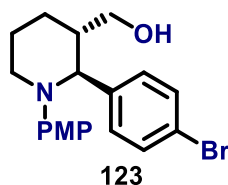
298.1804 ($[M+H]^+$); $[\alpha]_D^{25} = +2.3$ ($c = 0.5$, CHCl_3), lit. $[\alpha]_D^{25} = +2.6$ ($c = 1.0$, CHCl_3 , 73% ee). Data was consistent with the literature values.¹²⁰

((2*S*,3*S*)-2-Phenylpiperidin-3-yl)methanol (86)



Procedure: Prepared as per procedure D; Yield: 56%, a pale-red oil; IR (neat) 3286 (br), 3028 (w), 2927 (s), 2855 (m), 1448 (m), 1091 (m), 756 (s); ^1H NMR (400 MHz, CDCl_3) δ 7.40 – 7.24 (m, 5H), 3.41 – 3.32 (m, 2H), 3.24 (dd, $J = 11.0, 5.9$ Hz, 1H), 3.18 – 3.10 (m, 1H), 2.80 – 2.70 (m, 1H), 2.04 – 1.95 (m, 1H), 1.82 – 1.73 (m, 3H, overlapping with OH brs), 1.71 – 1.66 (m, 1H), 1.63 (brs, 1H, NH), 1.41 – 1.28 (m, 1H); ^{13}C NMR (101 MHz, CDCl_3) δ 143.24, 128.77 (2C), 127.83 (2C), 116.38, 65.47, 65.37, 47.62, 45.37, 28.65, 26.11; LRMS (+ESI) m/z 192.2 ($[M+H]^+$); HRMS (+ESI) m/z calcd for $\text{C}_{12}\text{H}_{18}\text{NO}^+$ ($[M+H]^+$) 192.1388, found 192.1389 ($[M+H]^+$); $[\alpha]_D^{25} = +5.8$ ($c = 1.0$, CHCl_3).

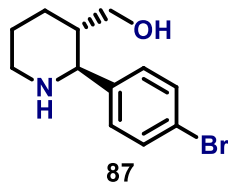
((2*S*,3*S*)-2-(4-Bromophenyl)-1-(4-methoxyphenyl)piperidin-3-yl)methanol (123)¹²⁰



Procedure: Prepared as per procedure B, using aldimine **103**; Yield: 64%, a dark brown oil; IR (neat) 3378 (br), 2937 (m), 2833 (w), 1508 (s), 1239 (s), 832 (m), 731 (m); ^1H NMR (400 MHz, CDCl_3) δ 7.29 – 7.24 (m, 2H), 7.12 (d, $J = 8.4$ Hz, 2H), 6.88 (d, $J = 9.0$ Hz, 2H), 6.63 (d, $J = 9.0$ Hz, 2H), 3.83 (d, $J = 9.0$ Hz, 1H), 3.68 (s, 3H), 3.45 – 3.38 (m, 1H), 3.31 – 3.21 (m, 2H), 2.86 – 2.78 (m, 1H), 2.01 – 1.94 (m, 1H), 1.91 – 1.80 (m, 4H, overlapping with OH brs), 1.53 – 1.42 (m, 1H); ^{13}C NMR (101 MHz, CDCl_3) δ 155.59, 145.96, 141.54, 131.26 (2C), 130.33 (2C), 125.48 (2C), 120.43, 113.92 (2C), 66.62, 65.07, 57.05, 55.38, 46.10, 27.52, 25.71; LRMS (+ESI) m/z 376.0 ($[M+H]^+$), 378.1 ($[M+H]^+$), 398.0 ($[M+\text{Na}]^+$), 400.0 ($[M+\text{Na}]^+$); HRMS (+ESI) m/z calcd for $\text{C}_{19}\text{H}_{23}^{79}\text{BrNO}_2^+$ ($[M+H]^+$) 376.0912, found 376.0912 ($[M+H]^+$) and calcd for $\text{C}_{19}\text{H}_{23}^{81}\text{BrNO}_2^+$ ($[M+H]^+$) 378.0886, found 378.0898

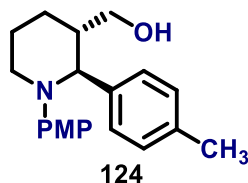
([M+H]⁺); $[\alpha]_{\text{D}}^{25} = -6.8$ (c = 1.0, CHCl₃), lit. $[\alpha]_{\text{D}}^{25} = -6.4$ (c = 1.0, CHCl₃, 90% ee). Data was consistent with the literature values.¹²⁰

((2*S*,3*S*)-2-(4-Bromophenyl)piperidin-3-yl)methanol (87)



Procedure: Prepared as per procedure D; Yield: 62%, a bright orange oil; IR (neat) 3278 (br), 2928 (s), 1489 (s), 1010 (s), 814 (m); ¹H NMR (400 MHz, CDCl₃) δ 7.45 (d, *J* = 8.4 Hz, 2H), 7.29 – 7.24 (m, 2H), 3.40 (d, *J* = 10.0 Hz, 1H), 3.34 (dd, *J* = 10.9, 3.9 Hz, 1H), 3.22 (dd, *J* = 10.8, 5.7 Hz, 1H), 3.14 (d, *J* = 11.4 Hz, 1H), 2.80 – 2.68 (m, 1H), 2.03 – 1.95 (m, 1H), 1.82 – 1.75 (m, 2H, overlapping with OH brs), 1.74 – 1.65 (m, 2H), 1.53 (brs, 1H, NH), 1.45 – 1.31 (m, 1H); ¹³C NMR (101 MHz, CDCl₃) δ 142.33, 131.80 (2C), 129.61 (2C), 121.47, 65.02, 64.41, 47.53, 45.31, 28.48, 26.01; LRMS (+ESI) *m/z* 270.1 ([M+H]⁺), 272.2 ([M+H]⁺); HRMS (+ESI) *m/z* calcd for C₁₂H₁₇⁷⁹BrNO⁺ ([M+H]⁺) 270.0494, found 270.0494 ([M+H]⁺) and calcd for C₁₂H₁₇⁸¹BrNO⁺ ([M+H]⁺) 272.0468, found 272.0485 ([M+H]⁺); $[\alpha]_{\text{D}}^{25} = -9.8^{\circ}$ (c = 1.0, CHCl₃).

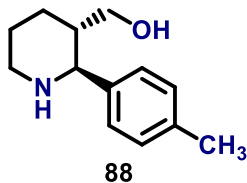
((2*S*,3*S*)-1-(4-Methoxyphenyl)-2-(*p*-tolyl)piperidin-3-yl)methanol (124)



Procedure: Prepared as per procedure B, using aldimine **104**; Yield: 51% (60.4% ee), a clear brown oil; IR (neat) 3366 (br), 2932 (m), 1509 (s), 1240 (s), 805 (m); ¹H NMR (400 MHz, CDCl₃) δ 7.11 (d, *J* = 8.0 Hz, 2H), 6.96 (d, *J* = 7.9 Hz, 2H), 6.89 (d, *J* = 9.0 Hz, 2H), 6.64 (d, *J* = 9.0 Hz, 2H), 3.78 (d, *J* = 8.6 Hz, 1H), 3.67 (s, 3H), 3.43 (dd, *J* = 11.0, 4.7 Hz, 1H), 3.34 – 3.22 (m, 2H), 2.88 – 2.80 (m, 1H), 2.21 (s, 3H), 2.00 – 1.79 (m, 5H, overlapping with OH brs), 1.48 – 1.37 (m, 1H); ¹³C NMR (101 MHz, CDCl₃) δ 155.27, 146.32, 139.16, 136.34, 128.96 (2C), 128.42 (2C), 125.23 (2C), 113.79 (2C), 67.43, 65.67, 56.84, 55.37, 46.21, 27.66, 25.70, 21.19; LRMS (+ESI) *m/z* 312.2 ([M+H]⁺), 334.2 ([M+Na]⁺); HRMS

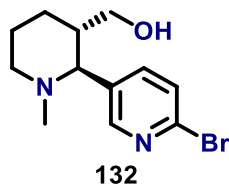
(+ESI) m/z calcd for $C_{20}H_{26}NO_2^+$ ($[M+H]^+$) 312.1964, found 312.1964 ($[M+H]^+$); $[\alpha]_D^{25} = +7.9$ ($c = 1.0$, MeOH).

((2S,3S)-2-(p-Tolyl)piperidin-3-yl)methanol (88)

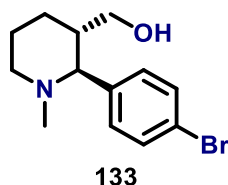


Procedure: Prepared as per procedure D; Yield: 43%, a pale-orange oil; IR (neat) 3296 (br), 2924 (s), 2856 (m), 1514 (s), 1036 (s), 808 (s); 1H NMR (400 MHz, $CDCl_3$) δ 7.29 – 7.23 (m, 2H), 7.14 (d, $J = 7.8$ Hz, 2H), 3.39 – 3.33 (m, 2H), 3.23 (dd, $J = 11.0, 5.6$ Hz, 1H), 3.14 (d, $J = 11.4$ Hz, 1H), 2.78 – 2.70 (m, 1H), 2.33 (s, 3H), 2.02 – 1.94 (m, 1H), 1.82 – 1.63 (m, 5H, overlapping with OH and NH brs), 1.39 – 1.27 (m, 1H); ^{13}C NMR (101 MHz, $CDCl_3$) δ 140.09, 137.54, 129.48 (2C), 127.72 (2C), 65.55, 65.32, 47.62, 45.36, 28.66, 26.04, 21.27; LRMS (+ESI) m/z 206.2 ($[M+H]^+$); HRMS (+ESI) m/z calcd for $C_{13}H_{20}NO^+$ ($[M+H]^+$) 206.1545, found 206.1549 ($[M+H]^+$); $[\alpha]_D^{25} = +3.8$ ($c = 1.0$, MeOH).

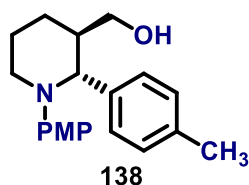
((2S,3S)-2-(6-Bromopyridin-3-yl)-1-methylpiperidin-3-yl)methanol (132)



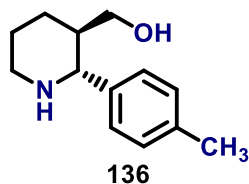
Procedure: Prepared as per procedure E, using piperidine **84**; Yield: 93%, a dark red oil; IR (neat) 3383 (br), 2991 (s), 2790 (m), 1506 (s), 1424 (s), 798 (s); 1H NMR (400 MHz, $CDCl_3$) 8.27 (s, 1H), 7.57 (d, $J = 8.0$ Hz, 1H), 7.47 (d, $J = 8.2$ Hz, 1H), 3.28 (d, $J = 10.6$ Hz, 1H), 3.18 – 3.09 (m, 1H), 2.99 (d, $J = 11.4$ Hz, 1H), 2.75 (d, $J = 10.1$ Hz, 1H), 2.18 – 2.07 (m, 1H), 1.99 – 1.90 (m, 4H, overlapping with OH brs), 1.84 – 1.63 (m, 4H), 1.44 – 1.32 (m, 1H); ^{13}C NMR (101 MHz, $CDCl_3$) δ 150.46, 141.08, 138.28, 137.74, 128.38, 68.76, 64.48, 57.14, 45.42, 44.85, 27.79, 25.25; LRMS (+ESI) m/z 285.6 ($[M+H]^+$), 287.0 ($[M+H]^+$); HRMS (+ESI) m/z calcd for $C_{12}H_{18}^{79}BrN_2O^+$ ($[M+H]^+$) 285.0597, found 285.0598 ($[M+H]^+$) and calcd for $C_{12}H_{18}^{81}BrN_2O^+$ ($[M+H]^+$) 287.0577, found 287.0577 ($[M+H]^+$); $[\alpha]_D^{25} = +13.3$ ($c = 1.0$, $CHCl_3$).

((2*S*,3*S*)-2-(4-Bromophenyl)-1-methylpiperidin-3-yl)methanol (133)

Procedure: Prepared as per procedure E, using piperidine **87** ; Yield: 87%, a dark red oil; IR (neat) 3339 (brs), 2935 (s), 2851 (m), 1487 (s), 1004 (s), 813 (s); ¹H NMR (400 MHz, CDCl₃) δ 7.45 (d, *J* = 8.5 Hz, 2H), 7.21 (d, *J* = 8.0 Hz, 2H), 3.28 (dd, *J* = 10.8, 3.5 Hz, 1H), 3.13 (dd, *J* = 10.8, 5.8 Hz, 1H), 3.06 – 2.98 (m, 1H), 2.66 (d, *J* = 10.2 Hz, 1H), 2.16 – 2.08 (m, 1H), 1.96 – 1.90 (m, 4H, overlapping with OH brs), 1.87 – 1.68 (m, 4H), 1.38 – 1.22 (m, 1H); ¹³C NMR (101 MHz, CDCl₃) δ 141.45, 131.84 (2C), 130.01 (2C), 121.25, 72.13, 65.06, 57.30, 45.49, 44.68, 27.93, 25.31; LRMS (+ESI) *m/z* 284.1 ([M+H]⁺), 286.1 ([M+H]⁺), 306.0; HRMS (+ESI) *m/z* calcd for C₁₃H₁₉⁷⁹BrNO⁺ (M+H)⁺ 284.0650, found 284.0651 (M+H)⁺ and calcd for C₁₃H₁₉⁸¹BrNO⁺ (M+H)⁺ 286.0630, found 286.0633 (M+H)⁺; [α]_D²⁵ = -7.1 (c = 1.0, CHCl₃).

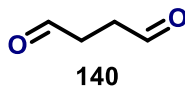
((2*R*,3*R*)-1-(4-Methoxyphenyl)-2-(*p*-tolyl)piperidin-3-yl)methanol (138)

Procedure: Prepared as per procedure B, using aldimine **104** and D-proline as a catalyst; Yield: 62% (69.6% ee), a clear pale-brown oil; IR, NMR and MS analytical data were the same as data for piperidine **124**; [α]_D²⁵ = -7.9 (c = 1.0, MeOH)

((2*R*,3*R*)-2-(*p*-Tolyl)piperidin-3-yl)methanol (136)

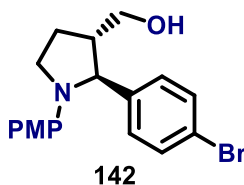
Procedure: Prepared as per procedure D; Yield: 49%, a bright red oil; IR, NMR and MS analytical data were same as data for piperidine **88**; $[\alpha]_D^{25} = -3.8$ ($c = 1.0$, MeOH).

Succinaldehyde (**140**)¹³²



Procedure: To a round bottom flask containing a stirring solution of 2,5-dimethoxytetrahydrofuran **139** (10.2 g, 10 ml, 77.25 mmol) in water (25 ml), was heated to 75 °C (oil bath temperature) for 4 h and distillate (2 – 3 ml) was collected during this period in a separate flask to remove the methanol formed. The temperature was then increased to 120 °C (oil bath temperature) and again distillate (20 -25 ml) collected during this period in a separate flask to remove excess water. The mixture was cooled to ambient temperature and extracted with DCM (20 × 5 ml). The combined organic phases were dried over Na₂SO₄, filtered, and concentrated under reduced pressure to give succinaldehyde **140** (4.8 g) as a yellow liquid. Succinaldehyde can be stored at -20 °C in water or DCM for 2-3 days; Yield: 72%; IR (neat) 2912 (s), 2819 (m), 2740 (w), 1725 (m), 1405 (s); ¹H NMR (400 MHz, CDCl₃) δ 9.82 (s, 2H), 2.80 (s, 4H).; ¹³C NMR (101 MHz, CDCl₃) δ 199.73 (2C), 36.14 (2C). Data was consistent with the literature values.¹³²

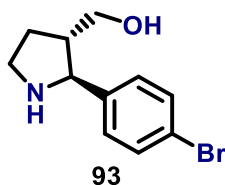
((2*S*,3*S*)-2-(4-Bromophenyl)-1-(4-methoxyphenyl)pyrrolidin-3-yl)methanol (**142**)¹²¹



Procedure: Prepared as per procedure C, using aldimine **103**; Yield: 67%, a dark brown oil; IR (neat) 3339 (br), 2925 (m), 2889 (w), 1515 (s), 1140 (s), 847 (m); ¹H NMR (400 MHz, CDCl₃) δ 7.43 (d, $J = 8.5$ Hz, 2H), 7.15 (d, $J = 8.3$ Hz, 2H), 6.76 (d, $J = 9.1$ Hz, 2H), 6.46 – 6.37 (m, 2H), 4.47 (d, $J = 2.6$ Hz, 1H), 3.71 (s, 4H), 3.69 – 3.63 (m, 2H), 3.50 – 3.39 (m, 1H), 2.34 – 2.28 (m, 1H), 2.22 – 2.10 (m, 1H), 1.93 – 1.82 (m, 1H), 1.57 (brs, 1H, OH); ¹³C NMR (101 MHz, CDCl₃) δ 151.29, 143.60, 141.78, 131.84 (2C), 127.96 (2C), 120.53, 114.99 (2C), 113.45 (2C), 65.33, 64.31, 55.99, 51.70, 48.55, 25.70; LRMS (+ESI) m/z 362.0 ([M+H]⁺), 364.4 ([M+H]⁺); HRMS (+ESI) m/z calcd for C₁₈H₂₁⁷⁹BrNO₂⁺ ([M+H]⁺)

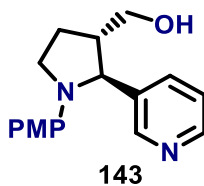
362.0750, found 362.0752 ($[M+H]^+$) and calcd for $C_{18}H_{21}^{81}BrNO_2^+$ ($[M+H]^+$) 364.0730, found 364.0730 ($[M+H]^+$); $[\alpha]_D^{25} = -42.1$ ($c = 1.0$, $CHCl_3$), lit. $[\alpha]_D^{22} = -43.2$ ($c = 1.0$, $CHCl_3$, 90% ee). Data was consistent with the literature values.¹²¹

((2S,3S)-2-(4-Bromophenyl)pyrrolidin-3-yl)methanol (93)



Procedure: Prepared as per procedure D; Yield: 69%, a clear red oil; IR (neat) 3263 (br), 2996 (s), 1457 (s), 768 (m); 1H NMR (400 MHz, $CDCl_3$) δ 7.43 (d, $J = 8.4$ Hz, 2H), 7.28 – 7.24 (m, 2H), 3.95 – 3.82 (m, 1H), 3.72 – 3.60 (m, 2H), 3.25 – 3.15 (m, 1H), 3.12 – 3.01 (m, 1H), 2.24 – 2.03 (m, 4H, overlapping with OH brs), 1.98 (brs, 1H, NH), 1.78 – 1.66 (m, 1H); ^{13}C NMR (101 MHz, $CDCl_3$) δ 143.30, 131.70 (2C), 128.83 (2C), 120.97, 64.86, 64.74, 49.93, 46.21, 29.12; LRMS (+ESI) m/z 256.8 ($[M+H]^+$), 258.4 ($[M+H]^+$); HRMS (+ESI) m/z calcd for $C_{11}H_{15}^{79}BrNO^+$ ($[M+H]^+$) 256.0332, found 256.0335 ($[M+H]^+$) and calcd for $C_{11}H_{15}^{81}BrNO^+$ ($[M+H]^+$) 258.0311, found 258.0312 ($[M+H]^+$); $[\alpha]_D^{25} = -24.7$ ($c = 1.0$, $CHCl_3$).

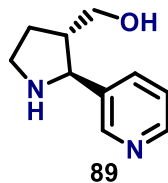
((2S,3S)-1-(4-Methoxyphenyl)-2-(pyridin-3-yl)pyrrolidin-3-yl)methanol (143)



Procedure: Prepared as per procedure C, using aldimine **105**; Yield: 65%, a clear brown oil; IR (neat) 3321 (br), 2946 (m), 1536 (s), 1239 (s); 1H NMR (400 MHz, $CDCl_3$) δ 8.56 (s, 1H), 8.47 (d, $J = 4.1$ Hz, 1H), 7.57 (d, $J = 7.8$ Hz, 1H), 7.24 – 7.18 (m, 1H), 6.76 (d, $J = 9.1$ Hz, 2H), 6.40 (d, $J = 9.0$ Hz, 2H), 4.62 – 4.55 (m, 1H), 3.77 – 3.72 (m, 1H), 3.70 (s, 4H, overlapping with OH brs), 3.50 – 3.39 (m, 1H), 2.40 – 2.27 (m, 1H), 2.23 – 2.13 (m, 1H), 1.99 – 1.80 (m, 3H); ^{13}C NMR (101 MHz, $CDCl_3$) δ 151.44, 148.33, 148.24, 141.60, 140.00, 134.05, 123.77, 115.03 (2C), 113.58 (2C), 64.04, 63.57, 55.98, 51.71, 48.67, 25.76; LRMS

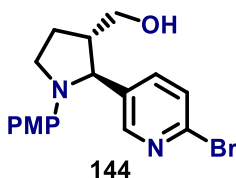
(+ESI) m/z 307.6 ($[M+Na]^+$); HRMS (+ESI) m/z calcd for $C_{17}H_{21}N_2O_2^+$ ($[M+H]^+$) 285.1598, found 285.1598 ($[M+H]^+$); $[\alpha]_D^{25} = -35.9$ ($c = 1.0$, $CHCl_3$).

((2S,3S)-2-(Pyridin-3-yl)pyrrolidin-3-yl)methanol (89)

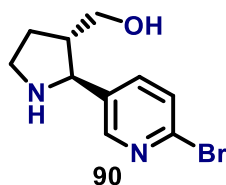


Procedure: Prepared as per procedure D; Yield: 66%, a bright orange oil; IR (neat) 3413 (br), 3248 (w), 2930 (s), 2862 (s), 1431 (s); 1H NMR (400 MHz, $CDCl_3$) δ 8.23 (d, $J = 2.0$ Hz, 1H), 8.01 – 7.92 (m, 1H), 7.62 – 7.55 (m, 1H), 7.29 – 7.22 (m, 1H), 3.87 (d, $J = 9.8$ Hz, 1H), 3.55 – 3.47 (m, 1H), 3.34 – 3.21 (m, 1H), 3.20 – 3.08 (m, 1H), 2.92 – 2.85 (m, 1H), 2.11 (brs, 1H, NH), 1.98 – 1.88 (m, 1H), 1.74 – 1.65 (m, 3H, overlapping with OH brs); ^{13}C NMR (101 MHz, $CDCl_3$) δ 149.17, 148.21, 138.01, 136.22, 125.14, 65.67, 62.92, 49.31, 48.88, 29.15; LRMS (+ESI) m/z 179.3 ($[M+H]^+$); HRMS (+ESI) m/z calcd for $C_{10}H_{15}N_2O^+$ ($[M+H]^+$) 179.1179, found 179.1180 ($[M+H]^+$); $[\alpha]_D^{25} = +18.3$ ($c = 1.0$, $CHCl_3$).

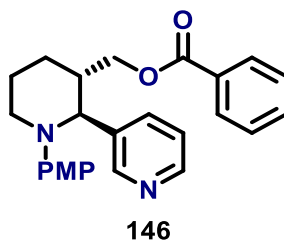
((2S,3S)-2-(6-Bromopyridin-3-yl)-1-(4-methoxyphenyl)pyrrolidin-3-yl)methanol (144)



Procedure: Prepared as per procedure C, using aldimine **106**; Yield: 70%, a dark brown oil; IR (neat) 3316 (br), 2900 (m), 1525 (s), 1489 (s), 1251 (s); 1H NMR (400 MHz, $CDCl_3$) δ 8.31 (s, 1H), 7.48 – 7.35 (m, 2H), 6.77 (d, $J = 9.0$ Hz, 2H), 6.48 – 6.31 (m, 2H), 4.56 (d, $J = 2.4$ Hz, 1H), 3.78 – 3.64 (m, 6H), 3.49 – 3.38 (m, 1H), 2.38 – 2.26 (m, 1H), 2.23 – 2.11 (m, 1H), 1.98 – 1.86 (m, 1H), 1.76 – 1.52 (m, 3H); ^{13}C NMR (101 MHz, $CDCl_3$) δ 151.66, 148.91, 141.35, 140.53, 139.48, 136.79, 128.18 (2C), 115.08 (2C), 113.71, 63.94, 63.07, 55.98, 51.57, 48.75, 25.76; LRMS (+ESI) m/z 363.8 ($[M+H]^+$), 365.5 ($[M+H]^+$); HRMS (+ESI) m/z calcd for $C_{17}H_{20}^{79}BrN_2O_2^+$ ($[M+H]^+$) 363.0703, found 363.0708 ($[M+H]^+$) and calcd for $C_{17}H_{20}^{81}BrN_2O_2^+$ ($[M+H]^+$) 365.0682, found 365.0687 ($[M+H]^+$); $[\alpha]_D^{25} = +16.8$ ($c = 1.0$, $CHCl_3$).

((2*S*,3*S*)-2-(6-Bromopyridin-3-yl)pyrrolidin-3-yl)methanol (90)

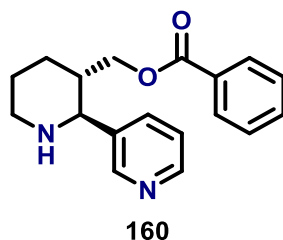
Procedure: Prepared as per procedure D; Yield: 73%, a clear brown oil; IR (neat) 3483 (br), 2969 (s), 1580 (s), 1452 (s), 796 (s); ^1H NMR (400 MHz, CDCl_3) δ 8.35 (d, $J = 2.5$ Hz, 1H), 7.64 (dd, $J = 8.2, 2.5$ Hz, 1H), 7.43 (d, $J = 8.2$ Hz, 1H), 3.97 (d, $J = 6.8$ Hz, 1H), 3.67 (d, $J = 5.8$ Hz, 2H), 3.21 – 3.14 (m, 1H), 3.13 – 3.05 (m, 1H), 2.22 – 2.03 (m, 2H), 1.85 (brs, 2H, overlapping OH and NH brs), 1.75 – 1.65 (m, 1H); ^{13}C NMR (101 MHz, CDCl_3) δ 149.30, 140.64, 139.60, 137.58, 128.04, 64.37, 62.25, 50.01, 46.32, 29.08; LRMS (+ESI) m/z 257.3 ($[\text{M}+\text{H}]^+$), 259.6 ($[\text{M}+\text{H}]^+$); HRMS (+ESI) m/z calcd for $\text{C}_{11}\text{H}_{16}^{79}\text{BrN}_2\text{O}^+$ ($[\text{M}+\text{H}]^+$) 257.0284, found 257.0285 ($[\text{M}+\text{H}]^+$) and calcd for $\text{C}_{11}\text{H}_{16}^{81}\text{BrN}_2\text{O}^+$ ($[\text{M}+\text{H}]^+$) 259.0264, found 259.0268 ($[\text{M}+\text{H}]^+$); $[\alpha]_{\text{D}}^{25} = +22.1$ ($c = 1.0$, CHCl_3).

((2*S*,3*S*)-1-(4-Methoxyphenyl)-2-(pyridin-3-yl)piperidin-3-yl)methyl benzoate (146)

Procedure: To a round bottom flask containing a solution of piperidine alcohol (1 mmol, 100 mg) in DCM (5 ml), TEA (3 mmol) and benzoyl chloride (1.1 mmol) was added at 0 °C and stirred for 1 h. The mixture was diluted with saturated NaHCO_3 solution, extracted with ethyl acetate (3 x 5 ml) and dried over Na_2SO_4 . The combined organic extract was concentrated under reduced pressure and the residue was purified by column chromatography (EtOAc:Hex, 1:5) to afford piperidine-benzoate ester **146** as clear pale-yellow oil; Yield: 77%; IR (neat) 2969 (m), 1755 (w), 1555 (s), 1307 (m), 817 (m); ^1H NMR (400 MHz, CDCl_3) δ 8.46 (d, $J = 1.7$ Hz, 1H), 8.28 (dd, $J = 4.8, 1.6$ Hz, 1H), 7.98 – 7.93 (m, 2H), 7.60 – 7.52 (m, 2H), 7.48 – 7.41 (m, 2H), 7.07 – 7.01 (m, 1H), 6.90 (d, $J = 8.9$ Hz, 2H), 6.63 (d, $J = 9.0$ Hz, 2H), 4.14 (dd, $J = 11.2, 4.4$ Hz, 1H), 3.99 – 3.89 (m, 2H), 3.66 (s, 3H), 3.33 – 3.23 (m, 1H), 2.91 – 2.81 (m, 1H), 2.33 – 2.19 (m, 1H), 2.12 – 2.04 (m, 1H),

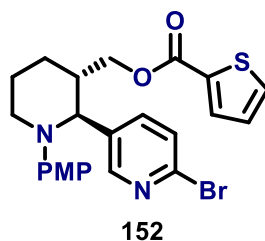
2.01 – 1.82 (m, 2H), 1.64 – 1.49 (m, 1H); ^{13}C NMR (101 MHz, CDCl_3) δ 166.43, 156.04, 150.37, 148.46, 145.37, 137.33, 136.04, 133.14, 130.17, 129.65 (2C), 128.52 (2C), 126.09 (2C), 123.39, 114.06 (2C), 66.71, 65.94, 57.39, 55.36, 43.52, 28.16, 25.75; LRMS (+ESI) m/z 425.4 ($[\text{M}+\text{Na}]^+$); HRMS (+ESI) m/z calcd for $\text{C}_{25}\text{H}_{27}\text{N}_2\text{O}_3^+$ ($[\text{M}+\text{H}]^+$) 403.2016, found 403.2019 ($[\text{M}+\text{H}]^+$); $[\alpha]_{\text{D}}^{25} = +27.4$ ($c = 1.0$, CHCl_3).

((2S,3S)-2-(Pyridin-3-yl)piperidin-3-yl)methyl benzoate (160)



Procedure: Prepared as per procedure D; Yield: 66%, a clear bright red oil; IR (neat) 3443 (br), 2993 (s), 1742 (w), 1439 (s), 820 (s), 717 (s); ^1H NMR (400 MHz, CDCl_3) δ 8.62 (d, $J = 1.8$ Hz, 1H), 8.48 (dd, $J = 4.7, 1.5$ Hz, 1H), 7.88 – 7.83 (m, 2H), 7.75 (d, $J = 7.9$ Hz, 1H), 7.54 (t, $J = 7.2$ Hz, 1H), 7.44 – 7.37 (m, 2H), 7.25 – 7.19 (m, 1H), 4.05 (dd, $J = 11.3, 4.3$ Hz, 1H), 3.92 (dd, $J = 11.3, 5.5$ Hz, 1H), 3.58 (d, $J = 9.9$ Hz, 1H), 3.21 (d, $J = 11.5$ Hz, 1H), 2.86 – 2.74 (m, 1H), 2.23 (s, 1H), 2.13 – 2.01 (m, 2H), 1.87 – 1.67 (m, 2H), 1.55 – 1.37 (m, 1H); ^{13}C NMR (101 MHz, CDCl_3) δ 166.40, 149.61, 149.40, 138.36, 135.33, 133.09, 130.09, 129.59 (2C), 128.44 (2C), 123.82, 66.66, 63.07, 47.46, 42.40, 28.86, 25.82; LRMS (+ESI) m/z 297.3 ($[\text{M}+\text{H}]^+$); HRMS (+ESI) m/z calcd for $\text{C}_{18}\text{H}_{21}\text{N}_2\text{O}_2^+$ ($[\text{M}+\text{H}]^+$) 297.1598, found 297.1600 ($[\text{M}+\text{H}]^+$); $[\alpha]_{\text{D}}^{25} = +31.5$ ($c = 1.0$, CHCl_3).

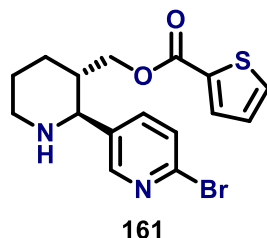
((2S,3S)-2-(6-Bromopyridin-3-yl)-1-(4-methoxyphenyl)piperidin-3-yl)methyl thiophene-2-carboxylate (152)



Procedure: Prepared as per procedure F, using thiophene-2-carboxylic acid **147**; Yield: 68%, a dark yellow oil; IR (neat) 2953 (m), 1737 (w), 1523 (s), 1312 (s), 810 (s); ^1H NMR

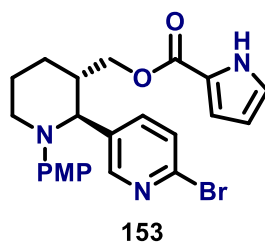
(400 MHz, CDCl₃) δ 8.20 (s, 1H), 7.69 (d, $J = 3.4$ Hz, 1H), 7.56 (d, $J = 4.9$ Hz, 1H), 7.43 (d, $J = 7.4$ Hz, 1H), 7.23 (d, $J = 8.2$ Hz, 1H), 7.11 (t, $J = 4.3$ Hz, 1H), 6.90 (d, $J = 8.6$ Hz, 2H), 6.63 (d, $J = 8.4$ Hz, 2H), 4.12 (dd, $J = 11.2, 4.2$ Hz, 1H), 3.95 – 3.84 (m, 2H), 3.68 (s, 3H), 3.30 – 3.20 (m, 1H), 2.87 – 2.75 (m, 1H), 2.22 – 2.08 (m, 1H), 2.08 – 1.99 (m, 1H), 1.88 (d, $J = 3.8$ Hz, 2H), 1.57 – 1.43 (m, 1H); ¹³C NMR (101 MHz, CDCl₃) δ 161.96, 156.31, 150.65, 145.00, 140.57, 138.59, 136.92, 133.65, 133.40, 132.65, 128.03, 127.89, 126.22 (2C), 114.23 (2C), 66.66, 65.42, 57.59, 55.38, 43.57, 28.12, 25.72; LRMS (+ESI) m/z 487.2 ([M+H]⁺), 489.4 ([M+H]⁺); HRMS (+ESI) m/z calcd for C₂₃H₂₄⁷⁹BrN₂O₃S⁺ ([M+H]⁺) 487.0686, found 487.0686 ([M+H]⁺) and calcd for C₂₃H₂₄⁸¹BrN₂O₃S⁺ ([M+H]⁺) 487.0665, found 487.0666 ([M+H]⁺); $[\alpha]_D^{25} = -18.5$ (c = 1.0, CHCl₃).

((2*S*,3*S*)-2-(6-Bromopyridin-3-yl)piperidin-3-yl)methyl thiophene-2-carboxylate (161)



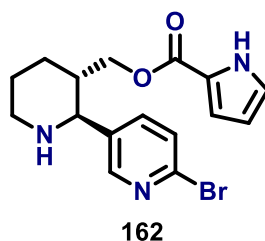
Procedure: Prepared as per procedure D; Yield: 75%, a pale-brown oil; IR (neat) 3386 (br), 2913 (s), 1742 (w), 1555 (s), 1218 (s), 805 (s); ¹H NMR (400 MHz, CDCl₃) δ 8.38 (s, 1H), 7.67 – 7.59 (m, 2H), 7.54 (d, $J = 4.9$ Hz, 1H), 7.41 (d, $J = 8.2$ Hz, 1H), 7.13 – 7.06 (m, 1H), 4.05 (dd, $J = 11.3, 4.7$ Hz, 1H), 3.88 (dd, $J = 11.4, 4.8$ Hz, 1H), 3.55 (d, $J = 9.7$ Hz, 1H), 3.15 (d, $J = 11.2$ Hz, 1H), 2.83 – 2.72 (m, 1H), 2.10 – 1.95 (m, 2H), 1.93 (brs, 1H, NH), 1.85 – 1.65 (m, 2H), 1.50 – 1.33 (m, 1H); ¹³C NMR (101 MHz, CDCl₃) δ 161.92, 149.94, 141.64, 138.02, 137.46, 133.61, 133.28, 132.67, 128.35, 127.98, 66.52, 62.37, 47.27, 42.29, 28.60, 25.46; LRMS (+ESI) m/z 381.2 ([M+H]⁺), 383.4 ([M+H]⁺); HRMS (+ESI) m/z calcd for C₁₆H₁₈⁷⁹BrN₂O₂S⁺ ([M+H]⁺) 381.0267, found 381.0267 ([M+H]⁺) and calcd for C₁₆H₁₈⁸¹BrN₂O₂S⁺ ([M+H]⁺) 383.0246, found 383.0247 ([M+H]⁺); $[\alpha]_D^{25} = -7.7$ (c = 1.0, CHCl₃).

((2*S*,3*S*)-2-(6-Bromopyridin-3-yl)-1-(4-methoxyphenyl)piperidin-3-yl)methyl 1H-pyrrole-2-carboxylate (153)



Procedure: Prepared as per procedure F, using 1H-pyrrole-2-carboxylic acid **148**; Yield: 55%, a brown oil; IR (neat) 3310 (br), 2959 (m), 1722 (w), 1558 (s), 1103 (s), 827 (s); ¹H NMR (400 MHz, CDCl₃) δ 8.91 (brs, 1H, NH), 8.20 (d, *J* = 2.2 Hz, 1H), 7.44 (dd, *J* = 8.2, 2.3 Hz, 1H), 7.23 (d, *J* = 8.2 Hz, 1H), 6.99 – 6.93 (m, 1H), 6.89 (d, *J* = 8.7 Hz, 2H), 6.85 – 6.80 (m, 1H), 6.65 (d, *J* = 8.9 Hz, 2H), 6.31 – 6.23 (m, 1H), 4.03 (dd, *J* = 11.3, 4.7 Hz, 1H), 3.93 (dd, *J* = 11.3, 5.1 Hz, 1H), 3.83 (d, *J* = 9.5 Hz, 1H), 3.69 (s, 3H), 3.29 – 3.19 (m, 1H), 2.88 – 2.75 (m, 1H), 2.15 – 2.10 (m, 1H), 2.06 – 1.99 (m, 1H), 1.97 – 1.84 (m, 2H), 1.53 – 1.46 (m, 1H); ¹³C NMR (101 MHz, CDCl₃) δ 160.83, 156.32, 150.72, 145.02, 140.50, 138.65, 137.11, 127.85, 126.22 (2C), 123.27, 122.47, 115.41, 114.25 (2C), 110.69, 65.91, 65.57, 57.54, 55.39, 43.63, 34.11, 28.11; LRMS (+ESI) *m/z* 470.0 ([M+H]⁺), 472.2 ([M+H]⁺); HRMS (+ESI) *m/z* calcd for C₂₃H₂₅⁷⁹BrN₃O₃⁺ ([M+H]⁺) 470.1074, found 470.1079 ([M+H]⁺) and calcd for C₂₃H₂₅⁸¹BrN₃O₃⁺ ([M+H]⁺) 472.1053, found 472.1054 ([M+H]⁺); [α]_D²⁵ = +28.2 (c = 1.0, CHCl₃).

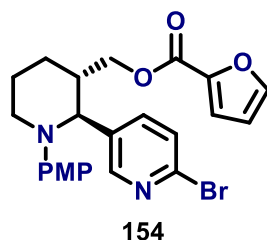
((2*S*,3*S*)-2-(6-Bromopyridin-3-yl)piperidin-3-yl)methyl 1H-pyrrole-2-carboxylate (162)



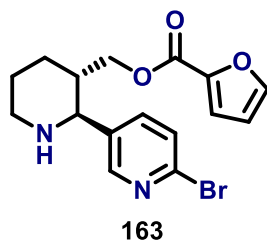
Procedure: Prepared as per procedure D; Yield: 63%, a red oil; IR (neat) 3468 (br), 3439 (br), 2914 (s), 1738 (w), 1511 (s), 1222 (s); ¹H NMR (400 MHz, CDCl₃) δ 8.92 (brs, 1H, NH), 8.36 (d, *J* = 2.4 Hz, 1H), 7.60 (dd, *J* = 8.1, 2.4 Hz, 1H), 7.41 (d, *J* = 8.4 Hz, 1H), 6.96 – 6.90 (m, 1H), 6.77 – 6.70 (m, 1H), 6.30 – 6.20 (m, 1H), 3.97 (dd, *J* = 11.3, 5.1 Hz, 1H),

3.88 (dd, $J = 11.3, 5.0$ Hz, 1H), 3.53 (d, $J = 9.9$ Hz, 1H), 3.21 – 3.11 (m, 1H), 2.83 – 2.69 (m, 1H), 2.06 – 1.95 (m, 2H), 1.84 – 1.65 (m, 3H, overlapping with NH brs), 1.46 – 1.30 (m, 1H); ^{13}C NMR (101 MHz, CDCl_3) δ 160.76, 149.95, 141.49, 138.06, 137.88, 128.29, 123.25, 122.36, 115.40, 110.66, 65.80, 62.52, 47.31, 42.46, 28.63, 25.55; LRMS (+ESI) m/z 386.3 ($[\text{M}+\text{Na}]^+$), 388.5 ($[\text{M}+\text{Na}]^+$); HRMS (+ESI) m/z calcd for $\text{C}_{16}\text{H}_{19}^{79}\text{BrN}_3\text{O}_2^+$ ($[\text{M}+\text{H}]^+$) 364.0655, found 364.0658 ($[\text{M}+\text{H}]^+$) and calcd for $\text{C}_{16}\text{H}_{19}^{81}\text{BrN}_3\text{O}_2^+$ ($[\text{M}+\text{H}]^+$) 366.0635, found 366.0636 ($[\text{M}+\text{H}]^+$); $[\alpha]_{\text{D}}^{25} = +16.9$ ($c = 1.0$, MeOH).

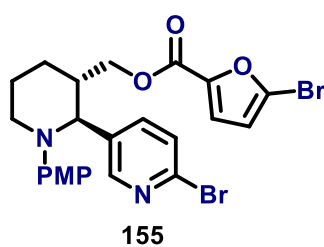
((2S,3S)-2-(6-Bromopyridin-3-yl)-1-(4-methoxyphenyl)piperidin-3-yl)methyl furan-2-carboxylate (154)



Procedure: Prepared as per procedure F, using furan-2-carboxylic acid **149**; Yield: 51%, a brown oil; IR (neat) 2958 (m), 1745 (w), 1524 (s), 1413 (s), 1301 (s); ^1H NMR (400 MHz, CDCl_3) δ 8.12 (s, 1H), 7.51 (s, 1H), 7.39 – 7.32 (m, 1H), 7.14 (d, $J = 8.1$ Hz, 1H), 6.98 (d, $J = 3.1$ Hz, 1H), 6.80 (d, $J = 8.5$ Hz, 2H), 6.56 (d, $J = 8.5$ Hz, 2H), 6.44 (s, 1H), 4.07 – 3.97 (m, 1H), 3.88 (dd, $J = 11.4, 5.2$ Hz, 1H), 3.77 (d, $J = 9.4$ Hz, 1H), 3.62 (s, 3H), 3.15 (d, $J = 11.8$ Hz, 1H), 2.81 – 2.69 (m, 1H), 2.17 – 2.03 (m, 1H), 1.98 – 1.92 (m, 1H), 1.90 – 1.71 (m, 2H), 1.46 – 1.35 (m, 1H); ^{13}C NMR (101 MHz, CDCl_3) δ 159.82, 154.77, 150.88, 147.97, 142.36, 141.53, 139.24, 133.30, 132.87, 129.30, 125.21 (2C), 118.45, 117.23, 113.52 (2C), 66.79, 64.91, 55.40, 52.37, 40.62, 28.15, 23.31; LRMS (+ESI) m/z 471.1 ($[\text{M}+\text{H}]^+$), 473.4 ($[\text{M}+\text{H}]^+$); HRMS (+ESI) m/z calcd for $\text{C}_{23}\text{H}_{24}^{79}\text{BrN}_2\text{O}_4^+$ ($[\text{M}+\text{H}]^+$) 471.0914, found 471.0919 ($[\text{M}+\text{H}]^+$) and calcd for $\text{C}_{23}\text{H}_{24}^{81}\text{BrN}_2\text{O}_4^+$ ($[\text{M}+\text{H}]^+$) 473.0893, found 473.0894 ($[\text{M}+\text{H}]^+$); $[\alpha]_{\text{D}}^{25} = -28.3$ ($c = 1.0$, MeOH).

((2*S*,3*S*)-2-(6-Bromopyridin-3-yl)piperidin-3-yl)methyl furan-2-carboxylate (163)

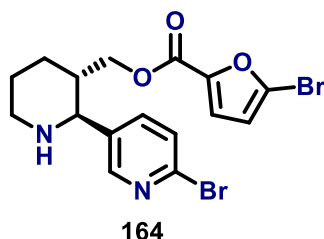
Procedure: Prepared as per procedure D; Yield: 69%, a brown oil; IR (neat) 3447 (br), 2922 (s), 1731 (w), 1533 (s), 1291 (s); ^1H NMR (400 MHz, CDCl_3) δ 8.31 (d, $J = 2.1$ Hz, 1H), 7.55 (dd, $J = 8.2, 2.1$ Hz, 1H), 7.51 – 7.46 (m, 1H), 7.34 (d, $J = 8.2$ Hz, 1H), 6.90 (d, $J = 3.4$ Hz, 1H), 6.44 – 6.40 (m, 1H), 3.96 (dd, $J = 11.3, 5.3$ Hz, 1H), 3.85 (dd, $J = 11.4, 5.1$ Hz, 1H), 3.48 (d, $J = 9.9$ Hz, 1H), 3.14 – 3.05 (m, 1H), 2.75 – 2.66 (m, 1H), 2.01 (brs, 1H, NH), 1.98 – 1.89 (m, 2H), 1.79 – 1.60 (m, 3H); ^{13}C NMR (101 MHz, CDCl_3) δ 158.40, 149.96, 149.36, 146.63, 144.29, 141.62, 138.07, 128.28, 118.14, 112.02, 66.29, 62.37, 47.14, 42.05, 28.47, 25.25; LRMS (+ESI) m/z 387.6 ($[\text{M}+\text{Na}]^+$), 389.2 ($[\text{M}+\text{Na}]^+$); HRMS (+ESI) m/z calcd for $\text{C}_{16}\text{H}_{18}^{79}\text{BrN}_2\text{O}_3^+$ ($[\text{M}+\text{H}]^+$) 365.0495, found 365.0498 ($[\text{M}+\text{H}]^+$) and calcd for $\text{C}_{16}\text{H}_{18}^{81}\text{BrN}_2\text{O}_3^+$ ($[\text{M}+\text{H}]^+$) 367.0475, found 367.0475 ($[\text{M}+\text{H}]^+$); $[\alpha]_{\text{D}}^{25} = -13.5$ ($c = 1.0, \text{CHCl}_3$).

((2*S*,3*S*)-2-(6-Bromopyridin-3-yl)-1-(4-methoxyphenyl)piperidin-3-yl)methyl 5-bromofuran-2-carboxylate (155)

Procedure: Prepared as per procedure F, using 5-bromofuran-2-carboxylic acid **150**; Yield: 57%, a dark red oil; IR (neat) 2981 (m), 1722 (w), 1524 (s), 1455 (s), 775 (s); ^1H NMR (400 MHz, CDCl_3) δ 8.17 (d, $J = 2.1$ Hz, 1H), 7.41 (dd, $J = 8.1, 2.4$ Hz, 1H), 7.23 (d, $J = 8.1$ Hz, 1H), 6.96 (d, $J = 3.5$ Hz, 1H), 6.87 (d, $J = 8.8$ Hz, 2H), 6.65 (d, $J = 8.9$ Hz, 2H), 6.45 (d, $J = 3.5$ Hz, 1H), 4.07 (dd, $J = 11.3, 5.0$ Hz, 1H), 3.96 (dd, $J = 11.4, 5.4$ Hz, 1H), 3.81 (d, $J = 9.3$ Hz, 1H), 3.68 (s, 3H), 3.28 – 3.19 (m, 1H), 2.87 – 2.76 (m, 1H), 2.21 – 2.14 (m, 1H), 2.06 – 1.98 (m, 1H), 1.94 – 1.80 (m, 3H), 1.53 – 1.41 (m, 1H); ^{13}C NMR (101 MHz, CDCl_3)

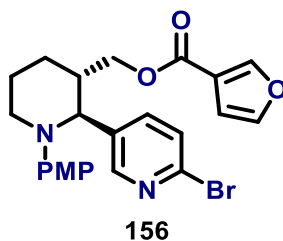
δ 157.35, 156.35, 150.64, 145.97, 144.90, 140.53, 138.63, 136.89, 127.92, 127.86, 126.24 (2C), 120.29, 114.25 (2C), 114.15, 66.74, 65.58, 57.44, 55.39, 43.39, 28.03, 25.64; LRMS (+ESI) m/z 549.6 ($[M+H]^+$), 551.4 ($[M+H]^+$); HRMS (+ESI) m/z calcd for $C_{23}H_{23}^{79}Br_2N_2O_4^+$ ($[M+H]^+$) 549.0019, found 549.0020 ($[M+H]^+$) and calcd for $C_{23}H_{23}^{81}Br_2N_2O_4^+$ ($[M+H]^+$) 551.0008, found 551.0010 ($[M+H]^+$); $[\alpha]_D^{25} = +27.3$ ($c = 1.0$, $CHCl_3$).

((2S,3S)-2-(6-Bromopyridin-3-yl)piperidin-3-yl)methyl 5-bromofuran-2-carboxylate (164)



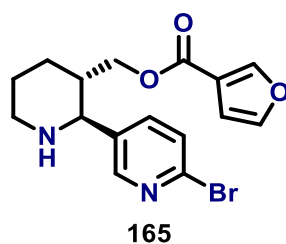
Procedure: Prepared as per procedure D; Yield: 72%, a dark brown oil; IR (neat) 3311 (br), 2961 (s), 1749 (w), 1552 (s), 1473 (s); 1H NMR (400 MHz, $CDCl_3$) δ 8.35 (d, $J = 2.5$ Hz, 1H), 7.62 (dd, $J = 8.2, 2.3$ Hz, 1H), 7.42 (d, $J = 8.1$ Hz, 1H), 6.90 (d, $J = 3.5$ Hz, 1H), 6.44 (d, $J = 3.5$ Hz, 1H), 4.04 (dd, $J = 11.3, 5.2$ Hz, 1H), 3.89 (dd, $J = 11.3, 5.0$ Hz, 1H), 3.50 (d, $J = 9.8$ Hz, 1H), 3.21 – 3.11 (m, 1H), 2.82 – 2.69 (m, 1H), 2.10 – 1.93 (m, 1H), 1.88 – 1.61 (m, 4H, overlapping with NH brs), 1.44 – 1.29 (m, 1H); ^{13}C NMR (101 MHz, $CDCl_3$) δ 157.28, 149.91, 145.88, 141.55, 138.07, 137.55, 128.29, 127.91, 120.25, 114.13, 66.62, 62.47, 47.23, 42.17, 28.54, 25.42; LRMS (+ESI) m/z 442.7 ($[M+H]^+$), 444.8 ($[M+H]^+$); HRMS (+ESI) m/z calcd for $C_{16}H_{17}^{79}Br_2N_2O_3^+$ ($[M+H]^+$) 442.9600, found 442.9601 ($[M+H]^+$) and calcd for $C_{16}H_{17}^{81}Br_2N_2O_3^+$ ($[M+H]^+$) 444.9580, found 444.9580 ($[M+H]^+$); $[\alpha]_D^{25} = +32.7$ ($c = 1.0$, $CHCl_3$).

((2S,3S)-2-(6-Bromopyridin-3-yl)-1-(4-methoxyphenyl)piperidin-3-yl)methyl furan-3-carboxylate (156)



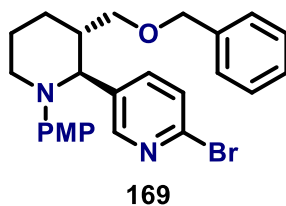
Procedure: Prepared as per procedure F, using furan-3-carboxylic acid **151**; Yield: 45%, a dark yellow oil; IR (neat) 2938 (m), 1739 (w), 1539 (s), 1280 (s), 1080 (s); ^1H NMR (400 MHz, CDCl_3) δ 8.14 (s, 1H), 7.81 – 7.76 (m, 2H), 7.60 (s, 1H), 7.19 (d, $J = 8.1$ Hz, 1H), 6.98 – 6.84 (m, 1H), 6.77 (d, $J = 8.5$ Hz, 2H), 6.60 – 6.49 (m, 2H), 4.27 – 4.05 (m, 1H), 3.94 (dd, $J = 11.4, 5.2$ Hz, 1H), 3.80 (d, $J = 9.4$ Hz, 1H), 3.60 (s, 3H), 3.35 – 3.23 (m, 1H), 2.92 – 2.77 (m, 2H), 2.10 – 1.94 (m, 1H), 1.89 – 1.71 (m, 2H), 1.56 – 1.45 (m, 1H); ^{13}C NMR (101 MHz, CDCl_3) δ 160.95, 153.21, 149.03, 147.33, 143.29, 142.83, 140.11, 132.66, 131.09, 129.12, 122.45 (2C), 118.32, 115.44 (2C), 110.42, 66.66, 64.23, 55.43, 50.19, 40.53, 28.02, 23.71; LRMS (+ESI) m/z 471.2 ($[\text{M}+\text{H}]^+$), 473.0 ($[\text{M}+\text{H}]^+$); HRMS (+ESI) m/z calcd for $\text{C}_{23}\text{H}_{24}^{79}\text{BrN}_2\text{O}_4^+$ ($[\text{M}+\text{H}]^+$) 471.0916, found 471.0916 ($[\text{M}+\text{H}]^+$) and calcd for $\text{C}_{23}\text{H}_{24}^{81}\text{BrN}_2\text{O}_4^+$ ($[\text{M}+\text{H}]^+$) 473.0888, found 473.0890 ($[\text{M}+\text{H}]^+$); $[\alpha]_{\text{D}}^{25} = +17.9$ ($c = 1.0$, CHCl_3).

((2*S*,3*S*)-2-(6-Bromopyridin-3-yl)piperidin-3-yl)methyl furan-3-carboxylate (165)



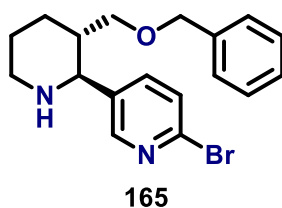
Procedure: Prepared as per procedure D; Yield: 61%, a pale-yellow oil; IR (neat) 3300 (br), 2981 (s), 1760 (w), 1555 (s), 1473 (s), 792 (s); ^1H NMR (400 MHz, CDCl_3) δ 8.35 (d, $J = 2.4$ Hz, 1H), 7.85 – 7.80 (m, 1H), 7.61 (dd, $J = 8.3, 2.5$ Hz, 1H), 7.43 – 7.38 (m, 2H), 6.57 – 6.53 (m, 1H), 3.98 (dd, $J = 11.5, 5.1$ Hz, 1H), 3.86 (dd, $J = 11.3, 5.1$ Hz, 1H), 3.49 (d, $J = 9.7$ Hz, 1H), 3.20 – 3.11 (m, 1H), 2.81 – 2.68 (m, 1H), 2.06 – 1.94 (m, 2H), 1.86 – 1.63 (m, 3H, overlapping with NH brs), 1.44 – 1.28 (m, 1H); ^{13}C NMR (101 MHz, CDCl_3) δ 162.79, 149.90, 147.70, 143.93, 141.54, 137.99, 137.77, 128.28, 119.05, 109.69, 66.04, 62.57, 47.31, 42.31, 28.66, 25.52; LRMS (+ESI) m/z 387.4 ($[\text{M}+\text{Na}]^+$), 389.1 ($[\text{M}+\text{Na}]^+$); HRMS (+ESI) m/z calcd for $\text{C}_{16}\text{H}_{18}^{79}\text{BrN}_2\text{O}_3^+$ ($[\text{M}+\text{H}]^+$) 365.0490, found 365.0491 ($[\text{M}+\text{H}]^+$) and calcd for $\text{C}_{16}\text{H}_{18}^{81}\text{BrN}_2\text{O}_3^+$ ($[\text{M}+\text{H}]^+$) 367.0480, found 367.0481 ($[\text{M}+\text{H}]^+$); $[\alpha]_{\text{D}}^{25} = +14.8$ ($c = 1.0$, CHCl_3).

5-((2*S*,3*S*)-3-((Benzyloxy)methyl)-1-(4-methoxyphenyl)piperidin-2-yl)-2-bromopyridine (169)



Procedure: Prepared as per procedure G, using benzyl bromide **166**; Yield: 82%, a dark brown oil; IR (neat) 2926 (m), 1559 (s), 1478 (s), 1008 (s); ^1H NMR (400 MHz, CDCl_3) δ 8.17 (d, $J = 2.4$ Hz, 1H), 7.41 (dd, $J = 8.2, 2.5$ Hz, 1H), 7.37 – 7.28 (m, 3H), 7.24 (s, 1H), 7.20 (d, $J = 8.2$ Hz, 1H), 6.87 (d, $J = 8.8$ Hz, 2H), 6.63 (d, $J = 8.8$ Hz, 2H), 4.34 (s, 2H), 3.95 (d, $J = 9.3$ Hz, 1H), 3.68 (s, 3H), 3.25 – 3.15 (m, 2H), 3.04 (dd, $J = 9.3, 4.8$ Hz, 1H), 2.84 – 2.75 (m, 1H), 2.02 – 1.92 (m, 1H), 1.91 – 1.78 (m, 4H), 1.65 (td, $J = 12.1, 4.7$ Hz, 1H); ^{13}C NMR (101 MHz, CDCl_3) δ 156.00, 150.69, 145.53, 140.07, 138.61, 138.34, 137.65, 128.51 (2C), 127.77 (2C), 127.74, 127.66, 125.91 (2C), 114.18 (2C), 73.35, 71.96, 64.11, 57.42, 55.39, 44.63, 28.21, 25.89; LRMS (+ESI) m/z 467.1 ($[\text{M}+\text{H}]^+$), 469.4 ($[\text{M}+\text{H}]^+$); HRMS (+ESI) m/z calcd for $\text{C}_{25}\text{H}_{27}^{79}\text{BrN}_2\text{O}_2^+$ ($[\text{M}+\text{H}]^+$) 467.1329, found 467.1330 ($[\text{M}+\text{H}]^+$) and calcd for $\text{C}_{25}\text{H}_{27}^{81}\text{BrN}_2\text{O}_2^+$ ($[\text{M}+\text{H}]^+$) 469.1308, found 469.1312 ($[\text{M}+\text{H}]^+$); $[\alpha]_{\text{D}}^{25} = -5.8$ ($c = 1.0$, CHCl_3).

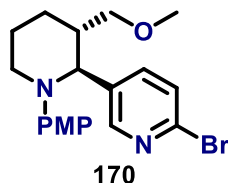
5-((2*S*,3*S*)-3-((Benzyloxy)methyl)piperidin-2-yl)-2-bromopyridine (165)



Procedure: Prepared as per procedure D; Yield: 69%, a bright red oil; IR (neat) 3392 (br), 2981 (s), 1568 (s), 1480 (s), 1029 (s), 818 (s); ^1H NMR (400 MHz, CDCl_3) δ 8.32 (d, $J = 2.3$ Hz, 1H), 7.58 (dd, $J = 8.2, 2.3$ Hz, 1H), 7.41 (d, $J = 8.2$ Hz, 1H), 7.35 – 7.26 (m, 3H), 7.21 – 7.16 (m, 2H), 4.29 (s, 2H), 3.55 (d, $J = 10.0$ Hz, 1H), 3.17 – 3.09 (m, 2H), 3.04 (dd, $J = 9.3, 5.2$ Hz, 1H), 2.80 – 2.67 (m, 1H), 2.02 – 1.92 (m, 1H), 1.83 – 1.70 (m, 3H, overlapping with NH brs), 1.70 – 1.59 (m, 1H), 1.57 – 1.44 (m, 1H); ^{13}C NMR (101 MHz, CDCl_3) δ 149.94, 141.06, 138.40, 138.26, 138.07, 128.46 (2C), 128.09, 127.69, 127.63

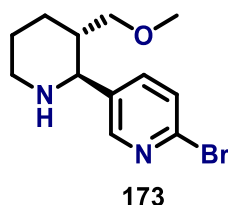
(2C), 73.24, 72.00, 61.50, 47.43, 43.68, 28.98, 25.97; LRMS (+ESI) m/z 383.6 ($[M+Na]^+$), 385.9 ($[M+Na]^+$); HRMS (+ESI) m/z calcd for $C_{18}H_{22}^{79}BrN_2O^+$ ($[M+H]^+$) 361.0910, found 361.0910 ($[M+H]^+$) and calcd for $C_{18}H_{22}^{81}BrN_2O^+$ ($[M+H]^+$) 363.0890, found 363.0892 ($[M+H]^+$); $[\alpha]_D^{25} = +4.5$ ($c = 0.5$, $CHCl_3$).

2-Bromo-5-((2S,3S)-3-(methoxymethyl)-1-(4-methoxyphenyl)piperidin-2-yl)pyridine (170)



Procedure: Prepared as per procedure G, using methyl iodide **167**; Yield: 79%, a clear pale-orange oil; IR (neat) 2955 (m), 2863 (w), 1524 (s), 1400 (s), 1304 (s), 850 (s); 1H NMR (400 MHz, $CDCl_3$) δ 8.17 (d, $J = 1.8$ Hz, 1H), 7.47 (dd, $J = 8.0, 2.1$ Hz, 1H), 7.26 – 7.21 (m, 1H), 6.89 (d, $J = 8.7$ Hz, 2H), 6.65 (d, $J = 8.8$ Hz, 2H), 3.95 (d, $J = 9.3$ Hz, 1H), 3.68 (s, 3H), 3.25 – 3.18 (m, 4H), 3.09 (dd, $J = 9.3, 3.1$ Hz, 1H), 2.93 (dd, $J = 9.2, 4.9$ Hz, 1H), 2.84 – 2.72 (m, 1H), 1.98 – 1.89 (m, 1H), 1.88 – 1.75 (m, 3H), 1.66 – 1.53 (m, 1H); ^{13}C NMR (101 MHz, $CDCl_3$) δ 156.00, 150.69, 145.54, 140.09, 138.54, 137.69, 127.71, 125.92 (2C), 114.18 (2C), 74.39, 63.89, 59.08, 57.51, 55.39, 44.63, 28.10, 25.91; LRMS (+ESI) m/z 391.4 ($[M+H]^+$), 393.5 ($[M+H]^+$); HRMS (+ESI) m/z calcd for $C_{19}H_{24}^{79}BrN_2O_2^+$ ($[M+H]^+$) 391.1016, found 391.1016 ($[M+H]^+$) and calcd for $C_{19}H_{24}^{81}BrN_2O_2^+$ ($[M+H]^+$) 393.0995, found 393.0998 ($[M+H]^+$); $[\alpha]_D^{25} = +13.9$ ($c = 0.5$, $CHCl_3$).

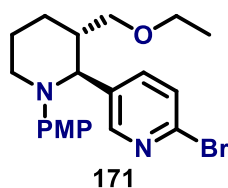
2-Bromo-5-((2S,3S)-3-(methoxymethyl)piperidin-2-yl)pyridine (173)



Procedure: Prepared as per procedure D; Yield: 71%, a pale-orange oil; IR (neat) 3410 (br), 2995 (s), 1540 (s), 1459 (s), 1235(s), 818 (s); 1H NMR (400 MHz, $CDCl_3$) δ 8.32 (d, $J = 2.3$ Hz, 1H), 7.64 (dd, $J = 8.3, 2.5$ Hz, 1H), 7.46 (d, $J = 8.2$ Hz, 1H), 3.54 (d, $J = 10.1$ Hz, 1H), 3.15 (s, 3H), 3.13 – 3.08 (m, 1H), 3.01 (dd, $J = 9.3, 3.1$ Hz, 1H), 2.91 (dd, $J = 9.3, 5.4$

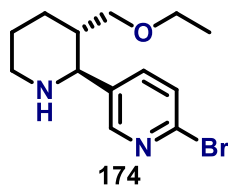
Hz, 1H), 2.79 – 2.68 (m, 1H), 2.00 – 1.90 (m, 1H), 1.84 (brs, 1H, NH), 1.81 – 1.74 (m, 1H), 1.72 – 1.62 (m, 2H), 1.54 – 1.40 (m, 1H); ^{13}C NMR (101 MHz, CDCl_3) δ 150.01, 141.22, 138.05, 138.01, 128.15, 74.30, 61.25, 59.04, 47.37, 43.61, 28.80, 25.82; LRMS (+ESI) m/z 285.7 ($[\text{M}+\text{H}]^+$), 297.5 ($[\text{M}+\text{H}]^+$); HRMS (+ESI) m/z calcd for $\text{C}_{12}\text{H}_{18}^{79}\text{BrN}_2\text{O}^+$ ($[\text{M}+\text{H}]^+$) 285.0597, found 285.0599 ($[\text{M}+\text{H}]^+$) and calcd for $\text{C}_{12}\text{H}_{18}^{81}\text{BrN}_2\text{O}^+$ ($[\text{M}+\text{H}]^+$) 287.0577, found 287.0560 ($[\text{M}+\text{H}]^+$); $[\alpha]_{\text{D}}^{25} = +9.9$ ($c = 1.0$, CHCl_3).

2-Bromo-5-((2S,3S)-3-(ethoxymethyl)-1-(4-methoxyphenyl)piperidin-2-yl)pyridine (171)



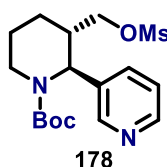
Procedure: Prepared as per procedure G, using EtBr **168**; Yield: 87%, a dark brown oil; IR (neat) 2962 (m), 1571 (s), 1408 (s), 1223 (s), 888 (s); ^1H NMR (400 MHz, CDCl_3) δ 8.16 (d, $J = 2.3$ Hz, 1H), 7.45 (dd, $J = 8.2, 2.3$ Hz, 1H), 7.24 (d, $J = 8.3$ Hz, 1H), 6.88 (d, $J = 8.7$ Hz, 2H), 6.64 (d, $J = 8.7$ Hz, 2H), 3.93 (d, $J = 9.3$ Hz, 1H), 3.68 (s, 3H), 3.33 – 3.25 (m, 2H), 3.26 – 3.18 (m, 1H), 3.12 (dd, $J = 9.4, 3.4$ Hz, 1H), 2.97 (dd, $J = 9.4, 5.1$ Hz, 1H), 2.86 – 2.71 (m, 1H), 2.01 – 1.91 (m, 1H), 1.89 – 1.75 (m, 2H), 1.64 – 1.52 (m, 2H), 1.12 (t, $J = 7.0$ Hz, 3H); ^{13}C NMR (101 MHz, CDCl_3) δ 155.93, 150.68, 145.54, 140.00, 138.57, 137.75, 127.68, 125.94 (2C), 114.12 (2C), 72.18, 66.63, 64.11, 57.52, 55.37, 44.57, 28.22, 25.90, 15.25; LRMS (+ESI) m/z 405.8 ($[\text{M}+\text{H}]^+$), 407.4 ($[\text{M}+\text{H}]^+$); HRMS (+ESI) m/z calcd for $\text{C}_{20}\text{H}_{26}^{79}\text{BrN}_2\text{O}_2^+$ ($[\text{M}+\text{H}]^+$) 405.1172, found 405.1172 ($[\text{M}+\text{H}]^+$) and calcd for $\text{C}_{20}\text{H}_{26}^{81}\text{BrN}_2\text{O}_2^+$ ($[\text{M}+\text{H}]^+$) 407.1152, found 407.1153 ($[\text{M}+\text{H}]^+$); $[\alpha]_{\text{D}}^{25} = +9.7$ ($c = 0.5$, CHCl_3).

2-Bromo-5-((2S,3S)-3-(ethoxymethyl)piperidin-2-yl)pyridine (174)



Procedure: Prepared as per procedure D; Yield: 62%, a red oil; IR (neat) 3333 (br), 2998 (s), 1570 (s), 1482 (s), 899 (s); ^1H NMR (400 MHz, CDCl_3) δ 8.33 (d, $J = 2.4$ Hz, 1H), 7.68 (dd, $J = 8.2, 2.5$ Hz, 1H), 7.45 (d, $J = 8.2$ Hz, 1H), 3.56 (d, $J = 10.1$ Hz, 1H), 3.29 – 3.18 (m, 2H), 3.16 – 3.09 (m, 1H), 3.05 (dd, $J = 9.4, 3.4$ Hz, 1H), 2.95 (dd, $J = 9.4, 5.3$ Hz, 1H), 2.80 – 2.70 (m, 1H), 2.00 – 1.91 (m, 1H), 1.81 – 1.68 (m, 4H, overlapping with NH brs), 1.54 – 1.42 (m, 1H), 1.06 (t, $J = 7.0$ Hz, 3H); ^{13}C NMR (101 MHz, CDCl_3) δ 150.05, 141.27, 138.07, 137.54, 128.14, 71.96, 66.57, 61.39, 47.23, 43.30, 28.77, 25.51, 15.17; LRMS (+ESI) m/z 299.6 ($[\text{M}+\text{H}]^+$), 301.2 ($[\text{M}+\text{H}]^+$); HRMS (+ESI) m/z calcd for $\text{C}_{13}\text{H}_{20}^{79}\text{BrN}_2\text{O}^+$ ($[\text{M}+\text{H}]^+$) 299.0754, found 299.0756 ($[\text{M}+\text{H}]^+$) and calcd for $\text{C}_{13}\text{H}_{20}^{81}\text{BrN}_2\text{O}^+$ ($[\text{M}+\text{H}]^+$) 301.0733, found 301.0736 ($[\text{M}+\text{H}]^+$); $[\alpha]_{\text{D}}^{25} = +15.1$ ($c = 1.0, \text{CHCl}_3$).

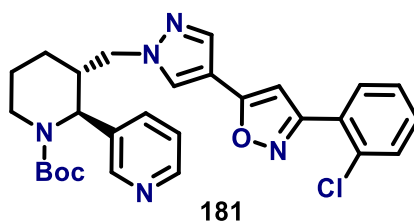
***tert*-Butyl (2*S*,3*S*)-3-(((methylsulfonyl)oxy)methyl)-2-(pyridin-3-yl)piperidine-1-carboxylate (178)**



Procedure: To a round bottom flask containing a stirring solution of piperidine **83** (1 mmol, 100 mg) in methanol (5 ml), TEA (3 mmol) and di-*tert*-butyl dicarbonate (1.1 mmol) was added. The reaction was stirred for 12 h at room temperature. The mixture was concentrated under reduced pressure, diluted with THF (5 ml) and stirred at 0 °C for 15 mins. To the stirring solution, methanesulfonyl chloride (1.2 mmol) was added dropwise. The reaction was warmed up to room temperature and stirred for 1 h. The mixture was neutralised with saturated NaHCO_3 solution, extracted with ethyl acetate (3 x 5 ml) and dried over Na_2SO_4 . The combined organic extract was concentrated under reduced pressure and the residue was purified by column chromatography (EtOAc:Hex, 1:5) to afford Boc-protected mesylated piperidine **178** (145 mg) as clear brown oil; Yield: 75%; IR (neat) 2961 (m), 2852 (w), 1687 (m), 1176 (s), 939 (s); ^1H NMR (400 MHz, CDCl_3) δ 8.54 (s, 2H), 7.56 (d, $J = 8.0$ Hz, 1H), 7.38 – 7.29 (m, 1H), 5.49 (s, 1H), 4.47 – 4.39 (m, 1H), 4.35 – 4.28 (m, 1H), 4.15 – 4.06 (m, 1H), 3.08 (s, 3H), 2.83 – 2.68 (m, 2H), 1.76 – 1.68 (m, 2H), 1.66 – 1.55 (m, 1H), 1.48 (s, 9H), 1.46 – 1.41 (m, 1H); ^{13}C NMR (101 MHz, CDCl_3) δ 162.91, 155.80, 148.30, 148.14, 134.84, 123.85, 80.91, 70.13, 52.09, 39.79, 37.62, 35.46, 28.48 (3C), 21.20, 20.50; LRMS

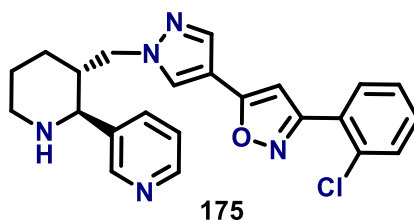
(+ESI) m/z 371.4 ($[M+H]^+$), 393.1 ($[M+Na]^+$); HRMS (+ESI) m/z calcd for $C_{17}H_{27}N_2O_5S^+$ ($[M+H]^+$) 371.1635, found 371.1637 ($[M+H]^+$). $[\alpha]_D^{25} = +4.1$ ($c = 0.5$, $CHCl_3$).

***tert*-Butyl (2*S*,3*R*)-3-((4-(3-(2-chlorophenyl)isoxazol-5-yl)-1*H*-pyrazol-1-yl)methyl)-2-(pyridin-3-yl)piperidine-1-carboxylate (181)**



Procedure: Prepared as per procedure H, using pyrazole **179**; Yield: 52%, a dark brown oil; IR (neat) 3130 (m), 2972 (m), 1690 (m), 1640 (s), 1479 (s), 930 (s); 1H NMR (400 MHz, $CDCl_3$) δ 8.53 – 8.45 (m, 2H), 7.93 (d, $J = 8.6$ Hz, 2H), 7.77 – 7.72 (m, 1H), 7.53 – 7.46 (m, 2H), 7.42 – 7.31 (m, 2H), 7.30 – 7.24 (m, 1H), 6.72 (s, 1H), 5.21 (s, 1H), 4.42 (dd, $J = 13.7, 8.8$ Hz, 1H), 4.34 (dd, $J = 13.8, 6.2$ Hz, 1H), 4.16 (d, $J = 13.3$ Hz, 1H), 3.18 – 3.09 (m, 1H), 2.82 – 2.73 (m, 1H), 1.77 – 1.63 (m, 2H), 1.58 – 1.49 (m, 2H), 1.48 (s, 9H); ^{13}C NMR (101 MHz, $CDCl_3$) δ 163.77, 161.33, 155.76, 148.37, 148.30, 138.19, 134.44, 134.24, 132.91, 130.96, 130.82, 130.40, 129.06, 128.36, 127.09, 123.50, 110.49, 99.73, 80.78, 53.78, 52.67, 39.66, 36.40, 28.37 (3C), 21.70, 20.21; LRMS (+ESI) m/z 520.9 ($[M+H]^+$); HRMS (+ESI) m/z calcd for $C_{28}H_{31}ClN_5O_3^+$ ($[M+H]^+$) 520.2110, found 520.2110 ($[M+H]^+$); $[\alpha]_D^{25} = +28.9$ ($c = 0.5$, $CHCl_3$).

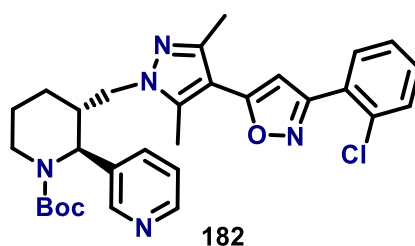
3-(2-Chlorophenyl)-5-(1-(((2*S*,3*R*)-2-(pyridin-3-yl)piperidin-3-yl)methyl)-1*H*-pyrazol-4-yl)isoxazole (175)



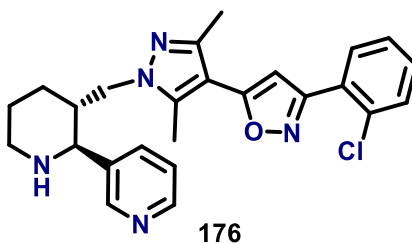
Procedure: Prepared as per procedure I; Yield: 74%, a pale-red oil; IR (neat) 3422 (br), 3084 (m), 2985 (m), 1640 (s), 1497 (s); 1H NMR (400 MHz, $CDCl_3$) δ 8.64 (d, $J = 1.6$ Hz, 1H), 8.54 (dd, $J = 4.7, 1.5$ Hz, 1H), 7.84 – 7.78 (m, 2H), 7.77 – 7.73 (m, 1H), 7.56 (s, 1H), 7.52 – 7.47 (m, 1H), 7.42 – 7.33 (m, 2H), 7.31 – 7.26 (m, 1H), 6.67 (s, 1H), 3.93 – 3.74 (m,

2H), 3.55 (d, $J = 10.2$ Hz, 1H), 3.18 – 3.09 (m, 1H), 2.81 – 2.71 (m, 1H), 2.42 – 2.28 (m, 1H), 1.81 – 1.64 (m, 3H), 1.30 – 1.20 (m, 1H), NH brs not observed; ^{13}C NMR (101 MHz, CDCl_3) δ 163.92, 161.48, 149.95, 149.84, 137.68, 136.89, 135.48, 133.07, 131.12, 130.97, 130.56, 128.59, 128.53, 127.24, 124.03, 110.62, 99.77, 63.38, 55.12, 47.06, 42.78, 29.10, 25.23; LRMS (+ESI) m/z 420.5 ($[\text{M}+\text{H}]^+$), 442.8 ($[\text{M}+\text{Na}]^+$); HRMS (+ESI) m/z calcd for $\text{C}_{23}\text{H}_{23}\text{ClN}_5\text{O}^+$ ($[\text{M}+\text{H}]^+$) 420.1586, found 420.1592 ($[\text{M}+\text{H}]^+$); $[\alpha]_{\text{D}}^{25} = +23.7$ ($c = 0.5$, CHCl_3).

***tert*-Butyl (2*S*,3*R*)-3-((4-(3-(2-chlorophenyl)isoxazol-5-yl)-3,5-dimethyl-1*H*-pyrazol-1-yl)methyl)-2-(pyridin-3-yl)piperidine-1-carboxylate (182)**



Procedure: Prepared as per procedure H, using pyrazole **180**; Yield: 57%, an orange oil; IR (neat) 3156 (m), 2949 (m), 1693 (m), 1488 (s), 891 (s); ^1H NMR (400 MHz, CDCl_3) δ 8.51 (s, 2H), 7.80 – 7.74 (m, 1H), 7.57 – 7.47 (m, 2H), 7.43 – 7.28 (m, 3H), 6.63 (s, 1H), 5.14 (s, 1H), 4.33 (dd, $J = 13.7, 8.6$ Hz, 1H), 4.23 – 4.14 (m, 1H), 4.08 (dd, $J = 13.6, 6.4$ Hz, 1H), 3.22 – 3.15 (m, 1H), 2.90 – 2.79 (m, 1H), 2.56 (s, 3H), 2.45 (s, 3H), 1.82 – 1.71 (m, 1H), 1.70 – 1.49 (m, 3H), 1.42 (s, 9H); ^{13}C NMR (101 MHz, CDCl_3) δ 165.58, 161.14, 155.95, 148.47, 148.36, 147.08, 139.45, 134.44, 134.38, 133.11, 131.13, 130.88, 130.57, 128.77, 127.24, 123.60, 107.10, 100.62, 80.77, 53.09, 49.79, 40.11, 36.67, 28.47 (3C), 21.75, 20.44, 13.92, 11.28; LRMS (+ESI) m/z 548.4 ($[\text{M}+\text{H}]^+$); HRMS (+ESI) m/z calcd for $\text{C}_{30}\text{H}_{35}\text{ClN}_5\text{O}_3^+$ ($[\text{M}+\text{H}]^+$) 548.2423, found 548.2422 ($[\text{M}+\text{H}]^+$); $[\alpha]_{\text{D}}^{25} = +36.1$ ($c = 0.5$, CHCl_3).

3-(2-Chlorophenyl)-5-(3,5-dimethyl-1-(((2*S*,3*R*)-2-(pyridin-3-yl)piperidin-3-yl)methyl)-1H-pyrazol-4-yl)isoxazole (176)

Procedure: Prepared as per procedure I; Yield: 76%, a bright orange oil; IR (neat) 3372 (br), 3139 (m), 2920 (m), 1643 (s), 1483 (s); ^1H NMR (400 MHz, CDCl_3) δ 8.65 (s, 1H), 8.53 (d, $J = 3.8$ Hz, 1H), 7.81 (d, $J = 7.9$ Hz, 1H), 7.78 – 7.72 (m, 1H), 7.54 – 7.47 (m, 1H), 7.43 – 7.33 (m, 2H), 7.27 (s, 1H), 6.55 (s, 1H), 3.76 – 3.61 (m, 3H), 3.12 (d, $J = 11.9$ Hz, 1H), 2.82 – 2.71 (m, 1H), 2.49 – 2.41 (m, 1H), 2.37 (s, 3H), 2.30 (s, 3H), 1.84 – 1.66 (m, 3H), 1.32 – 1.22 (m, 1H), NH brs not observed; ^{13}C NMR (101 MHz, CDCl_3) δ 165.32, 160.97, 149.88, 149.77, 146.28, 138.58, 135.38, 135.32, 132.93, 130.97, 130.73, 130.42, 128.59, 127.09, 123.66, 106.95, 100.32, 63.01, 50.82, 46.52, 41.75, 28.56, 24.43, 13.62, 11.09; LRMS (+ESI) m/z 448.9 ($[\text{M}+\text{H}]^+$), 470.2 ($[\text{M}+\text{Na}]^+$); HRMS (+ESI) m/z calcd for $\text{C}_{25}\text{H}_{27}\text{ClN}_5\text{O}^+$ ($[\text{M}+\text{H}]^+$) 448.1899, found 448.1900 ($[\text{M}+\text{H}]^+$); $[\alpha]_{\text{D}}^{25} = +19.8$ ($c = 0.5$, CHCl_3).

REFERENCES

1. Hurst, R.; Rollema, H.; Bertrand, D., Nicotinic acetylcholine receptors: from basic science to therapeutics. *Pharmacology & therapeutics* **2013**, *137*, 22-54.
2. Unwin, N., Refined structure of the nicotinic acetylcholine receptor at 4 Å resolution. *Journal of molecular biology* **2005**, *346*, 967-989.
3. Changeux, J.-P., The nicotinic acetylcholine receptor: the founding father of the pentameric ligand-gated ion channel superfamily. *Journal of Biological Chemistry* **2012**, *287*, 40207-40215.
4. Zouridakis, M.; Zisimopoulou, P.; Poulas, K.; Tzartos, S. J., Recent advances in understanding the structure of nicotinic acetylcholine receptors. *IUBMB life* **2009**, *61*, 407-423.
5. Chatzidaki, A.; Millar, N. S., Allosteric modulation of nicotinic acetylcholine receptors. *Biochemical pharmacology* **2015**, *97*, 408-417.
6. Taly, A.; Corringer, P.-J.; Guedin, D.; Lestage, P.; Changeux, J.-P., Nicotinic receptors: allosteric transitions and therapeutic targets in the nervous system. *Nature reviews Drug discovery* **2009**, *8*, 733-750.
7. Jensen, A. A.; Frølund, B.; Liljefors, T.; Krogsgaard-Larsen, P., Neuronal nicotinic acetylcholine receptors: structural revelations, target identifications, and therapeutic inspirations. *Journal of medicinal chemistry* **2005**, *48*, 4705-4745.
8. Wonnacott, S.; Barik, J., Nicotinic ACh receptors. Tocris Bioscience Scientific Review Series 2007.
9. Fambrough, D. M.; Drachman, D. B.; Satyamurti, S., Neuromuscular junction in myasthenia gravis: decreased acetylcholine receptors. *Science* **1973**, *182*, 293-295.
10. Janhunen, S.; Ahtee, L., Differential nicotinic regulation of the nigrostriatal and mesolimbic dopaminergic pathways: implications for drug development. *Neuroscience & Biobehavioral Reviews* **2007**, *31*, 287-314.
11. Livingstone, P. D.; Srinivasan, J.; Kew, J. N.; Dawson, L. A.; Gotti, C.; Moretti, M.; Shoaib, M.; Wonnacott, S., $\alpha 7$ and non- $\alpha 7$ nicotinic acetylcholine receptors modulate dopamine release in vitro and in vivo in the rat prefrontal cortex. *European Journal of Neuroscience* **2009**, *29*, 539-550.
12. Whitehouse, P. J.; Martino, A. M.; Antuono, P. G.; Lowenstein, P. R.; Coyle, J. T.; Price, D. L.; Kellar, K. J., Nicotinic acetylcholine binding sites in Alzheimer's disease. *Brain research* **1986**, *371*, 146-151.
13. Marubio, L. M.; del Mar Arroyo-Jimenez, M.; Cordero-Erausquin, M.; Léna, C.; Le Novère, N.; de Kerchove d'Exaerde, A.; Huchet, M.; Damaj, M. I.; Changeux, J.-P., Reduced antinociception in mice lacking neuronal nicotinic receptor subunits. *Nature* **1999**, *398*, 805-810.

14. Janowsky, D.; Davis, J.; El-Yousef, M. K.; Sekerke, H. J., A cholinergic-adrenergic hypothesis of mania and depression. *The Lancet* **1972**, *300*, 632-635.
15. Picciotto, M. R.; Zoli, M.; Rimondini, R.; Léna, C.; Marubio, L. M.; Pich, E. M.; Fuxe, K.; Changeux, J.-P., Acetylcholine receptors containing the $\beta 2$ subunit are involved in the reinforcing properties of nicotine. *Nature* **1998**, *391*, 173-177.
16. Albuquerque, E. X.; Pereira, E. F.; Alkondon, M.; Rogers, S. W., Mammalian nicotinic acetylcholine receptors: from structure to function. *Physiological reviews* **2009**, *89*, 73-120.
17. Celie, P. H.; van Rossum-Fikkert, S. E.; van Dijk, W. J.; Brejc, K.; Smit, A. B.; Sixma, T. K., Nicotine and carbamylcholine binding to nicotinic acetylcholine receptors as studied in AChBP crystal structures. *Neuron* **2004**, *41*, 907-914.
18. Brejc, K.; van Dijk, W. J.; Klaassen, R. V.; Schuurmans, M.; van der Oost, J.; Smit, A. B.; Sixma, T. K., Crystal structure of an ACh-binding protein reveals the ligand-binding domain of nicotinic receptors. *Nature* **2001**, *411*, 269-276.
19. Karlin, A., Emerging structure of the nicotinic acetylcholine receptors. *Nature Reviews Neuroscience* **2002**, *3*, 102-114.
20. Sine, S. M.; Engel, A. G., Recent advances in Cys-loop receptor structure and function. *Nature* **2006**, *440*, 448-455.
21. Hansen, S. B.; Sulzenbacher, G.; Huxford, T.; Marchot, P.; Taylor, P.; Bourne, Y., Structures of Aplysia AChBP complexes with nicotinic agonists and antagonists reveal distinctive binding interfaces and conformations. *The EMBO journal* **2005**, *24*, 3635-3646.
22. Xiu, X.; Puskar, N. L.; Shanata, J. A.; Lester, H. A.; Dougherty, D. A., Nicotine binding to brain receptors requires a strong cation- π interaction. *Nature* **2009**, *458*, 534-537.
23. Blum, A. P.; Lester, H. A.; Dougherty, D. A., Nicotinic pharmacophore: the pyridine N of nicotine and carbonyl of acetylcholine hydrogen bond across a subunit interface to a backbone NH. *Proceedings of the National Academy of Sciences* **2010**, *107*, 13206-13211.
24. Sine, S. M.; Claudio, T.; Sigworth, F. J., Activation of Torpedo acetylcholine receptors expressed in mouse fibroblasts. Single channel current kinetics reveal distinct agonist binding affinities. *The Journal of General Physiology* **1990**, *96*, 395-437.
25. Colquhoun, D.; Sakmann, B., Fluctuations in the microsecond time range of the current through single acetylcholine receptor ion channels. *Nature* **1981**, *294*, 464-466.
26. Chang, Y.-c.; Wu, W.; Zhang, J.-l.; Huang, Y., Allosteric activation mechanism of the cys-loop receptors. *Acta Pharmacologica Sinica* **2009**, *30*, 663-672.
27. Taly, A.; Corringer, P.-J.; Grutter, T.; de Carvalho, L. P.; Karplus, M.; Changeux, J.-P., Implications of the quaternary twist allosteric model for the physiology and pathology of nicotinic acetylcholine receptors. *Proceedings of the National Academy of Sciences* **2006**, *103*, 16965-16970.

28. Taly, A.; Delarue, M.; Grutter, T.; Nilges, M.; Le Novere, N.; Corringer, P.-J.; Changeux, J.-P., Normal mode analysis suggests a quaternary twist model for the nicotinic receptor gating mechanism. *Biophysical journal* **2005**, *88*, 3954-3965.
29. Hilf, R. J.; Dutzler, R., X-ray structure of a prokaryotic pentameric ligand-gated ion channel. *Nature* **2008**, *452*, 375-379.
30. Bocquet, N.; Nury, H.; Baaden, M.; Le Poupon, C.; Changeux, J.-P.; Delarue, M.; Corringer, P.-J., X-ray structure of a pentameric ligand-gated ion channel in an apparently open conformation. *Nature* **2009**, *457*, 111-114.
31. Hilf, R. J.; Dutzler, R., Structure of a potentially open state of a proton-activated pentameric ligand-gated ion channel. *Nature* **2009**, *457*, 115-118.
32. Hales, T. G.; Dunlop, J. I.; Deeb, T. Z.; Carland, J. E.; Kelley, S. P.; Lambert, J. J.; Peters, J. A., Common determinants of single channel conductance within the large cytoplasmic loop of 5-hydroxytryptamine type 3 and $\alpha 4\beta 2$ nicotinic acetylcholine receptors. *Journal of Biological Chemistry* **2006**, *281*, 8062-8071.
33. Kalamida, D.; Poulas, K.; Avramopoulou, V.; Fostieri, E.; Lagoumintzis, G.; Lazaridis, K.; Sideri, A.; Zouridakis, M.; Tzartos, S. J., Muscle and neuronal nicotinic acetylcholine receptors. *The FEBS journal* **2007**, *274*, 3799-3845.
34. Le Novere, N.; Corringer, P. J.; Changeux, J. P., The diversity of subunit composition in nAChRs: evolutionary origins, physiologic and pharmacologic consequences. *Journal of neurobiology* **2002**, *53*, 447-456.
35. Monod, J.; Wyman, J.; Changeux, J.-P., On the nature of allosteric transitions: a plausible model. *J Mol Biol* **1965**, *12*, 88-118.
36. Changeux, J.-P.; Edelstein, S. J., Allosteric receptors after 30 years. *Neuron* **1998**, *21*, 959-980.
37. Giniatullin, R.; Nistri, A.; Yakel, J. L., Desensitization of nicotinic ACh receptors: shaping cholinergic signaling. *Trends in neurosciences* **2005**, *28*, 371-378.
38. Quick, M. W.; Lester, R. A., Desensitization of neuronal nicotinic receptors. *Journal of neurobiology* **2002**, *53*, 457-478.
39. Daly, J. W., Nicotinic agonists, antagonists, and modulators from natural sources. *Cellular and molecular neurobiology* **2005**, *25*, 513-552.
40. Sharples, C. G.; Wonnacott, S., Neuronal nicotinic receptors. *Tocris reviews* **2001**, *19*, 1-12.
41. Beers, W.; Reich, E., Structure and activity of acetylcholine. *Nature* **1970**, *228*, 917-922.
42. Nicolotti, O.; Pellegrini-Calace, M.; Carrieri, A.; Altomare, C.; Centeno, N. B.; Sanz, F.; Carotti, A., Neuronal nicotinic receptor agonists: a multi-approach development of the pharmacophore. *Journal of computer-aided molecular design* **2001**, *15*, 859-872.

43. Whiteaker, P.; Sharples, C. G.; Wonnacott, S., Agonist-induced up-regulation of $\alpha 4\beta 2$ nicotinic acetylcholine receptors in M10 cells: pharmacological and spatial definition. *Molecular pharmacology* **1998**, *53*, 950-962.
44. Verbitsky, M.; Rothlin, C. V.; Katz, E.; Elgoyhen, A. B., Mixed nicotinic–muscarinic properties of the $\alpha 9$ nicotinic cholinergic receptor. *Neuropharmacology* **2000**, *39*, 2515-2524.
45. Millar, N. S.; Harkness, P. C., Assembly and trafficking of nicotinic acetylcholine receptors. *Molecular membrane biology* **2008**, *25*, 279-292.
46. Coe, J. W.; Vetelino, M. G.; Bashore, C. G.; Wirtz, M. C.; Brooks, P. R.; Arnold, E. P.; Lebel, L. A.; Fox, C. B.; Sands, S. B.; Davis, T. I., In pursuit of $\alpha 4\beta 2$ nicotinic receptor partial agonists for smoking cessation: Carbon analogs of (–)-cytisine. *Bioorganic & medicinal chemistry letters* **2005**, *15*, 2974-2979.
47. Mihalak, K. B.; Carroll, F. I.; Luetje, C. W., Varenicline is a partial agonist at $\alpha 4\beta 2$ and a full agonist at $\alpha 7$ neuronal nicotinic receptors. *Molecular pharmacology* **2006**, *70*, 801-805.
48. Garrison, G. D.; Dugan, S. E., Varenicline: a first-line treatment option for smoking cessation. *Clinical therapeutics* **2009**, *31*, 463-491.
49. Gerzanich, V.; Peng, X.; Wang, F.; Wells, G.; Anand, R.; Fletcher, S.; Lindstrom, J., Comparative pharmacology of epibatidine: a potent agonist for neuronal nicotinic acetylcholine receptors. *Molecular Pharmacology* **1995**, *48*, 774-782.
50. Dwoskin, L. P.; Crooks, P. A., Competitive neuronal nicotinic receptor antagonists: a new direction for drug discovery. *Journal of Pharmacology and Experimental Therapeutics* **2001**, *298*, 395-402.
51. Bertrand, D.; Ballivet, M.; Rungger, D., Activation and blocking of neuronal nicotinic acetylcholine receptor reconstituted in *Xenopus* oocytes. *Proceedings of the National Academy of Sciences* **1990**, *87*, 1993-1997.
52. Peng, C.; Kimbrell, M. R.; Tian, C.; Pack, T. F.; Crooks, P. A.; Fifer, E. K.; Papke, R. L., Multiple modes of $\alpha 7$ nAChR noncompetitive antagonism of control agonist-evoked and allosterically enhanced currents. *Molecular pharmacology* **2013**, *84*, 459-475.
53. Alkondon, M.; Pereira, E.; Wonnacott, S.; Albuquerque, E. X., Blockade of nicotinic currents in hippocampal neurons defines methyllycaconitine as a potent and specific receptor antagonist. *Molecular pharmacology* **1992**, *41*, 802-808.
54. Quek, G. X.; Lin, D.; Halliday, J. I.; Absalom, N.; Ambrus, J. I.; Thompson, A. J.; Lochner, M.; Lummis, S. C.; McLeod, M. D.; Chebib, M., Identifying the binding site of novel methyllycaconitine (MLA) analogs at $\alpha 4\beta 2$ nicotinic acetylcholine receptors. *ACS chemical neuroscience* **2010**, *1*, 796-809.
55. Arias, H. R.; Rosenberg, A.; Targowska-Duda, K. M.; Feuerbach, D.; Jozwiak, K.; Moaddel, R.; Wainer, I. W., Tricyclic antidepressants and mecamylamine bind to different sites in the human $\alpha 4\beta 2$ nicotinic receptor ion channel. *The international journal of biochemistry & cell biology* **2010**, *42*, 1007-1018.

56. Uteshev, V. V., The therapeutic promise of positive allosteric modulation of nicotinic receptors. *European journal of pharmacology* **2014**, *727*, 181-185.
57. Gill-Thind, J. K.; Dhankher, P.; D'Oyley, J. M.; Sheppard, T. D.; Millar, N. S., Structurally similar allosteric modulators of $\alpha 7$ nicotinic acetylcholine receptors exhibit five distinct pharmacological effects. *Journal of Biological Chemistry* **2015**, *290*, 3552-3562.
58. Williams, D. K.; Wang, J.; Papke, R. L., Positive allosteric modulators as an approach to nicotinic acetylcholine receptor-targeted therapeutics: advantages and limitations. *Biochemical pharmacology* **2011**, *82*, 915-930.
59. Sala, F.; Mulet, J.; Reddy, K. P.; Bernal, J. A.; Wikman, P.; Valor, L. M.; Peters, L.; König, G. M.; Criado, M.; Sala, S., Potentiation of human $\alpha 4\beta 2$ neuronal nicotinic receptors by a *Flustra foliacea* metabolite. *Neuroscience letters* **2005**, *373*, 144-149.
60. Timmermann, D.; Sandager-Nielsen, K.; Dyhring, T.; Smith, M.; Jacobsen, A. M.; Nielsen, E.; Grunnet, M.; Christensen, J.; Peters, D.; Kohlhaas, K., Augmentation of cognitive function by NS9283, a stoichiometry-dependent positive allosteric modulator of $\alpha 2$ -and $\alpha 4$ -containing nicotinic acetylcholine receptors. *British journal of pharmacology* **2012**, *167*, 164-182.
61. Morales-Perez, C. L.; Noviello, C. M.; Hibbs, R. E., X-ray structure of the human $\alpha 4\beta 2$ nicotinic receptor. *Nature* **2016**, *538*, 411-415.
62. Miller, P. S.; Aricescu, A. R., Crystal structure of a human GABA A receptor. *Nature* **2014**, *512*, 270-275.
63. Harpsøe, K.; Ahring, P. K.; Christensen, J. K.; Jensen, M. L.; Peters, D.; Balle, T., Unraveling the high- and low-sensitivity agonist responses of nicotinic acetylcholine receptors. *Journal of Neuroscience* **2011**, *31*, 10759-10766.
64. Nelson, M. E.; Kuryatov, A.; Choi, C. H.; Zhou, Y.; Lindstrom, J., Alternate stoichiometries of $\alpha 4\beta 2$ nicotinic acetylcholine receptors. *Molecular pharmacology* **2003**, *63*, 332-341.
65. Anand, R.; Conroy, W.; Schoepfer, R.; Whiting, P.; Lindstrom, J., Neuronal nicotinic acetylcholine receptors expressed in *Xenopus* oocytes have a pentameric quaternary structure. *Journal of Biological Chemistry* **1991**, *266*, 11192-11198.
66. Cooper, E.; Couturier, S.; Ballivet, M., Pentameric structure and subunit stoichiometry of a neuronal nicotinic acetylcholine receptor. *Nature* **1991**, *350*, 235-238.
67. Zwart, R.; Vijverberg, H. P., Four Pharmacologically Distinct Subtypes of $\alpha 4\beta 2$ Nicotinic Acetylcholine Receptor Expressed in *Xenopus laevis* Oocytes. *Molecular pharmacology* **1998**, *54*, 1124-1131.
68. Kuryatov, A.; Gerzanich, V.; Nelson, M.; Olale, F.; Lindstrom, J., Mutation causing autosomal dominant nocturnal frontal lobe epilepsy alters Ca^{2+} permeability, conductance, and gating of human $\alpha 4\beta 2$ nicotinic acetylcholine receptors. *Journal of Neuroscience* **1997**, *17*, 9035-9047.

69. Buisson, B.; Bertrand, D., Chronic exposure to nicotine upregulates the human $\alpha 4\beta 2$ nicotinic acetylcholine receptor function. *Journal of Neuroscience* **2001**, *21*, 1819-1829.
70. Mazzaferro, S.; Benallegue, N.; Carbone, A.; Gasparri, F.; Vijayan, R.; Biggin, P. C.; Moroni, M.; Bermudez, I., Additional acetylcholine (ACh) binding site at $\alpha 4/\alpha 4$ interface of ($\alpha 4\beta 2$) $2\alpha 4$ nicotinic receptor influences agonist sensitivity. *Journal of Biological Chemistry* **2011**, *286*, 31043-31054.
71. Carbone, A. L.; Moroni, M.; Groot-Kormelink, P. J.; Bermudez, I., Pentameric concatenated ($\alpha 4$) $2(\beta 2)$ 3 and ($\alpha 4$) $3(\beta 2)$ 2 nicotinic acetylcholine receptors: subunit arrangement determines functional expression. *British journal of pharmacology* **2009**, *156*, 970-981.
72. Walsh, R. M.; Roh, S.-H.; Gharpure, A.; Morales-Perez, C. L.; Teng, J.; Hibbs, R. E., Structural principles of distinct assemblies of the human $\alpha 4\beta 2$ nicotinic receptor. *Nature* **2018**, *557*, 261-265.
73. Shafae, N.; Houg, M.; Truong, A.; Viseshakul, N.; Figl, A.; Sandhu, S.; Forsayeth, J. R.; Dwoskin, L. P.; Crooks, P. A.; Cohen, B. N., Pharmacological similarities between native brain and heterologously expressed $\alpha 4\beta 2$ nicotinic receptors. *British journal of pharmacology* **1999**, *128*, 1291-1299.
74. Lee, C.-H.; Zhu, C.; Malysz, J.; Campbell, T.; Shaughnessy, T.; Honore, P.; Polakowski, J.; Gopalakrishnan, M., $\alpha 4\beta 2$ neuronal nicotinic receptor positive allosteric modulation: an approach for improving the therapeutic index of $\alpha 4\beta 2$ nAChR agonists in pain. *Biochemical pharmacology* **2011**, *82*, 959-966.
75. Zhu, C. Z.; Chin, C.-I.; Rustay, N. R.; Zhong, C.; Mikusa, J.; Chandran, P.; Salyers, A.; Gomez, E.; Simler, G.; Lewis, L. G., Potentiation of analgesic efficacy but not side effects: co-administration of an $\alpha 4\beta 2$ neuronal nicotinic acetylcholine receptor agonist and its positive allosteric modulator in experimental models of pain in rats. *Biochemical pharmacology* **2011**, *82*, 967-976.
76. Grupe, M.; Grunnet, M.; Laursen, B.; Bastlund, J. F., Neuropharmacological modulation of the P3-like event-related potential in a rat two-tone auditory discrimination task with modafinil and NS9283, a positive allosteric modulator of $\alpha 4\beta 2$ nAChRs. *Neuropharmacology* **2014**, *79*, 444-455.
77. Liu, X., Positive allosteric modulation of $\alpha 4\beta 2$ nicotinic acetylcholine receptors as a new approach to smoking reduction: evidence from a rat model of nicotine self-administration. *Psychopharmacology* **2013**, *230*, 203-213.
78. Maurer, J. J.; Sandager-Nielsen, K.; Schmidt, H. D., Attenuation of nicotine taking and seeking in rats by the stoichiometry-selective $\alpha 4\beta 2$ nicotinic acetylcholine receptor positive allosteric modulator NS9283. *Psychopharmacology* **2017**, *234*, 475-484.
79. Mohler, E. G.; Franklin, S. R.; Rueter, L. E., Discriminative-stimulus effects of NS9283, a nicotinic $\alpha 4\beta 2^*$ positive allosteric modulator, in nicotine-discriminating rats. *Psychopharmacology* **2014**, *231*, 67-74.

80. Grupe, M.; Jensen, A. A.; Ahring, P. K.; Christensen, J. K.; Grunnet, M., Unravelling the mechanism of action of NS9283, a positive allosteric modulator of $(\alpha 4) 3 (\beta 2) 2$ nicotinic ACh receptors. *British journal of pharmacology* **2013**, *168*, 2000-2010.
81. Weltzin, M. M.; Schulte, M. K., Pharmacological characterization of the allosteric modulator desformylfluorobromine and its interaction with $\alpha 4\beta 2$ neuronal nicotinic acetylcholine receptor orthosteric ligands. *Journal of Pharmacology and Experimental Therapeutics* **2010**, *334*, 917-926.
82. Malysz, J.; Grønlien, J. H.; Anderson, D. J.; Håkerud, M.; Thorin-Hagene, K.; Ween, H.; Wetterstrand, C.; Briggs, C. A.; Faghieh, R.; Bunnelle, W. H., In vitro pharmacological characterization of a novel allosteric modulator of $\alpha 7$ neuronal acetylcholine receptor, 4-(5-(4-chlorophenyl)-2-methyl-3-propionyl-1H-pyrrol-1-yl) benzenesulfonamide (A-867744), exhibiting unique pharmacological profile. *Journal of Pharmacology and Experimental Therapeutics* **2009**, *330*, 257-267.
83. Olsen, J. A.; Ahring, P. K.; Kastrup, J. S.; Gajhede, M.; Balle, T., Structural and functional studies of the modulator NS9283 reveal agonist-like mechanism of action at $\alpha 4\beta 2$ nicotinic acetylcholine receptors. *Journal of Biological Chemistry* **2014**, *289*, 24911-24921.
84. Wang, J.; Kuryatov, A.; Sriram, A.; Jin, Z.; Kamenecka, T. M.; Kenny, P. J.; Lindstrom, J., An accessory agonist binding site promotes activation of $\alpha 4\beta 2^*$ nicotinic acetylcholine receptors. *Journal of Biological Chemistry* **2015**, *290*, 13907-13918.
85. Nielsen, S. F.; Nielsen, E. Ø.; Olsen, G. M.; Liljefors, T.; Peters, D., Novel potent ligands for the central nicotinic acetylcholine receptor: synthesis, receptor binding, and 3D-QSAR analysis. *Journal of medicinal chemistry* **2000**, *43*, 2217-2226.
86. Rohde, L. A. H.; Ahring, P. K.; Jensen, M. L.; Nielsen, E. Ø.; Peters, D.; Helgstrand, C.; Krintel, C.; Harpsøe, K.; Gajhede, M.; Kastrup, J. S., Intersubunit Bridge Formation Governs Agonist Efficacy at Nicotinic Acetylcholine $\alpha 4\beta 2$ Receptors UNIQUE ROLE OF HALOGEN BONDING REVEALED. *Journal of Biological Chemistry* **2012**, *287*, 4248-4259.
87. Ahring, P. K.; Olsen, J. A.; Nielsen, E. Ø.; Peters, D.; Pedersen, M. H.; Rohde, L. A.; Kastrup, J. S.; Shahsavari, A.; Indurthi, D. C.; Chebib, M., Engineered $\alpha 4\beta 2$ nicotinic acetylcholine receptors as models for measuring agonist binding and effect at the orthosteric low-affinity $\alpha 4-\alpha 4$ interface. *Neuropharmacology* **2015**, *92*, 135-145.
88. Shahsavari, A.; Ahring, P. K.; Olsen, J. A.; Krintel, C.; Kastrup, J. S.; Balle, T.; Gajhede, M., Acetylcholine-binding protein engineered to mimic the $\alpha 4-\alpha 4$ binding pocket in $\alpha 4\beta 2$ nicotinic acetylcholine receptors reveals interface specific interactions important for binding and activity. *Molecular pharmacology* **2015**, *88*, 697-707.
89. Post, M. R.; Tender, G. S.; Lester, H. A.; Dougherty, D. A., Secondary ammonium agonists make dual cation- π interactions in $\alpha 4\beta 2$ nicotinic receptors. *ENeuro* **2017**, *4*.
90. Audouze, K.; Nielsen, E. Ø.; Olsen, G. M.; Ahring, P.; Jørgensen, T. D.; Peters, D.; Liljefors, T.; Balle, T., New ligands with affinity for the $\alpha 4\beta 2$ subtype of nicotinic acetylcholine receptors. Synthesis, receptor binding, and 3D-QSAR modeling. *Journal of medicinal chemistry* **2006**, *49*, 3159-3171.

91. Paul, F.; Patt, J.; Hartwig, J. F., Palladium-catalyzed formation of carbon-nitrogen bonds. Reaction intermediates and catalyst improvements in the hetero cross-coupling of aryl halides and tin amides. *Journal of the American Chemical Society* **1994**, *116*, 5969-5970.
92. Guram, A. S.; Buchwald, S. L., Palladium-catalyzed aromatic aminations with in situ generated aminostannanes. *Journal of the American Chemical Society* **1994**, *116*, 7901-7902.
93. Guram, A. S.; Rennels, R. A.; Buchwald, S. L., A simple catalytic method for the conversion of aryl bromides to arylamines. *Angewandte Chemie International Edition in English* **1995**, *34*, 1348-1350.
94. Surry, D. S.; Buchwald, S. L., Dialkylbiaryl phosphines in Pd-catalyzed amination: a user's guide. *Chemical Science* **2011**, *2*, 27-50.
95. Kurti, L.; Czako, B., *Strategic applications of named reactions in organic synthesis*. Elsevier2005.
96. Huang, X.; Anderson, K. W.; Zim, D.; Jiang, L.; Klapars, A.; Buchwald, S. L., Expanding Pd-catalyzed C–N bond-forming processes: the first amidation of aryl sulfonates, aqueous amination, and complementarity with Cu-catalyzed reactions. *Journal of the American Chemical Society* **2003**, *125*, 6653-6655.
97. Jo, Y. S.; van der Vlies, A. J.; Gantz, J.; Thacher, T. N.; Antonijevic, S.; Cavadini, S.; Demurtas, D.; Stergiopoulos, N.; Hubbell, J. A., Micelles for delivery of nitric oxide. *Journal of the American Chemical Society* **2009**, *131*, 14413-14418.
98. Bartoli, S.; Cipollone, A.; Squarcia, A.; Madami, A.; Fattori, D., Electrophilic bromination of meta-substituted anilines with N-bromosuccinimide: Regioselectivity and solvent effect. *Synthesis* **2009**, *2009*, 1305-1308.
99. Breman, A. C.; Ruiz-Olalla, A.; van Maarseveen, J. H.; Ingemann, S.; Hiemstra, H., Synthesis of Quinuclidines by Intramolecular Silver-Catalysed Amine Additions to Alkynes. *European Journal of Organic Chemistry* **2014**, *2014*, 7413-7425.
100. Suzuki, A., Cross coupling reactions in organic synthesis themed issue.
101. Moon, K. S.; Kim, H. J.; Lee, E.; Lee, M., Self-Assembly of T-Shaped Aromatic Amphiphiles into Stimulus-Responsive Nanofibers. *Angewandte Chemie International Edition* **2007**, *46*, 6807-6810.
102. Castanet, A.-S.; Colobert, F.; Broutin, P.-E., Mild and regioselective iodination of electron-rich aromatics with N-iodosuccinimide and catalytic trifluoroacetic acid. *Tetrahedron letters* **2002**, *43*, 5047-5048.
103. Singh, R.; Just, G., Rates and regioselectivities of the palladium-catalyzed ethynylation of substituted bromo- and dibromobenzenes. *The Journal of Organic Chemistry* **1989**, *54*, 4453-4457.
104. Frost; Bunnelle, W. H.; Tietje, K. R.; Anderson, D. J.; Rueter, L. E.; Curzon, P.; Surowy, C. S.; Ji, J.; Daanen, J. F.; Kohlhaas, K. L., Synthesis and structure–activity

relationships of 3, 8-diazabicyclo [4.2. 0] octane ligands, potent nicotinic acetylcholine receptor agonists. *Journal of medicinal chemistry* **2006**, *49*, 7843-7853.

105. Ji, J.; Schrimpf, M. R.; Sippy, K. B.; Bunnelle, W. H.; Li, T.; Anderson, D. J.; Faltynek, C.; Surowy, C. S.; Dyhring, T.; Ahring, P. K., Synthesis and Structure– Activity Relationship Studies of 3, 6-Diazabicyclo [3.2. 0] heptanes as Novel $\alpha 4\beta 2$ Nicotinic Acetylcholine Receptor Selective Agonists. *Journal of medicinal chemistry* **2007**, *50*, 5493-5508.

106. Sippy, K. B.; Anderson, D. J.; Bunnelle, W. H.; Hutchins, C. W.; Schrimpf, M. R., Preparation and characterization of N-(3-pyridinyl) spirocyclic diamines as ligands for nicotinic acetylcholine receptors. *Bioorganic & medicinal chemistry letters* **2009**, *19*, 1682-1685.

107. Tosco, P.; Ahring, P. K.; Dyhring, T.; Peters, D.; Harpsøe, K.; Liljefors, T.; Balle, T., Complementary three-dimensional quantitative structure– activity relationship modeling of binding affinity and functional potency: a study on $\alpha 4\beta 2$ nicotinic ligands. *Journal of medicinal chemistry* **2009**, *52*, 2311-2316.

108. Weltzin, M. M.; George, A. A.; Lukas, R. J.; Whiteaker, P., Distinctive single-channel properties of $\alpha 4\beta 2$ -nicotinic acetylcholine receptor isoforms. *PloS one* **2019**, *14*.

109. Dallanoce, C.; Magrone, P.; Matera, C.; Frigerio, F.; Grazioso, G.; De Amici, M.; Fucile, S.; Piccari, V.; Frydenvang, K.; Pucci, L., Design, Synthesis, and Pharmacological Characterization of Novel Spirocyclic Quinuclidinyl- $\Delta 2$ -Isoxazoline Derivatives as Potent and Selective Agonists of $\alpha 7$ Nicotinic Acetylcholine Receptors. *ChemMedChem* **2011**, *6*, 889-903.

110. Rucktooa, P.; Haseler, C. A.; van Elk, R.; Smit, A. B.; Gallagher, T.; Sixma, T. K., Structural characterization of binding mode of smoking cessation drugs to nicotinic acetylcholine receptors through study of ligand complexes with acetylcholine-binding protein. *Journal of Biological Chemistry* **2012**, *287*, 23283-23293.

111. Hansen, S. B.; Taylor, P., Galanthamine and non-competitive inhibitor binding to ACh-binding protein: evidence for a binding site on non- α -subunit interfaces of heteromeric neuronal nicotinic receptors. *Journal of molecular biology* **2007**, *369*, 895-901.

112. Ihara, M.; Okajima, T.; Yamashita, A.; Oda, T.; Hirata, K.; Nishiwaki, H.; Morimoto, T.; Akamatsu, M.; Ashikawa, Y.; Kuroda, S. i., Crystal structures of *Lymnaea stagnalis* AChBP in complex with neonicotinoid insecticides imidacloprid and clothianidin. *Invertebrate Neuroscience* **2008**, *8*, 71-81.

113. Zhang, H.; Tückmantel, W.; Eaton, J. B.; Yuen, P.-w.; Yu, L.-F.; Bajjuri, K. M.; Fedolak, A.; Wang, D.; Ghavami, A.; Caldarone, B., Chemistry and behavioral studies identify chiral cyclopropanes as selective $\alpha 4\beta 2$ -nicotinic acetylcholine receptor partial agonists exhibiting an antidepressant profile. *Journal of medicinal chemistry* **2012**, *55*, 717-724.

114. Hibbs, R. E.; Sulzenbacher, G.; Shi, J.; Talley, T. T.; Conrod, S.; Kem, W. R.; Taylor, P.; Marchot, P.; Bourne, Y., Structural determinants for interaction of partial

agonists with acetylcholine binding protein and neuronal $\alpha 7$ nicotinic acetylcholine receptor. *The EMBO journal* **2009**, *28*, 3040-3051.

115. Kaczanowska, K.; Harel, M.; Radić, Z.; Changeux, J.-P.; Finn, M.; Taylor, P., Structural basis for cooperative interactions of substituted 2-aminopyrimidines with the acetylcholine binding protein. *Proceedings of the National Academy of Sciences* **2014**, *111*, 10749-10754.

116. Albrecht, B. K.; Berry, V.; Boezio, A. A.; Cao, L.; Clarkin, K.; Guo, W.; Harmange, J.-C.; Hierl, M.; Huang, L.; Janosky, B., Discovery and optimization of substituted piperidines as potent, selective, CNS-penetrant $\alpha 4\beta 2$ nicotinic acetylcholine receptor potentiators. *Bioorganic & medicinal chemistry letters* **2008**, *18*, 5209-5212.

117. Hamouda, A. K.; Deba, F.; Wang, Z.-J.; Cohen, J. B., Photolabeling a nicotinic acetylcholine receptor (nAChR) with an ($\alpha 4$) 3 ($\beta 2$) 2 nAChR-selective positive allosteric modulator. *Molecular pharmacology* **2016**, *89*, 575-584.

118. Giera, D. S.; Sickert, M.; Schneider, C., A straightforward synthesis of (S)-Anabasine via the catalytic, enantioselective vinylogous mukaiyama-Mannich reaction. *Synthesis* **2009**, *2009*, 3797-3802.

119. Hughes, G.; Kimura, M.; Buchwald, S. L., Catalytic enantioselective conjugate reduction of lactones and lactams. *Journal of the American Chemical Society* **2003**, *125*, 11253-11258.

120. Kumar, I.; Ramaraju, P.; Mir, N. A.; Singh, D.; Gupta, V. K., Highly enantioselective [4+ 2] annulation via organocatalytic Mannich-reductive cyclization: one-pot synthesis of functionalized piperidines. *Chemical Communications* **2013**, *49*, 5645-5647.

121. Kumar, I.; Mir, N. A.; Gupta, V. K., An organocatalytic direct Mannich-cyclization cascade as [3+ 2] annulation: asymmetric synthesis of 2, 3-substituted pyrrolidines. *Chemical Communications* **2012**, *48*, 6975-6977.

122. Shaghafi, M. B.; Grote, R. E.; Jarvo, E. R., Oxazolidine synthesis by complementary stereospecific and stereoconvergent methods. *Organic letters* **2011**, *13*, 5188-5191.

123. Kii, S.; Akao, A.; Iida, T.; Mase, T.; Yasuda, N., Bromine-magnesium exchange of 5-bromo-2-picoline via an organomagnesium complex nBu₂iPrMgLi: A new preparation methodology of functionalized picolines under noncryogenic conditions. *Tetrahedron letters* **2006**, *47*, 1877-1879.

124. Van Den Heuvel, M.; van den Berg, T. A.; Kellogg, R. M.; Choma, C. T.; Feringa, B. L., Synthesis of a non-heme template for attaching four peptides: an approach to artificial iron (II)-containing peroxidases. *The Journal of organic chemistry* **2004**, *69*, 250-262.

125. Wang, X.; Rabbat, P.; O'Shea, P.; Tillyer, R.; Grabowski, E.; Reider, P. J., Selective monolithiation of 2, 5-dibromopyridine with butyllithium. *Tetrahedron Letters* **2000**, *41*, 4335-4338.

126. Hanan, E. J.; Eigenbrot, C.; Bryan, M. C.; Burdick, D. J.; Chan, B. K.; Chen, Y.; Dotson, J.; Heald, R. A.; Jackson, P. S.; La, H., Discovery of selective and noncovalent

diaminopyrimidine-based inhibitors of epidermal growth factor receptor containing the T790M resistance mutation. *Journal of medicinal chemistry* **2014**, *57*, 10176-10191.

127. Jeon, A. R.; Kim, M. E.; Park, J. K.; Shin, W. K.; An, D. K., Mild and direct conversion of esters to morpholine amides using diisobutyl (morpholino) aluminum: application to efficient one-pot synthesis of ketones and aldehydes from esters. *Tetrahedron* **2014**, *70*, 4420-4424.

128. Park, J. K.; Shin, W. K.; An, D. K., An effective one-pot conversion of acid chlorides to aldehydes and ketones. *Tetrahedron Letters* **2013**, *54*, 3199-3203.

129. Abels, F.; Schneider, C., A Modified and Highly Useful Protocol for the Brønsted Acid Catalyzed, Enantioselective, Vinylogous Mannich Reaction with Aliphatic Aldimines. *Synthesis* **2011**, *2011*, 4050-4058.

130. Jarrahpour, A.; Zarei, M., Synthesis of novel N-(4-ethoxyphenyl) azetidin-2-ones and their oxidative N-deprotection by ceric ammonium nitrate. *Molecules* **2007**, *12*, 2364-2379.

131. Mattson, R. J.; Pham, K. M.; Leuck, D. J.; Cowen, K. A., An improved method for reductive alkylation of amines using titanium (IV) isopropoxide and sodium cyanoborohydride. *The Journal of Organic Chemistry* **1990**, *55*, 2552-2554.

132. Coulthard, G.; Erb, W.; Aggarwal, V. K., Stereocontrolled organocatalytic synthesis of prostaglandin PGF 2 α in seven steps. *Nature* **2012**, *489*, 278-281.

133. Palmer, M. J.; Kenny, J. A.; Walsgrove, T.; Kawamoto, A. M.; Wills, M., Asymmetric transfer hydrogenation of ketones using amino alcohol and monotosylated diamine derivatives of indane. *Journal of the Chemical Society, Perkin Transactions 1* **2002**, 416-427.

134. Srimontree, W.; Chatupheeraphat, A.; Liao, H.-H.; Rueping, M., Amide to alkyne interconversion via a nickel/copper-catalyzed deamidative cross-coupling of aryl and alkenyl amides. *Organic letters* **2017**, *19*, 3091-3094.

135. Ye, X.; Petersen, J. L.; Shi, X., Nickel-catalyzed directed sulfenylation of sp² and sp³ C–H bonds. *Chemical Communications* **2015**, *51*, 7863-7866.

136. Verkade, J. M.; van der Pijl, F.; Willems, M. M.; Quaedflieg, P. J.; van Delft, F. L.; Rutjes, F. P., An enantioselective organocatalytic approach to both enantiomers of lasubine II. *The Journal of organic chemistry* **2009**, *74*, 3207-3210.

137. Neises, B.; Steglich, W., Simple method for the esterification of carboxylic acids. *Angewandte Chemie International Edition in English* **1978**, *17*, 522-524.